

# Design, performance and analysis of ducted axial flow fans : including tests on sheet metal bladed fans

**Author:**

Wallis, R. Allan (Raymond Allan)

**Publication Date:**

1953

**DOI:**

<https://doi.org/10.26190/unsworks/5299>

**License:**

<https://creativecommons.org/licenses/by-nc-nd/3.0/au/>

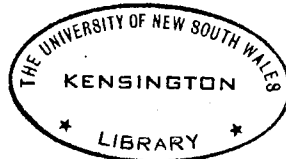
Link to license to see what you are allowed to do with this resource.

Downloaded from <http://hdl.handle.net/1959.4/56834> in <https://unsworks.unsw.edu.au> on 2024-03-29

DESIGN, PERFORMANCE AND ANALYSIS OF DUCTED AXIAL  
FLOW FANS, INCLUDING TESTS ON SHEET METAL BLADED FANS

by

R.A. Wallis A.S.T.C., A.M.I.E. Aust.



*A thesis submitted to the N.S.W. University of Technology,  
Master of Engineering Degree Course*

December 1953.



UNIVERSITY OF N.S.W.

27970 26.FEB.75

LIBRARY

(1)

### SUMMARY

A method of designing, analysing and estimating performance is given for the general case of a ducted axial flow fan rotor with prerotators upstream and straighteners downstream. The theory is based largely on data obtained from experimental tests on isolated aerofoils and aerofoils in cascade. This facilitates the design of both low and high pressure rise fans.

The design method, which is direct, is developed in terms of two parameters, namely, the flow and swirl coefficients. Recommendations for calculating the losses in the rotor, stators and over the tail fairing give an estimate of efficiency which is adequate for design purposes. As the method lends itself to graphical solution, the design variables have been presented as simple functions of the above two parameters.

A rapid estimate of the characteristic curve can be obtained from the method of analysis given, which is simple and of a general nature.

Experimental and performance data are presented which facilitate the design of axial flow fans made with circular arc blades. Relatively good efficiencies are possible with this industrial type of fan. The tests also include an investigation on the order of the losses over the tail fairing. A design example and a method of construction are appended.

CONTENTS

GENERAL DESIGN METHODS AND ANALYSIS - PART A

TESTS ON SHEET METAL BLADED FANS - PART B

PART APage

## NOTATION

1	INTRODUCTION	1
1.1	Basic design theories	2
1.2	Fan configurations	3
1.3	Swirl and flow coefficients	4
1.4	Load distribution	5
1.5	The blade element	6
1.6	Interference	8
1.7	Fan efficiency	10
1.8	Design assumptions	13
1.9	Design method	14
1.10	Fan analysis	17
2	ROTOR DESIGN	
2.1	General	17
2.2	Momentum Considerations	18
2.3	Blade Design Considerations	28
2.3.1	Choice of appropriate design method	34
2.4	Blade element design (isolated aerofoil theory)	37
2.5	Blade element design (aerofoils in cascade)	38

Contents Cont'd

	<u>Page</u>
3 STATOR DESIGN	41
3.1 Momentum considerations	41
3.2 Straightener design (N.P.L. type)	43
3.3 Straightener design (aerofoils in cascade)	45
3.4 Prerotator design (aerofoils in cascade)	47
4 ROTOR LOSSES	50
4.1 General	50
4.2 Momentum Considerations	52
4.3 Profile drag	53
4.4 Secondary drag	55
4.5 Annulus drag	57
4.6 Total drag	59
5 STATOR LOSSES	60
5.1 General	60
5.2 Momentum Considerations	60
5.3 Drag components	62
5.4 Total drag	63
6 DUCT AND TAIL FAIRING LOSSES	64
7 OVERALL EFFICIENCIES	66
⑧ DETAILED DESIGN PROCEDURES	69
8.1 Preliminary Procedure	69
8.2 Detail Rotor Design (isolated aerofoil theory)	74
8.3 Detail Rotor Design (aerofoils in cascade)	76
8.4 Detail Straightener Design	77
8.5 Detail Prerotator Design	78

<u>Contents Cont'd.</u>	<u>Page</u>
9 TORQUE, THRUST, AND POWER	79
10 ANALYSIS OF A GIVEN FAN	81
10.1 Rotor analysis	82
10.1.1 Effect of spanwise variations in axial velocity - free vortex design	91
10.2 Straightener analysis	94
10.3 Prerotator analysis	95
10.4 Power requirements	95
APPENDICES TO PART A	
APPENDIX A ANALYTICAL DETERMINATION OF CHARACTERISTIC CURVE FOR CONTRA-ROTATING FANS (REF. 45)	96
APPENDIX B AEROFOIL SECTION CO-ORDINATES	99
TABLES 1 - 16	
FIGURES 1 - 44	
PART B	
ADDITIONAL NOTATION	100
11 INTRODUCTION	10
11.1 General	10
11.2 Description of fans tested	10
11.3 General methods of fan testing	10
12 FAN TESTS	10
12.1 Equipment	10
12.2 Method of Analysis	10
12.3 Results	10

<u>Contents Cont'd.</u>	<u>Page</u>
12.3.1 Velocity distributions	110
12.3.2 Induced velocity distributions	110
12.3.3 Total head distributions	112
12.3.4 Characteristic curves	113
12.3.5 Power and efficiency	114
13 LOSSES OVER TAIL FAIRING	115
14 CONCLUSIONS	117
15 ACKNOWLEDGEMENTS	117
APPENDICES TO PART B	
APPENDIX C Design details of No. 3 fan	118
APPENDIX D Analysis of fan losses - test results	121
APPENDIX E Analytical determination of characteristic - cambered plate fan	123
APPENDIX F Design example	124
APPENDIX G Construction method for cambered blades.	143
TABLES 17 - 18	149
FIGURES 45 - 73	
REFERENCES	



NOTATION

$b$	Camber of aerofoil (cascade theory)
$C_D$	Total drag coefficient of rotor or stator blade element at radius $r$ .
$C_{D_P}$	Profile drag coefficient of rotor or stator blade element at radius $r$ .
$C_{D_S}$	Secondary drag coefficient of rotor or stator blade element at radius $r$ .
$C_{D_A}$	Annulus drag coefficient of rotor or stator blade element at radius $r$ .
$c$	Chord of the rotor or stator blade element at radius $r$ .
$C_L$	Lift coefficient of rotor or stator blade element at radius $r$ .
$C_L^*$	Optimum lift coefficient of rotor or stator blade element at radius $r$ (cascade theory)
$D$	Total drag of rotor or stator blade element at radius $r$ .
$f$	Fineness ratio of tail fairing
$H$	Total head in a streamline
$\Delta H$	Mean total head loss in duct system (exclusive of fan unit)
$\Delta H_D$	Mean total head loss over tail fairing

* $\Delta h_a$	Actual total head rise across rotor and stator blades in an elementary annulus.
$\Delta h_{th}$	Theoretical total head rise across the rotor in an elementary annulus.
$\Delta h_F$	Total head losses across the rotor due to drag in an elementary annulus.
$\Delta h_P$	Total head losses across the pre-rotator due to drag in an elementary annulus.
$\Delta h_S$	Total head losses across the straighteners due to drag in an elementary annulus.
$i$	Local angle of incidence (cascade theory)
$K$	Total head coefficient of duct loss $\left( \frac{\Delta H}{\frac{1}{2} \rho U_o^2} \right)$
$K_D$	Mean total head loss coefficient for tail fairing diffuser
$k_a$	Coefficient of total head rise across rotor and stators

---

\* Capital letters denote mean total head changes in duct or fan unit as a whole, whilst small letters are for changes in an elementary annulus.

Total head rises have small letter subscripts, losses have capital letter subscripts.

$k_{th}$	Coefficient of theoretical total head rise across rotor
* $k_F$	Coefficient of total head loss across rotor
$k_P$	Coefficient of total head loss across pre-rotator
$k_S$	Coefficient of total head loss across straightener
$k_{F_p}$	Coefficient of total head loss across rotor due to profile drag.
$k_{F_s}$	Coefficient of total head loss across rotor due to secondary drag
$k_{F_A}$	Coefficient of total head loss across rotor due to annulus drag.
$k_{P_p}$	Coefficient of total head loss across pre-rotator due to profile drag.
$k_{P_s}$	Coefficient of total head loss across pre-rotator due to secondary drag.
$k_{S_p}$	Coefficient of total head loss across straightener due to profile drag.
$k_{S_s}$	Coefficient of total head loss across straightener due to secondary drag.
L	Lift of rotor or stator blade element at radius r.

---

\* Capital letter, K, denotes coefficient of mean total head change; small letter, k, the coefficient for elementary annulus. All coefficients are based on  $\frac{1}{2}\rho u^2$

(ix)

$m$	Slope of lift curve ( $C_L = m \sin (\Phi - \varphi)$ )
$L$	Length of tail fairing
$N$	Number of rotor or stator blades
$P$	Horsepower
$P_c$	Power coefficient
$p$	Static pressure in a streamline
$\Delta p$	Static pressure rise across rotor in elementary annulus
$\Delta p_{th}$	Theoretical static pressure rise across rotor in elementary annulus
$Q$	Torque of rotor
$Q_c$	Torque coefficient
$R$	Radius of rotor tip
$R_{cur}$	Radius of curvature of camber line (cascade theory)
$r$	Radius of elementary annulus
$dr$	Width of elementary annulus
$r_o$	Radius of rotor boss
$s$	Gap between rotor or stator blades
$T$	Thrust of rotor
$T_c$	Thrust coefficient
$U_o$	Mean velocity in duct of radius $R$ ( $x_o = 0$ )
$u$	Axial component of velocity in elementary annulus (assumed constant for whole fan)
$V_1$	Resultant inlet velocity relative to blade
$V_2$	Resultant outlet velocity relative to blade

(x)

$w$	Mean effective resultant velocity relative to rotor blade
$w_p$	Mean effective resultant velocity relative to pre-rotator blade
$w_s$	Mean effective resultant velocity relative to straightener blade
$X$	Tangential force per blade element
$x$	Radius ratio $r/R$
$x_o$	Boss ratio $r_o/R$
$Y$	Axial force per blade element
$\alpha$	Angle of incidence (free aerofoil theory)
$\alpha_1$	Angle vector, $V_1$ , makes with fan axis.
$\alpha_2$	Angle vector, $V_2$ , makes with fan axis.
$\beta_1$	Angle leading edge camber line tangent makes with fan axis.
$\beta_2$	Angle trailing edge camber line tangent makes with fan axis
$\gamma$	Lift/drag ratio
$\delta$	Angle of deviation
* $\epsilon$	Ratio of induced velocity to axial velocity

---

\* Suffices o and m to  $\epsilon$  and  $\lambda$  denote values at  $r_o$  and the mid-span station respectively.


$\epsilon_p$	Ratio of induced velocity, produced by pre-rotators, to axial velocity
$\epsilon_s$	Ratio of induced velocity, removed by straighteners, to axial velocity
$\eta_a$	Efficiency of rotor and stators
$\eta_F$	Efficiency of rotor
$\eta_T$	Efficiency of complete unit
$\eta_D$	Diffuser efficiency over tail fairing
$\theta$	Camber angle of rotor or stator blades
$\Lambda$	Ratio of axial velocity to rotor tip velocity
$\lambda$	Ratio of axial velocity to blade velocity at radius $r$ .
$\xi$	Stagger angle
$\rho$	Density in slugs/ft. <sup>3</sup>
$\sigma$	Solidity (the reciprocal of $s/c$ )
$\Phi$	angle between no lift line of blade element section and the plane of rotation
$\varphi$	Angle vector, $w$ , makes with plane of rotation.
$\varphi_p$	Angle vector, $w_p$ , makes with plane of rotation.
$\varphi_s$	Angle vector, $w_s$ , makes with plane of rotation.
$\Psi$	Angle associated with rate of change of swirl with flow coefficient.
$\omega$	Angular velocity of induced rotation at radius $r$

$\omega_p$	Angular velocity of rotation induced by pre-rotators at radius $r$
$\omega_s$	Angular velocity of rotation removed by straighteners at radius $r$ .
$\Omega$	Angular velocity of rotor.



1

## INTRODUCTION



An axial flow fan adds momentum to a body of air without changing the general direction of the flow. There are two main types, namely, (i) non-ducted circulating fans, and (ii) ducted fans. Intermediate between these two are fans with shroud rings to prevent recirculation through the tips and fans mounted in a diaphragm plate, such as crude wall exhaust fans. Originally, axial flow fans were crudely designed and poorly installed and they suffered in comparison with the centrifugal fan. Nowadays, however, it is well known that very high efficiencies can be obtained from well designed axial flow fans.

The ducted axial flow fan, which is considered in the paper, is very amenable to mathematical computation, and advanced design techniques are now available. Such a fan can be considered as a means of forcing a quantity of air through a duct system against a resistance comprised of skin friction, flow separations, discharge losses and losses within the fan unit itself. It is intended to treat the design, performance and analysis of ducted fans in a manner which will permit a ready application of the data.



### 1.1 Basic Design Theories.

There are two basic design theories which are used conjointly to design fans to fulfil a specific task. The first, called the Momentum Theory, is only concerned with the momentum which the fan must add to the air and the overall effects on the stream. The second, called the Blade Element Theory, specifies the aerofoil blade details necessary to produce these overall effects.

Taking the air velocities relative to the blade, the outlet velocity is less than the inlet velocity and hence a static pressure rise occurs, as in diffusers. Relative to the duct, the outlet velocity is greater than the inlet velocity resulting in a tangential or swirl component. The torque of the fan is equal to the rate of change of angular momentum. The question of impulse or reaction fans is discussed in section 2.2.

From the pressure rise and flow requirements the momentum relationships can be established and the velocity vectors determined. The blade element theory then enables the blade shape and setting to be investigated. Each elementary length of blade is usually treated as a two dimensional blade section in a two dimensional flow.

## 1.2 Fan Configurations.

The change in angular momentum of the air represents a loss unless it is efficiently recovered as pressure. There are, in general, five main design possibilities, namely, (a) the swirl passes downstream and the energy is lost, (b) the swirl is removed by stators downstream of the fan, (c) stators are used to impart a pre-swirl in the opposite sense to the fan rotation, the rotor then removing the swirl, (d) a combination of the preceding two and (e) contra-rotating fans where the second removes the swirl of the first.

Multi-stage units are uncommon as centrifugal fans, due to their simplicity, are usually preferred in this pressure rise range. However, where efficiency is an important factor, the multi-stage unit is attractive.

In general, the fan-straightener unit is the one most commonly used as it is usually more efficient and convenient than the prerotator - fan unit; however, slightly higher pressure rises are possible with the latter for a given rotational speed. Straighteners are sometimes used in conjunction with prerotators in order to remove the residual rotation when the fan operates substantially away from the design case.

### 1.3 Swirl and Flow Coefficients.

On passing through prerotators, the air is deflected and accelerated with a subsequent pressure drop. Deflections of  $60^\circ$  or more are possible before stator stall conditions appear. However, the greater the swirl, the larger the pressure rise across the rotor and hence the danger of rotor stalling will impose some limitations on the preswirl permissible.

In the case of downstream stators, or straighteners as they are called when the swirl component is completely removed, the air is decelerated, i.e. a pressure rise occurs. A restriction has to be placed on the design swirl of the rotor to ensure that the straighteners do not stall. The angle of deflection through flow straighteners is limited, for most practical purposes, to  $45^\circ$ .

From the above it can be readily seen that the ratio between the swirl velocity and the axial component, which defines the deflection angle, is an important variable. The swirl imparted, or removed, by the fan is a measure of the change in angular momentum and thus of the torque of the fan. Assuming that for a given flow and pressure rise the efficiency remains constant, it is at once apparent that the amount of swirl

for a given power input can be changed by altering the design speed of the fan. This involves a second ratio between the axial component and the rotational speed of the blade element known as the flow coefficient. Most of the variables associated with fan design can be expressed as simple functions of these two ratios.

#### 1.4 Load Distribution.

It is possible to specify the load distribution along the span of the blade in terms of the swirl and flow coefficients. The most common design distribution is obtained by assuming that the angular velocity of swirl is inversely proportional to the radius. In such a flow, the centrifugal forces are balanced by the radial pressure gradient (e.g. see Ref. 1) and hence the flow particles are confined to an elementary annulus of fixed radius. This condition, which gives no radial component of velocity and results in a constant total head rise along the span, is known as "free vortex" flow.

With "solid body" rotation, the angular velocity is directly proportional to the radius, as the name would imply. This distribution is very seldom used owing to the radial flows introduced. The total head rise increases as the tip is approached and because

of this it has been shown that, for moderate boss diameter to fan diameter ratios, the working capacity of a fan can be increased whilst retaining high efficiency (Ref. 1). It is of course possible to design for this condition, or any other arbitrary distribution such as constant angular velocity, provided attention is paid to the radial flows, (Refs. 1, 2 and 3).

#### 1.5 The Blade Element.

As a consequence of the relative velocity between the blade and the air, the blade experiences lift and drag forces. When compounded along the fan axis and in the plane of rotation, these forces define respectively the thrust and torque on the blade element. The lift is dependent on three main factors, namely, the dynamic head due to the relative velocity, the blade chord and the angle of incidence which the velocity vector makes with the blade. Increasing each of these, within limits, will increase the pressure rise which the fan is capable of producing.

For a given mass flow, the relative velocity may be increased by increasing (a) the axial component, (b) the rotational component. The first is achieved by increasing the boss diameter and/or by

reducing the fan diameter. It must be borne in mind, however, that the flow has to be diffused back to the mean velocity in the duct. The losses involved in this process, as will be shown later, can reduce the overall efficiency by a considerable amount. The second expedient, that of increasing the fan speed, also has its limitations. Due to an increase in the absolute drag, the loss in efficiency at small flow coefficients, i.e. large relative rotational speeds, can be considerable. At the tip, where the relative velocity is greatest, compressibility troubles may arise if the relative velocity exceeds 500 - 550 ft./sec. (Refs. 11 and 5). Noise is, of course, augmented with increasing tip speed.

Instead of considering the blade chord it is more convenient to use the non-dimensional ratio of blade chord to circumferential gap between adjacent blade elements, namely the solidity. For solidities approaching unity and beyond, there is an aerodynamic interference between adjacent blades which results usually in a marked reduction in lift. Hence for this and obvious practical reasons there is a very definite limit to the amount which the chord can be increased for the purpose of obtaining higher pressure rises.

Lastly, there is in design a limitation on the angle of incidence of the blade, with respect to the relative velocity, fixed usually by a large increase in drag which precedes the stall. In order to obtain the highest efficiency it is necessary to use blade sections which have a high lift/drag ratio.

There is, of course, no lower limit on pressure rise; it is only necessary to ensure that the design gives the desired efficiency.

#### 1.6 Interference.

When the solidity is low, there is no mutual interference between the lifts of adjacent blades. In these circumstances, the two dimensional test data of suitable aerofoils, such as the RAF 6 and Clark Y (see Appendix B), can be directly applied. This approach is known as the isolated aerofoil theory. On the basis of experimental work (Refs. 6, 7, 8 and 9) this theory is assumed to be invalid for solidities greater than unity. An arbitrary limit of unity has also been placed on the product of lift coefficient and solidity (Ref. 6). In the light of recent experimental work on the performance of aerofoils in cascade, these criteria will be unreliable at small flow coefficients (see Section 2.3).

Some attempts (Refs. 5, 9, 10 and 11) have been made to extend the scope of the isolated aerofoil theory by introducing an interference factor sometimes defined as the ratio of the actual lift of the blade in cascade to the lift it would exert if the other blades were absent. Such methods, however, have failed in general to produce consistent results.

One approach (Refs. 11, 12 and 13) to the cascade aerofoil theory is to theoretically remove one blade and replace it by a simple circulation to represent the lift. This flow is then compounded with the flow field around the adjacent blade, the latter having been calculated for an isolated aerofoil. From the modified pressure distribution, the lift of the aerofoils can be determined. Other methods of calculating the potential flow through cascades of aerofoils are given in References 9, and 14-18. More recently, techniques have been evolved which enable cascade aerofoils to be designed with a specific velocity distribution (Refs. 19 to 23). Whilst such methods are promising, the majority of present day design is based on experimental data obtained from low speed two dimensional cascade wind tunnels (Refs. 3 and 24 to 30).



This data, which is considerable, owes its existence to the axial flow compressor research carried out in numerous countries. In general, the blade section is comprised of a specified camber line which is then clothed with a suitable symmetrical aerofoil section (see Appendix B). The camber line and its setting are usually sufficient to specify the duty which the blade fulfils in design.

#### 1.7 Fan Efficiency.

The efficiency of an axial flow fan depends greatly on the overall installation. Good inlet and outlet conditions are not always possible, (due possibly to space limitations or unavoidable obstructions,) and, when this is the case, no accurate measure of the losses can be obtained. In these circumstances, actual experience is almost essential in determining the losses although assistance can be obtained from published work such as Reference 31.

Provided, however, that flow separation is avoided within a reasonable compass of the fan, the fan losses can be predicted with a sufficient degree of accuracy. It is generally accepted now that the losses may be arbitrarily subdivided into three components namely, profile drag, secondary drag and annulus drag. (e.g. see Refs. 32, 33 and 34).

The first, which is a two dimensional loss, is fully understood but the latter two, which are three dimensional, are still receiving considerable attention

Secondary flow, i.e. flow having a component normal to the local stream direction, arises as a result of a non uniform inlet total head caused by wall boundary layers and wakes. The centrifugal forces acting on the air in these retarded regions are insufficient to balance the pressure gradients associated with turning the flow through the fan. This leads to secondary flow near the extremities of the blade. This superimposed motion represents momentum lost to the main flow as it cannot be recovered; the motion is dissipated finally as turbulence.

There are, in general, two approaches to the problem. The theory which is more fundamentally sound, treats the secondary flow as one depending on the properties of the passage through which it is passing (Refs. 35, 36). It has not as yet, however, yielded much in the way of reliable quantitative data although qualitatively the losses are known to depend on the turning angle and the solidity (Ref. 37).

Howell and Carter (Refs. 3, 32 and 34) have endeavoured to identify the motion with the normal

trailing vortex system found downstream of finite wings. Although valid objections (Ref. 37) can be raised to such a treatment it has nevertheless formed the basis of a quantitative analysis. The loss is presented as an equivalent induced drag coefficient. It has been shown (Ref. 34) that the real induced drag coefficient, due to a variation in lift along the blade, (not including the sudden loss of lift at the extremities,) is generally very small.

The origin of the annulus losses as given by Howell (Ref. 3), namely, high skin friction, is not completely satisfactory. A more satisfactory approach is indicated by Mager and others (Ref. 33) who undertook an analysis of the boundary layer deflections on the wall near the blade tips.

Despite the uncertainty associated with the exact nature of the three dimensional losses, enough is known to permit a reasonable quantitative estimate. A similar subdivision of losses can be made for the stators.

Because of the direct relationship between the fan design and the diffuser losses over the tail fairing, these losses have to be taken into consideration. Finally it will be reiterated that the losses outlined

are the major ones provided there are no flow separations in or near the fan.

For blade Reynolds numbers below the critical, the losses increase sharply with decreasing Reynolds number, (e.g. See Reference 34 and general aerofoil test data). Another factor which has an influence on the efficiency is the relative roughness of the surface. Usually, roughness only increases the skin friction, the main effect being a loss in efficiency. Roughness can, however, modify the characteristics of the fan rotor (See Ref. 38).

#### 1.8 Design Assumptions.

From the foregoing sub-sections, it is obvious that a complete cover of the subject is impossible; in this paper, therefore, some restriction has been necessary. A design method has been presented which is general enough to permit its application to most practical problems without introducing undue complication. An extension of the theory to meet any special need should not prove difficult. Axial flow compressors are not considered.

The design method is based on the following:

- (i) Only high efficiency ducted fans are treated in detail. In Part B an extension to sheet metal bladed fans is indicated.

- (ii) The general case of a rotor with stators upstream and downstream is treated.
- (iii) Experimental data on isolated and cascade aerofoils has been used in order to cover the complete pressure range.
- (iv) The flow is incompressible, i.e. the relative velocity at the tip is less than 550 ft/sec.
- (v) Free vortex flow which involves assuming constant total head rise and axial velocity along the blade span.
- (vi) The swirl coefficient removed by the straighteners not to exceed 1.0 and that produced by prerotators to be less than 1.5 (See section 1.3).
- (vii) A lower limit of 0.2 on flow coefficient,  $\lambda$ , due to efficiency considerations and an upper limit of 1.5 fixed by design difficulties.

Contra-rotating fans can be designed from the above by taking the swirl of the front fan as being the prerotation for the rear fan.

### 1.9 Design Method.

In developing the present design method, an attempt has been made to combine the best features of existing design methods (Refs. 1, 4-7, 9-11, 24, 39-43)

and at the same time carry out developments aimed at simplifying the processes. The use of thrust and torque gradings along the span in determining the blade element characteristics, either on a reiterative (Refs. 4 and 5) or a direct basis (Refs. 6 and 42), has been eliminated; their use can be traced to an extension of airscrew theory to ducted fan design.

This present design method is an extension of Patterson's (Refs. 6, 39-41) and hence, wherever possible, the same non-dimensional coefficients and notation have been retained. The virtue of a non-dimensional treatment is self evident as it permits the extensive use of design graphs, simplifies the design and gives a ready appreciation of design limits. In cascade theory (Refs. 3 and 24), which was developed for compressor design, the flow characteristics are often defined by angles or functions of angles; this is due to density variations which prevent, in such work, the use of the non-dimensional fan coefficients. However, wherever possible, this data has been reduced to a suitable non-dimensional form enabling it to be integrated into the general design method for both low and high pressure in fans. The standard conventions of Ref. 44 has been adopted where additional notation is

required. This theory is usually limited to high pressure rise fans with moderately high boss/fan ratios.

It has been found that most design variables can be expressed as simply functions of the swirl and flow coefficients. This has simplified the procedure and opened the way to a greater use of design graphs. The data from which the accompanying figures are plotted, are tabulated to facilitate the preparation of graphs large enough for design purposes.

It has been found more convenient to develop the design in terms of the theoretical, rather than the actual, total head rise. This permits greater use of the swirl and flow coefficients as parameters in design graphs. The losses are more conveniently handled separately and as functions of the same two coefficients.

Although the design theory of Patterson (Ref. 6) constituted a starting point for the present investigation, most of the design theory and method have been recast. In Reference 6, a constant efficiency is assumed along the blade from which the lift/profile drag ratio to give that efficiency is calculated for a specific blade element. Knowing the characteristics of the particular aerofoil to be used, the lift coefficient

and blade incidence corresponding to the above lift/drag ratio can be determined. The computation of the blade chord then follows, thus completing the design of a specific blade element.

The present method is more direct and only involves the solution of a small number of simple equations.

#### 1.10 Fan Analysis

An important part of fan design is the determination of the operating characteristic for the requisite range of working conditions. A number of methods have been suggested (e.g. Refs. 7, 10, 45 to 48) which entail varying degrees of labour. In this paper a simple method of analysis is presented which is very suitable for the analysis of free vortex fans and can be used, within reason, for other types. As before, the general case of a rotor with both preswirl and afterswirl is considered. An alternative method for cascade type aerofoils is also given.

## 2 FAN DESIGN

### 2.1 General.

From experience it is found that the assumption of a constant axial velocity component, made



in section 1.8, is very reliable. The use of a nose fairing and a moderate boss/fan ratio tend to improve the velocity distribution. When this assumption is combined with that of constant total head rise it can be shown (Section 2.2) that the flow satisfies the free vortex equation, namely,

$$\omega r^2 = \text{constant} \qquad 2.1.1$$

where  $\omega$  is the angular velocity of swirl.

The air is then retained between co-axial cylinders of radius  $r$  and  $(r + dr)$ .

The theory, as mentioned previously, has been developed for the generalized case in which stators have been fitted upstream and downstream of the fan. Although such a design is rarely encountered, the more usual configurations with either prerotators or straighteners can be readily designed by substituting the appropriate values.

Irrespective of whether isolated aerofoil or cascade data is used, the initial steps of design are identical as these depend only on momentum considerations.

## 2.2 Momentum Considerations.

From the assumptions just made and taking a blade element of length  $dr$ , the following diagram can be drawn,

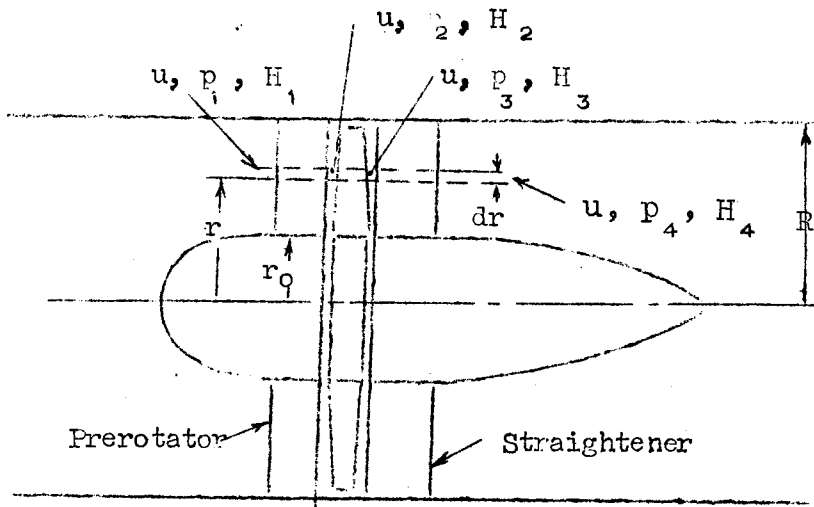


DIAGRAM 1

Air entering the prerotators axially is deflected tangentially in a direction opposite to the fan rotation. It is assumed that the air then leaves the fan rotor with a tangential component of opposite sign to that given by the prerotators thus leaving the straighteners the task of deflecting the air back into the axial direction.

The total heads at each position are given by the expressions:

$$\begin{aligned}
 H_1 &= p_1 + \frac{1}{2}\rho u^2 \\
 H_2 &= p_2 + \frac{1}{2}\rho u^2 + \frac{1}{2}\rho(\omega_p r)^2 \\
 H_3 &= p_3 + \frac{1}{2}\rho u^2 + \frac{1}{2}\rho(\omega_s r)^2 \\
 H_4 &= p_4 + \frac{1}{2}\rho u^2
 \end{aligned}$$

2.2.1

where  $H$ ,  $p$ ,  $u$  and  $\omega r$  are the total head, static pressure, axial velocity component and tangential velocity component respectively.

The overall change in total head in the annulus can be written -

$$H_4 - H_1 = \Delta h_a = \Delta h_{th} - \Delta h_F - \Delta h_P - \Delta h_S \quad 2.2.2$$

where  $\Delta h_{th}$  is the theoretical head rise assuming no losses; the other terms denote the losses in the fan, prerotators and straighteners respectively.

Expressing the above non-dimensionally by dividing throughout by  $\frac{1}{2}\rho u^2$ .

$$k_a = k_{th} - k_F - k_P - k_S \quad 2.2.3$$

This represents also the non-dimensional static pressure rise between stations 1 and 4. The static pressure rise across the fan rotor is given by -

$$p_3 - p_2 = \Delta p = \frac{1}{2}\rho u^2(k_{th} - k_F + \epsilon_p^2 - \epsilon_s^2) \quad 2.2.4$$

where  $\frac{\omega r}{u} = \epsilon$  and  $H_2 - H_3 = \Delta h_{th} - \Delta h_F$

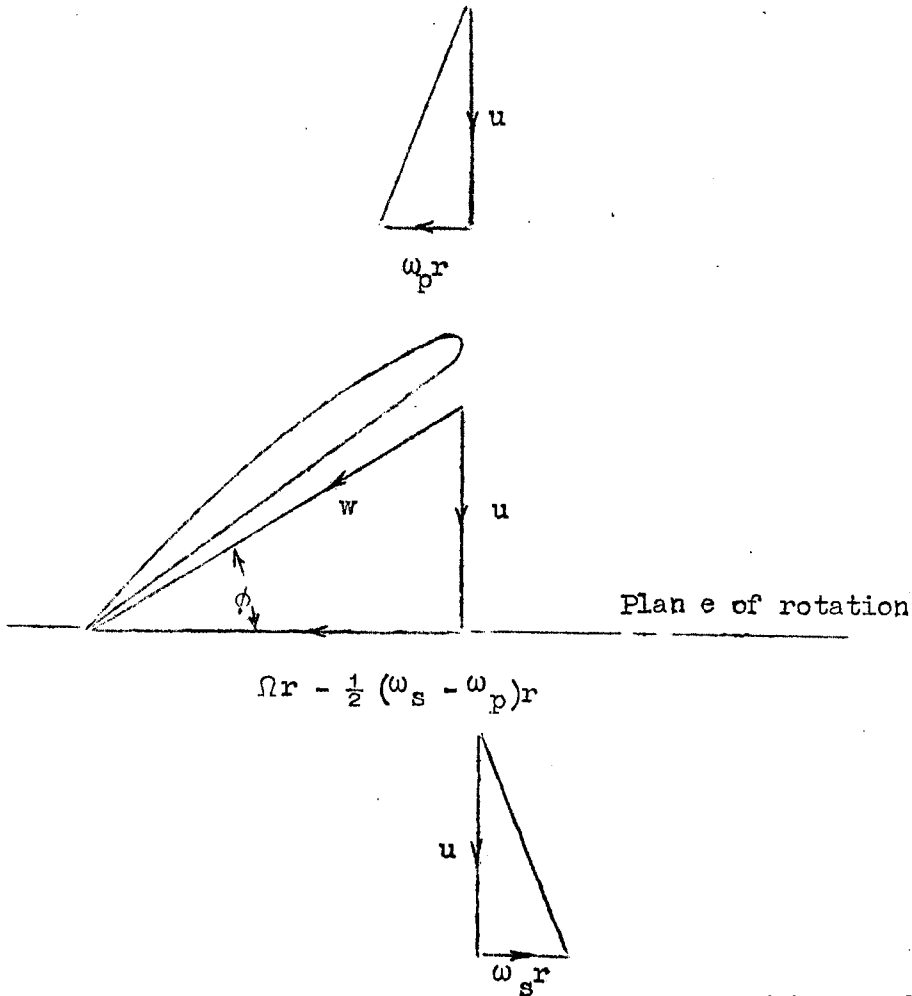


DIAGRAM 2

Neglecting for a while the flow through the stators, the preceding diagram illustrates the absolute velocity vectors for an element of fan blade of length  $dr$ . The prerotator gives the air entering the fan a rotational component of  $\omega_p r$  which the fan removes and at the same time the fan produces an additional component of  $\omega_s r$  at outlet as described before.

In order to determine the mean resultant vector which the fan experiences it is necessary to make some assumption concerning the effective swirl. This is taken to be the mean change in swirl assuming the swirl changes linearly from inlet to outlet from the blade. The resultant tangential velocity experienced by the blade is then given by

$$\Omega r - \frac{1}{2}(\omega_s - \omega_p)r$$

where  $\Omega r$  is the blade speed at radius  $r$ .

The angle which the resultant velocity makes with the plane of rotation,  $\phi$ , can be expressed by

$$\left. \begin{aligned} \tan \phi &= \frac{u}{\Omega r - \frac{1}{2}(\omega_s - \omega_p)r} \\ &= \frac{\lambda}{1 - \frac{1}{2}(\epsilon_s - \epsilon_p)\lambda} \end{aligned} \right\} \quad 2.2.5$$

where  $\lambda$ , the flow coefficient =  $\frac{u}{\Omega r}$

This indicates the direction in which the lift and drag forces act. From the force vector diagram below -

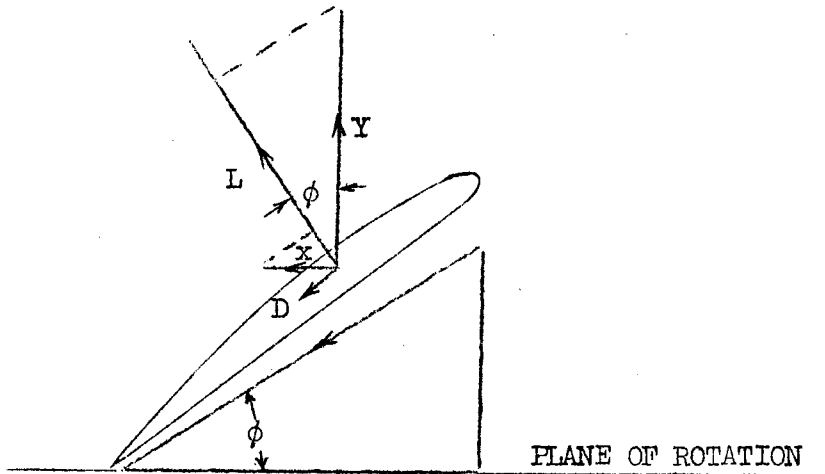


DIAGRAM 3

it will be seen that the lift is comprised of components of both the axial and tangential forces Y and X; the drag has a similar composition.

The axial force, Y, per blade element equals

$$\Delta p s dr \quad 2.2.6$$

where s is the gap defined by  $\frac{2\pi r}{N}$

and N is the number of blades.

The rate of change of swirl momentum gives the tangential force, X, as follows:

$$\begin{aligned} X &= sp u (\omega_p r + \omega_s r) dr \\ &= sp u^2 (\epsilon_p + \epsilon_s) dr \end{aligned} \quad 2.2.7$$

Hence the drag of a blade element is

$$D = X \cos \phi - Y \sin \phi$$

$$= \rho u^2 (\epsilon_p + \epsilon_s) dr \cos \phi - s \Delta p dr \sin \phi$$

Substituting for  $\Delta p$  and dividing by  $\frac{1}{2} \rho u^2 c dr$  where  $c$  is the blade chord, and substituting  $\sin \phi$  for  $\frac{u}{W}$

$$C_D = \frac{s}{c} \sin^2 \phi \{ 2(\epsilon_p + \epsilon_s) \cos \phi - (k_{th} - \epsilon_s^2 + \epsilon_p^2) \sin \phi \} \\ + \frac{s}{c} k_F \sin^3 \phi$$

Assuming no losses in the fan, the work done will equal the work put into the fan by the shaft, hence for a complete annulus:

$$\Delta h_{th} 2\pi r dr u = 2\pi r dr \rho u^2 (\epsilon_p + \epsilon_s) \Omega r$$

$$\therefore \frac{k_{th} \lambda}{2(\epsilon_p + \epsilon_s)} = 1 \quad 2.2.8$$

Eliminating  $k_{th}$  and substituting

$\cot \phi$  for

$$\frac{1 - \frac{1}{2}(\epsilon_s - \epsilon_p) \lambda}{\lambda}$$

$$C_D = 2 \frac{s}{c} \sin^2 \phi (\epsilon_p + \epsilon_s) \{ \cos \phi - \cot \phi \sin \phi \} + \frac{s}{c} k_F \sin^3 \phi$$

$$\therefore C_D = \frac{s}{c} k_F \sin^3 \phi \quad 2.2.9$$

Similarly the lift, L, is

$$\begin{aligned} L &= X \sin \phi + Y \cos \phi \\ &= \rho u^2 (\epsilon_p + \epsilon_s) dr \sin \phi + s \Delta p dr \cos \phi \end{aligned}$$

hence

$$\begin{aligned} C_L &= \frac{s}{c} \sin^2 \phi \{ 2(\epsilon_p + \epsilon_s) \sin \phi + (k_{th} - \epsilon_s^2 + \epsilon_p^2) \cos \phi \} \\ &\quad - \frac{s}{c} k_F \sin^2 \phi \cos \phi \end{aligned}$$

Making the same substitution as before and in addition substituting  $C_D$  for  $\frac{s}{c} k_F \sin^3 \phi$

$$C_L = 2 \left( \frac{s}{c} \right) (\epsilon_p + \epsilon_s) \sin \phi - C_D \cot \phi \quad 2.2.10$$

writing  $\frac{c}{s}$  as  $\sigma$  which is the normal symbol for propeller solidity.

$$C_L \sigma = 2(\epsilon_p + \epsilon_s) \sin \phi - \sigma C_D \cot \phi \quad 2.2.11$$

As mentioned previously, (para. 2.1) the condition of constant total head rise and constant axial velocity through the fan at all stations ensures a free vortex flow. From equation 2.2.8

$$2\Omega r \left\{ \frac{\omega_p r}{u} + \frac{\omega_s r}{u} \right\} = k_{th} u$$

$$\text{i.e.} \quad \omega_p r^2 + \omega_s r^2 = \text{const.} \quad 2.2.12$$



The design equation thus satisfies the condition given in reference 1 for no radial flow.

Another momentum consideration which proves of interest is the question of impulse and reaction blading. With impulse blades, there is no acceleration or retardation of the flow, the sole purpose of the blades being to change the sense of the tangential velocity component relative to the blade. This means there is no static pressure rise through a stage of impulse blading. With 100% reaction blading, the static pressure rise across the blades is equal to the total static pressure rise of the unit i.e. rotor and stators. In this report it is intended that this definition should apply only to the rotor. (A similar definition can be applied to stators e.g. in a fan-straightener unit with an impulse rotor, the static pressure rise across the stators is equal to the pressure rise of the unit and hence the stators have 100% reaction blading).

From equation 2.2.4

$$\Delta p_{th} = \frac{1}{2} \rho u^2 (k_{th} + \epsilon_p^2 - \epsilon_s^2) \quad 2.2.13$$

where  $\Delta p_{th} = \Delta p + k_F \frac{1}{2} \rho u^2$

and is the theoretical static pressure rise across the rotor.

Since it is assumed that the air enters and leaves the unit in an axial direction, the theoretical static pressure rise of the unit is equal to the theoretical total head rise,  $k_{th} \frac{1}{2} \rho u^2$ . Therefore re-arranging equation 2.2.13 we get -

$$\frac{\Delta p_{th} / \frac{1}{2} \rho u^2}{k_{th}} = 1 + \frac{\epsilon_p^2}{k_{th}} - \frac{\epsilon_s^2}{k_{th}} \quad 2.2.14$$

which expresses the degree of reaction in the rotor blading. When only prerotators are used, the rotor has more than 100% reaction whilst with straighteners it has always less than this value. A combination of the two types of stators results in a wide range of possibilities. It should be mentioned that there is another type of prerotator which is used in high speed axial flow compressors. The stators instead of imparting a swirl velocity of opposite sense to the blade velocity, add the swirl in the same sense in order to reduce the local air velocities on the blade; this avoids the formation of shock waves on the blades. The  $\epsilon_p^2 / k_{th}$  term in equation 2.2.14 then becomes negative.

The initial design centres around equations 2.2.8, 2.2.5 and 2.2.11. From the first, the swirl can be

calculated whilst the second and third give the direction of the velocity vector,  $w$ , and the blade loading respectively. There are still, however, a few unknowns one of which is the value of  $k_{th}$ . This depends, amongst other things, on a knowledge of the loss coefficients  $k_F$ ,  $k_P$  and  $k_S$ . However, before considering the stator properties, the fan design, based on  $k_{th}$ , will be studied in detail.

### 2.3 Blade Design Considerations.

The blade must be designed to fulfil the requirements of equation 2.2.11. As the second term is a second order one, it can usually be neglected, thus -

$$C_L \sigma = 2(\epsilon_p + \epsilon_s) \sin \phi \quad 2.3.1$$

When this product of the lift coefficient and solidity is well below unity, no difficulty is experienced in designing the blade. As will be shown later, careful attention must be paid to choosing an appropriate lift coefficient when the product approaches unity. In order to study the problem it is necessary to consider the relative velocity diagrams at the inlet and outlet to the blade.

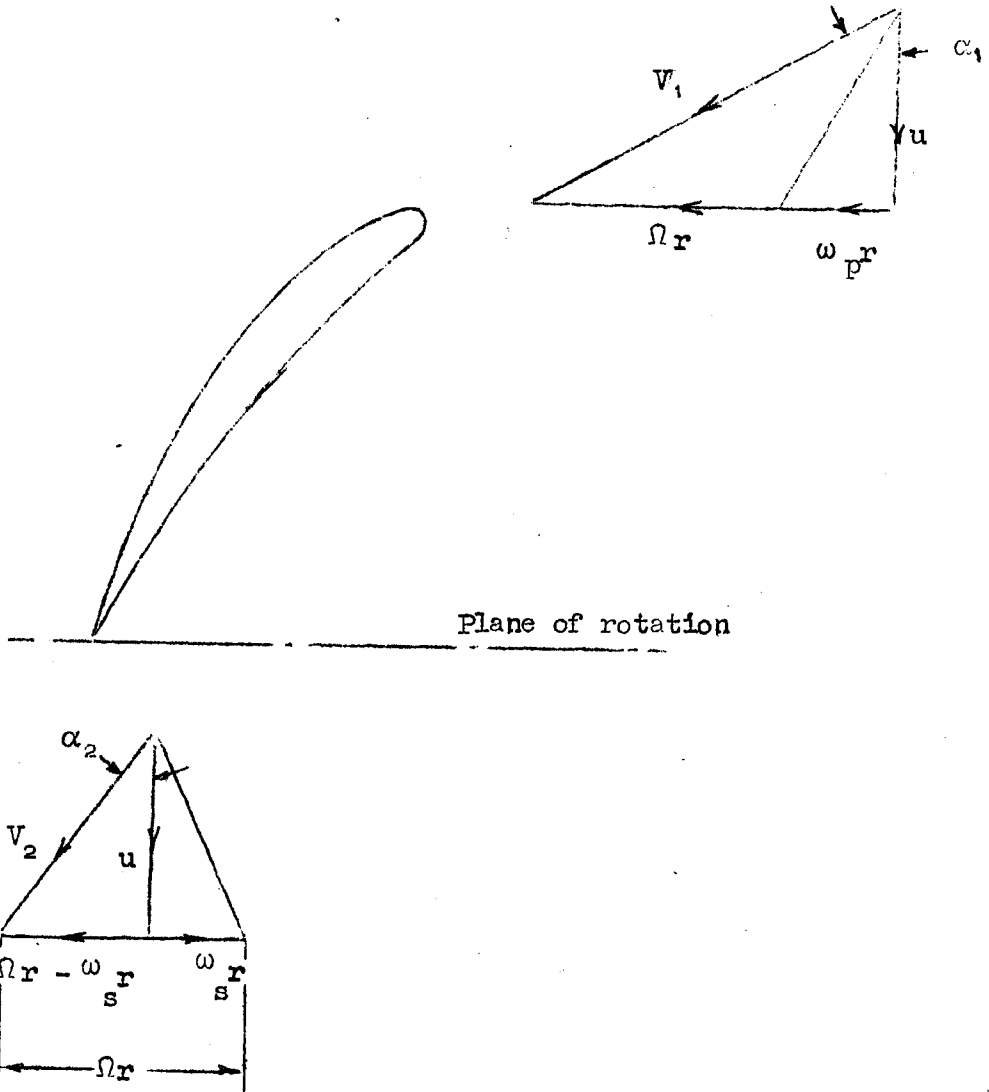


DIAGRAM 4.

The theoretical pressure rise through the fan is given by -

$$\Delta p_{th} = \frac{1}{2} \rho V_1^2 - \frac{1}{2} \rho V_2^2 \quad 2.3.2$$

The optimum lift coefficient has been found from experimental work on cascades of cambered aerofoils

(reference 43) to be

$$C_L^* = 2 \left\{ 1 - \frac{\Delta p_{th}}{\frac{1}{2} \rho V_1^2} \right\}^{1.375} \quad \text{for } \sigma = \frac{2}{3} \text{ to } 2 \quad 2.3.3$$

which occurs when the deflection for a given s/c is approximately 80% of the maximum deflection,  $(\alpha_1 - \alpha_2)_{\max}$ , achieved just prior to the stall.

Substituting  $u/\cos\alpha_1$  and  $u/\cos\alpha_2$  for  $V_1$  and  $V_2$  respectively and eliminating  $\Delta p_{th}$ ,

$$C_L^* = 2 \left\{ \frac{\cos \alpha_1}{\cos \alpha_2} \right\}^{2.75} \quad 2.3.4$$

From the preceding diagram it can be seen that

$$\epsilon_p + \epsilon_s = \tan\alpha_1 - \tan\alpha_2 \quad 2.3.5$$

and from equation 2.2.5

$$\begin{aligned} \cot\phi &= \frac{\Omega r - \frac{1}{2} (\omega_s - \omega_p) r}{u} \\ &= \frac{1}{2} (\tan\alpha_1 + \tan\alpha_2) \end{aligned} \quad 2.3.6$$

Substituting equations 2.3.5 and 2.3.6 in equation 2.3.1

$$C_L = \frac{2}{\sigma} (\tan\alpha_1 - \tan\alpha_2) \sin \cot^{-1} \left\{ \frac{1}{2} (\tan\alpha_1 + \tan\alpha_2) \right\} \quad 2.3.7$$

From equations 2.3.4 and 2.3.7 several graphical relationships can be drawn; three of these are presented in Figs. 1 to 3 and Table I for solidities from 0.6 to 2.0. The abscissa in each case is the outlet angle  $\alpha_2$ . In determining the sign of the angles  $\alpha_1$  and  $\alpha_2$ ,

it is sufficient to accept the cascade theory convention (Ref. 44) that the flow deflection,  $(\alpha_1 - \alpha_2)$ , is always positive. It can be shown that  $\alpha_1$  is always positive for a retarding cascade and  $\alpha_2$  always negative for an accelerating one.

The inlet and outlet angles can also be expressed as follows

$$\left. \begin{aligned} \tan \alpha_1 &= \frac{1 + \varepsilon_p \lambda}{\lambda} \\ \tan \alpha_2 &= \frac{1 - \varepsilon_s \lambda}{\lambda} \end{aligned} \right\} \quad 2.3.8$$

For the type of rotor design considered in this report, the inlet angle will always be positive and provided the product  $\varepsilon_s \lambda$  is less than unity,  $\alpha_2$  will also be positive.

Equation 2.3.4 now becomes -

$$C_L^* = 2 \left\{ \frac{\cos \tan^{-1} \frac{1 + \varepsilon_p \lambda}{\lambda}}{\cos \tan^{-1} \frac{1 - \varepsilon_s \lambda}{\lambda}} \right\}^{2.75} \quad 2.3.9$$

$$\therefore C_L^* = f(\varepsilon_p, \varepsilon_s, \lambda) \quad 2.3.10$$

From equation 2.3.1 and the relation

$$\varphi = \tan^{-1} \frac{\lambda}{1 - \frac{1}{2}(\varepsilon_s - \varepsilon_p)\lambda}$$

$$C_L = \int_2 (\varepsilon_p, \varepsilon_s, \alpha, \lambda) \quad 2.3.11$$

Simple graphical presentations of equations 2.3.10 and 2.3.11 are possible when either  $\varepsilon_p$  or  $\varepsilon_s$  is assumed to be zero. This is not impractical as, in most designs, straighteners and prerotators are seldom used together.

Assuming  $\varepsilon_p$  is zero and hence

$$\tan \alpha_1 = \frac{1}{\lambda}$$

equation 2.3.9 becomes

$$C_L^* = 2 \left\{ \frac{\cos \tan^{-1} \frac{1}{\lambda}}{\cos \tan^{-1} \left( \frac{1 - \varepsilon_s \lambda}{\lambda} \right)} \right\}^{2.75} \quad 2.3.12$$

thus enabling  $C_L^*$  to be plotted against  $\lambda$  for lines of constant  $\varepsilon_s$ . Similarly when  $\varepsilon_s$  is zero

$$\tan \alpha_2 = \frac{1}{\lambda} \quad \text{and}$$

$$C_L^* = 2 \left\{ \frac{\cos \tan^{-1} \left( \frac{1 + \varepsilon_p \lambda}{\lambda} \right)}{\cos \tan^{-1} \frac{1}{\lambda}} \right\}^{2.75} \quad 2.3.13$$

Equations 2.3.12 and 2.3.13 have been plotted in figures 4 and 5 on which the limits of solidity appropriate to the cascade theory have been superimposed. (The lower limit of  $\frac{2}{3}$  mentioned previously is extended for convenience to 0.6 at which the cascade theory should still hold with sufficient accuracy).

It is also possible to obtain two simple graphical solutions of equation 2.3.1. These are presented in Figs. 6 and 7 for  $\epsilon_p$  and  $\epsilon_s$  equal to zero respectively.

Finally by equating 2.3.10 and 2.3.11, the optimum solidity is obtained in terms of  $\epsilon$  and  $\lambda$  (Figs. 8 & 9). Data from which the above figures were constructed are given in Tables 2 to 5.

In the above general considerations, an optimum lift coefficient based on experimental data from cascade aerofoils was introduced. The scope of application was limited by lack of experimental data to a range of solidities from  $\frac{2}{3}$  to 2. The upper limit is, for obvious reasons, a fairly practical one but many low pressure fans require a much lower solidity than  $\frac{2}{3}$ . In contrast, there is no lower limit on the values of solidity which can be used in the isolated aerofoil theory.



### 2.3.1 Choice of Appropriate Design Method.

It can be seen that, due to limited experimental data, one design method cannot cover the entire range of ducted axial flow fans. The problem which arises is fixing a nominal boundary between the isolated aerofoil theory and the cascade theory of design. This is fairly difficult as the information available concerning the multi-plane interference between adjacent blades is not completely satisfactory. Theory, however, seems to indicate that when  $\phi$  is approximately  $40^\circ$  and the solidity less than unity, the interference between adjacent blades is small (Reference 9). For a given solidity, the actual lift coefficient for  $\phi$  greater than  $40^\circ$  is liable to be less than for the isolated aerofoil and vice versa.

In practice however good results have been obtained with the isolated aerofoil theory. Tests on a fan so designed gave complete satisfaction, although the design values of solidity and  $\phi$  exceeded the above at the root section (Reference 45). Any loss of design lift at the blade root may have been countered by an increase in lift toward the tip; some justification for this assumption is found in the systematic deviation of the measured  $c$  from the design curve in going from blade root to blade tip. However, with a much larger boss ratio than

that used, namely 0.5, a nett loss in lift may result from exceeding the theoretical values.

On the basis of existing knowledge the following general rule is suggested. If the product of the lift coefficient and solidity for a given blade element lies above the lines of unit solidity given in Figs. 6 and 7, the cascade theory of design should be employed. Below the lines of  $\sigma = 0.7$ , the isolated aerofoil theory is the appropriate one. Between the lines  $\sigma = 1$  and 0.7 either method may be employed, although in the case of straighteners only, i.e.  $\epsilon_p = 0$ , the cascade method is preferable for values of  $\lambda$  greater than 0.8. In this region  $\phi$  may exceed  $40^\circ$  (Figs. 10 and 11) due to multiplane interference; loss of lift may result as indicated previously. It should be mentioned that the lines of constant solidity on Figs. 6 and 7 are for the optimum lift coefficients of equation 2.3.4.

The preceding recommendations apply to a specific blade element. When the fan as a whole is considered, modifications may be necessary. As an example, the case of a fan with a moderate boss ratio of 0.5 and high loading locally at the root will be considered. The greater portion of the blade can be designed by the free aerofoil theory but special attention has to be paid to the

root. Two alternatives which suggest themselves are

- (i) use the cascade theory near the root and blend the sections so obtained into a similar cambered aerofoil of which the two-dimensional characteristics are known;
- (ii) use the isolated aerofoil theory with suitable modifications at the blade root, such as, increasing the blade incidence to counter a probable drop in the design lift coefficient and use the optimum lift coefficient (equation 2.3.4) or less; this may involve increasing the solidity.

As mentioned in section 1.9, fans designed entirely by the cascade method for free vortex flow tend to be high pressure rise fans with large boss ratios.

The choice of the appropriate design method is not difficult once a little experience has been gained. The actual determination of the blade element sections and their settings will now be indicated. In isolated aerofoil theory, the shape of the blade section is assumed and it is a simple matter to determine the chord and blade setting; the cascade theory includes, as well, the development of the blade section.

## 2.4 Blade Element Design (Isolated Aerofoil Theory).

Provided the value of  $k_{th}$  is known, sufficient data is available to permit the design of a fan rotor employing the isolated aerofoil theory. From the design equations 2.2.8, 2.2.5 and 2.2.11 the direction of the velocity vector relative to the blade and the blade loading are known. If the blade loading does not exceed the recommendations made in the previous section, it is only necessary to have aerofoil data giving the variation of the lift and drag coefficients with incidence to complete the design. The optimum lift/drag ratio is usually attained just after the drag starts to increase appreciably with incidence (see Fig. 12). The design procedure is then to choose a lift coefficient near the optimum incidence and calculate the solidity from equation 2.2.11. From the following diagram the angle of setting relative to the plane of rotation is  $\phi + \alpha$  where  $\alpha$  is the angle of incidence.

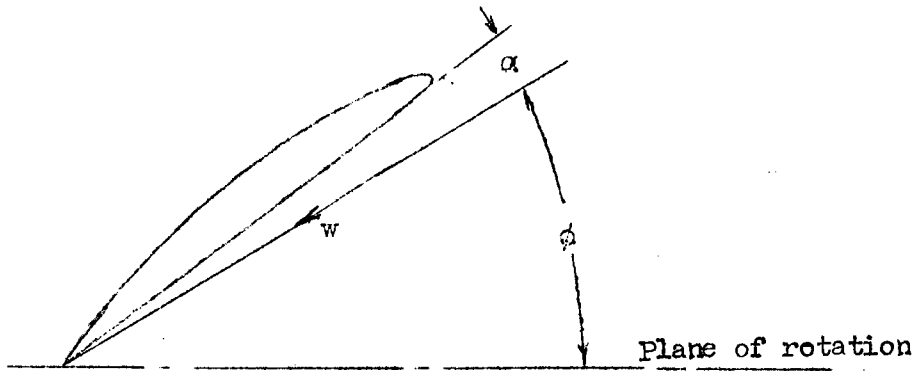


DIAGRAM 5

The detailed design procedure will be summarized in a later section as it not possible at this stage to outline the determination of  $k_{th}$ .

## 2.5 Blade Element Design (Aerofoils in Cascade).

To obtain the aerofoil section, a symmetrical aerofoil is superimposed on a given camber line. Only circular arc type camber will be treated here; this is the more common variety. The following sketch defines the main variables involved in determining the blade shape.

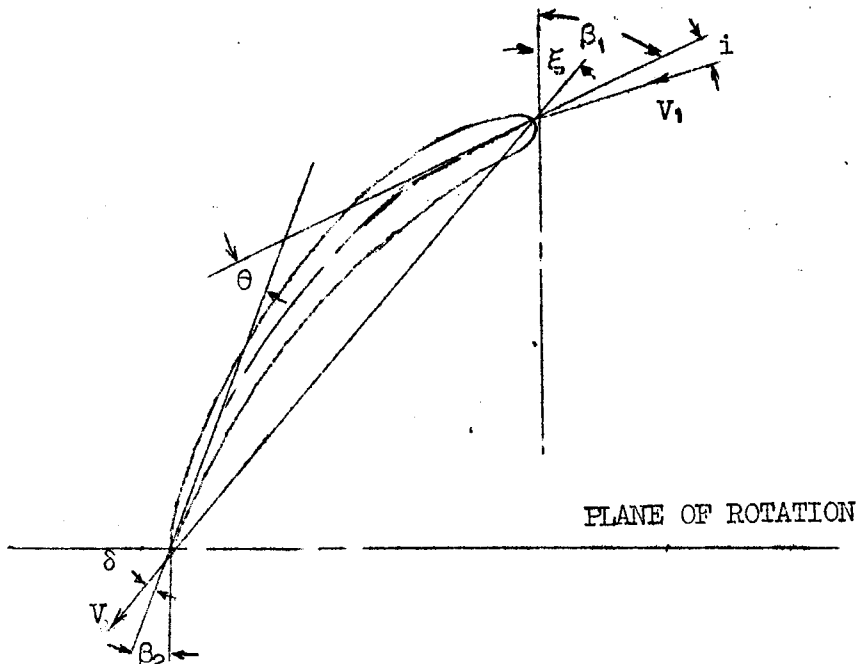


DIAGRAM 6

The tangents at the leading and trailing edges of the blades make angles  $\beta_1$  and  $\beta_2$  respectively with the axial direction; the flow enters and leaves the blade at angles of  $i$  and  $\delta$  to these tangential lines. By joining the leading and trailing edges with a straight line, the stagger,  $\xi$ , is obtained.

An important parameter in developing the blade shape is the camber angle  $\theta$

$$\theta = \beta_1 - \beta_2 = (\alpha_1 - i) - (\alpha_2 - \delta) \quad 2.5.1$$

hence

$$\alpha_2 = \delta + \beta_2 \quad 2.5.2$$

Provided the incidence,  $i$ , remains within the limits  $\pm 5^\circ$ , the outlet angle  $\alpha_2$  is not sensibly altered (Reference 32). For this range of incidence, the angle of deviation,  $\delta$ , is given approximately by Constant's rule (Reference 25), namely:

$$\delta = 0.26\theta \sqrt{s/c} \quad 2.5.3$$

and substituting for  $\delta$

$$\theta = \frac{(\alpha_1 - \alpha_2) - i}{1 - 0.26 \sqrt{s/c}} \quad 2.5.4$$

Finally the stagger,  $\xi$ , is given by

$$\xi = \beta_1 - \frac{\theta}{2} \quad 2.5.5$$

For design, it is usually desirable and convenient to make  $i = 0$ . A further simplification can be made by assuming, as before, that either  $\varepsilon_p$  or  $\varepsilon_s$  is zero.

When  $\varepsilon_p$  is zero, equation 2.5.4 reduces to

$$\theta = \frac{\tan^{-1} \frac{1}{\lambda} - \tan^{-1} \left( \frac{1 - \varepsilon_s \lambda}{\lambda} \right)}{1 - 0.26 \sqrt{S/c}} \quad 2.5.6$$

and hence  $\theta = f(\varepsilon, \lambda)$  as  $\frac{S}{c}$  can be expressed in terms of  $\varepsilon$  and  $\lambda$  (see Figs. 8 and 9) when the optimum value  $C_L^*$  is used.

Similarly when  $\varepsilon_s = 0$

$$\theta = \frac{\tan^{-1} \left( \frac{1 + \varepsilon_p \lambda}{\lambda} \right) - \tan^{-1} \frac{1}{\lambda}}{1 - 0.26 \sqrt{S/c}} \quad 2.5.7$$

Equations 2.5.6 and 2.5.7 have been presented graphically in Figs. 13 or 14, (Tables 6 and 7).

The stagger,  $\xi$ , is now given by

$$\xi = \tan^{-1} \frac{1}{\lambda} - \frac{\theta}{2} \quad 2.5.8$$

when  $\varepsilon_p = 0$

$$\text{and} \quad \xi = \tan^{-1} \left( \frac{1 + \varepsilon_p \lambda}{\lambda} \right) - \frac{\theta}{2} \quad 2.5.9$$

when  $\varepsilon_s = 0$

These relationships are given in Figs. 15 and 16, (Tables 6 and 7).

Two of the geometric properties of the camber,  $\theta$ , can be expressed as follows:-

$$(i) \quad \frac{R_{cur}}{c} = \frac{1}{2 \sin \frac{\theta}{2}} \quad 2.5.10$$

where  $R_{cur}$  is the radius of curvature.

$$(ii) \quad \text{Camber/chord ratio, } \frac{b}{c} = \frac{1 - \cos \frac{\theta}{2}}{2 \sin \frac{\theta}{2}} \quad 2.5.11$$

Equation 2.5.11 can be written approximately as

$$\frac{b}{c} \approx 0.00221 \theta \text{ for the range}$$

$$\theta = 0 \text{ to } 50^\circ \text{ where } \theta \text{ is in degrees.}$$

### 3 STATOR DESIGN

Before dealing with fan performance, it will be advantageous to consider the design of the stators.

#### 3.1 Momentum Considerations.

An analysis of stator design can be carried out in a similar way to that followed in section 2.2 for the fan rotor. For a blade element at radius  $r$  we have the following diagrams, where the effective swirl component is assumed to be the mean of the inlet and outlet swirl.



## Straightener

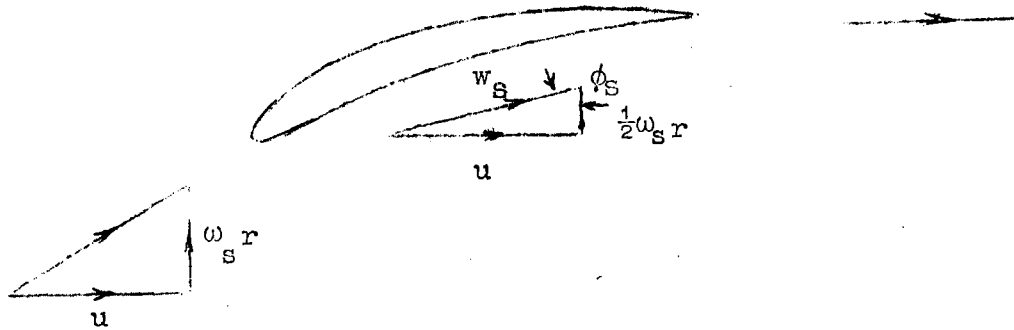


DIAGRAM 7

## Prerotator

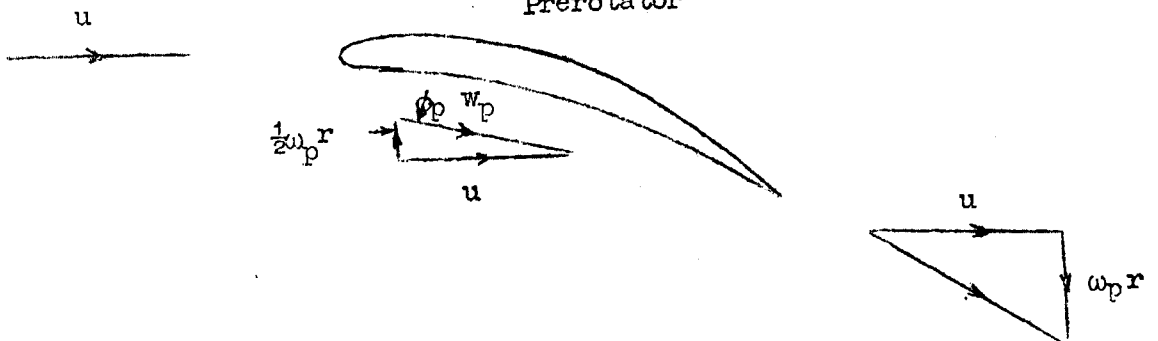


DIAGRAM 8

Expressions similar to that of equation 2.2.9 can be developed for the stators, the relationships being,

$$C_D = \frac{s}{c} k_s \sin^3 \phi_s \text{ for straighteners} \quad 3.1.1$$

and

$$C_D = \frac{s}{c} k_p \sin^3 \phi_p \text{ for prerotators} \quad 3.1.2$$

The lift coefficients can be shown to be

$$C_L = 2 \frac{s}{c} \epsilon_s \sin \phi_s - C_D \frac{\epsilon_s}{2} \text{ for straighteners} \quad 3.1.3$$

and

$$C_L = 2 \frac{s}{c} \epsilon_p \sin \phi_p - C_D \frac{\epsilon_p}{2} \text{ for prerotators} \quad 3.1.4$$

### 3.2 Straightener Design (N.P.L. Type)

When the swirl velocity is small, a simple solution evolved at the N.P.L. is often employed, (Reference 9 ). This consists of using stators with a gap/chord ratio of unity, the stators being so arranged that in a purely axial flow, there is no lift on the stators, i.e. the "no lift" line of the section is parallel with the fan axis. Provided the stators are not stalled, all swirls can be removed with a single stator setting. Although this is only approximately true, it is for all practical purposes an adequate solution, particularly in wind tunnel installations where a symmetrical section such as the N.A.C.A. 0012 is often used. The flow diagram for such a section is given below.

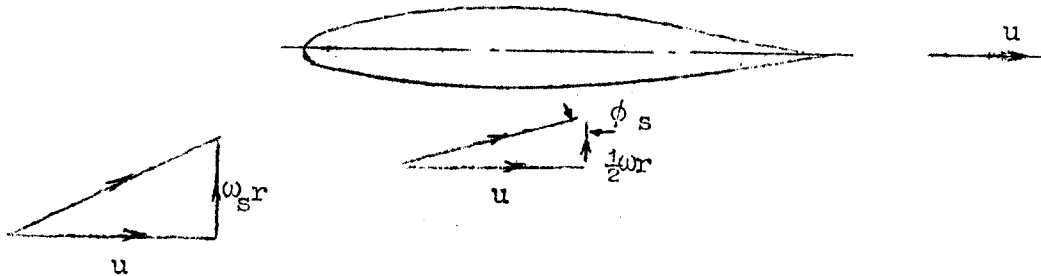


DIAGRAM 9

From the diagram, the angle of incidence is  $(90^\circ - \phi_s)$  where

$$\begin{aligned}\cot \phi_s &= \frac{1}{2} \omega_s r / u \\ &= \epsilon_s / 2\end{aligned}\quad 3.2.1$$

Assuming the two-dimensional N.A.C.A. 0012 aerofoil commences to stall at  $14^\circ$  incidence, we have  $\epsilon_s = 0.5$  as a limiting value. Hence this type of straightener can be considered satisfactory for the design range.

$$\epsilon_s = 0 \text{ to } 0.4 \quad (\text{Ref. 40})$$

Although this method of design can be extended to higher values of  $\epsilon_s$  by using cambered sections, it is not advisable or desirable to do so. The cascade theory is the better approach to this problem.

### 3.3 Straightener Design (Aerofoils in Cascade).

When the value of  $\epsilon_s$  exceeds 0.4 the cascade theory of design is usually resorted to. The design details of the stator blades can be found in a similar fashion to that employed in section 2.5.

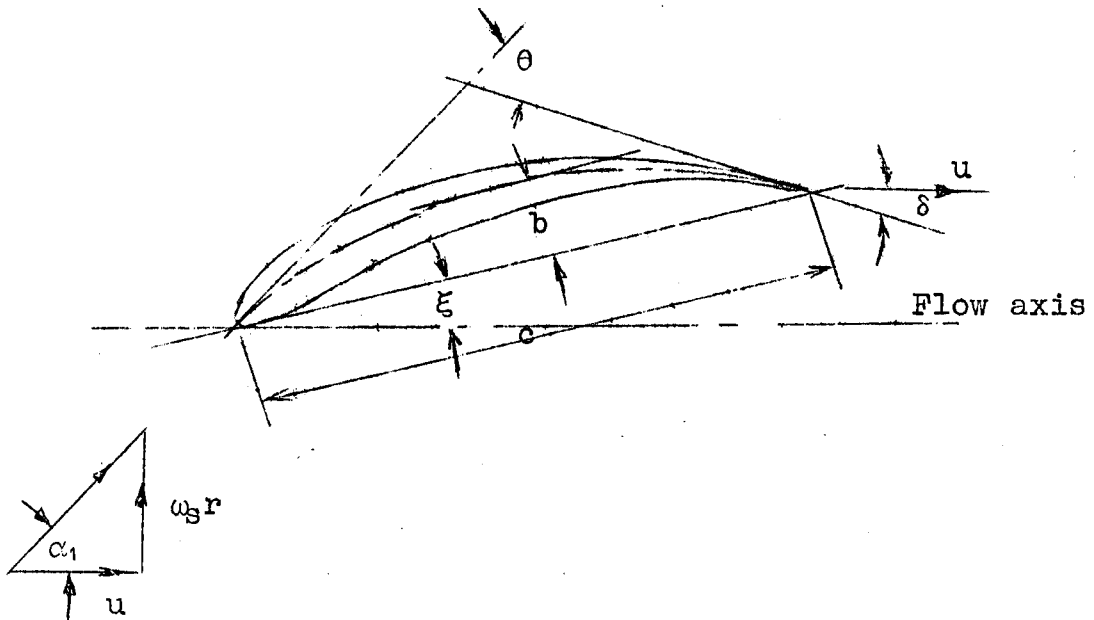


DIAGRAM 10

The above diagram gives the important details of the flow, and the main parameters involved in designing a circular arc camber line aerofoil. It has been assumed that the angle of incidence,  $i$ , is zero as this normally is the case (see Section 2.5). When the stator is not working at the design case, the outlet angle will remain constant provided the incidence,  $i$ , does not exceed the limits,  $-5$  to  $+5$ , mentioned previously.

This is in substantial agreement with the assumed behaviour of the N.P.L. type of straightener.

From diagram 10 we have the following relationships.

$$\theta = \alpha_1 + \delta \quad 3.3.1$$

and substituting for  $\delta$  from equation 2.5.3

$$\theta = \frac{\alpha_1}{1 - 0.26 \sqrt{s/c}} \quad 3.3.2$$

The radius of curvature and percentage camber follow from equations 2.5.10 and 2.5.11.

The stagger angle,  $\xi$ , is given by

$$\xi = \alpha_1 - \frac{\theta}{2} \quad 3.3.3$$

Since  $\tan \alpha_1 = \epsilon_s$  and  $\alpha_2 = 0$ , the optimum  $s/c$  can be determined from Fig. 2 as a function of  $\epsilon_s$ . This relationship is plotted in Fig. 17 and compared with the approximate expression given in reference 32 namely -

$$\tan \alpha_1 - \tan \alpha_2 = \frac{1.55}{1 + 1.5 (s/c)} \quad 3.3.4$$

However, in this report, the one derived from Fig. 2 will be employed. It will be noted from Fig. 2 that, for the field covered in the cascade tests, i.e.  $s/c = 0.5$  to  $1.5$ , the parameter  $\epsilon_s$  varies between  $0.5$  and  $0.94$ . There appears to be no reason why  $\epsilon_s$  cannot

be extended to 1.0 as an upper limit. Beyond this value, however, the gap/chord ratio is for practical purposes, becoming excessively small. For values of  $\epsilon_s$  less than 0.5 it is desirable to maintain  $s/c$  at 1.5 as no experimental data exist for values higher than this; the working  $C_L$  is then less than the optimum. The lift coefficient corresponding to the foregoing values of  $s/c$  can be obtained from the approximate form of equation 3.1.3, namely,

$$C_L = 2 \frac{s}{c} \epsilon_s \sin \phi_s \quad 3.3.5$$

For  $\epsilon_s > 0.5$ , when optimum values of  $C_L$  are employed, the variation of  $C_L^*$  with  $\epsilon_s$  can be approximated by (Fig. 17.)

$$C_L^* = 2.18 - 1.43 \epsilon_s \quad 3.3.6$$

The variables  $\theta$  and  $\xi$  are presented in Fig. 18 as functions of  $s/c$  and  $\epsilon_s$ ; values corresponding to optimum  $\frac{s}{c}$  are indicated. Design data for the condition,  $\frac{s}{c} = 1.5$ , when  $\epsilon_s$  is less than 0.5 and for optimum conditions when  $\epsilon_s = 0.5$  to 1.0 are given in Table 8.

### 3.4 Prerotator design.

A prerotator accelerates the air and produces a pressure drop across the stator. This makes

it less critical in design than the straighteners and as a result lower solidities and higher lift coefficients are possible.

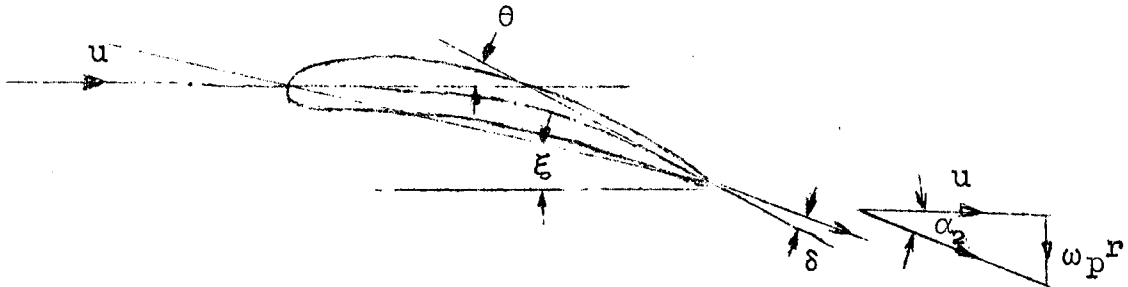


DIAGRAM 11

From the diagram

$$\theta = \alpha_2 + \delta \quad 3.4.1$$

when it is assumed that  $i = 0$ .

For accelerating cascades and optimum design conditions, the angle of deviation,  $\delta$ , is given approximately by Reeman's rule (Ref. 27), namely -

$$\delta = 0.20 \frac{s}{c} \theta \quad (\text{See Refs. 43 and 26 also}) \quad 3.4.2$$

Substituting for  $\delta$  in equation 3.4.1

$$\theta = \frac{\alpha_2}{1 - 0.20 \frac{s}{c}} \quad 3.4.3$$

The radius of curvature and the camber/chord ratio are, as before, given by equations 2.5.10 and 2.5.11 respectively.

The stagger angle,  $\xi$ , is

$$\xi = \frac{\theta}{2} \quad 3.4.4$$

Using the approximate form of equation 3.1.4, namely

$$C_L = 2 \frac{s}{c} \epsilon_p \sin \phi_p \quad 3.4.5$$

the lift coefficient has been plotted in Fig. 19 (Table 9) as a function of  $\epsilon_p$  for various values of  $\frac{s}{c}$ .

It can be shown from section 2.3 that, due to the accelerating flow, the angle  $\alpha_2$  is negative. Hence using Fig. 2 it can be seen that gap/chord ratios in excess of 1.5 appear permissible. However, as no experimental and design data is available for greater values, this will be accepted as the maximum.

For  $\frac{s}{c} = 1.5$  and increasing swirl, the design lift coefficient reaches a value of 2 at  $\epsilon_p = 0.7$  (see Fig. 19). To avoid the possibility of increased secondary flow losses it is desirable to place an arbitrary limit of 2 on  $C_L$ ; this reduces  $\frac{s}{c}$  to 0.84 at  $\epsilon_p = 1.5$  (Figs. 19 & 20). The change in camber angle,  $\theta$ , with  $\frac{s}{c}$  and  $\epsilon_p$  is given in Fig. 20 (Table 10); the limit,  $C_L = 2$ , is indicated. Reference 27 tends to confirm the above recommendations as satisfactory turning and low losses have resulted from similar values of gap/chord ratios.



The above assumes the use of camber lines clothed with aerofoil sections. When sheet metal prerotators are used, i.e. aerofoils with constant thickness, there is a suggestion that overturning may result unless special attention is paid to the design (Ref.49). This is discussed in detail in Part B.

#### 4 ROTOR LOSSES

##### 4.1 General.

In the preceding sections, the design has been based on the pressure coefficient  $k_{th}$  but before this coefficient can be determined, the rotor losses, among others, have to be assessed.

In the following development, the capital letter K will be used for the mean losses and k for those in an elementary annulus. The coefficient k will vary considerably along the blade, particularly near the ends. It is normal practice to ascertain the mean value of the losses and assume these losses are uniformly distributed along the blade. However, it is convenient to develop the momentum relations for an elementary annulus in order to study the effects of the various parameters on efficiency. The non-dimensional losses will be expressed as functions of the two parameters,  $\lambda$  and  $\epsilon$ , wherever possible.

The losses in the rotor have been shown Reference 32, to consist of three components, namely,

- (i) profile drag,
- (ii) secondary drag, and
- (iii) annulus drag.

The first is that associated with the skin friction and form drag of the aerofoil. Secondly, as the blade has a finite length, vortices formed at the extremities introduce secondary losses. Thirdly consideration must be given to the skin friction and other losses on the boss and on the ducting around the fan, as at this point the boundary layer has to overcome a severe pressure rise. Clearance between the blade tip and the ducting must be kept to a minimum in order to curtail losses.

The rotor efficiency is given by

$$\eta_F = \frac{k_{th} - K_F}{k_{th}} \quad 4.1.1$$

where  $K_F = K_{F_P} + K_{F_S} + K_{F_A}$ , the loss coefficients depending on the corresponding drag coefficients, namely,

$$C_D = C_{D_P} + C_{D_S} + C_{D_A}.$$

If we consider component losses it can be shown that

$$\frac{K_{F_P}}{K_F} = \frac{C_{D_P}}{C_D}$$

and so on.

## 4.2 Momentum Considerations.

Before discussing each separate contribution to the drag, the variation of  $k_F$  with  $\lambda$  and  $\epsilon$  will be examined.

$$C_D = \frac{8}{c} k_F \sin^3 \phi \quad \text{or}$$

$$\frac{k_F}{C_D} = \frac{\sigma}{\sin^3 \phi} \quad 4.2.1$$

Multiplying by  $C_L/k_{th}$

$$\gamma \frac{k_F}{k_{th}} = \frac{C_L \sigma}{k_{th} \sin^3 \phi} \quad 4.2.2.$$

where

$$\gamma = \frac{C_L}{C_D}$$

Substituting for  $C_L \sigma$ , (equation 2.2.11), and  $k_{th}$ , (equation 2.2.8),

$$\gamma \frac{k_F}{k_{th}} = \frac{\lambda}{\sin \phi} - \frac{\sigma C_D \cot \phi}{k_{th} \sin^3 \phi}$$

and substituting for  $C_D$  (equation 2.2.9)

$$(\gamma + \cot \phi) \frac{k_F}{k_{th}} = \frac{\lambda}{\sin^2 \phi} \quad 4.2.3.$$

Normally  $\cot \phi$  will be small compared to  $\gamma$  and equation 4.2.3 may be rewritten

$$\gamma \frac{k_F}{k_{th}} = \frac{\lambda}{\sin^2 \phi} \quad 4.2.4$$

Following the procedure of section 2.3 in assuming either  $\epsilon_p$  or  $\epsilon_s$  is zero, equation 4.2.4 has been plotted in Figs. 21 and 22, (see Tables 2 and 3).

When the fan is designed by the cascade theory, the above analysis can be carried a step further. For a given  $\epsilon$  and  $\lambda$  there is an optimum value,  $C_L^*$ , as described in sections 2.3. Rewriting the equation we get,

$$\frac{k_F}{C_D k_{th}} = \frac{\lambda}{\sin^2 \phi C_L^*} \quad 4.2.5$$

This expression has been plotted in Figs. 23 and 24 (see Tables 11 and 12) for  $\epsilon_p = 0$  and  $\epsilon_s = 0$ ; an auxiliary scale has been added for the arbitrary case when  $C_D = 0.02$ .

It should be remembered that these graphs have been constructed by omitting the  $\cot \phi$  term in equation 4.2.3, which for practical purposes is quite acceptable.

Having discussed the drag collectively each component is now treated separately.

#### 4.3 Profile Drag.

The estimation of the loss in efficiency due to profile drag will depend on whether the fan is designed on free aerofoil theory or on cascade principles.

In the first case, the drag coefficient can be ascertained from the aerofoil characteristics once the design lift coefficient has been chosen, (e.g. Fig. 12). From the value of  $C_L/C_{D_P}$  thus obtained, the loss in efficiency is found from equation 4.2.4 or Figs. 21 and 22.

Limited data on the drag of aerofoils in cascade (Ref. 25) indicate that the coefficient (See Fig. 44) varies between 0.014 and 0.018 for  $\frac{s}{c} = 1.5$  and 0.5 respectively at chord Reynolds numbers,  $R_e > 3 \times 10^5$ . For  $R_e < 1 \times 10^5$  it is appropriate to add 0.007 to the above values. These drag coefficients are with respect to the dynamic head at inlet to the blade, namely  $\frac{1}{2}\rho V_1^2$ . When the deflection of the air is small, the inlet velocity,  $V_1$ , is approximately equal to the mean relative velocity,  $w$ . For convenience in comparing the relative merits of alternative designs it will be assumed in subsequent developments that the drag coefficients above are with respect to  $\frac{1}{2}\rho w^2$ . Since the blade thickness normally remains constant as the solidity is increased, it is obvious that there will be a constriction followed by increased diffusion towards the trailing edge. This gives rise to an increase in the drag coefficient with solidity as noted above.

The loss in efficiency due to profile drag is obtained from equation 4.2.5 (Figs. 23, 24). Although the efficiency will vary from root to tip, the variation will be small. Hence a mean value can be used in design calculations.

When the blade has a rough surface, allowance must be made for the increase in profile drag.

#### 4.4 Secondary Drag.

From the discussion of this component given in the introduction it can be concluded that very little is known quantitatively of the losses involved. Howell (Ref. 3) made efforts to correlate experimental data of  $C_{DS}$  with blade aspect ratio and gap/chord ratio as well as with  $C_L^2$ . The best results were obtained from the relation

$$C_{DS} = a C_L^2$$

where "a" is a function of chord Reynolds number only being 0.019 at  $R_e = 1 \times 10^5$  and 0.015 at  $R_e = 5 \times 10^5$  and  $C_L$  is a mean value for the blade. As in the previous subsection,  $C_{DS}$  is with respect to  $\frac{1}{2}\rho V_i^2$ . The value of "a" frequently used is 0.018 (Ref. 25) giving

$$C_{DS} = 0.018 C_L^2$$

4.4.1

Subsequent efforts by Carter (Refs. 34 and 50) using wall boundary layer parameters, in addition to those investigated by Howell, have not proved particularly successful. Hence, until the position is clarified it would be advisable to use an equation of the form given in 4.4.1. For fans with conventional aerofoil sections, the value of 0.018 will be retained as the results obtained appear to be of the right order of magnitude; a modification for sheet metal bladed fans is suggested in Part B. As before,  $C_{Ds}$  will be assumed to be based on  $\frac{1}{2}\rho V^2$  instead of  $\frac{1}{2}\rho V_1^2$ . The resulting loss in efficiency follows from equation 4.2.4,

$$\frac{k_{Fs}}{k_{th}} = \frac{0.018 C_L \lambda}{\sin^2 \phi} \quad 4.4.2$$

where  $C_L$  is the mean design value. When the cascade theory is used and the optimum lift coefficient,  $C_L^*$ , employed, the loss of efficiency can be expressed directly as a function of  $\epsilon$  and  $\lambda$  (Figs. 25 and 26; Tables 11 and 12).

It should be emphasised that the drag coefficient given by equation 4.4.1 is a mean value for the whole blade. Hence it is sufficient to ascertain its value at the mid-span station and assume it uniformly distributed along the span.

#### 4.5 Annulus Drag.

This aspect of fan performance is completely arbitrary. The drag is assumed (Ref. 3 ) to be that associated with the skin friction of the side walls i.e. the boss and the wall swept by the blade tips. Attention has been focussed on these localities because of the severe pressures rises which occur and the subsequent deterioration of the boundary layers. In cascade practice the equivalent drag coefficient (Ref. 3 ) is expressed as

$$C_{D_A} = 0.020 \frac{s}{h} \quad 4.5.1$$

where h is the height (span) of the blade and s the mean gap.

The constant, 0.020, is based on a skin friction coefficient of 0.010; this appears to be much too high, particularly in an adverse pressure gradient where skin friction is greatly reduced (Ref. 51). A more fundamental approach (Ref. 33) attributes the losses to tip effects and endeavours to present a basis for further research.

Portion of the losses associated with tip clearance may be considered to be included in the annulus drag. Howell states (Refs. 3 and 32) that provided the tip clearance is between 1% and 2% of the blade height,



no additional allowance for tip losses is necessary. For every additional 1% increase in clearance there is 3% drop in rotor efficiency. Closely controlled experiments carried out by Ruden (Ref. 11) gave a linear increase in loss as the clearance was increased, the rate being 9% loss for 1% change in the clearance/fan diameter ratio. These figures refer to the peak efficiencies. A limited series of tests (Ref. 1) gave a slightly higher rate of loss. The small tip clearances necessary for high efficiency are usually not difficult to obtain and when this is so the losses may be assumed to be included in secondary and annulus losses.

The effect of wall boundary layer thickness has been investigated by Boxer (Ref. 52). Spoilers were used to thicken the boundary layers on both the inner and outer walls of the annulus. Despite considerable thickening, the fan characteristics were not greatly affected and the maximum drop in peak efficiency was 2.5%.

In conclusion, it can be said that expression 4.5.1 is not suitable for general use in designing fans. As an alternative, it will be assumed that the effect of annulus drag does not vary greatly from fan to fan, and hence the loss coefficient,  $K_{FA}/k_{th}$ , may be taken as

constant and equal to 0.02; this is a fair average value. If the tip clearances are unavoidably large, allowance must be made along the lines suggested above. The same applies when the velocity distribution at inlet differs greatly from the assumed design condition (i.e.  $u = \text{constant}$ ).

#### 4.6 Total Drag.

In addition to the foregoing rotor losses there is a disk drag associated with the rotor surfaces internal to the flow annulus. However, provided the clearances between the rotor boss and the fairings are small and there is no leak through lightening holes and the like, the losses are negligible.

Having assumed the loss in efficiency due to annulus drag to be constant, the total rotor efficiency depends mainly on the ratio  $C_L/(C_{DF} + C_{DS})$ . This ratio has been plotted in Fig. 27 as a function of  $C_L$  and  $C_{DF}$  using  $C_{DS} = 0.018 C_L^2$ . Hence, design values of  $C_L$  near unity appear desirable provided the limitations imposed in the cascade theory permit their use. Making the assumptions that for cascade theory,  $C_{DP} = 0.016$  and optimum design values are used, the loss in efficiency due to these two components can be determined for the two cases, namely  $\epsilon_p$  or  $\epsilon_s$  equal zero (Figs. 28 & 29 ; Tables 11 and 12).

5 STATOR LOSSES.5.1 General.

The losses in the stators are made up of similar components to those outlined for rotors, namely the losses due to

- (i) profile drag,
- (ii) secondary drag, and
- (iii) annulus drag.

Only the essentials will be presented as the treatment is similar to the rotor case.

5.2 Momentum Considerations.

Substituting  $\phi_s$  or  $\phi_p$  for  $\phi$  and  $k_s$  or  $k_p$  for  $k_F$  in the equations of section 4.2, we obtain for straighteners -

$$\left( \gamma + \frac{\epsilon_s}{2} \right) \frac{k_s}{k_{th}} = \frac{\lambda}{\sin^2 \phi_s} \quad 5.2.1$$

where  $\cot \phi_s = \frac{\epsilon_s}{2}$  and  $\gamma$  is the appropriate lift/drag ratio.

or

$$\gamma \frac{k_s}{k_{th}} = \frac{\lambda}{\sin^2 \phi_s} \quad 5.2.2$$

where  $\gamma > \epsilon_s/2$

Similarly for pre-rotators

$$\left( \gamma + \frac{\epsilon_p}{2} \right) \frac{k_p}{k_{th}} = \frac{\lambda}{\sin^2 \phi_p} \quad 5.2.3$$

or

$$\gamma \frac{k_p}{k_{th}} = \frac{\lambda}{\sin^2 \phi_p} \quad 5.2.4$$

The angles  $\phi_s$  and  $\phi_p$  are functions of  $\epsilon_s$  and  $\epsilon_p$  respectively which enable equations 5.2.2 and 5.2.4 to be plotted as in Fig. 30, (Table 13).

With the design recommendations of Section 3 the loss in efficiency can be obtained from  $C_D$ ,  $\lambda$  and  $\epsilon$  only. The appropriate equations are given in the following;

(i) N.P.L. type of straightener.

Since the solidity is unity, equation 5.2.2 reduces to

$$\frac{1}{C_D} \frac{k_s}{k_{th}} = \frac{\lambda}{2 \epsilon_s \sin^3 \phi_s} \quad 5.2.5$$

when the approximate expression for  $C_L$ , namely equation 3.3.5 is used. Equation 5.2.5 has been plotted in Fig.31 (Table 14).

(ii) Straightener; cascade theory.

For the range  $0.5 < \epsilon_s < 1.0$ , the optimum lift coefficient is given by equation 3.3.6 and hence we have -

$$\frac{1}{C_D} \frac{k_s}{k_{th}} = \frac{\lambda}{(2.18 - 1.43 \epsilon_s) \sin^2 \phi_s} \quad 5.2.6$$

If we can assume that for  $\varepsilon_s < 0.5$  the gap/chord ratio is 1.5 the appropriate equation is -

$$\frac{1}{C_D} \frac{k_s}{k_{th}} = \frac{\lambda}{3\varepsilon_s \sin^3 \phi_s} \quad 5.2.7$$

These two expressions have been plotted in Fig. 32 (Table 15).

(iii) Prerotator; cascade theory.

Since the lift coefficient was assumed to be 2 for all values of  $\varepsilon_p$  greater than 0.7 -

$$\frac{1}{C_D} \frac{k_p}{k_{th}} = \frac{\lambda}{2 \sin^2 \phi_p} \quad 5.2.8$$

and for  $\varepsilon_p < 0.7$ ,  $s/c = 1.5$

$$\frac{1}{C_D} \frac{k_p}{k_{th}} = \frac{\lambda}{3\varepsilon_p \sin^3 \phi_p} \quad 5.2.9$$

These equations are plotted in Fig. 33 (Table 16)

### 5.3 Drag Components.

Information on the component drag coefficients for accelerating and decelerating stators (Refs. 27, 32 and 53), is presented in a slightly different form for each type of stator. However, the total drag coefficient is of the same order of magnitude with the secondary drag (Refs. 32 and 53) a function of  $C_L^2$  in each case. In view of the relative unimportance of the precise value of the drag, the drag coefficients recommended in Section 4 will be adopted for both the straighteners and the prerotators.

(i) Profile Drag.

The loss in efficiency can be estimated from equations 5.2.5 to 5.2.9 (Figs. 31 to 33) using the recommendations of Section 4.3.

(ii) Secondary Drag.

Equation 4.4.1 can be used for determining the drag coefficient,  $C_{D_S}$ ; substitution of  $C_{D_S}$  for  $C_D$  in Figs. 31 to 33 will give the loss in efficiency due to secondary drag.

(iii) Annulus Drag.

In prerotators there is a pressure drop and hence the wall boundary layers will be thinned. The pressure rise through the stators will usually be much smaller than that through the rotor; the tip clearance losses can be avoided by proper sealing. Hence it would appear that for both prerotators and straighteners this drag can be neglected when the above conditions apply.

5.4 Total Drag.

The ratio,  $C_L / (C_{D_P} + C_{D_S})$ , (Fig. 27) enables the loss in efficiency to be determined from either equation 5.2.2 or 5.2.4. When the recommendations of sections 3.3 and 3.4 are followed, the efficiency loss is obtained directly as a function of  $\lambda$  and  $\epsilon$  (Figs. 34 and 35).

6 DUCT AND TAIL FAIRING LOSSES

As the boss diameter in normal fan installations is an appreciable proportion of the fan diameter, considerable diffusion occurs along the tail fairing and surrounding duct. The subsequent loss in efficiency can be very high for large boss/fan ratios, particularly when flow separations occur on the fairing.

Diffuser efficiency (Ref. 54) can be expressed as -

$$\eta_D = 1 - \frac{\Delta H_D}{\frac{1}{2} \rho u^2 \left( 1 - \left( \frac{A_1}{A_2} \right)^2 \right)} \quad 6.1$$

where  $\Delta H_D$  is the difference in mean total head between stations at each end of the fairing,  $u$  is the mean axial velocity through the fan and  $A_1$  and  $A_2$  are the areas at the upstream and downstream stations respectively.

A loss coefficient can be defined as

$$K_D = \frac{\Delta H_D}{\frac{1}{2} \rho u^2}$$

and assuming the duct diameter is constant in the region of the fairing,

$$K_D = [1 - \eta_D] [x_o^2 (2 - x_o^2)] \quad 6.2$$

where  $x_o$  is boss dia./fan dia. ratio.

This equation is graphically presented in Figure 36. Tests carried out by the author suggested that the appropriate value of  $\eta_D$  is 0.80, provided there is no flow separation (see Part B); the duct Reynolds number  $\left(\frac{u \cdot 2R}{\nu}\right)$  was approximately  $5 \times 10^5$ . The value assumed in Reference 11 is 0.85 but it is suggested by Ruden that the value is possibly a little high; no experimental determination was carried out. However, these values are lower than the ones associated with ordinary small angle diffusers and this is probably due to the additional "wetted" surface provided by the fairing.

In view of the dearth of experimental data, it is suggested that the diffuser efficiency be taken as 0.80; Fig. 37 presents this component loss in efficiency as a function of  $k_{th}$  and  $x_0$ . It can be inferred from Figs. 36 and 37 that a small boss ratio is an advantage and low diffuser efficiencies resulting from separated flow must be avoided.

Limited tests carried out (Part B) showed that tail fairings based on an equivalent  $8^\circ$  included angle were satisfactory. The equivalent diffuser is considered to have a length  $L$ , equal to the length of the fairing and to open from a duct of diameter,  $2R\sqrt{1 - x_0^2}$  to a duct of diameter,  $2R$ . It then follows that the fineness ratio is -



$$\begin{aligned}
 f &= \frac{L}{2r_0} \\
 &= \frac{1 - \sqrt{1 - x_0^2}}{2x_0 \tan 4^\circ}
 \end{aligned}
 \tag{6.3}$$

This relationship becomes invalid for small boss ratios as the diffusion in the duct can no longer be considered as general and it is more appropriate to treat the fairing as though it were in an infinite stream. From reference 55 it appears that streamlined shapes with a total fineness ratio of 3 are the most efficient. Assuming that a tail fairing constitutes the last 60% of the complete streamline shape,  $f$  is equal to 1.8.

The recommendations for  $f$  which are plotted in Fig. 38 again emphasise the desirability of keeping the boss ratio small in order to avoid long fairings.

The co-ordinates of the streamlined shape used in the tests just mentioned were obtained from Reference 56.

## 7 OVERALL EFFICIENCIES

One of the main considerations in fan design is the achievement of high overall efficiencies. The total head rise required of the fan unit can be expressed as

$$K = \frac{\Delta H}{\frac{1}{2}\rho U_0^2} \tag{7.1}$$

where  $U_0$  is the mean velocity through a duct of radius  $R(x_0 = 0)$ , and  $\Delta H$  is the mean total head loss.

From equation 2.2.3 we have

$$\begin{aligned}
 k_a &= \frac{\Delta h_a}{\frac{1}{2}\rho u^2} \\
 &= k_{th} - k_F - k_P - k_S \text{ or alternatively} \\
 K_a &= K(1 - x_o^2)^2 + K_D \qquad 7.2
 \end{aligned}$$

where mean values are considered.

The rotor efficiency is given by equation 4.1.1 namely -

$$\eta_F = \frac{k_{th} - K_F}{k_{th}}$$

whilst the efficiency of the fan and stators is

$$\eta_a = \frac{K_a}{k_{th}} \qquad 7.3$$

Finally the total efficiency of the unit

$$\left. \begin{aligned}
 \eta_T &= \frac{K_a - K_D}{k_{th}} \\
 &= \frac{K(1 - x_o^2)^2}{k_{th}}
 \end{aligned} \right\} \qquad 7.4$$

When there are no stators, the swirl momentum is not recovered as pressure and hence must be considered a loss. Assuming the flow is purely axial on entry to the fan, equation 2.2.4 reduces to -

$$\Delta p = \frac{1}{2}\rho u^2 (k_{th} - k_F - \epsilon^2) \qquad 7.5$$

which gives the loss in static pressure rise as  $\frac{1}{2}\rho u^2 \epsilon^2$ . Using equation 2.2.8 the subsequent loss in efficiency is then given as

$$\frac{\epsilon^2}{k_{th}} = \frac{1}{2}\epsilon\lambda \quad 7.6$$

and is expressed graphically in figure 39. Although  $\epsilon$  varies from tip to root the mean loss in efficiency can be obtained from the values of  $\epsilon$  and  $\lambda$  at the mid-span station. Figure 39 can also be used to assess the degree of reaction in rotor blading (see equation 2.2.14).

From the design point of view, an exact estimate of the overall efficiency is not essential. Besides providing the means for estimating  $k_{th}$ , the loss coefficients recommended in sections 4 to 6 allow an assessment of the relative merits of alternative designs and indicate ways of improving the design.

For low pressure rise fans, the value of  $C_L/C_{Dp}$  can be assumed to be high and constant over a wide range of design flow coefficients,  $\lambda$ . From Figs. 21 and 22 it follows that there is an optimum  $\lambda$  near unity. It can be seen that  $\epsilon$  has a significant effect on fan efficiency due to the increase or decrease in absolute drag brought about by a change in relative velocity between the fan blades and the air. Using this argument it can be shown

that the fan rotor with prerotators must be less efficient than one with straighteners (See Fig. 21 and 22). The sharp increase in losses for decreasing values of  $\lambda$  is also largely due to the increase in relative velocity for a given work output.

When secondary drag is included, it follows from Fig. 27 that the optimum value of  $C_L$  approaches unity; this agrees with the optimum for profile drag only (See Fig. 12).

In the case of high pressure rise fans designed by the cascade theory, the ratio,  $C_L/C_{DP}$ , is a function of the operating conditions and hence when  $C_{DP}$  is assumed constant in Figs. 23 and 24, no optimum  $\lambda$  is apparent. Inclusion of the secondary drag, however, gives an optimum  $\lambda$  near unity and gives similar variations of efficiency with  $\epsilon$  and  $\lambda$  as observed in the previous case, (Figs. 28 and 29).

There is no significant difference between the total losses in straighteners and prerotators (See Figs. 32 to 35).

## 8 DETAILED DESIGN PROCEDURES

### 8.1 Preliminary Procedure.

From the foregoing developments it is possible to evolve a rational method of design. The first step, and

in many ways the most important, is to choose a flow coefficient  $\Lambda$ , which, for the given flow requirements will give an optimum design. Whilst it is realized that certain features such as fan speed or fan diameter may already be fixed by circumstances outside the designer's control, the following procedure can be readily modified to suit.

- (i) Establish the values of fan and boss diameters and hence  $x_0$ .
- (ii) Express the total head loss in the duct system non-dimensionally as  $K$  (equation 7.1) and determine a tentative value of  $k_{th}$  from equation 7.4 by assuming a value for  $\eta_T$ ; the efficiency,  $\eta_T$ , will normally be in the vicinity of 0.85. (This value of  $k_{th}$  is used to assess the practicability of the design and to obtain a reasonably accurate estimate of the fan unit efficiency)
- (iii) From the mass flow requirement, the axial component of velocity,  $u$ , can be determined.
- (iv) When the fan speed has been fixed the value of  $\Lambda = \frac{u}{\Omega R}$  can be determined together with  $\lambda_o = \frac{u}{\Omega r_o}$  and  $\lambda_m = \frac{u}{\Omega r_m}$  where  $\lambda_m$  is the value at the mid-span station.

It can be readily shown that the most critical part of the design occurs at the blade root as here both  $\lambda$  and  $\epsilon$  reach their maximum values. Hence a study of this station usually suffices in determining whether from a loading point of view the tentative values of  $k_{th}$  and  $\Lambda$  are practical.

(v) Find  $(\epsilon_p + \epsilon_s)_0$  from equation 2.2.8 (Fig. 40) using above values of  $\lambda_0$  and  $k_{th}$ .

(vi) Determine  $\phi_0$  from equation 2.2.5

(vii) Calculate  $(C_L \sigma)_0$  from equation 2.3.1.

When either  $\epsilon_p$  or  $\epsilon_s$  is equal to zero, (vi) can be omitted and  $(C_L \sigma)_0$  obtained directly from Fig. 6 or 7.

It is now possible to determine whether the recommended design limits have been exceeded. The swirl,  $(\epsilon_s)_0$ , should be less than unity and  $(\epsilon_p)_0$  less than 1.5. If  $(C_L \sigma)_0$  is somewhat less than unity, there is no difficulty in providing sufficient blade area to produce the desired total head rise. However, for values approaching or greater than unity the cascade design method may be appropriate. The upper limit of  $\sigma = 2$  must not be exceeded and this can be checked from Fig. 3, the angle  $\alpha_2$  having previously been obtained from equation 2.3.8. When either  $\epsilon_p$  or  $\epsilon_s$  equals zero,

Figs. 8 or 9 will give the required solidity.

In the advent of one of the design limits being exceeded at the root station, it becomes necessary to make fresh initial assumptions in steps (i) and (iv). As a guide in this direction, an increase of  $\lambda$  results in an increase of both  $\epsilon$  and  $C_L \sigma$  and vice versa. It should be remembered however, that for small values of  $\lambda$ , which are conducive to high pressure rises, the overall efficiency tends to be low (section 4) and hence a more satisfactory solution might be a multi-stage fan, each stage being of equal capacity.

The second aspect, that of overall efficiency,  $\eta_T$ , may be approached in the following manner -

(vii) The loss of efficiency in the rotor can be obtained assuming the mean loss is equal to the loss at the mid-span station.

(a) Loss due to profile drag - Obtained from equation 4.2.4 (Figs. 21 and 22) for the isolated aerofoil, where  $\gamma$  is obtained from aerofoil characteristics when suitable tentative values of  $C_L$  and Reynolds number are chosen (See Fig. 12.) When cascade theory is

- indicated, (see Section 2.3.1), equation 4.2.5 (Figs. 23 and 24) is used where  $C_{DP}$  can be given a mean value of 0.016.
- (b) Loss due to secondary drag - Obtained from equation 4.4.2 and in the case of cascade theory from figures 25 and 26.
  - (c) Loss due to annulus drag - Assume 2% loss.
- (viii) In a similar way, the loss of efficiency due to the stators can be determined using the parameters  $\eta_m$  and  $\lambda_m$ .
- (a) Loss due to profile drag - Obtained from the relevant equation (equations 5.2.5 to 5.2.9 - Figs. 31 to 33) by assuming a suitable value for  $C_{DP}$ , say 0.016.
  - (b) Loss due to secondary drag - Obtained from equation 4.4.1, and equations 5.2.5 to 5.2.9 (Fig. 31 to 33).
- (ix) The loss in efficiency due to the tail fairing can be obtained from equation 6.2 (Fig. 36) or when  $\eta_D = 0.80$  from Fig. 37.

By summing the above losses, the overall efficiency of the unit can be obtained namely,

$\eta_T = 1 - (K_F + K_S + K_P + K_D) / \eta_{kth}$ . This efficiency can now be compared with the original assumption for  $\eta_T$  and



provided they agree within 2 or 3%, the calculated figure may be accepted without recourse to a second approximation.

The preliminary design is now complete as the maximum rotor and stator loadings are known, and the overall efficiency has been established. One of the advantages of such a preliminary design is the ease with which a number of alternative designs can be compared.

Whilst working through the preliminary design, the appropriate method of design i.e. isolated or cascade aerofoils, and the desired type of stator will have become obvious. Hence, now that a more exact value of  $\eta_T$  is known,  $k_{th}$  can be recalculated.

## 8.2 Detail Rotor Design (isolated aerofoil theory).

Since  $k_{th}$  is assumed constant along the blade and the design value of  $\Lambda$  is known from the preliminary design, the detail design for a number of blade elements along the span can be commenced; five or six such stations usually suffice.

### (a) Fan with straighteners and prerotators.

- (i) Determine  $\lambda$  for each station ( $\lambda = \frac{\Lambda}{x}$ )
- (ii) Find  $(\varepsilon_p + \varepsilon_s)$  from equation 2.2.8 (Fig. 40)

- (iii) Choose value for  $\epsilon_p$  and arrange spanwise variation so that  $\epsilon_p x$  is a constant (see equation 2.1.1).

The value of  $\epsilon_s$  then follows.

- (iv) Calculate the product,  $C_L \sigma$ , (equation 2.3.1).

- (v) Determine the angle  $\phi$  (equation 2.2.5).

- (vi) Choose either  $C_L$  or  $\sigma$  and calculate the other.

Aspect ratios less than 2 are not recommended due to increasing secondary flow losses. Provided the lift/profile drag ratio is in excess of 40, (see Fig. 12), relatively high efficiencies can be obtained. It is inadvisable to select lift coefficients which exceed the recommendation of equation 2.3.9.

- (vii) From aerofoil characteristics (e.g. Fig. 12) obtain angle of incidence,  $\alpha$ .

- (b) Fan with either straighteners or prerotators.

The design procedure is very similar to the preceding one as it is only necessary to substitute the appropriate values of  $\epsilon_p$  or  $\epsilon_s$ . In the fourth step, Figures 6 and 7 can be employed and in the fifth, figures 10 and 11. The third step is of course omitted. Equation 2.3.9 in the sixth step is presented in Figs. 4 or 5 for  $\epsilon_p$  or  $\epsilon_s$  equal to zero.

Two refinements which may be made to the above design are modifications to the lift coefficient for Reynolds number (see Fig. 12) and for the effect of the second order term in equation 2.2.11, which was neglected in equation 2.3.1. In the first case any of the lift curves (see Fig. 12) may be used for the initial design and when the design is fixed, the appropriate Reynolds number calculated. It is then only necessary to make a small adjustment to  $\alpha$  to ensure the design  $C_L$  is obtained. The approximation used in equation 2.3.1 results in an over-estimation of the required  $C_L$  by an amount,  $C_D \cot \phi$ ; the appropriate correction, therefore, is a small reduction in the angle of incidence,  $\alpha$ .

### 8.3 Detail Rotor Design (aerofoils in cascade).

In general, this method of design has its greatest application when both the pressure rise and boss/fan ratio are large.

#### (a) Fan with straighteners and prerotators.

- (i) Complete the first four steps of section 8.2
- (ii) Calculate  $C_L^*$  from equation 2.3.9
- (iii) Determine  $\sigma$  from the product,  $C_L \sigma$
- (iv) Derive  $\theta$  from equations 2.5.4 and 2.3.8
- (v) Establish  $\xi$  from equation 2.5.5 where  $\beta_1 = \alpha_1$ ,  
i.e.  $i = 0$ .

(vi) Set out aerofoil shape (see Appendix B) on camber line defined by  $\theta$ .

(b) Fan with either straighteners or prerotators.

As in section 8.2, the design procedure only requires minor modifications. Steps two and three may be omitted and the value of  $\sigma$  determined directly from the appropriate figure (Figs. 8 and 9). The angles in steps four and five can then be determined from Figures 13 and 14 and Figures 15 and 16 respectively.

One of the basic aerofoil sections used in cascade theory is given in Reference 32 and reproduced in Appendix B.

There are occasions when, for specific reasons, it is not desirable to use the optimum values of  $C_L$  recommended in Reference 43 (see equation 2.3.9). In such cases the procedure outlined in (a) can be followed except for step two where the desired values of lift coefficient are substituted for the optimum ones. Figures 13 to 16 are not relevant as these are based on  $C_L^*$ .

#### 8.4 Detail Straightener Design.

In the case of the N.P.L. straightener the design method is self evident. An aerofoil section, such as the N.A.C.A. 0012, (see Appendix B) is arranged so that

$s/c$  is unity at each spanwise station and the axis of symmetry is parallel to the fan axis. In order to prevent a resonant beat frequency, the number of vanes should differ from the number of rotor blades and should not have a common multiplier.

When the cascade method is employed we have the following steps for each spanwise station.

- (i) Determine optimum  $s/c$  ratio from figure 17 for required value of  $\epsilon_s$ .
- (ii) Calculate angle  $\theta$  from equation 3.3.2 where  $\tan \alpha_1 = \epsilon_s$  (Fig. 18).
- (iii) Establish stagger angle,  $\xi$ , equation 3.3.3 (Fig. 18).
- (iv) Set out aerofoil shape (see Appendix B) on camber line defined by  $\theta$ .

When the optimum value of  $s/c$  is departed from, step one should be replaced by a solution of equation 3.3.5.

It is assumed in the above design that the angle of incidence,  $i$ , is zero.

#### 8.5 Detail Prerotator Design.

The procedure is very similar to that followed in section 8.4.

- (i) Choose the desired  $s/c$  ratio (suggested values are given in Fig. 20)
- (ii) Calculate  $\theta$  from equation 3.4.3 (Fig. 20) where  $\tan \alpha_2 = \epsilon_p$ .
- (iii) Determine stagger angle,  $\xi$ , (Fig. 20) from equation 3.4.4.
- (iv) Clothe camber line with aerofoil shape.

As before the angle of incidence,  $i$ , is assumed to be zero.

## 9 TORQUE, THRUST AND POWER

From reference 6 we have by definition

$$Q_c = \frac{Q}{\frac{1}{2}\rho u^2 \pi R^3} \quad 9.1$$

where  $Q$  is the shaft torque and  $Q_c$  the torque coefficient.

It is also shown that

$$Q_c = \int_{x_0}^1 4\epsilon x^2 dx = \int_{x_0}^1 4(\epsilon_p + \epsilon_s)x^2 dx \quad 9.2$$

which when we substitute for  $(\epsilon_p + \epsilon_s)$  from equation 2.2.8 gives

$$Q_c = \int_{x_0}^1 2k_{th} \Lambda x dx \quad \text{and when } k_{th} \text{ is constant along the blade,}$$

$$Q_c = k_{th} \Lambda (1 - x_0^2) \quad 9.3$$

The torque can then be calculated from equation 9.1. When  $k_{th}$  is not constant along the blade, the integral must be evaluated.

In a similar way from Reference 6

$$T_c = \frac{T}{\frac{1}{2}\rho u^2 \pi R^2} \quad 9.4$$

where  $T$  is the thrust on the rotor and  $T_c$  the thrust coefficient.

and

$$T_c = \int_{x_0}^1 2x \frac{\Delta p}{\frac{1}{2}\rho u^2} dx \quad 9.5$$

Substituting for  $\Delta p$  (equation 2.2.4) and assuming  $k_{th}$  is constant along the blade,

$$T_c = k_{th} \int_{x_0}^1 2x \left( \eta_F - \frac{\varepsilon_s^2}{k_{th}} + \frac{\varepsilon_p^2}{k_{th}} \right) dx \quad 9.6$$

When  $\varepsilon_s = \varepsilon_p$

$$T_c = k_{th} \eta_F (1 - x_0^2) \quad 9.7$$

and when  $\varepsilon_p$  is zero and using equation 2.2.8

$$\begin{aligned} T_c &= k_{th} \int_{x_0}^1 (2x\eta_F - k_{th} \Delta^2 / 2x) dx \\ &= k_{th} \eta_F (1 - x_0^2) + \frac{1}{2} k_{th}^2 \Delta^2 [\log_e x_0] \quad 9.8 \end{aligned}$$

Similarly when  $\varepsilon_s$  is zero

$$T_c = k_{th} \eta_F (1 - x_0^2) - \frac{1}{2} k_{th}^2 \Delta^2 [\log_e x_0] \quad 9.9$$

The rotor thrust is then obtained from equation 9.4. As before, the integral in equation 9.5 must be evaluated if  $k_{th}$  is not constant.

When the power coefficient is taken to be

$$P_c = \frac{550P}{\frac{1}{2}\rho u^3 \pi R^2} \quad (\text{Ref. 6}) \quad 9.10$$

we have

$$P_c = \frac{Q_c}{\Lambda} \quad (\text{Ref. 6}) \quad 9.11$$

Alternatively, the power can be determined from the torque,  $Q$ .

$$\text{Shaft H.P.} = \frac{2\pi NQ}{33,000} \quad 9.12$$

where  $N = \text{R.P.M.}$

or from,

$$\text{Shaft H.P.} = \frac{\Delta H \times \text{C.F.M.}}{33,000 \times \eta_T} \quad 9.13$$

where  $\Delta H$  is in  $\text{lbs./ft.}^2$

In defining the torque, thrust and power coefficients it is tacitly assumed that  $u$  is the mean axial velocity through the fan; this is in accordance with our initial design assumption.

## 10 ANALYSIS OF GIVEN FAN

The characteristics of fan-stator combinations or contra-rotating fans can be determined by the following simple method. Information on existing methods may be obtained from references 7, 10, 45 to 48



As before, the blade element will be examined first and the application of such data to the fan as a whole will be indicated.

### 10.1 Rotor Analysis.

Using the same conventions for velocity vectors as in section 2.2, the following diagram can be drawn.

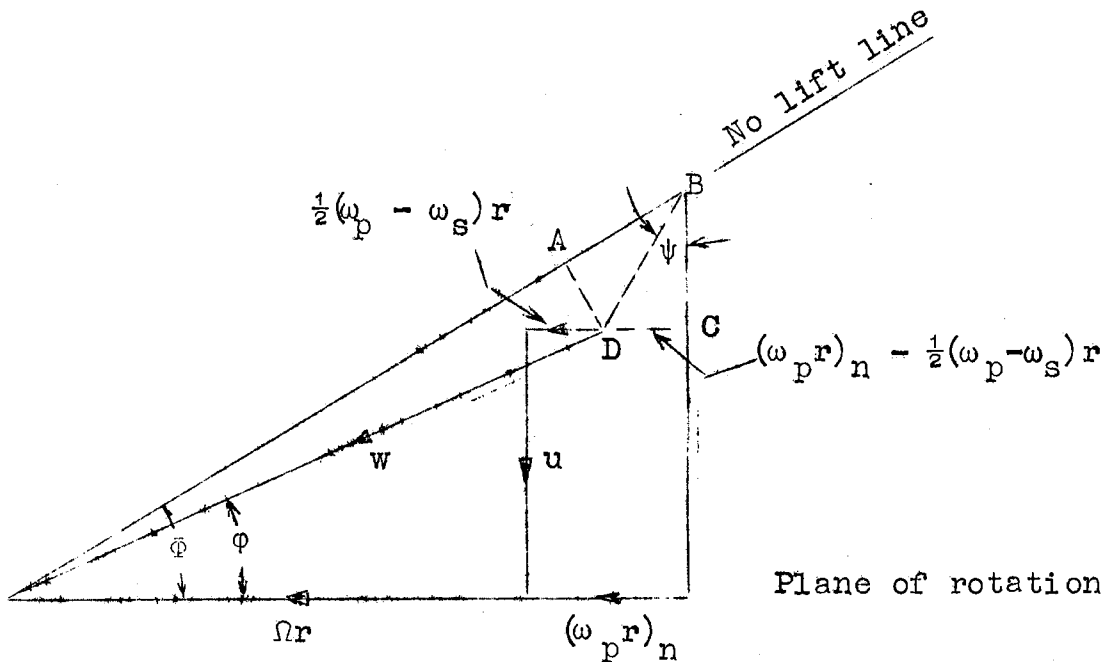


DIAGRAM 12.

This diagram represents a general case in which  $(\omega_p r)_n$  is the prerotation at zero rotor blade lift. When no work is done by the rotor, D will be coincident with B and the mean relative velocity vector will be along the no-lift line of the aerofoil section. From the diagram

$$u = [\Omega r + (\omega_p r)_n] \tan \phi - \left[ \frac{(\omega_p r)_n - \frac{1}{2}(\omega_p - \omega_s) r}{\tan \psi} \right]$$

Dividing by  $\Omega r$

$$\lambda = [1 + \epsilon_p \lambda_n] \tan \phi - \left[ \frac{\epsilon_p \lambda_n - \frac{1}{2}(\epsilon_p - \epsilon_s) \lambda}{\tan \psi} \right] \quad 10.1.1$$

where  $\lambda_n$  is the value of  $\lambda$  at zero lift and is given by

$$\lambda_n = \frac{1}{\cot \phi - \epsilon_p} \quad 10.1.2$$

When it is assumed that the prerotators deflect the flow through a constant angle,  $(\epsilon_p)_n = \epsilon_p$ ; this substitution has been made in equation 10.1.1.

It follows that

$$\epsilon_s = \frac{2 \tan \psi}{\lambda} [(1 + \epsilon_p \lambda_n) \tan \phi - \lambda] - \frac{2 \epsilon_p \lambda_n}{\lambda} + \epsilon_p \quad 10.1.3$$

The angle,  $\psi$ , can now be determined. From equation 2.3.1

$$C_L = 2 \left( \frac{s}{c} \right) (\epsilon_p + \epsilon_s) \sin \phi \quad \text{and for the}$$

working range of the blade element

$$C_L = m \sin (\Phi - \phi) \quad 10.1.4$$

where m for the RAF 6 type of blade section is 5.7.

From the diagram the following relationships are obtained, namely,

$$\begin{aligned} AD &= w \sin(\Phi - \phi) \\ &= BD \cos (\Phi + \psi) \\ &= DC \frac{\cos (\Phi + \psi)}{\sin \psi} \end{aligned}$$

$$\therefore w \sin(\Phi - \phi) = [(\omega_p r)_n - \frac{1}{2}(\omega_p - \omega_s) r] \frac{\cos (\Phi + \psi)}{\sin \psi} \quad 10.1.5$$

Equating equations 2.3.1 and 10.1.4 and substituting for  $\sin (\Phi - \phi)$  from equation 10.1.5 and u for  $w \sin \phi$ ,

$$\tan \psi = \frac{\cos \Phi}{\frac{2(\epsilon_p + \epsilon_s)}{m\sigma} \left[ \frac{1}{\epsilon_p \frac{\lambda_n}{\lambda} - \frac{1}{2} \epsilon_p + \frac{1}{2} \epsilon_s} \right] + \sin \Phi} \quad 10.1.6$$

Substituting this value in equation 10.1.3

$$\epsilon_s = \frac{2 \cos \Phi \left[ \frac{(1 + \epsilon_p \lambda_n)}{\lambda} \tan \Phi - 1 \right]}{\frac{2(\epsilon_p + \epsilon_s)}{m\sigma} \left[ \frac{1}{\epsilon_p \frac{\lambda_n}{\lambda} - \frac{1}{2} \epsilon_p + \frac{1}{2} \epsilon_s} \right] + \sin \Phi} - \frac{2\epsilon_p \lambda_n}{\lambda} + \epsilon_p \quad 10.1.7$$

When  $\varepsilon_p$  is known, the above equation can be solved for  $\varepsilon_s$ , since  $\Phi$ ,  $m$  and  $\sigma$  are known for the fan and the flow requirement is specified by  $\lambda$ .

Considerable simplification results when there is no prerotation, the equations 10.1.3 and 10.1.7 reducing to

$$\varepsilon_s = \frac{2 \tan \psi [\tan \Phi - \lambda]}{\lambda} \quad 10.1.8$$

and

$$\varepsilon_s = \frac{2 \cos \Phi \left[ \frac{\tan \Phi}{\lambda} - 1 \right]}{\frac{4}{m\sigma} + \sin \Phi} \quad 10.1.9$$

where

$$\tan \psi = \frac{\cos \Phi}{\frac{4}{m\sigma} + \sin \Phi} \quad * \quad 10.1.10.$$

From the above, the total head rise,  $k_{th}$ , can be determined using equation 2.2.8, namely,

$$\frac{k_{th} \lambda}{2(\varepsilon_p + \varepsilon_s)} = 1$$

A similar expression to equation 10.1.9 was developed in reference 48 for a fan without prerotators; the angle  $\psi$  was not introduced.

---

\* The author is indebted to Prof. A. Burn of the University of Tasmania for privately communicating this expression in October, 1947.

It will be noted that  $\tan \psi$ , as given by equation 10.1.10, is a constant. This results in a linear change in  $\omega_s r$  with  $u$  (see Diagram 12). It can be shown that a similar variation results when the actual prerotation  $\omega_p r$ , is kept constant over a range of operating conditions.

Assuming  $m = 5.7$ , the variation of  $\tan \psi$  with  $\Phi$  and  $\sigma$ , for  $\omega_p r$  zero or constant, has been plotted in Fig. 41. The greater the angle  $\Phi$  (large  $\lambda$ ), the greater the variation of  $u$  with pressure rise across the fan. Increasing the solidity reduces the variation.

It can be shown from equations 10.1.6 and 10.1.7 that by altering the amount of prerotation, the characteristic of the fan can be greatly modified. This is often done in practice by fitting variable pitch prerotator vanes (e.g. see Reference 57). As defined in Section 2.2 and in Diagram 12,  $\epsilon_p$  is negative and  $\epsilon_s$  is positive when taken in the direction of fan rotation. Although  $\epsilon_s$  is usually positive, it can be negative when the rotor is supplied with positive preswirl from stators or a contra-rotating fan.

The mean theoretical total head rise for the rotor as a whole is given by

$$\frac{2}{1 - x_0^2} \int_{x_0}^1 k_{th} x \, dx \quad 10.1.11$$

When the fan has been designed for free vortex flow, the off-design variation of  $k_{th}$  along the blade is generally small and hence it is satisfactory to take  $k_{th}$  at the mid-span section as representing the mean. At the mid span position of the blade, the losses are mainly due to profile drag and hence the local total head rise will be given by

$$k_{th} \left( 1 - \frac{k_{FP}}{k_{th}} \right) .$$

However, in estimating the mean total head rise for the fan, allowance should be made for the losses at the blade extremities. Following the recommendations of Sections 4 and 5 the mean total head rise is given by

$$k_{th} \left( 1 - \frac{k_F}{k_{th}} \right) \text{ where } k_F = k_{FP} + k_{FS} + k_{FA}$$

In determining  $\frac{k_F}{k_{th}}$ , the lift and drag

coefficients are required. The angle  $\phi$  can be found from equation 2.2.5 and  $C_L$  then follows from equation 2.3.1. Equation 4.2.4 then gives the loss in efficiency when the appropriate drag coefficients are assumed. When  $\epsilon_p = 0$ , use can be made of Figs. 6 and 21.

In order to illustrate the above method, the contra-rotating fans of reference 45 have been analysed. For the front fan, equation 10.1.9 was used to determine  $\epsilon_s$  at a number of flow coefficients and equation 2.2.8 gave  $k_{th}$ . The values of  $\epsilon_s$  then became  $\epsilon_p$  for the rear fan and equation 10.1.7 was solved for the same flow coefficient as before. For each flow coefficient,  $\Lambda$ , the value of  $\lambda_n$  was determined from equation 10.1.2 and equation 10.1.7 was solved by successive approximations. When properly tabulated these present no difficulty. Since the fans were designed for a free vortex flow, only the mid span stations ( $x = 0.75$ ) were analysed. Details of the calculations are given in Appendix A.

In Fig. 42, the calculated values of  $\epsilon_s$  for both fans are compared with the experimental curves. The values of  $k_{th}$ , calculated from the computed values of  $\epsilon_s$ , are superimposed on the experimental curves of  $K_r$ , the mean total head rise across the two rotors (Fig. 43). It is surprising that the values of  $k_{th}$  (no allowance for losses) are almost identical with  $K_r$ . These fans have previously been analysed in Ref. 45 and 46 for the flow coefficients,  $\Lambda = 0.555$  and  $0.65$  respectively. The main results, which are tabulated in Appendix 1, agree reasonably well with the present work and confirm the validity of the assumption,

that the total head rise at the mid span is representative of the fans as a whole. In reference 45 the fans were analysed by a method involving successive approximations of the design equations whilst reference 46 employed a nomogram method; both are more laborious and, it is thought, no more accurate than the present method.

No definite explanation can be offered for the apparent discrepancies, mentioned above, between the theoretical and experimental results of Fig. 43 but slightly incorrect blade angles may have contributed. However, the calculated trend of total head rise with flow coefficient is in good agreement with the experimental.

The preceding treatment can be applied to fans designed by the cascade method provided the lift curve slope and no-lift angle are known. This may not, in general, be the case. It has been found (Ref. 3) that when the ratio of the flow deflection,  $(\alpha_1 - \alpha_2)$ , to the optimum deflection,  $(\alpha_1 - \alpha_2)^*$ , is plotted against  $(i - i^*)/(\alpha_1 - \alpha_2)^*$ , the curve is fairly unique for all cascade results, (Fig. 44). The angle of incidence,  $i^*$ , is the angle at which the optimum deflection, defined by  $0.80 (\alpha_1 - \alpha_2)_{\max}$  is obtained. The value of  $i^*$ , at which these optimum conditions occur, does not appear to be critical, (Ref. 3).



When the recommendations of section 2.3 are used in design,  $(\alpha_1 - \alpha_2)^*$  is known and from Fig. 44 the data necessary for analysis can be obtained. Taking equations 2.3.8, namely,

$$\left. \begin{aligned} \tan \alpha_1 &= \frac{1 + \epsilon_p \lambda}{\lambda} \\ \tan \alpha_2 &= \frac{1 - \epsilon_s \lambda}{\lambda} \end{aligned} \right\} \quad 2.3.8$$

the angle  $\alpha_1$  can be determined for known values of  $\epsilon_p$  and  $\lambda$ ; if the design value of  $\alpha_1$  is called  $\alpha_1^*$ , then  $(1 - i^*)$  equals  $(\alpha_1 - \alpha_1^*)$ . The outlet angle,  $\alpha_2$ , follows from Fig. 44 enabling  $\epsilon_s$  to be calculated for a given value of  $\lambda$ . As before, equation 2.2.8 will then give the theoretical total head rise coefficient.

In section 2.5, it was stated that, provided the angle of incidence remains within the limits  $\pm 5^\circ$ ,  $\alpha_2$  remains sensibly constant. The value of  $\alpha_2$ , however, varies sufficiently to prevent the use of constant  $\alpha_2$  in determining  $\epsilon_s$  and  $k_{th}$ . In Fig. 44, the dotted line gives the relationship resulting from a constant angle. The limitations of this assumption can also be established from the general theory developed from diagram 12. If  $\alpha_2$  is a constant it can be shown from diagram 13 that

$\frac{d(\omega_s r)}{du}$  is a constant when  $\Omega r$  is assumed constant.

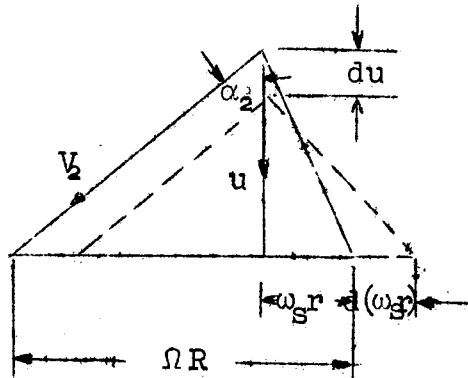


DIAGRAM 13

From equation 10.1.10 it was concluded that  $\frac{d(\omega_s r)}{du}$  is constant for a fan rotor without prerotation but constant  $\alpha_2$  is only one of a number of possibilities which satisfy this condition; the special case is

$\tan \alpha_2 = 2 \tan \psi$  when  $(\omega_p r)$  is zero or constant.

#### 10.1.1 Effect of spanwise variations in axial velocity - free vortex design.

In the theory to date,  $u$  has been assumed constant along the span. Small variations in velocity, however, such as might exist in some installations, can be

readily investigated. The following development is confined to the case  $\epsilon_p = 0$ .

Qualitatively it can be said that when the axial velocity is less than the mean, the blade element works at a greater incidence and hence adds more total head than it normally would and vice versa. When, as in Section 2.2, the theoretical work done is equated to the work put in by the shaft,

$$\Delta h_{th} 2\pi r dr u = 2\pi r dr \rho u \omega_s r \Omega r$$

$$\therefore \Delta h_{th} = \rho \omega_s r \Omega r \quad 10.1.1.1$$

From the above it can readily be shown that

$$\delta k_{th} = \frac{2 \delta \epsilon_s}{\lambda} \quad 10.1.1.2$$

where  $\delta k_{th}$  and  $\delta \epsilon_s$  are the small changes in these coefficients brought about by a change of  $\delta u$  from the mean velocity  $u$ . The coefficients  $\delta k_{th}$ ,  $\delta \epsilon_s$  and  $\lambda$  are with respect to the mean velocity.

$$\text{Now } \frac{\delta (\omega_s r)}{\delta u} = -2 \tan \psi \quad (\text{see diagram 12})$$

$$\text{hence } \delta \epsilon_s = - \frac{\delta u}{u} 2 \tan \psi$$

$$\therefore \delta k_{th} = -4 \frac{\delta u}{u} \cdot \frac{\tan \psi}{\lambda} \quad 10.1.1.3$$

When it is assumed that the static pressure upstream of a fan is constant on a given cross sectional plane, the

deficiency or excess of total head with respect to the mean is given by

$$\frac{1}{2}\rho(u + \delta u)^2 - \frac{1}{2}\rho u^2$$

or non-dimensionally

$$\delta k' = 2 \frac{\delta u}{u} + \left( \frac{\delta u}{u} \right)^2$$

$$\approx 2 \frac{\delta u}{u} \text{ when } \frac{\delta u}{u} \text{ is small} \quad 10.1.1.4$$

On comparing equations 10.1.1.3 and 10.1.1.4,  $\delta k_{th}$  equals  $\delta k'$  when  $2 \tan \psi = \lambda$  which is a distinct possibility. Even when this condition does not hold, it can be seen that the rotor tends to even out the initial total head variations. Provided the variations are not too great, a fan designed with a constant mean inlet axial velocity does fulfil the design requirements. Although not proven here, it can be said that a fan with designed prerotation will behave in a similar way.

The results of references 52 and 33 are of interest in connection with the above. In the first, the wall boundary layers were greatly thickened by means of spoilers on both the nose fairing and the duct walls. Both the above references recorded a thinning of the boundary layers on passing through the fan rotor. In

Reference 52, the losses in pressure rise and efficiency were not very great. Although the fan greatly re-energizes the boundary layer, a belief is expressed in Reference 33 that very little of this is useful due to tip and secondary losses absorbing a large proportion.

It may be concluded therefore that fans designed for a free vortex flow tend to even out total head variations except very close to the extremities of the blades where the additional work done on the slow moving air is lost in friction and secondary flow. Hence the design assumption of constant  $u$  along the blade does prove, in practice, to be very satisfactory. Fans designed with either increased or decreased incidence at the root and tip have not been very successful in improving fan performance.

## 10.2 Straightener Analysis.

When the N.P.L. type of straightener is used, slipstream rotations approaching  $\epsilon_s = 0.5$  can be removed. Normally, the critical station is at the root and since  $\epsilon$  is always greater than the computed value owing to the secondary flows, values of the calculated  $\epsilon_s$  much in excess of 0.4 will probably give local stator stalling.

As stated in Section 3.3, the cambered type of straightener will maintain a constant outlet angle provided the angle of incidence,  $i$ , does not exceed  $\pm 5^\circ$ . When  $\epsilon_s$  is less than the design and  $i$  less than  $-5^\circ$ , the air will tend to be over-turned. With increasing  $\epsilon_s$ , the straighteners may stall if  $(\alpha_1 - \alpha_2)$  for a given  $\frac{s}{c}$  exceeds the optimum design value by 25%, (See Fig. 44); when the flow leaves the stator axially,  $\alpha_2$  is zero.

Making use of equation 3.3.5, Fig. 27 and equation 5.2.2 the loss in efficiency can be estimated.

### 10.3 Prerotator Analysis

Prerotators will always work at the design condition unless there is a change in pitch or a non-design swirl upstream. As before, when  $i$  has the limit  $\pm 5^\circ$ , the outlet angle is sensibly constant and can be estimated from equation 3.4.2 (See Diagram 11). The loss in efficiency can be calculated in a similar fashion to that for the straighteners above.

### 10.4 Power Requirements.

From the foregoing analysis which gives the mean value of  $k_{th}$  (equation 10.1.11), the power can be estimated from equation 9.13, namely

$$\text{Shaft H.P.} = \frac{(k_{th} \frac{1}{2} \rho u^2) \times \text{C.F.M.}}{33000} \quad 10.4.1$$

$$\text{where } k_{th} \frac{1}{2} \rho u^2 = \Delta H / \eta_T$$

APPENDIX AANALYTICAL DETERMINATION OF CHARACTERISTIC  
CURVE OF CONTRA-ROTATING FANS (REF. 45)FRONT FAN

Equations:-

$$\tan \psi = \frac{\cos \Phi}{\frac{4}{m\sigma} + \sin \Phi} \quad 10.1.10$$

$$\varepsilon_s = \frac{2 \tan \psi}{\lambda} [\tan \Phi - \lambda] \quad 10.1.8$$

$$k_{th} = \frac{2 \varepsilon_s}{\lambda} \quad 2.2.8$$

Data:- For  $x = 0.75$ ;  $(\phi + \alpha) = 41.5$ ,  $\frac{N_c}{\pi R} = 0.95$ , RAF6E section, giving  $\Phi = 46.0^\circ$ ,  $m = 5.7$  and  $\sigma = 0.633$   
 $\therefore \tan \psi = 0.381$

	$\Lambda = 0.45$	$\Lambda = 0.50$	$\Lambda = 0.55$	$\Lambda = 0.60$	$\Lambda = 0.65$	$\Lambda = 0.70$
$\lambda$	0.600	0.666	0.733	0.800	0.866	0.933
$\tan \Phi - \lambda$	0.436	0.369	0.302	0.236	0.169	0.102
$2 \tan \psi / \lambda$	1.270	1.145	1.040	0.953	0.88	0.817
$\varepsilon_s$	0.553	0.423	0.314	0.225	0.149	0.083
$k_{th}$	1.84	1.270	0.856	0.563	0.344	0.178
Ref. 45	$\Lambda = 0.555, x = 0.75 :- \varepsilon_s = 0.316, k_{th} \left(1 - \frac{k_{FP}}{k_{th}}\right) = 0.827$					
Ref. 46	$\Lambda = 0.65, x = 0.75 :- \varepsilon_s = 0.158, k_{th} \left(1 - \frac{k_{FP}}{k_{th}}\right) = 0.340$					

REAR FAN

Equations:-

$$\epsilon_s = \frac{2 \cos \Phi \left[ \frac{(1 + \epsilon_p \lambda_n)}{\lambda} \tan \Phi - 1 \right]}{\frac{2(\epsilon_p + \epsilon_s)}{m\sigma} \left[ \frac{1}{\epsilon_p \frac{\lambda_n}{\lambda} - \frac{1}{2}\epsilon_p + \frac{1}{2}\epsilon_s} \right] + \sin \Phi} - \frac{2\epsilon_p \lambda_n}{\lambda} + \epsilon_p \quad 10.1.7$$

$$\lambda_n = \frac{1}{\cot \Phi - \epsilon_p} \quad 10.1.2$$

$$k_{th} = \frac{2(\epsilon_p + \epsilon_s)}{\lambda} \quad 2.2.8$$

Equation 10.1.7 can be written for a given  $\Lambda$  as

$$\epsilon_s = \frac{A}{B(\epsilon_p + \epsilon_s) \left[ \frac{1}{C + \frac{1}{2}\epsilon_s} \right] + \sin \Phi} - D + \epsilon_p$$

Data:- For  $x = 0.75$ ;  $(\phi + \alpha) = 37.2^\circ$ ,  $\frac{N_c}{\pi R} = 0.722$ , RAF6E section,

giving  $\Phi = 41.7^\circ$ ,  $m = 5.7$ ,  $\sigma = 0.481$ ,  $\epsilon_p = \epsilon_s$  of front fan,  $\sin \Phi = 0.665$   $\cos \Phi = 0.747$  and  $\tan \Phi = 0.891$ ,



	$\Lambda = 0.45$	$\Lambda = 0.50$	$\Lambda = 0.55$	$\Lambda = 0.60$	$\Lambda = 0.65$	$\Lambda = 0.70$
$\Lambda$	0.600	0.666	0.733	0.800	0.866	0.933
$\epsilon_p$	0.553	0.423	0.314	0.225	0.149	0.083
$\Lambda_n$	1.759	1.431	1.238	1.115	1.028	0.963
A	2.88	1.711	1.028	0.590	0.281	0.046
B	0.729	0.729	0.729	0.729	0.729	0.729
C	1.344	0.698	0.373	0.201	0.102	0.044
D	3.242	1.819	1.060	0.628	0.353	0.171
$\epsilon_s$	0.134	0.079	0.035	-0.005	-0.035	-0.064
$\epsilon_p + \epsilon_s$	0.687	0.502	0.349	0.220	0.114	0.019
$k_{th}$	2.29	1.51	0.953	0.550	0.263	0.041
Ref.45	$\Lambda = 0.555, x = 0.75:- \epsilon_s = 0.038, k_{th}\left(1 - \frac{k_{FP}}{k_{th}}\right) = 0.929$					
Ref.46	$\Lambda = 0.65, x = 0.75:- \epsilon_s = -0.028, k_{th}\left(1 - \frac{k_{FP}}{k_{th}}\right) = 0.280$					

## BOTH FANS

	$\Lambda = 0.45$	$\Lambda = 0.50$	$\Lambda = 0.55$	$\Lambda = 0.60$	$\Lambda = 0.65$	$\Lambda = 0.70$
$k_{th}$	4.13	2.78	1.81	1.11	0.606	0.219
Ref.45	$\Lambda = 0.555:- k_{th}\left(1 - \frac{k_{FP}}{k_{th}}\right) = 1.74^* \text{ (Exp. } K_r = 1.81)$					
Ref.46	$\Lambda = 0.65:- k_{th}\left(1 - \frac{k_{FP}}{k_{th}}\right) = 0.34 + 0.28 = 0.62^* \text{ (Exp. } K_r = 0.60)$					

\* These are mean values obtained by integrating the total head rise along the blade.

APPENDIX BAEROFOIL SECTION CO-ORDINATES

RAF 6E            Suitable for isolated aerofoil theory

C4                Base aerofoil for clothing camber line - cascade theo

NACA0012        Suitable for N.P.L. type straighteners

Distance from L.E.	Distance from Chord Line.		
	RAF 6E (Ref.6)	C4(Ref.32) Symmetrical	NACA0012 (Ref.58) Symmetrical
0	1.15	0	0
1.25	3.19	1.65	1.89
2.5	4.42	2.27	2.62
5.0	6.10	3.08	3.56
7.5	7.24	3.62	4.20
10	8.09	4.02	4.68
15	9.28	4.55	5.35
20	9.90	4.83	5.74
30	10.30	5.00	6.00
40	10.22	4.89	5.80
50	9.80	4.57	5.29
60	8.98	4.05	4.56
70	7.70	3.37	3.66
80	5.91	2.54	2.62
90	3.79	1.60	1.45
95	2.58	1.06	0.81
100	0.76	0	0.13
L.E. radius	1.15	1.2	1.58
T.E. radius	0.76	0.60	
Chord line	Flat under- surface of aerofoil	Axis of symmetry	Axis of symmetry

All distances given in percentage of chord distance.  
 (NOTE:- For details of CLARK Y section see Ref. 5.)

TABLE I  
OPTIMUM DESIGN VALUES FROM CASCADE THEORY

$\alpha$	$\alpha_2 = 70^\circ$			$\alpha_2 = 60^\circ$			$\alpha_2 = 50^\circ$			$\alpha_2 = 40^\circ$			$\alpha_2 = 30^\circ$			$\alpha_2 = 20^\circ$		
	$C_L^*$	$\xi$	$C_L \phi$	$C_L^*$	$\xi$	$C_L \phi$	$C_L^*$	$\xi$	$C_L \phi$	$C_L^*$	$\xi$	$C_L \phi$	$C_L^*$	$\xi$	$C_L \phi$	$C_L^*$	$\xi$	$C_L \phi$
0.6	0.950	0.960	0.570	0.970	0.670	0.582	1.020	0.545	0.612	1.061	0.464	0.637	1.125	0.434	0.675	1.230	0.428	0.738
0.7	0.885	1.062	0.620	0.907	0.738	0.635	0.952	0.595	0.667	0.995	0.515	0.696	1.059	0.478	0.741	1.148	0.470	0.804
0.8	0.830	1.153	0.664	0.855	0.803	0.684	0.900	0.647	0.720	0.937	0.561	0.750	1.000	0.521	0.800	1.085	0.511	0.868
0.9	0.782	1.235	0.704	0.807	0.864	0.726	0.848	0.695	0.763	0.885	0.604	0.796	0.945	0.562	0.850	1.030	0.550	0.927
1.0	0.740	1.318	0.740	0.764	0.922	0.764	0.800	0.740	0.800	0.840	0.645	0.840	0.897	0.600	0.897	0.980	0.587	0.980
1.1	0.705	1.395	0.775	0.727	0.978	0.800	0.760	0.785	0.836	0.800	0.681	0.880	0.856	0.634	0.942	0.935	0.622	1.029
1.2	0.674	1.472	0.809	0.695	1.030	0.834	0.724	0.825	0.869	0.764	0.717	0.917	0.820	0.667	0.983	0.893	0.656	1.071
1.3	0.648	1.541	0.842	0.667	1.077	0.866	0.694	0.862	0.901	0.732	0.750	0.950	0.786	0.696	1.021	0.857	0.683	1.112
1.4	0.623	1.610	0.872	0.642	1.124	0.898	0.668	0.900	0.935	0.704	0.782	0.985	0.757	0.726	1.060	0.825	0.715	1.154
1.5	0.600	1.675	0.900	0.618	1.166	0.927	0.644	0.935	0.966	0.678	0.813	1.019	0.730	0.754	1.095	0.797	0.741	1.196
1.6	0.578	1.735	0.925	0.596	1.210	0.954	0.620	0.969	0.992	0.655	0.844	1.048	0.703	0.781	1.125	0.770	0.770	1.232
1.7	0.558	1.793	0.948	0.577	1.250	0.981	0.600	1.00	1.020	0.633	0.872	1.076	0.680	0.808	1.155	0.747	0.796	1.270
1.8	0.540	1.850	0.972	0.557	1.290	1.002	0.580	1.032	1.042	0.612	0.900	1.101	0.657	0.832	1.183	0.722	0.820	1.300
1.9	0.523	1.905	0.994	0.540	1.325	1.026	0.560	1.061	1.063	0.595	0.925	1.130	0.636	0.855	1.209	0.700	0.843	1.330
2.0	0.506	1.960	1.012	0.522	1.365	1.044	0.541	1.090	1.082	0.578	0.951	1.156	0.618	0.876	1.236	0.677	0.865	1.354

$\alpha$	$\alpha_2 = 10^\circ$			$\alpha_2 = 0^\circ$			$\alpha_2 = -10^\circ$			$\alpha_2 = -20^\circ$			$\alpha_2 = -30^\circ$			$\alpha_2 = -40^\circ$		
	$C_L^*$	$\xi$	$C_L \phi$	$C_L^*$	$\xi$	$C_L \phi$	$C_L^*$	$\xi$	$C_L \phi$	$C_L^*$	$\xi$	$C_L \phi$	$C_L^*$	$\xi$	$C_L \phi$	$C_L^*$	$\xi$	$C_L \phi$
0.6	1.350	0.438	0.810	1.538	0.470	0.922	1.780	0.534	1.068	2.152	0.650	1.290						
0.7	1.270	0.463	0.869	1.440	0.520	1.009	1.672	0.593	1.170	2.030	0.711	1.420						
0.8	1.203	0.525	0.963	1.362	0.567	1.090	1.590	0.644	1.272	1.922	0.771	1.539	2.420	0.971	1.936			
0.9	1.142	0.586	1.029	1.294	0.610	1.165	1.511	0.690	1.360	1.827	0.823	1.643	2.284	1.030	2.061			
1.0	1.086	0.603	1.086	1.231	0.650	1.231	1.440	0.733	1.440	1.738	0.871	1.738	2.168	1.085	2.168			
1.1	1.036	0.637	1.139	1.177	0.685	1.293	1.372	0.772	1.510	1.655	0.915	1.820	2.055	1.135	2.260			
1.2	0.993	0.669	1.192	1.130	0.718	1.357	1.310	0.807	1.571	1.580	0.953	1.897	1.956	1.175	2.345	2.490	1.580	2.990
1.3	0.953	0.700	1.239	1.083	0.750	1.409	1.256	0.842	1.631	1.510	0.988	1.961	1.880	1.212	2.415	2.380	1.548	3.090
1.4	0.915	0.730	1.281	1.040	0.780	1.455	1.204	0.875	1.687	1.445	1.021	2.022	1.775	1.248	2.464	2.267	1.585	3.170
1.5	0.882	0.756	1.323	1.000	0.810	1.500	1.160	0.905	1.740	1.387	1.052	2.080	1.700	1.280	2.550	2.163	1.620	3.250
1.6	0.850	0.781	1.360	0.966	0.836	1.547	1.119	0.933	1.790	1.333	1.083	2.135	1.632	1.312	2.610	2.065	1.653	3.310
1.7	0.822	0.808	1.397	0.933	0.861	1.586	1.080	0.962	1.836	1.284	1.112	2.184	1.572	1.340	2.675	1.979	1.683	3.360
1.8	0.796	0.832	1.433	0.902	0.885	1.624	1.043	0.990	1.880	1.240	1.141	2.232	1.515	1.370	2.726	1.900	1.711	3.420
1.9	0.771	0.855	1.465	0.872	0.910	1.658	1.010	1.015	1.919	1.197	1.170	2.274	1.460	1.398	2.774	1.830	1.740	3.480
2.0	0.750	0.876	1.500	0.844	0.933	1.688	0.980	1.039	1.960	1.160	1.196	2.320	1.405	1.422	2.810	1.770	1.769	3.540

TABLE 2

DESIGN DATA FROM MOMENTUM CONSIDERATIONS.  $\epsilon p = 0$ 

	$\epsilon_s$	$\alpha_1^*$	$\alpha_2^*$	$\alpha_1^* \alpha_2^*$	$\phi^*$	$C_{LO}$	$h_{LH}$	$\delta_{LH}^*$
$\lambda = 0.2$	0.1		78.5	0.2	11.4	0.0396	1.0	5.12
	0.2		78.2	0.5	11.5	0.0600	2.0	5.00
	0.3		78.0	0.7	11.7	0.121	3.0	4.90
	0.4		77.7	1.0	11.8	0.183	4.0	4.62
	0.5	78.7	77.5	1.2	11.9	0.206	5.0	4.73
	0.6		77.2	1.5	12.0	0.250	6.0	4.62
	0.7		77.0	1.7	12.1	0.284	7.0	4.53
	0.8		76.6	2.1	12.3	0.340	8.0	4.43
	0.9		76.3	2.4	12.4	0.367	9.0	4.35
	1.0		76.0	2.7	12.5	0.434	10.0	4.26
$\lambda = 0.3$	0.1		72.8	0.5	17.0	0.0583	0.667	3.52
	0.2		72.3	1.0	17.2	0.118	1.333	3.45
	0.3		71.8	1.5	17.4	0.180	2.000	3.34
	0.4		71.2	2.1	17.7	0.243	2.667	3.25
	0.5	73.3	70.6	2.7	18.0	0.309	3.333	3.14
	0.6		69.9	3.4	18.3	0.376	4.000	3.06
	0.7		69.2	4.1	18.5	0.444	4.667	2.98
	0.8		68.5	4.8	18.8	0.518	5.333	2.88
	0.9		67.7	5.6	19.1	0.589	6.000	2.79
	1.0		66.8	6.5	19.5	0.667	6.667	2.71
$\lambda = 0.4$	0.1		67.4	0.8	22.2	0.0756	0.5	2.62
	0.2		66.5	1.7	22.8	0.154	1.0	2.70
	0.3		65.5	2.7	23.1	0.235	1.5	2.61
	0.4		64.5	3.7	23.5	0.319	2.0	2.51
	0.5	66.2	63.4	4.8	24.0	0.406	2.5	2.42
	0.6		62.3	5.9	24.5	0.497	3.0	2.34
	0.7		61.0	7.2	25.0	0.591	3.5	2.25
	0.8		59.5	8.7	25.5	0.688	4.0	2.16
	0.9		58.0	10.2	26.0	0.789	4.5	2.08
	1.0		56.3	11.9	26.6	0.894	5.0	2.00
$\lambda = 0.5$	0.1		62.2	1.3	27.2	0.091	0.4	2.40
	0.2		61.0	2.5	27.6	0.187	0.8	2.30
	0.3		59.5	4.0	28.4	0.285	1.2	2.21
	0.4		58.0	5.5	29.1	0.384	1.6	2.12
	0.5	63.5	56.3	7.2	29.8	0.487	2.0	2.03
	0.6		54.5	9.0	30.5	0.608	2.4	1.95
	0.7		52.4	11.1	31.2	0.725	2.8	1.86
	0.8		50.2	13.3	32.0	0.847	3.2	1.78
	0.9		48.0	15.5	32.8	0.975	3.6	1.70
	1.0		45.0	18.5	33.7	1.110	4.0	1.62
$\lambda = 0.6$	0.1		57.3	1.7	31.8	0.105	0.333	2.18
	0.2		55.7	3.3	32.6	0.215	0.667	2.07
	0.3		53.6	5.2	33.4	0.330	1.00	1.99
	0.4		51.7	7.3	34.3	0.451	1.333	1.89
	0.5	59.0	49.4	9.8	35.2	0.577	1.667	1.80
	0.6		46.9	12.1	36.2	0.709	2.000	1.72
	0.7		44.0	15.0	37.2	0.847	2.333	1.64
	0.8		40.9	18.1	38.3	0.991	2.667	1.56
	0.9		37.5	21.5	39.4	1.143	3.000	1.46
	1.0		33.7	25.3	40.6	1.302	3.333	1.42
$\lambda = 0.7$	0.1		53.0	2.0	36.0	0.117	0.286	2.03
	0.2		50.9	4.1	37.0	0.241	0.571	1.94
	0.3		48.5	6.5	38.0	0.370	0.857	1.84
	0.4		45.8	9.2	39.1	0.505	1.15	1.76
	0.5	55.0	42.9	12.1	40.3	0.647	1.43	1.67
	0.6		38.7	15.3	41.6	0.798	1.713	1.59
	0.7		36.1	18.9	42.6	0.952	2.00	1.52
	0.8		32.2	22.8	44.2	1.115	2.286	1.44
	0.9		27.9	27.1	45.6	1.287	2.57	1.37
	1.0		23.2	31.8	47.1	1.465	2.86	1.30
$\lambda = 0.8$	0.1		49.0	2.3	39.8	0.126	0.25	1.95
	0.2		46.4	4.9	41.0	0.262	0.50	1.86
	0.3		43.6	7.7	42.3	0.404	0.75	1.77
	0.4		40.4	10.9	43.6	0.551	1.00	1.68
	0.5	51.3	36.9	14.4	45.0	0.707	1.25	1.60
	0.6		33.0	18.3	46.5	0.869	1.50	1.52
	0.7		28.6	22.5	48.0	1.04	1.75	1.45
	0.8		24.2	27.1	49.7	1.22	2.00	1.38
	0.9		19.3	32.0	51.3	1.41	2.25	1.32
	1.0		14.0	37.3	53.1	1.60	2.50	1.25
	$\epsilon_s$	$\alpha_1^*$	$\alpha_2^*$	$\alpha_1^* \alpha_2^*$	$\phi^*$	$C_{LO}$	$h_{LH}$	$\delta_{LH}^*$
$\lambda = 0.9$	0.1		45.3	2.7	43.3	0.137	0.222	1.92
	0.2		42.3	5.7	44.7	0.281	0.445	1.82
	0.3		39.0	9.0	46.1	0.433	0.667	1.73
	0.4		35.4	12.6	47.7	0.591	0.890	1.65
	0.5	48.0	31.4	16.6	49.3	0.756	1.112	1.57
	0.6		27.1	20.9	50.9	0.932	1.333	1.50
	0.7		22.3	25.7	52.7	1.114	1.556	1.42
	0.8		17.3	30.7	54.6	1.304	1.780	1.36
	0.9		11.9	36.1	56.5	1.502	2.000	1.29
	1.0		6.3	41.7	58.6	1.706	2.222	1.24
$\lambda = 1.0$	0.1		42.0	3.0	46.5	0.145	0.2	1.90
	0.2		36.7	6.3	48.0	0.297	0.4	1.81
	0.3		35.0	10.0	49.8	0.457	0.6	1.72
	0.4		31.0	14.0	51.3	0.625	0.8	1.64
	0.5	45	26.6	18.4	53.1	0.800	1.0	1.56
	0.6		21.8	23.2	55.0	0.982	1.2	1.49
	0.7		16.7	28.3	57.0	1.171	1.4	1.43
	0.8		11.3	33.7	59.0	1.372	1.6	1.36
	0.9		5.7	39.3	61.2	1.579	1.8	1.30
	1.0		0.0	45.0	63.4	1.789	2.0	1.25
$\lambda = 1.1$	0.1		39.0	3.3	49.3	0.152	0.182	1.92
	0.2		35.3	7.0	51.0	0.311	0.364	1.84
	0.3		31.3	11.0	52.8	0.476	0.545	1.74
	0.4		27.0	15.3	54.7	0.653	0.727	1.66
	0.5	42.3	22.2	20.1	56.6	0.835	0.910	1.58
	0.6		17.2	25.1	58.7	1.025	1.091	1.51
	0.7		11.8	30.5	60.6	1.222	1.272	1.45
	0.8		6.2	36.1	63.0	1.426	1.454	1.39
	0.9		0.5	41.8	65.3	1.636	1.637	1.34
	1.0		-5.2	47.5	67.8	1.851	1.818	1.28
$\lambda = 1.2$	0.1		36.3	3.5	51.9	0.158	0.187	1.94
	0.2		32.4	7.4	53.8	0.323	0.333	1.85
	0.3		28.1	11.7	55.7	0.495	0.500	1.76
	0.4		23.4	16.4	57.7	0.678	0.667	1.69
	0.5	39.6	18.4	21.4	59.6	0.864	0.833	1.61
	0.6		13.1	26.7	61.9	1.059	1.000	1.54
	0.7		7.6	32.2	64.2	1.260	1.167	1.46
	0.8		1.9	37.9	66.6	1.466	1.333	1.43
	0.9		-3.8	43.6	69.0	1.681	1.500	1.36
	1.0		-9.5	49.3	71.6	1.897	1.667	1.33
$\lambda = 1.3$	0.1		33.6	3.8	54.3	0.162	0.154	1.97
	0.2		29.6	8.0	56.2	0.333	0.308	1.88
	0.3		25.1	12.5	58.2	0.510	0.482	1.80
	0.4		20.3	17.3	60.4	0.695	0.615	1.73
	0.5	37.6	15.1	22.5	62.6	0.886	0.769	1.65
	0.6		9.6	28.0	64.9	1.086	0.923	1.59
	0.7		3.9	33.7	67.3	1.291	1.078	1.53
	0.8		-1.8	39.4	69.7	1.501	1.230	1.46
	0.9		-7.5	45.1	72.3	1.715	1.385	1.43
	1.0		-13.0	50.6	74.9	1.931	1.540	1.39
$\lambda = 1.4$	0.1		31.6	4.0	56.4	0.167	0.143	2.02
	0.2		27.3	8.3	58.4	0.341	0.266	1.93
	0.3		22.5	13.1	60.6	0.523	0.429	1.85
	0.4		17.5	18.1	62.8	0.711	0.571	1.78
	0.5	35.6	12.1	23.5	65.1	0.907	0.714	1.71
	0.6		6.6	29.0	67.5	1.109	0.857	1.65
	0.7		0.9	34.7	70.0	1.315	1.000	1.59
	0.8		-4.9	40.5	72.6	1.528	1.143	1.54
	0.9		-10.5	46.1	75.2	1.740	1.286	1.50
	1.0		-15.9	51.5	77.9	1.956	1.429	1.47
$\lambda = 1.5$	0.1		28.6	4.1	58.3	0.170	0.133	2.07
	0.2		25.0	8.7	60.5	0.348	0.267	1.96
	0.3		20.2	13.5	62.7	0.533	0.400	1.90
	0.4		15.0	18.7	65.0	0.725	0.533	1.83
	0.5	33.7	9.5	24.2	67.6	0.923	0.667	1.76
	0.6		3.8	29.9	69.9	1.130	0.800	1.70
	0.7		-1.9	35.8	72.4	1.333	0.933	1.65
	0.8		-7.6	41.3	75.1	1.545	1.067	1.61
	0.9		-13.1	46.8	77.8	1.752	1.200	1.57
	1.0		-18.4	52.1	80.6	1.973	1.333	1.54

TABLE 3  
DESIGN DATA FROM MOMENTUM CONSIDERATIONS —  $E_s = 0$

	$E_p$	$\alpha_1^*$	$\alpha_2^*$	$\alpha_1^* - \alpha_2^*$	$\phi^*$	$C_{D0}$	$A_{R0}$	$\delta \frac{h}{h_{R0}}$
$\lambda = 0.2$	0.1	78.9		0.2	11.2	0.0389	1.0	5.31
	0.2	79.1		0.4	11.1	0.0770	2.0	5.40
	0.3	79.3		0.6	11.0	0.114	3.0	5.52
	0.4	79.5		0.8	10.9	0.151	4.0	5.62
	0.5	79.7		1.0	10.8	0.187	5.0	5.71
	0.6	79.9		1.2	10.7	0.223	6.0	5.81
	0.7	80.1		1.4	10.6	0.257	7.0	5.93
	0.8	80.2	78.7	1.5	10.5	0.292	8.0	6.04
	0.9	80.4		1.7	10.4	0.325	9.0	6.15
	1.0	80.5		1.8	10.3	0.358	10.0	6.26
	1.1	80.7		2.0	10.2	0.390	11.0	6.36
	1.2	80.8		2.1	10.1	0.422	12.0	6.47
	1.3	81.0		2.3	10.0	0.453	13.0	6.56
	1.4	81.1		2.4	10.0	0.484	14.0	6.69
	1.5	81.3		2.6	9.9	0.514	15.0	6.80
$\lambda = 0.3$	0.1	73.8		0.3	18.5	0.0588	0.667	3.72
	0.2	74.2		0.6	18.2	0.112	1.333	3.84
	0.3	74.6		1.3	18.0	0.165	2.000	3.94
	0.4	75.0		1.7	15.6	0.218	2.667	4.05
	0.5	75.4		2.1	15.6	0.269	3.333	4.16
	0.6	75.7		2.4	15.4	0.318	4.000	4.26
	0.7	76.1		2.8	15.2	0.368	4.667	4.35
	0.8	76.4	73.3	3.1	15.0	0.414	5.333	4.48
	0.9	76.7		3.4	14.8	0.458	6.000	4.60
	1.0	77.0		3.7	14.6	0.505	6.667	4.71
	1.1	77.3		4.0	14.5	0.549	7.333	4.81
	1.2	77.6		4.3	14.3	0.591	8.000	4.95
	1.3	77.8		4.5	14.1	0.632	8.667	5.07
	1.4	78.1		4.8	13.9	0.675	9.333	5.17
	1.5	78.3		5.0	13.8	0.712	10.000	5.32
$\lambda = 0.4$	0.1	68.0		0.8	21.4	0.0730	0.5	3.00
	0.2	69.7		1.5	21.0	0.144	1.0	3.10
	0.3	70.3		2.1	20.7	0.212	1.5	3.20
	0.4	71.0		2.8	20.3	0.278	2.0	3.33
	0.5	71.6		3.4	20.0	0.342	2.5	3.43
	0.6	72.1		3.9	18.7	0.404	3.0	3.54
	0.7	72.7		4.5	18.3	0.463	3.5	3.65
	0.8	73.2	68.2	5.0	19.0	0.522	4.0	3.77
	0.9	73.8		5.4	18.7	0.578	4.5	3.89
	1.0	74.1		5.9	18.4	0.632	5.0	4.02
	1.1	74.5		6.3	18.1	0.685	5.5	4.13
	1.2	74.9		6.7	17.9	0.737	6.0	4.26
	1.3	75.3		7.1	17.6	0.787	6.5	4.37
	1.4	75.6		7.4	17.4	0.835	7.0	4.50
	1.5	76.0		7.8	17.1	0.882	7.5	4.63
$\lambda = 0.5$	0.1	64.5		1.0	26.0	0.0877	0.4	2.80
	0.2	65.9		2.1	25.5	0.172	0.8	2.71
	0.3	66.5		3.0	24.8	0.253	1.2	2.62
	0.4	67.4		3.9	24.4	0.330	1.6	2.93
	0.5	68.2		4.7	24.0	0.406	2.0	3.04
	0.6	69.0		5.5	23.5	0.479	2.4	3.14
	0.7	69.7		6.2	23.1	0.549	2.8	3.26
	0.8	70.3	63.5	6.8	22.6	0.615	3.2	3.38
	0.9	71.0		7.5	22.2	0.680	3.6	3.51
	1.0	71.6		8.1	21.8	0.743	4.0	3.63
	1.1	72.1		8.8	21.4	0.803	4.4	3.76
	1.2	72.6		9.1	21.1	0.861	4.8	3.88
	1.3	73.1		9.6	20.7	0.917	5.2	4.02
	1.4	73.6		10.1	20.4	0.973	5.6	4.14
	1.5	74.1		10.6	20.0	1.028	6.0	4.26
$\lambda = 0.6$	0.1	60.5		1.5	30.2	0.101	0.333	2.37
	0.2	61.6		2.8	29.5	0.187	0.667	2.48
	0.3	63.0		4.0	28.8	0.268	1.000	2.59
	0.4	64.2		5.2	28.2	0.378	1.333	2.70
	0.5	65.2		6.2	27.8	0.483	1.667	2.82
	0.6	66.2		7.2	27.0	0.544	2.000	2.91
	0.7	67.1		8.1	26.4	0.622	2.333	3.04
	0.8	67.9	59.0	8.8	25.8	0.697	2.667	3.16
	0.9	68.7		9.7	25.3	0.769	3.000	3.30
	1.0	69.5		10.5	24.6	0.838	3.333	3.43
	1.1	70.1		11.1	24.3	0.905	3.667	3.55
	1.2	70.8		11.8	23.9	0.968	4.000	3.69
	1.3	71.4		12.4	23.4	1.030	4.333	3.82
	1.4	72.0		13.0	22.9	1.080	4.667	3.97
	1.5	72.5		13.5	22.5	1.128	5.000	4.11
$\lambda = 0.7$	0.1	56.6		1.8	34.1	0.112	0.266	2.23
	0.2	56.5		3.5	33.2	0.219	0.571	2.33
	0.3	60.0		5.0	32.4	0.321	0.857	2.44
	0.4	61.3		6.3	31.6	0.419	1.15	2.59
	0.5	62.6		7.5	30.8	0.513	1.43	2.67
	0.6	63.8		8.6	30.1	0.601	1.713	2.79
	0.7	64.6		9.6	29.4	0.689	2.00	2.91
	0.8	65.6	55.0	10.6	28.7	0.768	2.288	3.04
	0.9	66.6		11.6	28.0	0.848	2.57	3.17
	1.0	67.6		12.6	27.4	0.920	2.86	3.30
	1.1	68.4		13.4	26.8	0.993	3.15	3.43
	1.2	69.2		13.2	26.3	1.062	3.43	3.57
	1.3	69.9		13.9	25.7	1.128	3.71	3.72
	1.4	70.5		14.5	25.2	1.195	4.00	3.87
	1.5	71.1		15.1	24.7	1.277	4.29	4.02
$\lambda = 0.8$	0.1	53.5		2.2	37.6	0.122	0.25	2.15
	0.2	55.4		4.1	36.5	0.236	0.50	2.26
	0.3	57.2		5.9	35.5	0.349	0.75	2.37
	0.4	58.6		7.5	34.6	0.454	1.00	2.48
	0.5	60.3		9.0	33.7	0.555	1.25	2.60
	0.6	61.6		10.3	32.8	0.650	1.50	2.72
	0.7	62.9		11.6	32.0	0.741	1.75	2.85
	0.8	64.0	51.3	12.7	31.2	0.829	2.00	2.98
	0.9	65.1		13.6	30.5	0.913	2.25	3.11
	1.0	66.0		14.7	29.8	0.993	2.50	3.24
	1.1	67.0		15.7	29.1	1.070	2.75	3.39
	1.2	67.8		16.6	28.4	1.142	3.00	3.52
	1.3	68.6		17.3	27.6	1.210	3.25	3.69
	1.4	69.3		18.0	27.2	1.278	3.50	3.84
	1.5	70.0		18.7	26.8	1.341	3.75	4.00
$\lambda = 0.9$	0.1	50.7		2.7	40.7	0.131	0.222	2.12
	0.2	52.7		4.7	39.6	0.255	0.443	2.22
	0.3	54.7		6.7	38.4	0.373	0.667	2.33
	0.4	56.5		8.5	37.3	0.485	0.890	2.44
	0.5	58.2		10.2	36.5	0.592	1.112	2.57
	0.6	59.7		11.7	35.3	0.694	1.333	2.69
	0.7	61.1		13.1	34.4	0.791	1.556	2.82
	0.8	62.4	48.0	14.4	33.5	0.883	1.780	2.95
	0.9	63.6		15.6	32.7	0.971	2.000	3.09
	1.0	64.7		16.7	31.8	1.055	2.222	3.24
	1.1	65.7		17.7	31.1	1.135	2.443	3.39
	1.2	66.6		18.6	30.3	1.211	2.667	3.54
	1.3	67.5		19.5	29.6	1.284	2.890	3.69
	1.4	68.3		20.3	28.9	1.353	3.112	3.85
	1.5	69.0		21.0	28.3	1.420	3.333	4.02
$\lambda = 1.0$	0.1	47.7		2.7	43.6	0.138	0.2	2.10
	0.2	50.2		5.2	42.3	0.269	0.4	2.21
	0.3	52.4		7.4	41.0	0.394	0.6	2.33
	0.4	54.5		9.5	39.8	0.513	0.8	2.44
	0.5	56.3		11.3	38.7	0.625	1.0	2.56
	0.6	58.0		13.0	37.6	0.730	1.2	2.70
	0.7	59.5		14.5	36.5	0.835	1.4	2.83
	0.8	61.0	45	16.0	35.5	0.931	1.6	2.98
	0.9	62.3		17.3	34.6	1.021	1.8	3.09
	1.0	63.5		18.5	33.7	1.110	2.0	3.25
	1.1	64.5		19.5	32.8	1.191	2.2	3.40
	1.2	65.6		20.6	32.0	1.270	2.4	3.56
	1.3	66.5		21.5	31.2	1.347	2.6	3.73
	1.4	67.4		22.4	30.5	1.420	2.8	3.89
	1.5	68.2		23.2	29.8	1.490	3.0	4.06
$\lambda = 1.1$	0.1	45.3		3.0	46.2	0.144	0.182	2.12
	0.2	48.0		5.7	44.6	0.282	0.364	2.22
	0.3	50.4		8.1	43.4	0.412	0.545	2.34
	0.4	52.6		10.3	42.0	0.536	0.727	2.46
	0.5	54.6		12.3	40.8	0.653	0.910	2.58
	0.6	56.5		14.2	39.6	0.765	1.091	2.71
	0.7	58.2		15.9	38.5	0.871	1.272	2.84
	0.8	59.7	42.3	17.4	37.4	0.972	1.454	2.96
	0.9	61.1		18.6	36.4	1.067	1.637	3.13
	1.0	62.4		20.1	35.4	1.156	1.818	3.29
	1.1	63.5		21.2	34.4	1.244	2.00	3.44
	1.2	64.6		22.3	33.5	1.326	2.182	3.60
	1.3	65.6		23.3	32.7	1.404	2.364	3.76
	1.4	66.6		24.3	31.9	1.478	2.545	3.94
	1.5	67.5		25.2	31.1	1.549	2.727	4.12
$\lambda = 1.2$	0.1	43.0		3.2	46.8	0.150	0.187	2.14
	0.2	46.0		6.2	47.0	0.283	0.333	2.24
	0.3	48.6		8.9	45.6	0.428	0.500	2.36
	0.4	51.0		11.2	44.1	0.558	0.667	2.48
	0.5	53.1		13.3	42.7	0.678	0.833	2.61
	0.6	55.1		15.3	411			

TABLE 4  
OPTIMUM VALUES OF  $C_L^*$  AND  $\sigma$  FOR  $\varepsilon_p=0$  — CASCADE THEORY

	$\varepsilon_s=0.4$			$\varepsilon_s=0.5$			$\varepsilon_s=0.6$			$\varepsilon_s=0.7$			$\varepsilon_s=0.8$			$\varepsilon_s=0.9$			$\varepsilon_s=1.0$		
$\lambda$	$C_L^*$	$C_L\sigma$	$\sigma$	$C_L^*$	$C_L\sigma$	$\sigma$	$C_L^*$	$C_L\sigma$	$\sigma$	$C_L^*$	$C_L\sigma$	$\sigma$	$C_L^*$	$C_L\sigma$	$\sigma$	$C_L^*$	$C_L\sigma$	$\sigma$	$C_L^*$	$C_L\sigma$	$\sigma$
0.3																					
0.4							1.072	0.497	0.463	0.957	0.591	0.618	0.851	0.688	0.808	0.933	0.589	0.631	0.841	0.667	0.793
0.6				1.042	0.577	0.553	0.917	0.709	0.773	0.798	0.847	1.061	0.693	0.991	1.430	0.607	1.143	1.885	0.532	1.302	2.45
0.8	1.157	0.551	0.476	1.013	0.707	0.698	0.891	0.869	0.975	0.789	1.04	1.32	0.711	1.22	1.715	0.645	1.41	2.19	0.595	1.60	2.69
1.0	1.179	0.625	0.530	1.050	0.800	0.762	0.947	0.982	1.037	0.868	1.171	1.35	0.811	1.372	1.692	0.779	1.579	2.025	0.771	1.789	2.32
1.2	1.222	0.676	0.553	1.125	0.864	0.768	1.042	1.059	1.015	0.993	1.260	1.269	0.971	1.468	1.510	0.979	1.681	1.72	1.009	1.897	1.88
1.5	1.368	0.725	0.530	1.292	0.923	0.714	1.250	1.130	0.904	1.254	1.333	1.063	1.270	1.545	1.217	1.342	1.752	1.305	1.442	1.973	1.37

TABLE 5  
OPTIMUM VALUES OF  $C_L^*$  AND  $\sigma$  FOR  $\varepsilon_s=0$  — CASCADE THEORY

	$\varepsilon_p = 0.4$			$\varepsilon_p = 0.5$			$\varepsilon_p = 0.6$			$\varepsilon_p = 0.7$			$\varepsilon_p = 0.8$			$\varepsilon_p = 0.9$			$\varepsilon_p = 1.0$		
$\lambda$	$C_L^*$	$C_L\sigma$	$\sigma$	$C_L^*$	$C_L\sigma$	$\sigma$	$C_L^*$	$C_L\sigma$	$\sigma$	$C_L^*$	$C_L\sigma$	$\sigma$	$C_L^*$	$C_L\sigma$	$\sigma$	$C_L^*$	$C_L\sigma$	$\sigma$	$C_L^*$	$C_L\sigma$	$\sigma$
0.3																			1.021	0.505	0.495
0.4										1.098	0.463	0.422	1.010	0.522	0.517	0.940	0.578	0.615	0.874	0.632	0.723
0.6							1.025	0.544	0.531	0.927	0.622	0.671	0.842	0.697	0.828	0.766	0.769	1.003	0.698	0.838	1.200
0.8				1.060	0.555	0.524	0.944	0.650	0.689	0.842	0.741	0.881	0.752	0.829	1.102	0.679	0.913	1.345	0.614	0.993	1.619
1.0	1.171	0.513	0.438	1.021	0.625	0.611	0.900	0.730	0.811	0.800	0.835	1.042	0.710	0.931	1.310	0.635	1.021	1.610	0.566	1.110	1.960
1.2	1.159	0.556	0.480	1.010	0.678	0.671	0.890	0.794	0.892	0.783	0.904	1.153	0.693	1.008	1.455	0.611	1.107	1.810	0.545	1.200	2.203
1.5	1.225	0.604	0.493	1.079	0.737	0.683	0.939	0.862	0.918	0.826	0.981	1.187	0.720	1.092	1.516	0.638	1.200	1.862	0.564	1.301	2.31

	$\varepsilon_p = 1.1$			$\varepsilon_p = 1.2$			$\varepsilon_p = 1.3$			$\varepsilon_p = 1.4$			$\varepsilon_p = 1.5$								
$\lambda$	$C_L^*$	$C_L\sigma$	$\sigma$	$C_L^*$	$C_L\sigma$	$\sigma$	$C_L^*$	$C_L\sigma$	$\sigma$	$C_L^*$	$C_L\sigma$	$\sigma$	$C_L^*$	$C_L\sigma$	$\sigma$						
0.3	0.957	0.549	0.573	0.897	0.591	0.659	0.858	0.632	0.737	0.805	0.675	0.838	0.767	0.712	0.929						
0.4	0.811	0.685	0.844	0.759	0.737	0.971	0.711	0.787	1.106	0.666	0.835	1.254	0.619	0.862	1.425						
0.6	0.638	0.905	1.420	0.587	0.968	1.650	0.538	1.030	1.915	0.495	1.090	2.203	0.456	1.148	2.515						
0.8	0.552	1.070	1.939	0.500	1.142	2.285	0.456	1.210	2.67	0.416	1.276	3.07									
1.0	0.513	1.191	2.324	0.458	1.270	2.775															
1.2	0.484	1.289	2.662																		
1.5																					

**TABLE 6**  
**DESIGN DETAILS FOR CASCADE THEORY AEROFOILS— $\xi_p=0$**

	$\xi_s=0.4$		$\xi_s=0.5$		$\xi_s=0.6$		$\xi_s=0.7$		$\xi_s=0.8$		$\xi_s=0.9$		$\xi_s=1.0$	
$\lambda$	$\theta^\circ$	$\xi^\circ$	$\theta^\circ$	$\xi^\circ$	$\theta^\circ$	$\xi^\circ$	$\theta^\circ$	$\xi^\circ$	$\theta^\circ$	$\xi^\circ$	$\theta^\circ$	$\xi^\circ$	$\theta^\circ$	$\xi^\circ$
0.3									7.6	69.5	8.3	69.1	9.2	68.7
0.4					9.6	63.4	10.8	62.8	12.2	62.1	13.7	61.4	15.3	60.6
0.6			14.8	51.6	17.3	50.4	20.1	49.0	23.2	47.5	26.6	45.8	30.4	43.8
0.8	17.5	42.6	21.0	40.8	24.9	38.9	29.1	36.8	33.8	34.4	38.9	31.9	44.3	29.2
1.0	21.8	34.1	26.2	31.9	31.1	29.5	36.5	26.8	42.2	23.9	48.1	21.0	54.3	17.9
1.2	25.2	27.2	30.4	24.6	36.0	21.8	41.8	18.9	48.0	15.8	54.4	12.6	60.8	9.4
1.5	29.1	19.2	35.0	16.2	41.2	13.1	47.6	9.9	54.1	6.7	60.7	3.4	67.1	0.2

TABLE 7

DESIGN DETAILS FOR CASCADE THEORY AEROFOILS —  $\epsilon_s = 0$

[illegible]



TABLE 8  
RECOMMENDED VALUES FOR STRAIGHTENER DESIGN  
AS FUNCTIONS OF  $\epsilon_s$

$\epsilon_s$	0.1	0.2	0.3	0.4	0.5	0.6	0.7	0.8	0.9	1.0
S/C	1.5	1.5	1.5	1.5	1.5	1.14	0.88	0.665	0.540	0.430
$C_L$	0.300	0.597	0.890	1.178	1.458	1.310	1.162	1.016	0.866	0.770
$\theta$	8.4°	16.6°	24.6°	32.0°	39.0°	42.9°	46.3°	49.2°	51.9°	54.3°
%CAMBER	1.66	3.67	5.43	7.07	8.62	9.47	10.22	10.86	11.46	12.00
$\xi$	1.5°	3.0°	4.4°	5.8°	7.1°	9.5°	11.8°	14.1°	16.0°	17.8°

\* OPTIMUM VALUES

TABLE 10  
RECOMMENDED VALUES FOR PREROTATOR DESIGN  
AS FUNCTIONS OF  $\epsilon_p$

$\epsilon_p$	0.1	0.2	0.3	0.4	0.5	0.6	0.7	0.8	0.9	1.0	1.1	1.2	1.3	1.4	1.5
S/C	1.5	1.5	1.5	1.5	1.5	1.5	1.5	1.345	1.215	1.116	1.038	0.975	0.918	0.872	0.840
$C_L$	0.300	0.597	0.890	1.178	1.458	1.725	1.982	2.0	2.0	2.0	2.0	2.0	2.0	2.0	2.0
$\theta$	8.1°	16.2°	23.9°	31.1°	38.0°	44.3°	50.0°	52.9°	55.4°	57.9°	60.2°	62.4°	64.1°	66.1°	67.7°
%CAMBER	1.77	3.56	5.28	6.87	8.40	9.78	11.05	11.69	12.25	12.79	13.30	13.79	14.16	14.60	14.95
$\xi$	4.1°	8.1°	12.0°	15.6°	19.0°	22.2°	25.0°	26.5°	27.7°	29.0°	30.1°	31.2°	32.1°	33.1°	33.9°

TABLE 9  
VALUES OF  $C_L$  AS A FUNCTION OF  $\epsilon_s$  OR  $\epsilon_p$  AND  $\frac{S}{C}$   
FOR STATOR DESIGN—GENERAL APPLICATION

E	Sc										
	0.5	0.6	0.7	0.8	0.9	1.0	1.1	1.2	1.3	1.4	1.5
0.2	0.199	0.239	0.279	0.318	0.358	0.398	0.438	0.478	0.517	0.557	0.597
0.4	0.392	0.471	0.549	0.628	0.706	0.785	0.863	0.941	1.020	1.098	1.177
0.6	0.575	0.690	0.805	0.920	1.035	1.150	1.265	1.380	1.495	1.610	1.725
0.8	0.742	0.891	1.040	1.189	1.336	1.485	1.633	1.781	1.930	2.080	2.225
1.0	0.893	1.072	1.251	1.430	1.609	1.789	1.968	2.145	2.323		
1.2	1.029	1.234	1.440	1.646	1.851	2.059	2.264				
1.4	1.145	1.373	1.603	1.832	2.061	2.290					
1.5	1.200	1.440	1.680	1.920	2.160	2.400					

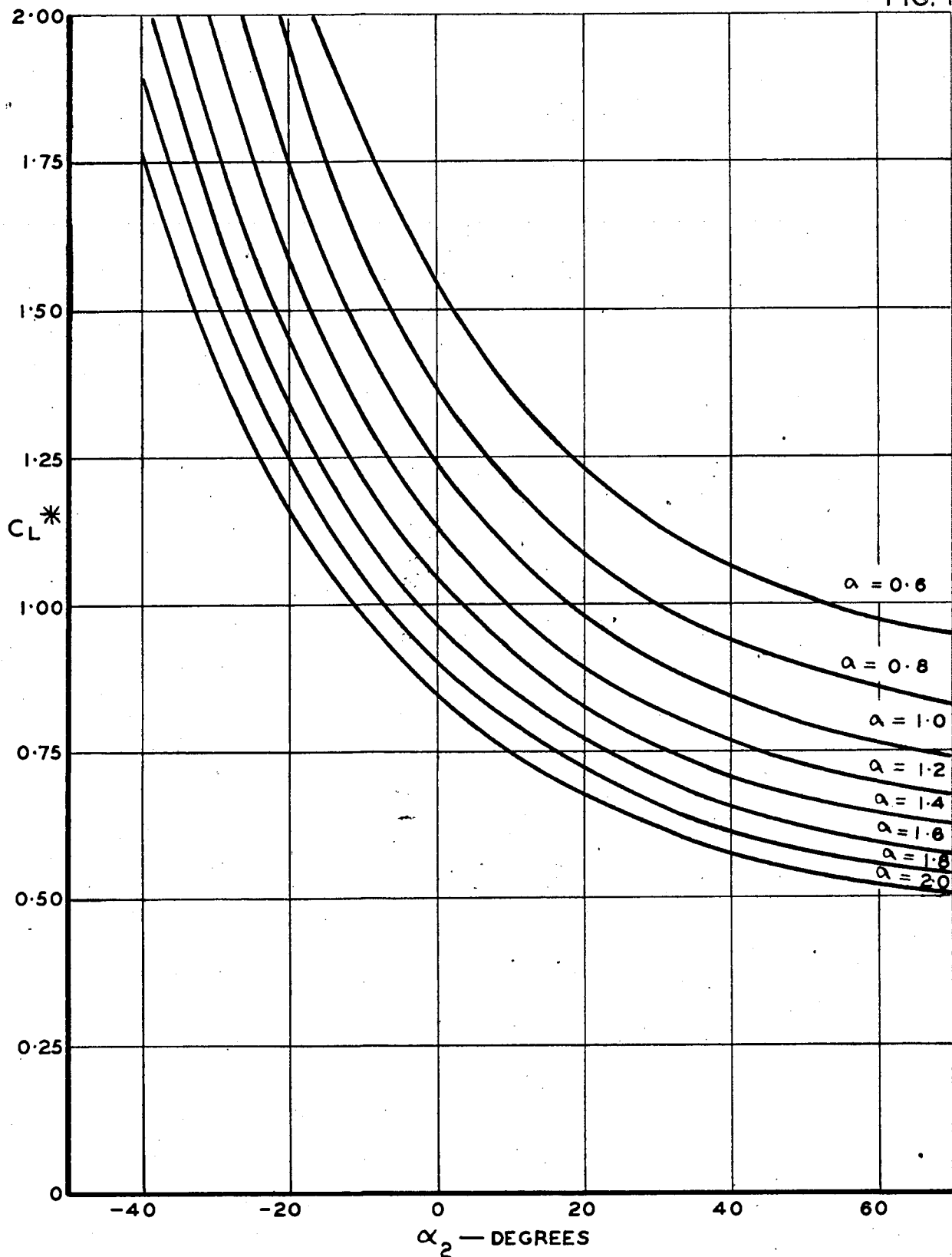
TABLE 11  
LOSS COEFFICIENTS FOR ROTOR,  $\epsilon_p=0$ —CASCADE THEORY

$\lambda$	$\epsilon_s=0.4$			$\epsilon_s=0.5$			$\epsilon_s=0.6$		
	$\frac{R_F}{C_D R_{th}}$	$\frac{R_F}{R_{th}}$	$\frac{(R_F+R_F)}{R_{th}}$	$\frac{R_F}{C_D R_{th}}$	$\frac{R_F}{R_{th}}$	$\frac{(R_F+R_F)}{R_{th}}$	$\frac{R_F}{C_D R_{th}}$	$\frac{R_F}{R_{th}}$	$\frac{(R_F+R_F)}{R_{th}}$
	$C_D R_{th}$	$R_{th}$	$R_{th}$	$C_D R_{th}$	$R_{th}$	$R_{th}$	$C_D R_{th}$	$R_{th}$	$R_{th}$
0.4				1.73	0.034	0.061	2.18	0.045	0.080
0.6				1.58	0.029	0.054	1.88	0.028	0.058
0.8	1.45	0.035	0.058	1.49	0.029	0.053	1.71	0.025	0.052
1.0	1.39	0.035	0.057	1.43	0.033	0.055	1.57	0.025	0.051
1.2	1.38	0.037	0.059	1.43	0.033	0.055	1.48	0.029	0.052
1.5	1.34	0.045	0.066	1.36	0.041	0.063	1.36	0.038	0.060
	$\epsilon_s=0.7$			$\epsilon_s=0.8$			$\epsilon_s=0.9$		
	$\frac{R_F}{C_D R_{th}}$	$\frac{R_F}{R_{th}}$	$\frac{(R_F+R_F)}{R_{th}}$	$\frac{R_F}{C_D R_{th}}$	$\frac{R_F}{R_{th}}$	$\frac{(R_F+R_F)}{R_{th}}$	$\frac{R_F}{C_D R_{th}}$	$\frac{R_F}{R_{th}}$	$\frac{(R_F+R_F)}{R_{th}}$
	$C_D R_{th}$	$R_{th}$	$R_{th}$	$C_D R_{th}$	$R_{th}$	$R_{th}$	$C_D R_{th}$	$R_{th}$	$R_{th}$
0.3				2.76	0.054	0.098	2.99	0.047	0.095
0.4	2.35	0.039	0.077	2.54	0.033	0.074	2.75	0.028	0.072
0.6	2.06	0.024	0.057	2.25	0.019	0.055	2.44	0.016	0.053
0.8	1.84	0.021	0.050	1.94	0.018	0.049	2.05	0.015	0.048
1.0	1.65	0.022	0.049	1.68	0.020	0.047	1.67	0.018	0.045
1.2	1.49	0.026	0.050	1.47	0.025	0.049	1.41	0.024	0.047
1.5	1.32	0.037	0.058	1.27	0.037	0.057	1.17	0.038	0.057
	$\epsilon_s=1.0$								
	$\frac{R_F}{C_D R_{th}}$	$\frac{R_F}{R_{th}}$	$\frac{(R_F+R_F)}{R_{th}}$	$\frac{R_F}{C_D R_{th}}$	$\frac{R_F}{R_{th}}$	$\frac{(R_F+R_F)}{R_{th}}$	$\frac{R_F}{C_D R_{th}}$	$\frac{R_F}{R_{th}}$	$\frac{(R_F+R_F)}{R_{th}}$
	$C_D R_{th}$	$R_{th}$	$R_{th}$	$C_D R_{th}$	$R_{th}$	$R_{th}$	$C_D R_{th}$	$R_{th}$	$R_{th}$
0.3	3.22	0.041	0.092						
0.4	2.99	0.024	0.072						
0.6	2.67	0.014	0.056						
0.8	2.10	0.014	0.047						
1.0	1.62	0.017	0.043						
1.2	1.32	0.024	0.045						
1.5	1.07	0.040	0.057						

NOTE: FOR ASSUMPTIONS, SEE SECTIONS 4.2 AND 4.6

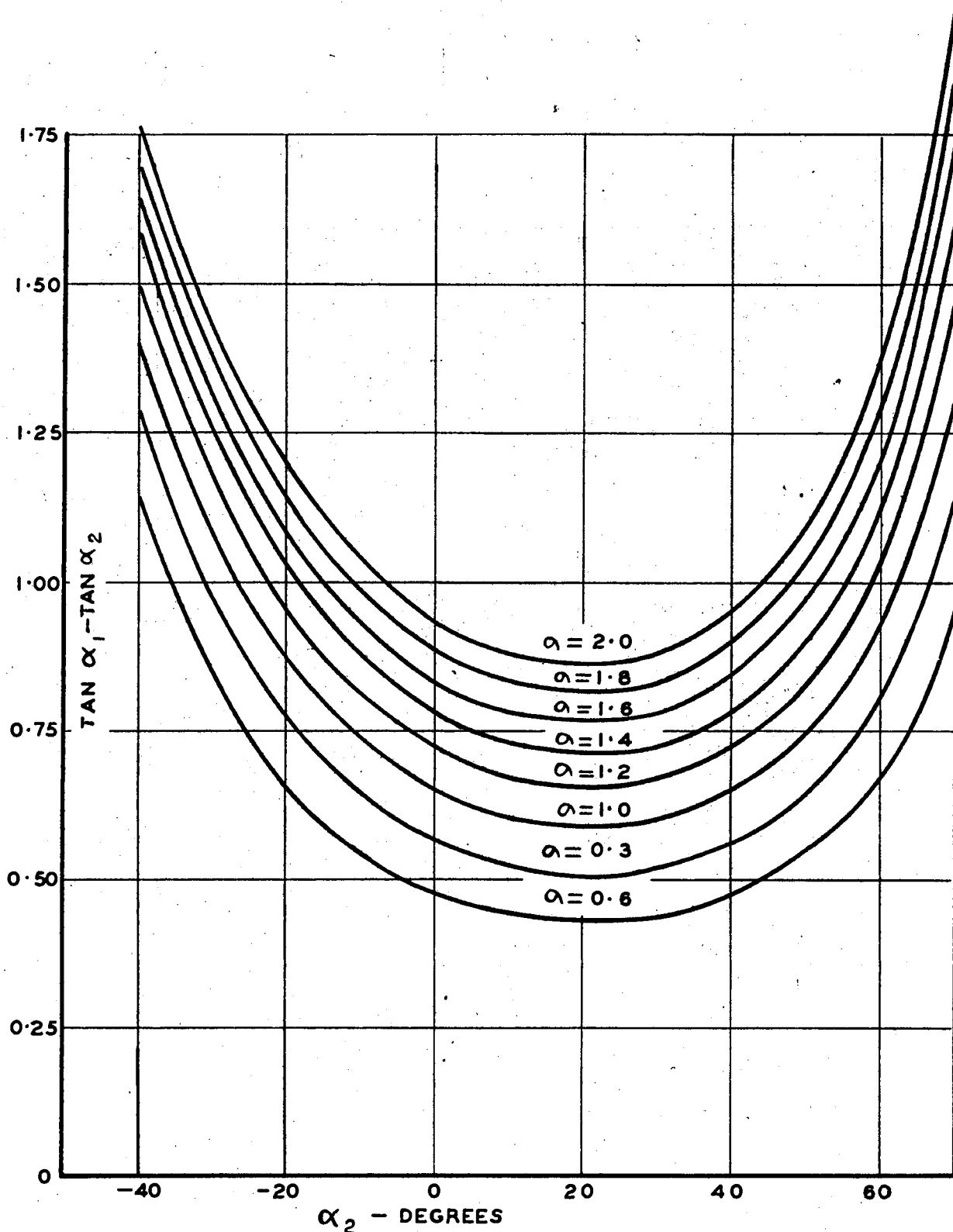


FIG. 1



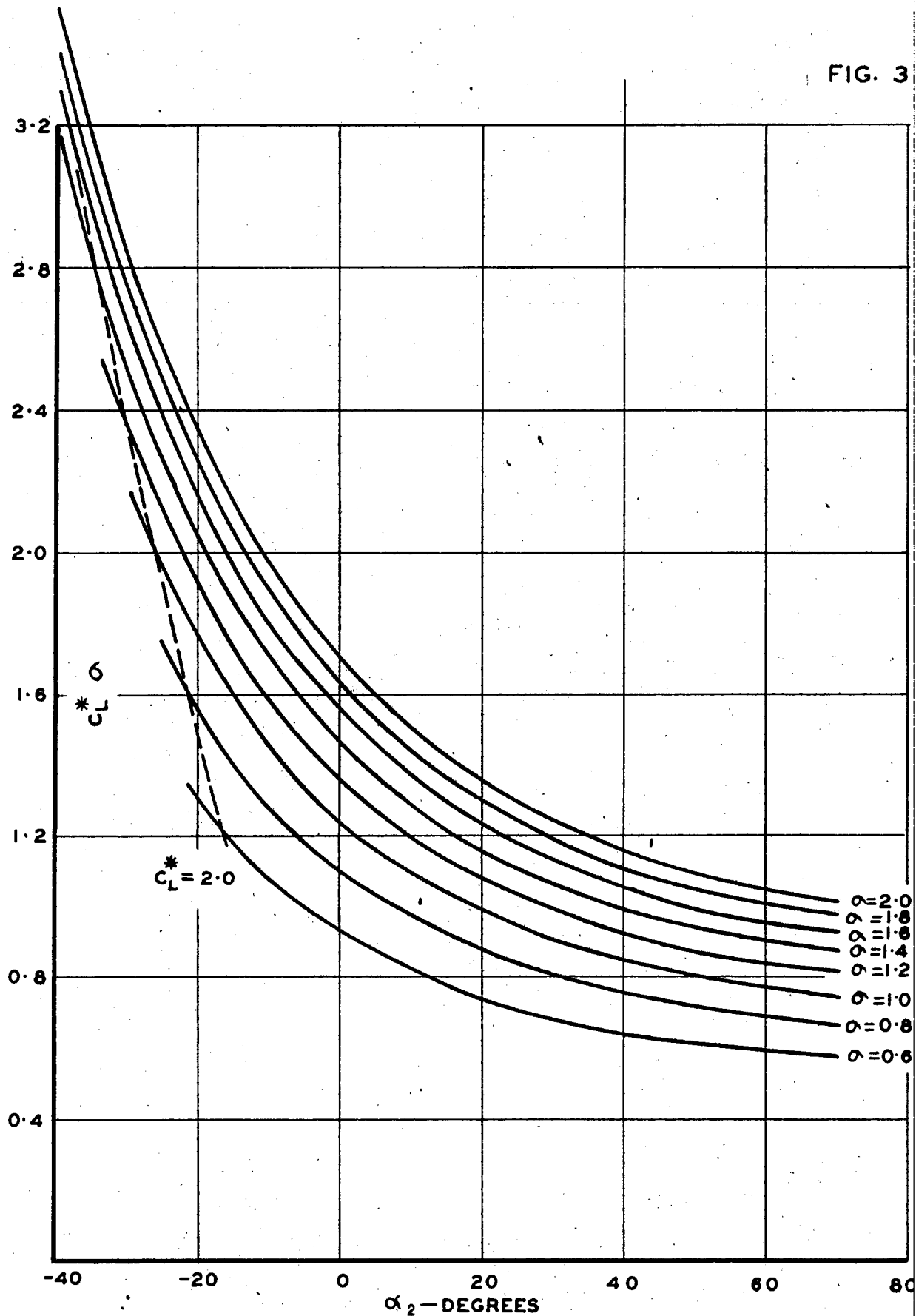
OPTIMUM LIFT COEFFICIENT—CASCADE THEORY

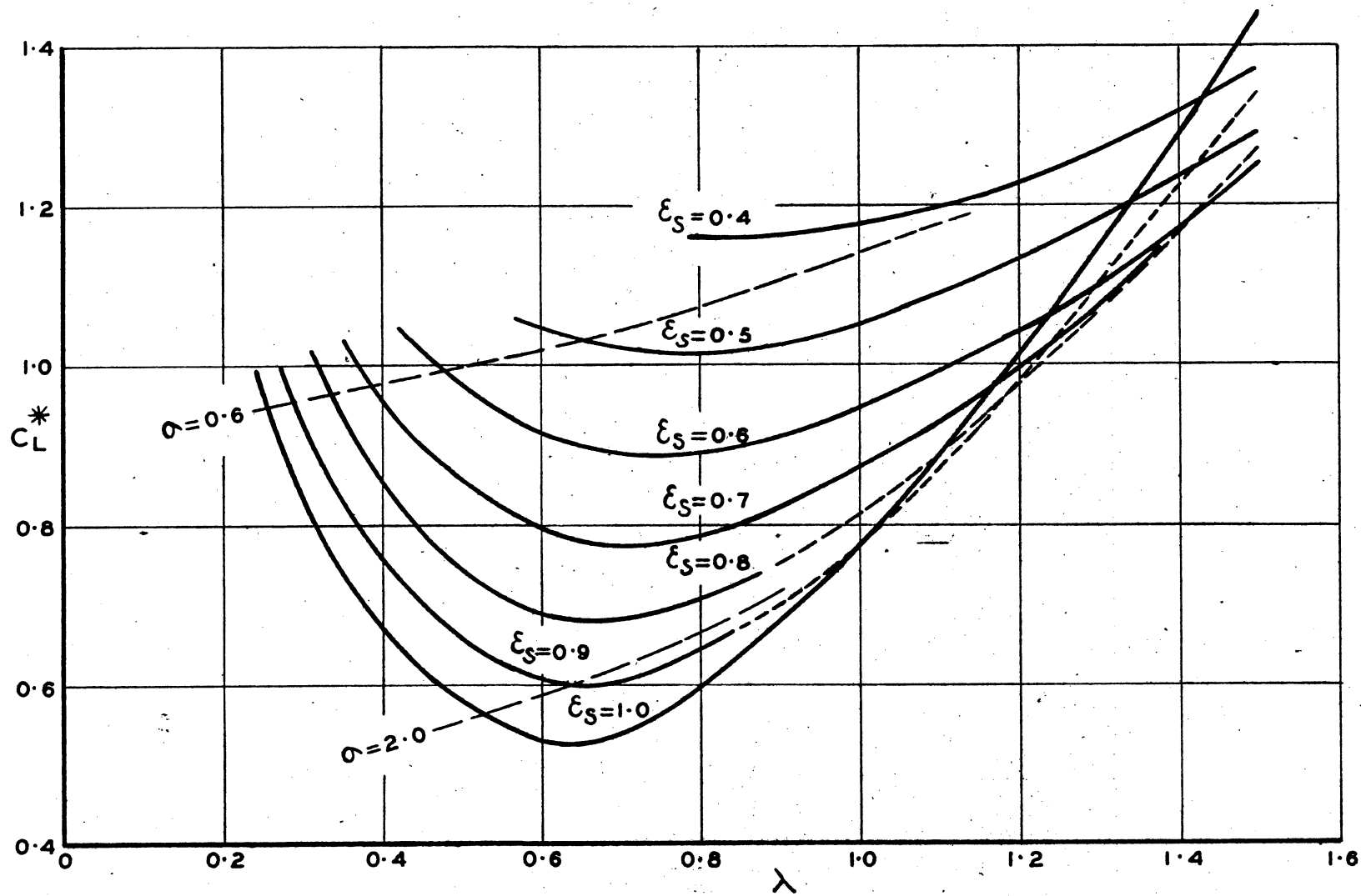
FIG. 2



OPTIMUM SOLIDITIES FOR GIVEN FLOW ROTATIONS  
CASCADE THEORY

FIG. 3

OPTIMUM SOLIDITIES FOR GIVEN  $C_L \alpha$  - CASCADE THEORY



OPTIMUM  $C_L$  WHEN  $\epsilon_p = 0$  - CASCADE THEORY

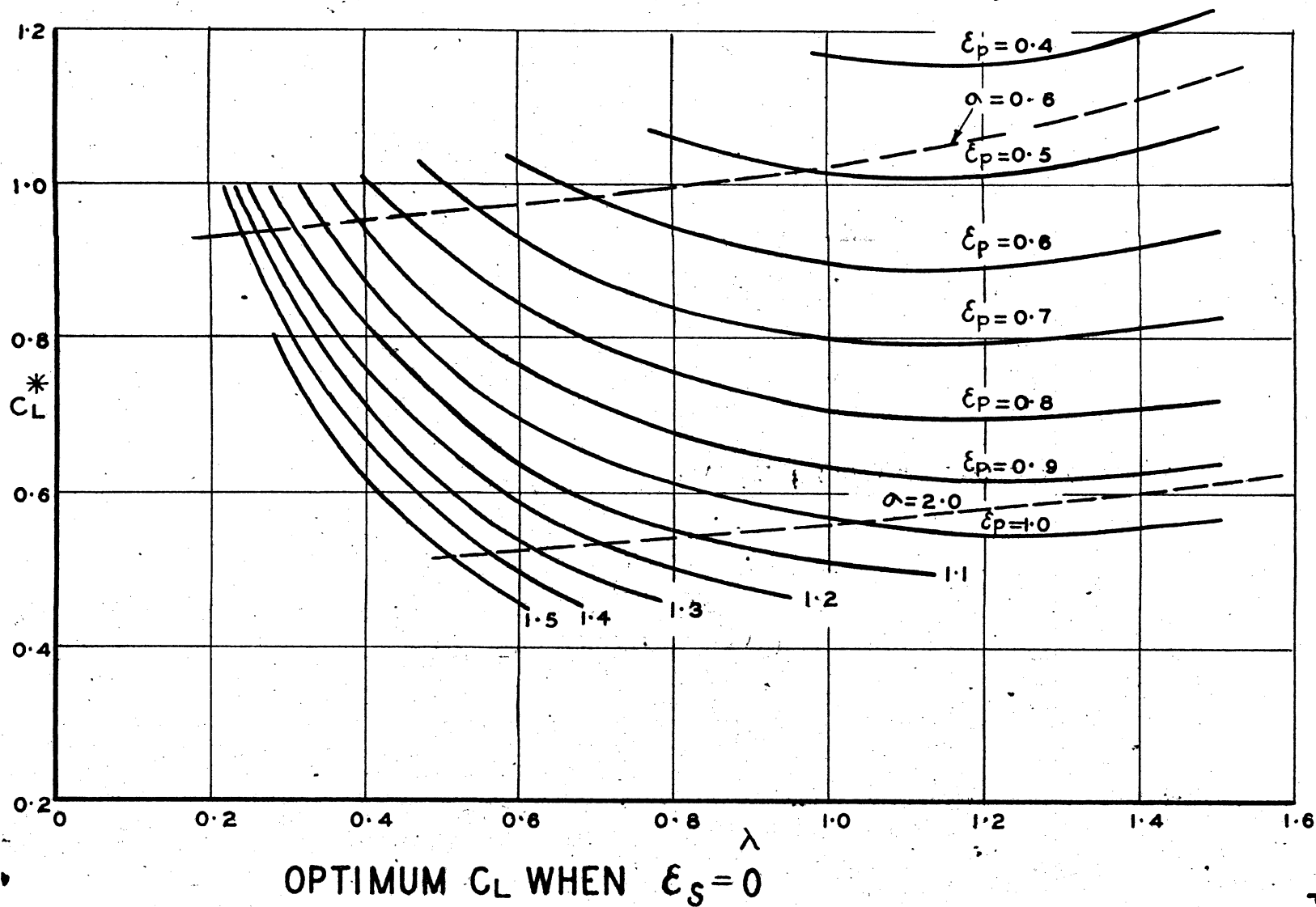
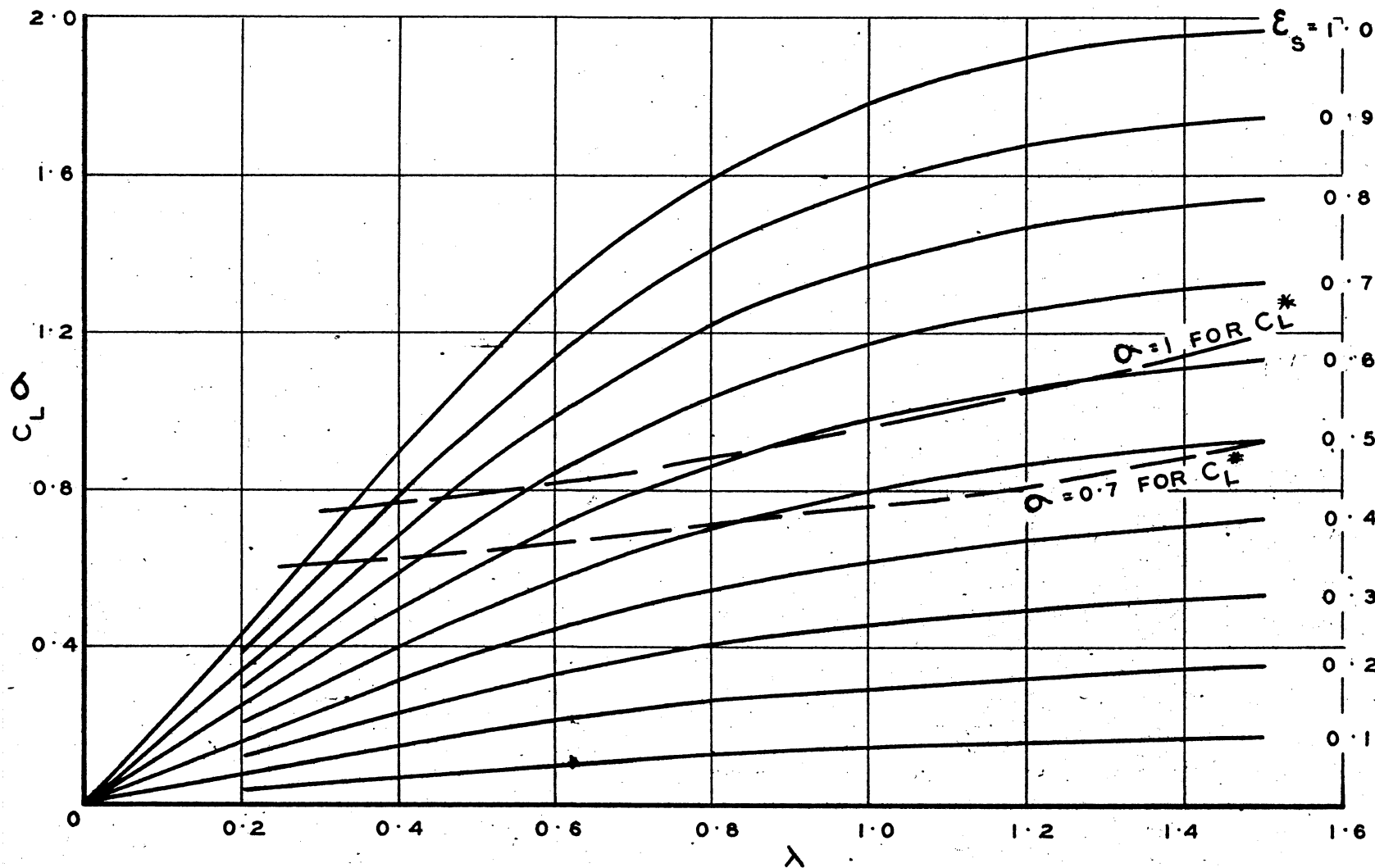
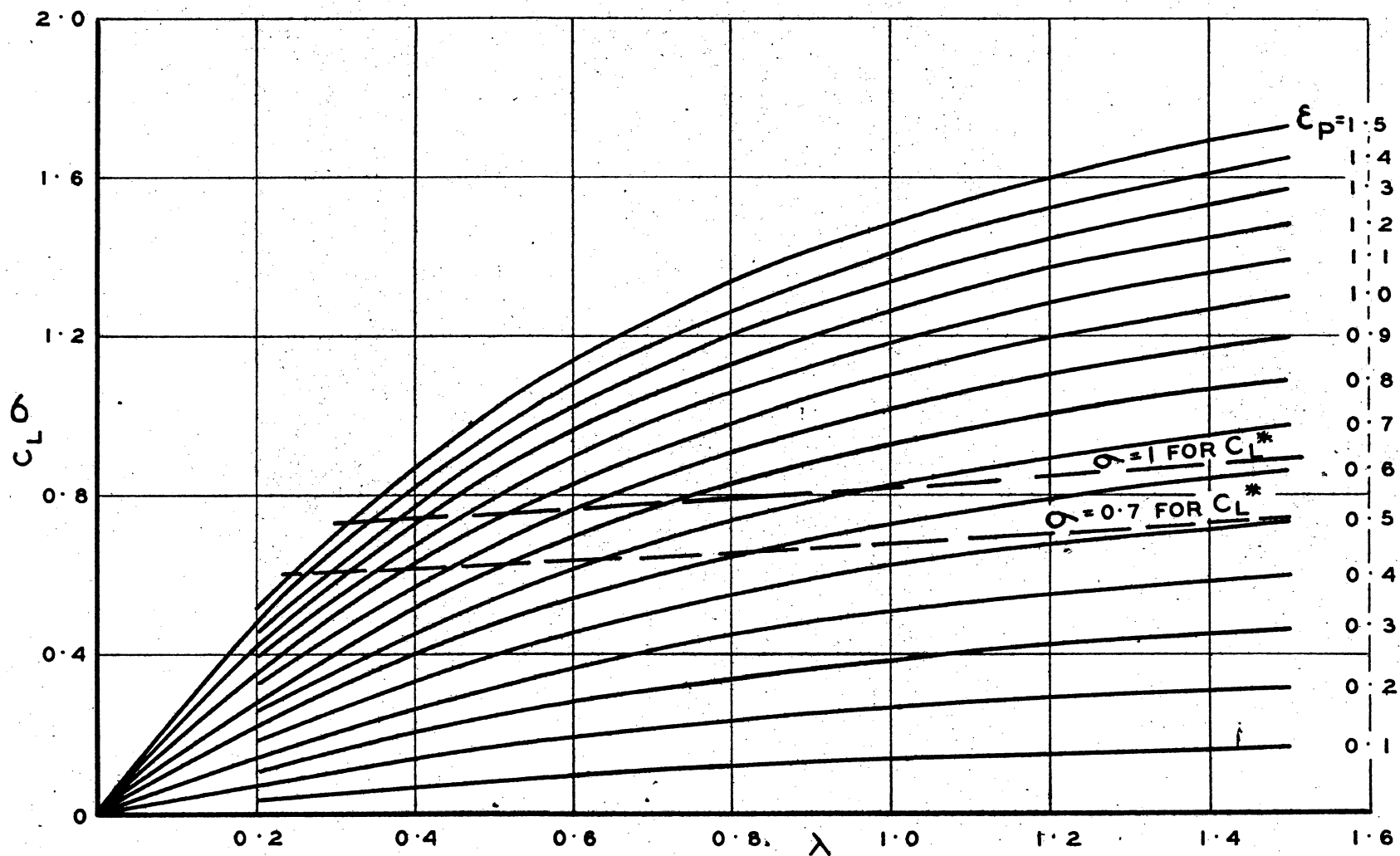


FIG. 5

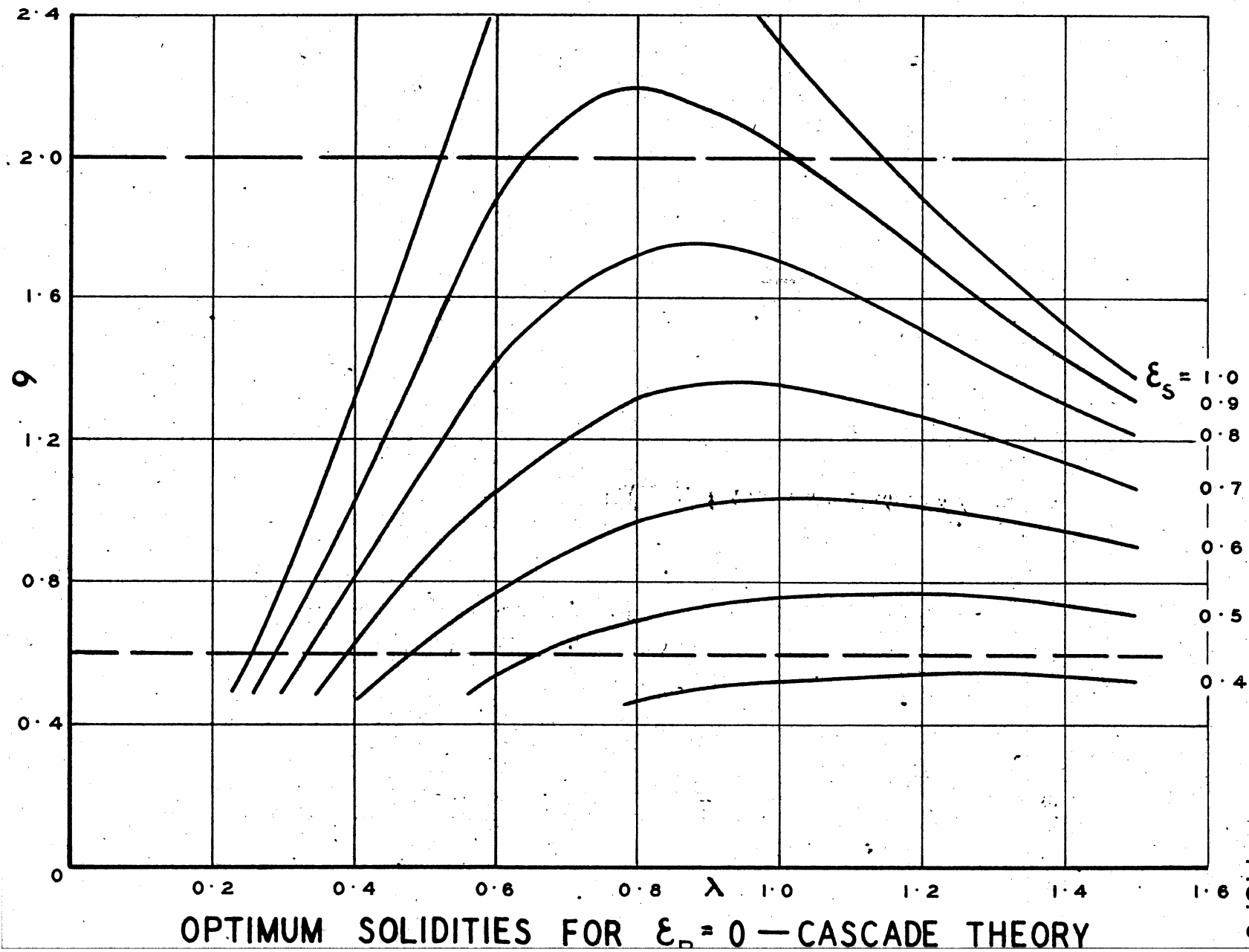


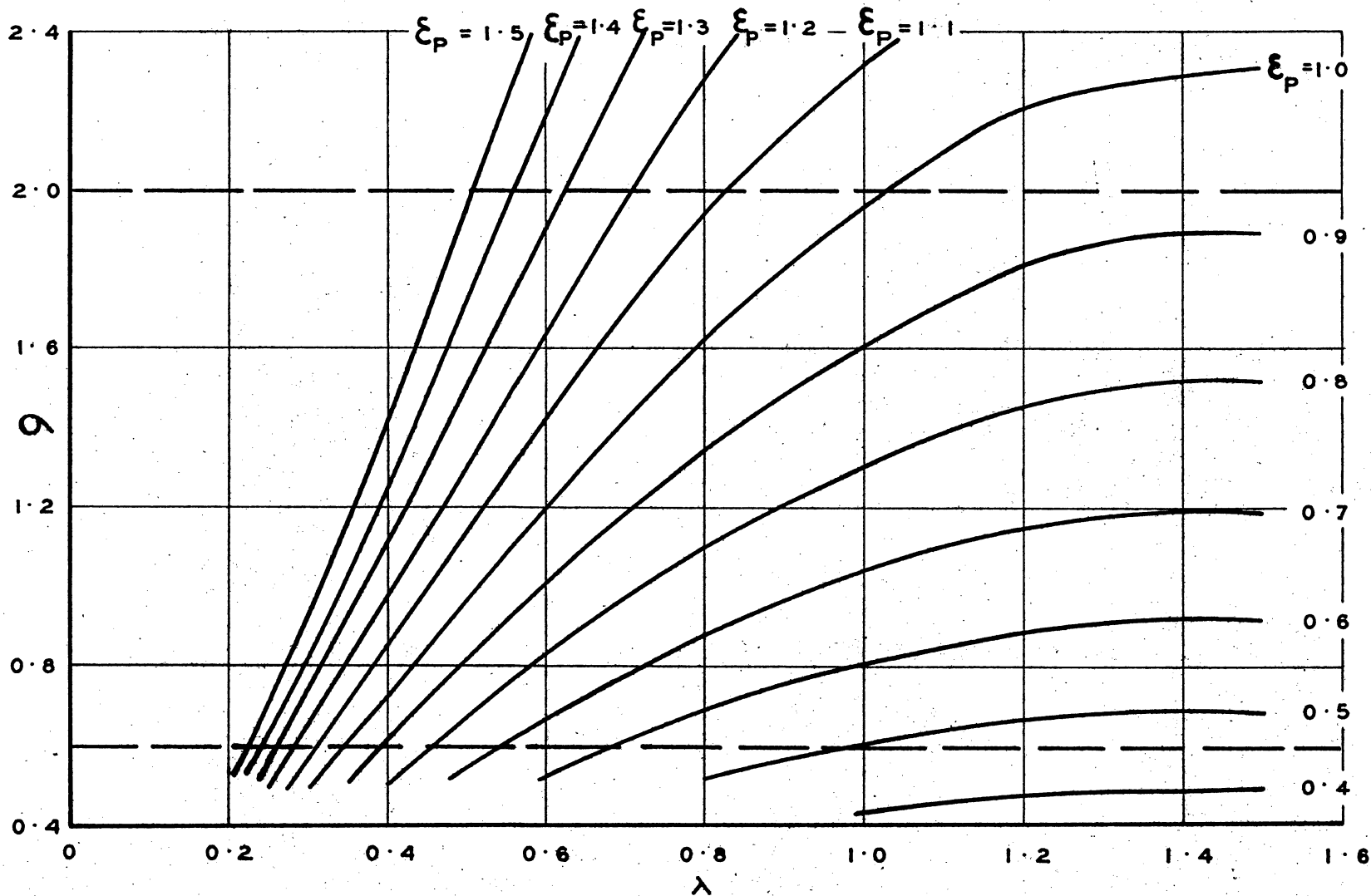
PRODUCT  $C_L \alpha$  FOR  $\epsilon_p = 0$  — GENERAL APPLICATION



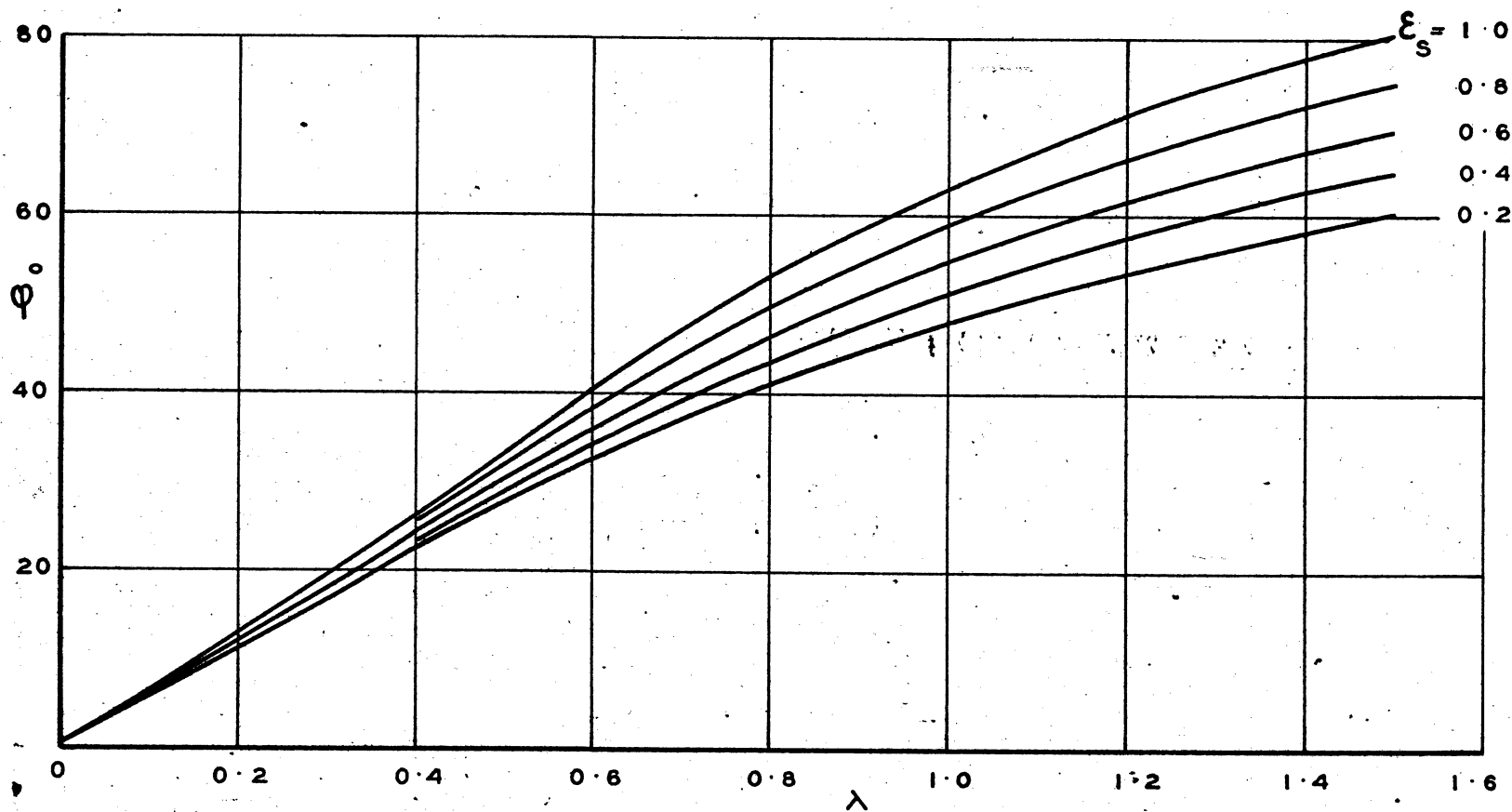


PRODUCT  $C_L \sigma$  FOR  $\epsilon_s = 0$  — GENERAL APPLICATION

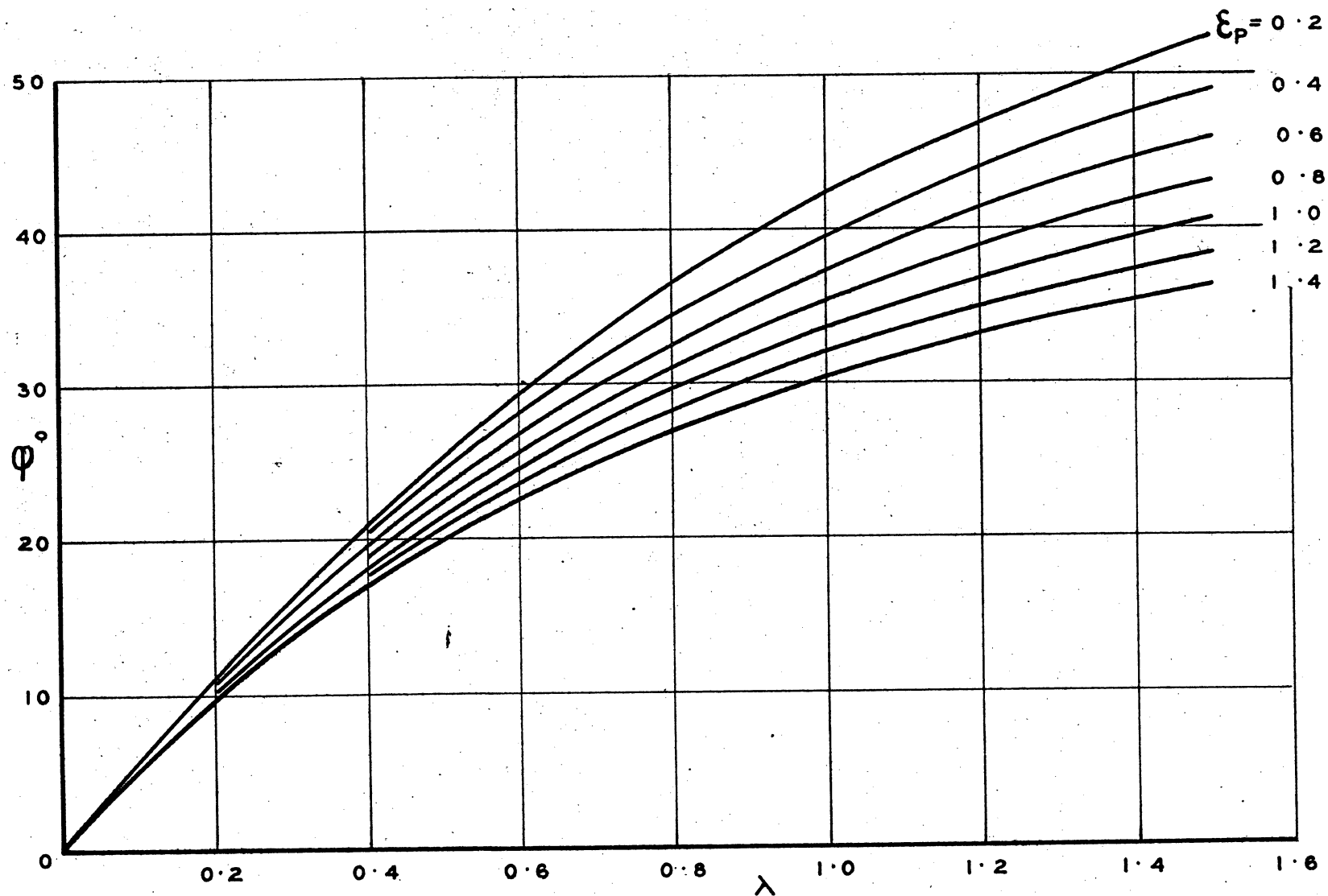




OPTIMUM SOLIDITIES FOR  $\epsilon_s = 0$  — CASCADE THEORY



FLOW ANGLE FOR  $\epsilon_p = 0$  — GENERAL APPLICATION



FLOW ANGLE FOR  $\epsilon_s = 0$  — GENERAL APPLICATION

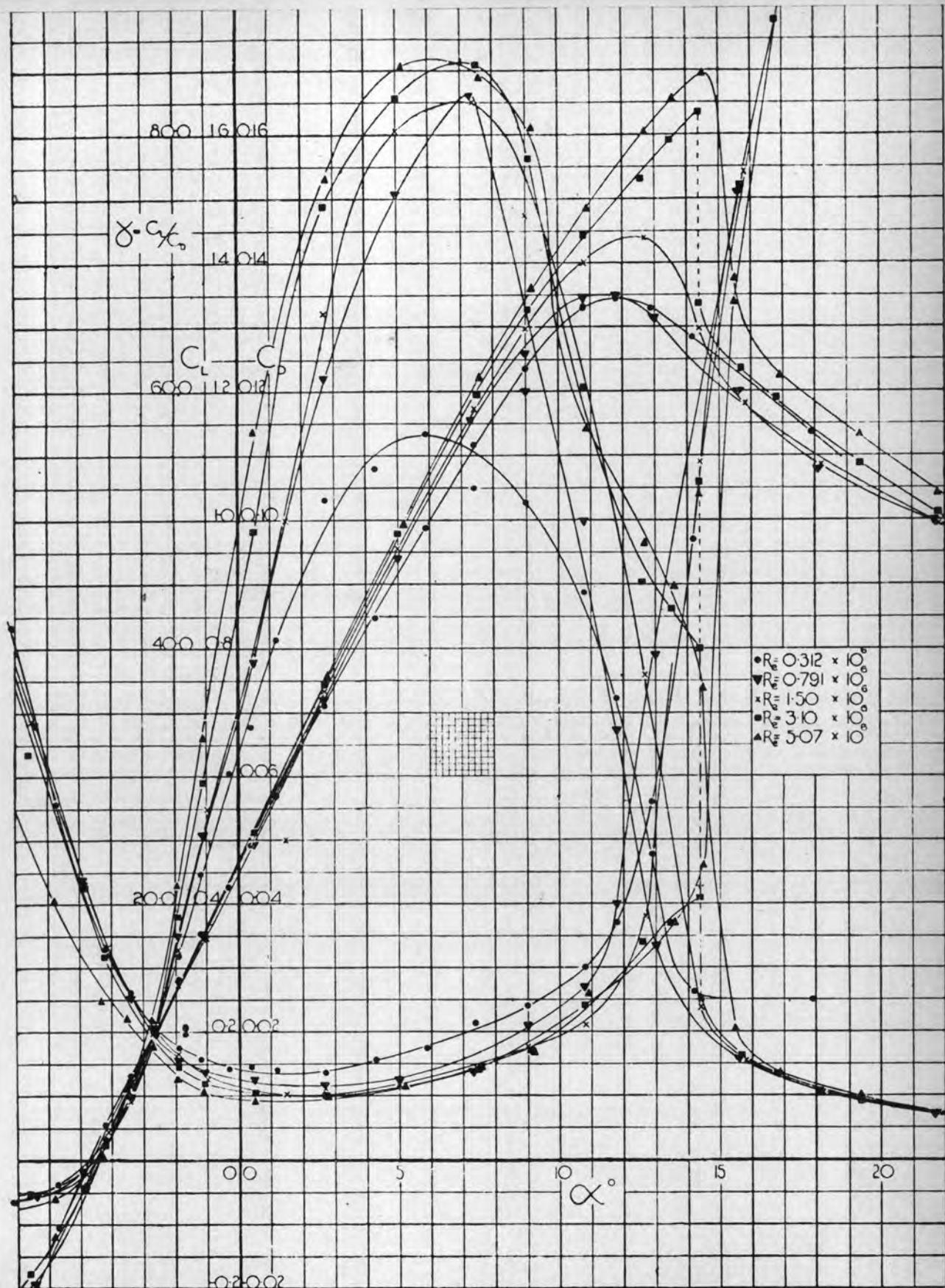
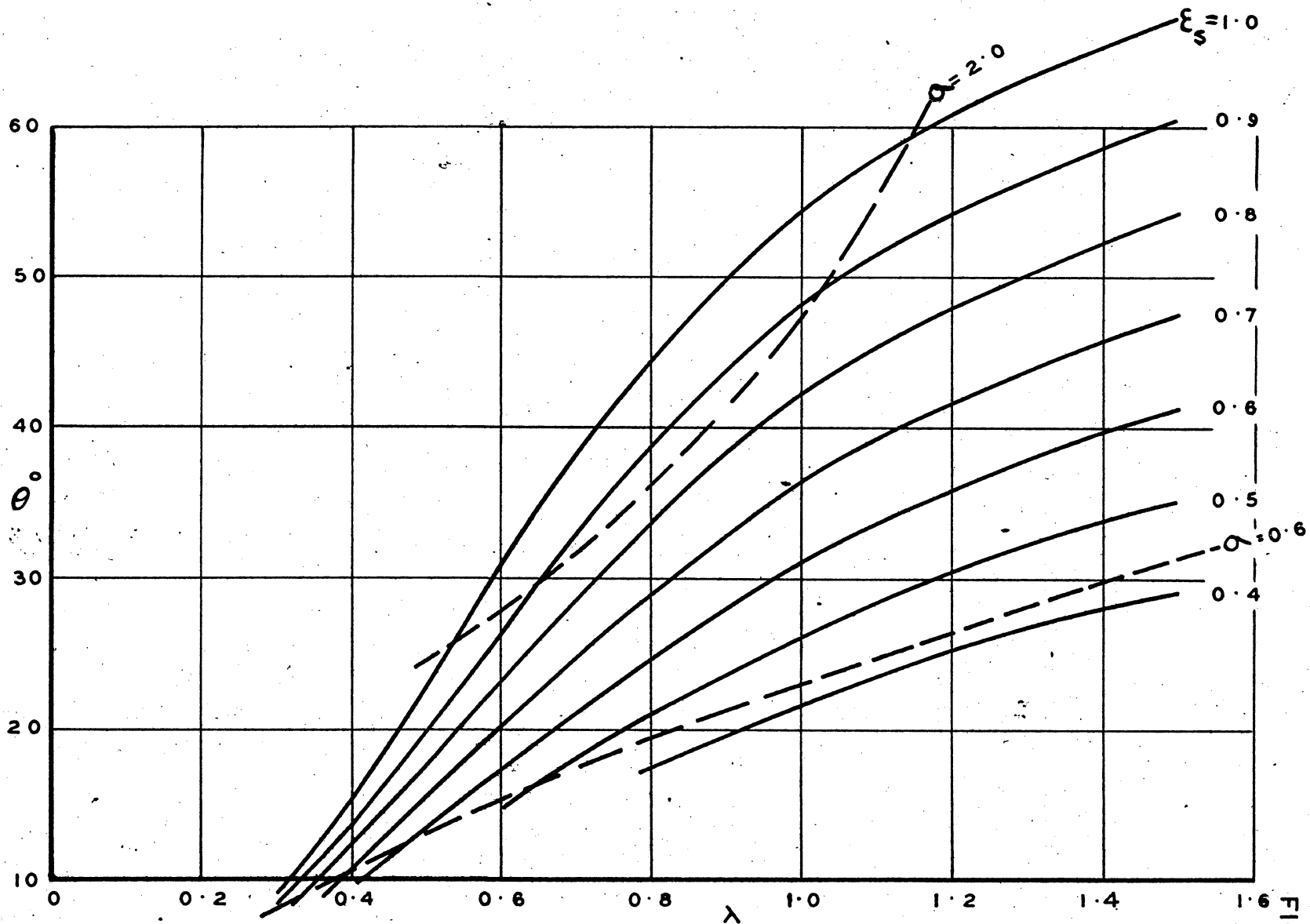
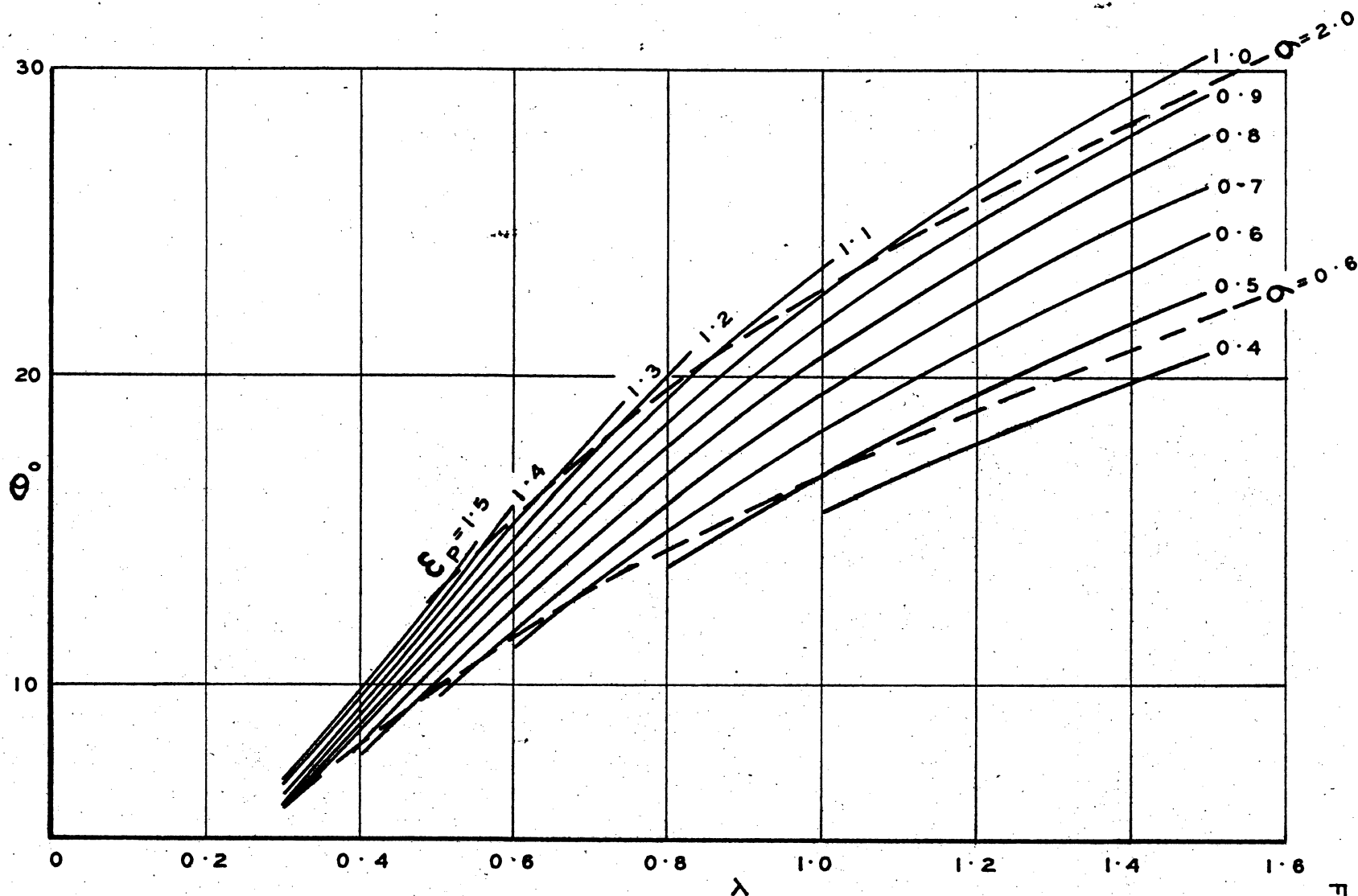


Fig. 12. Characteristic curves for fan blade element  
(PAE set type section)



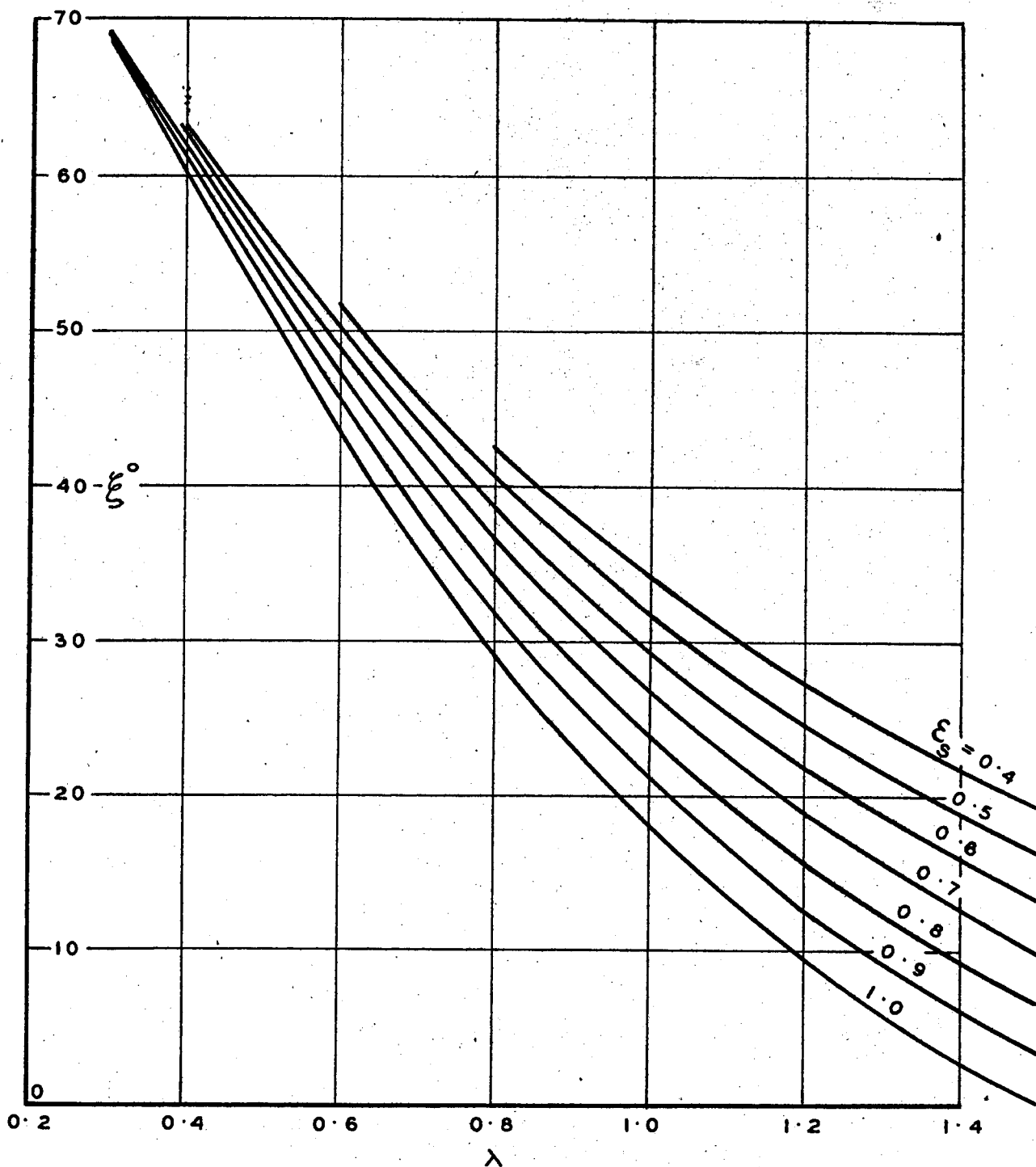
CAMBER ANGLE FOR CASCADE AEROFOIL —  $\epsilon_p = 0$



CAMBER ANGLE FOR CASCADE AEROFOIL —  $\epsilon_s = 0$



FIG. 15



STAGGER ANGLE FOR CASCADE AEROFOIL -  $\varepsilon_p = 0$

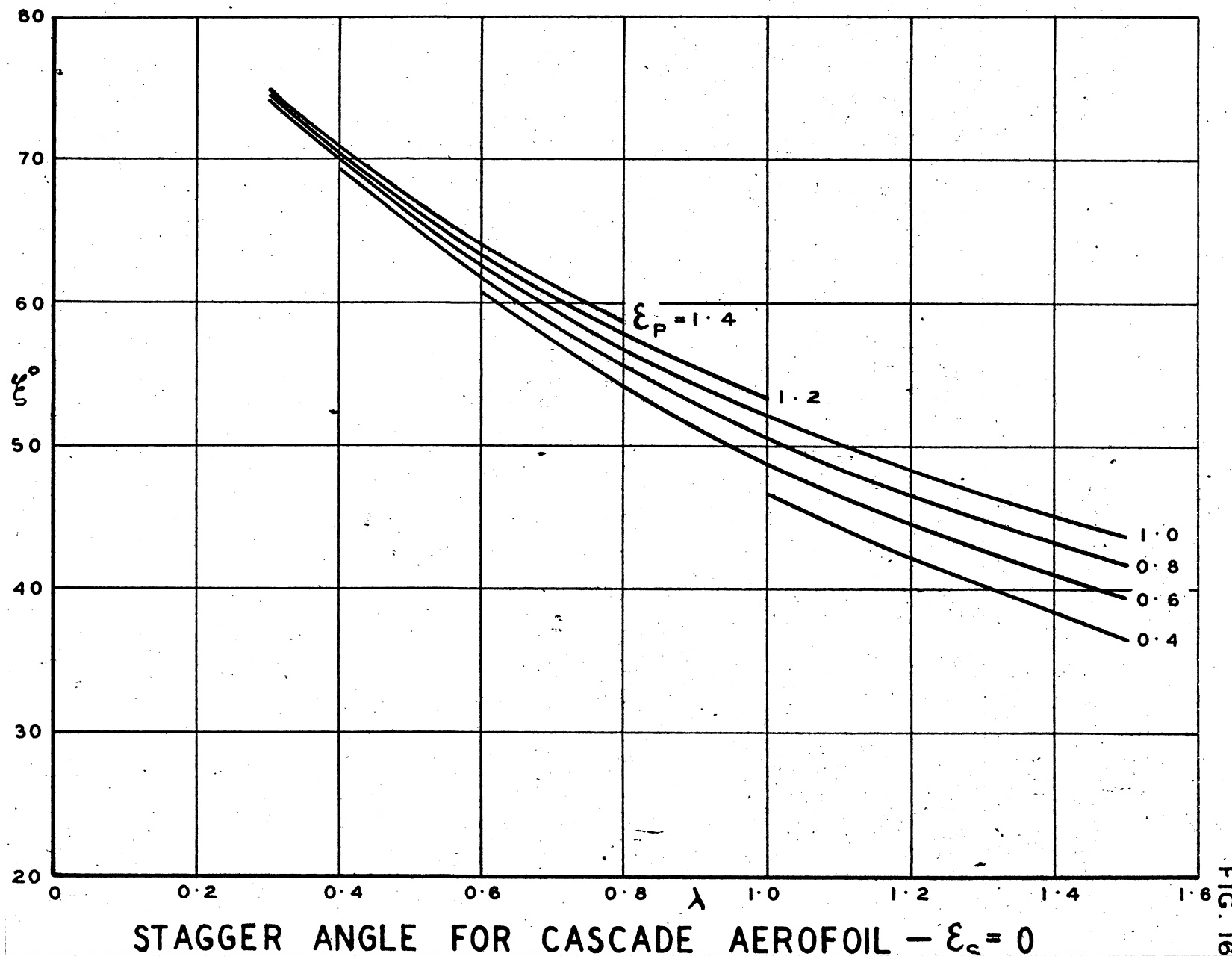
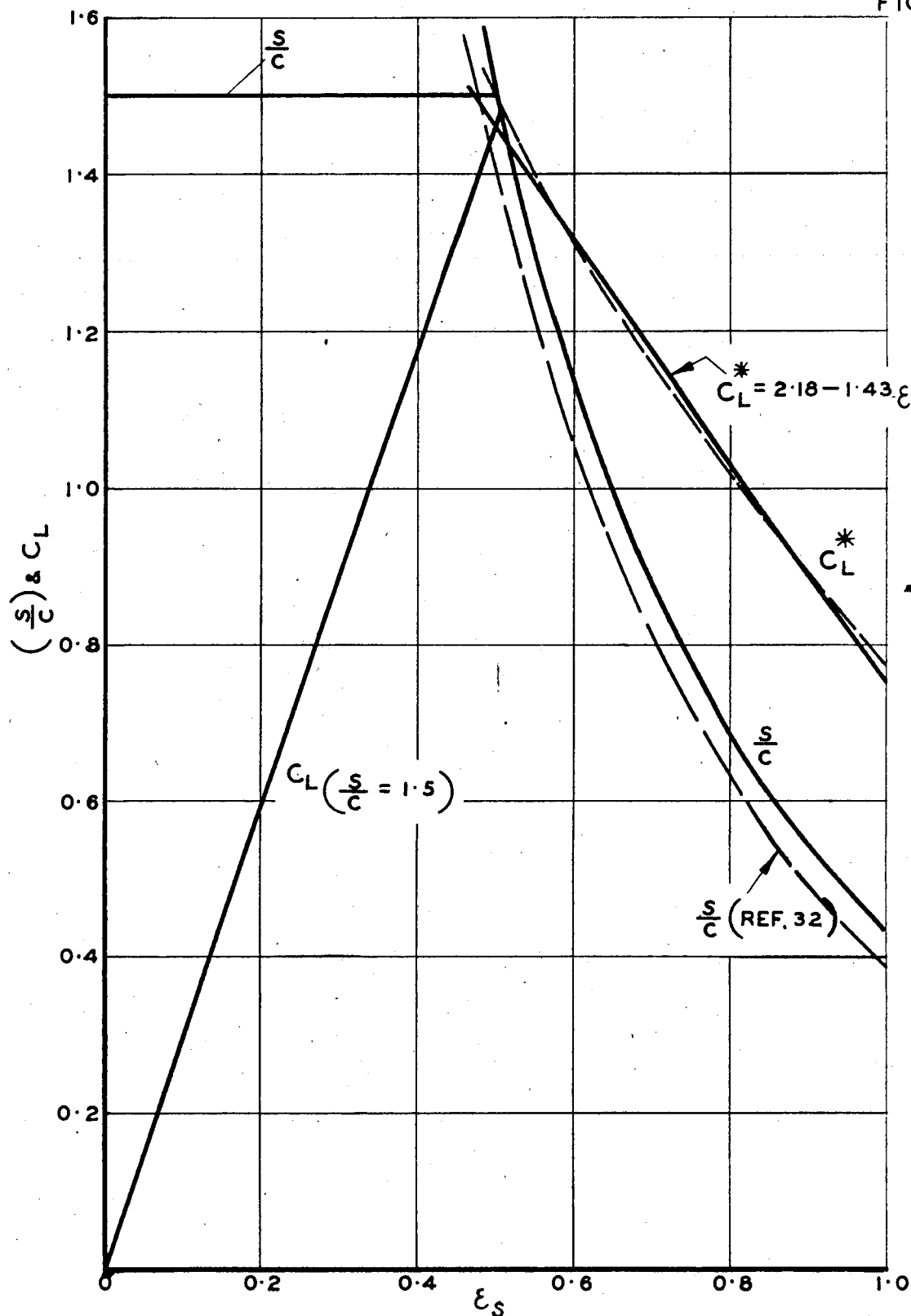
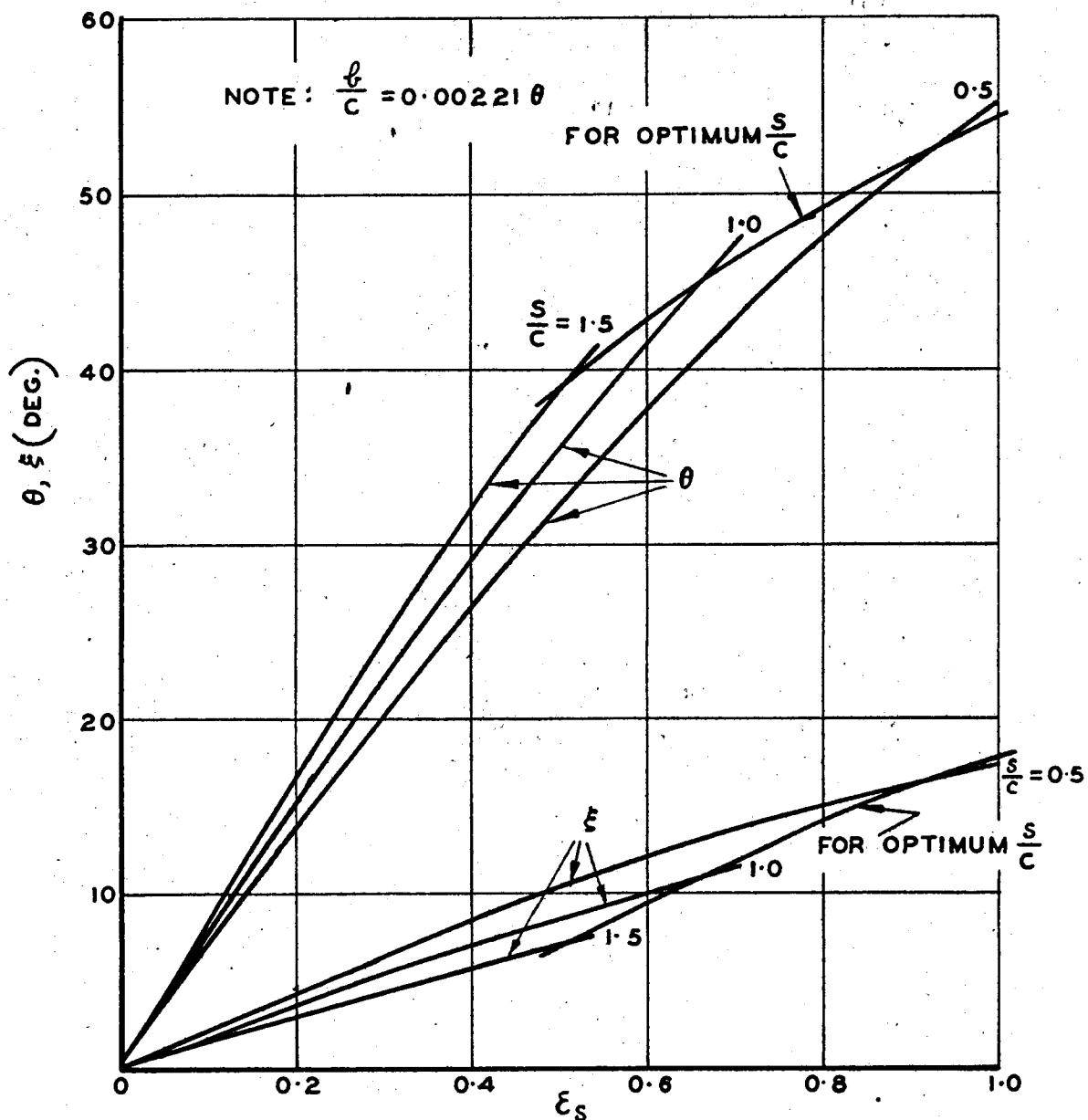


FIG. 17

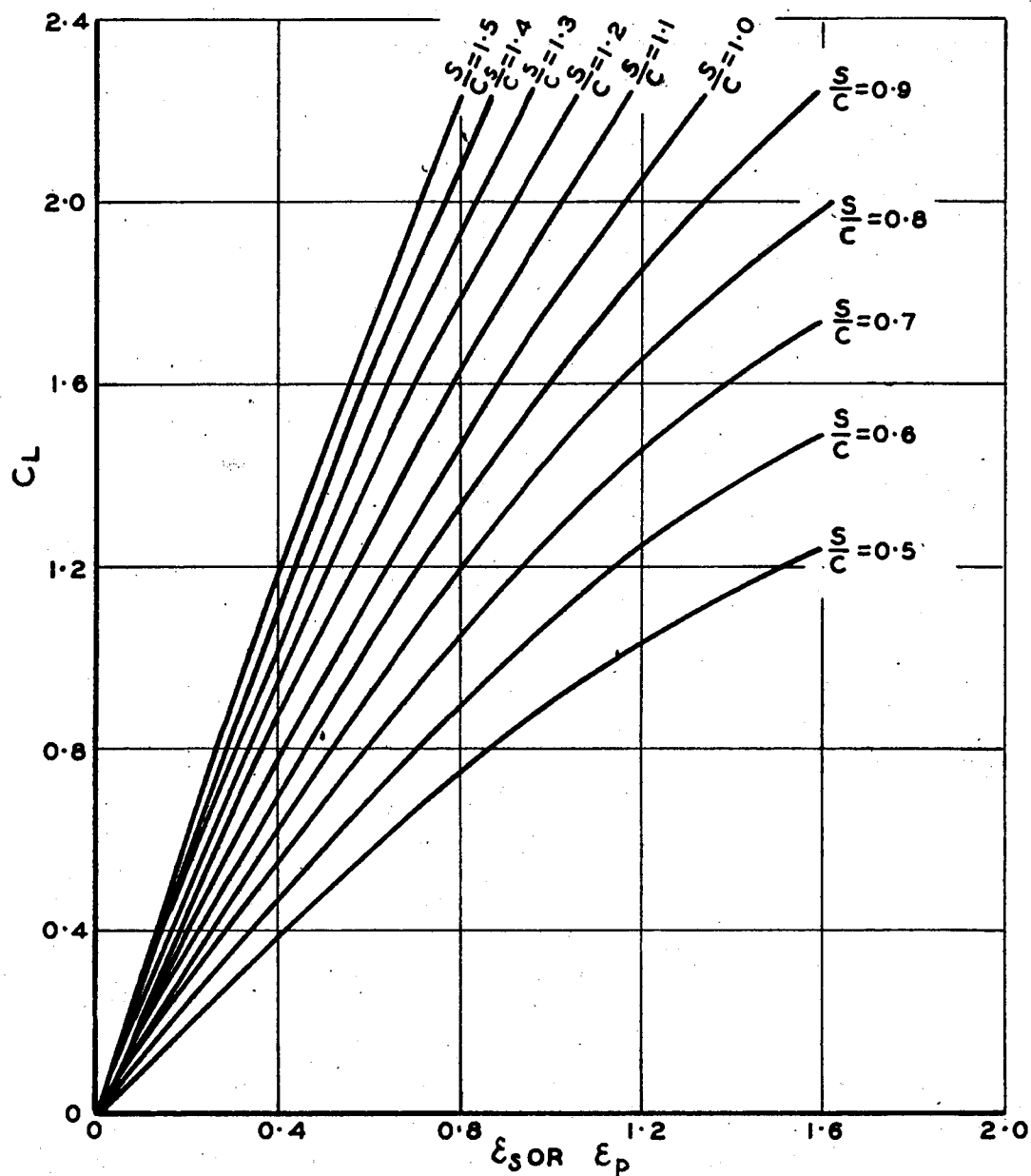


RECOMMENDED VALUES OF  $C_L$  AND  $\frac{S}{C}$  FOR  
CASCADE TYPE STRAIGHTENERS

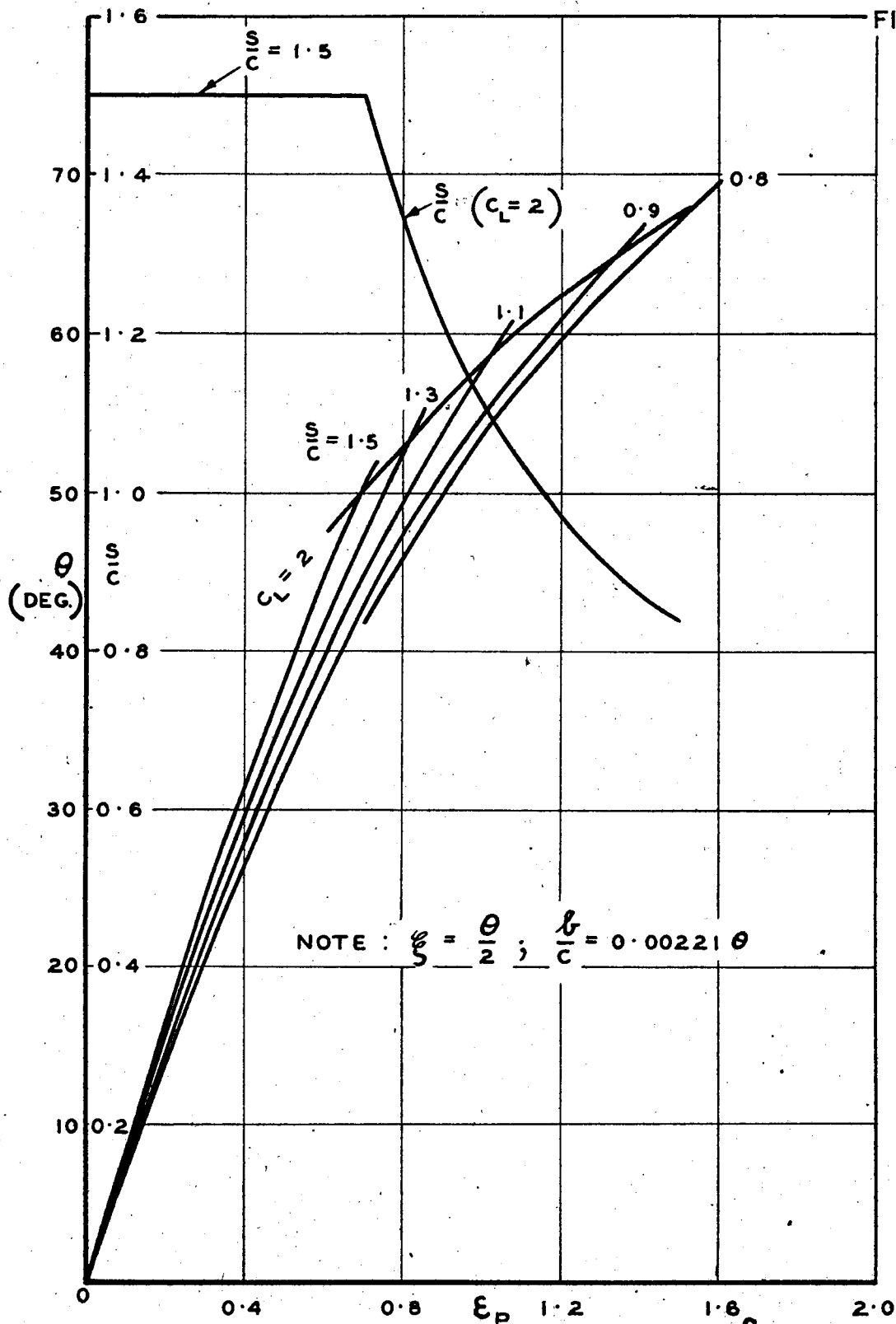


CAMBER AND STAGGER ANGLES FOR  
CASCADE TYPE STRAIGHTENERS

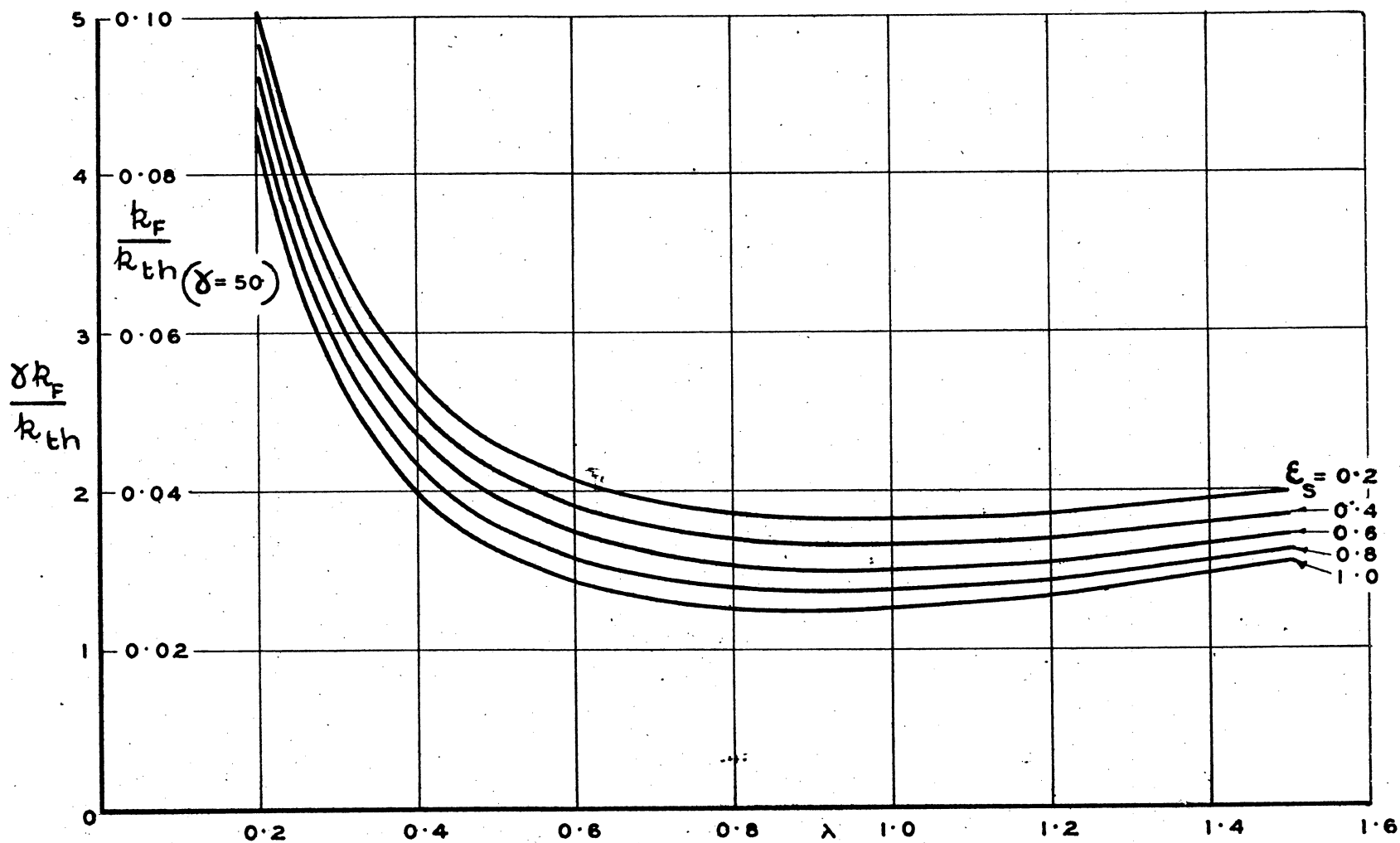
FIG. 19



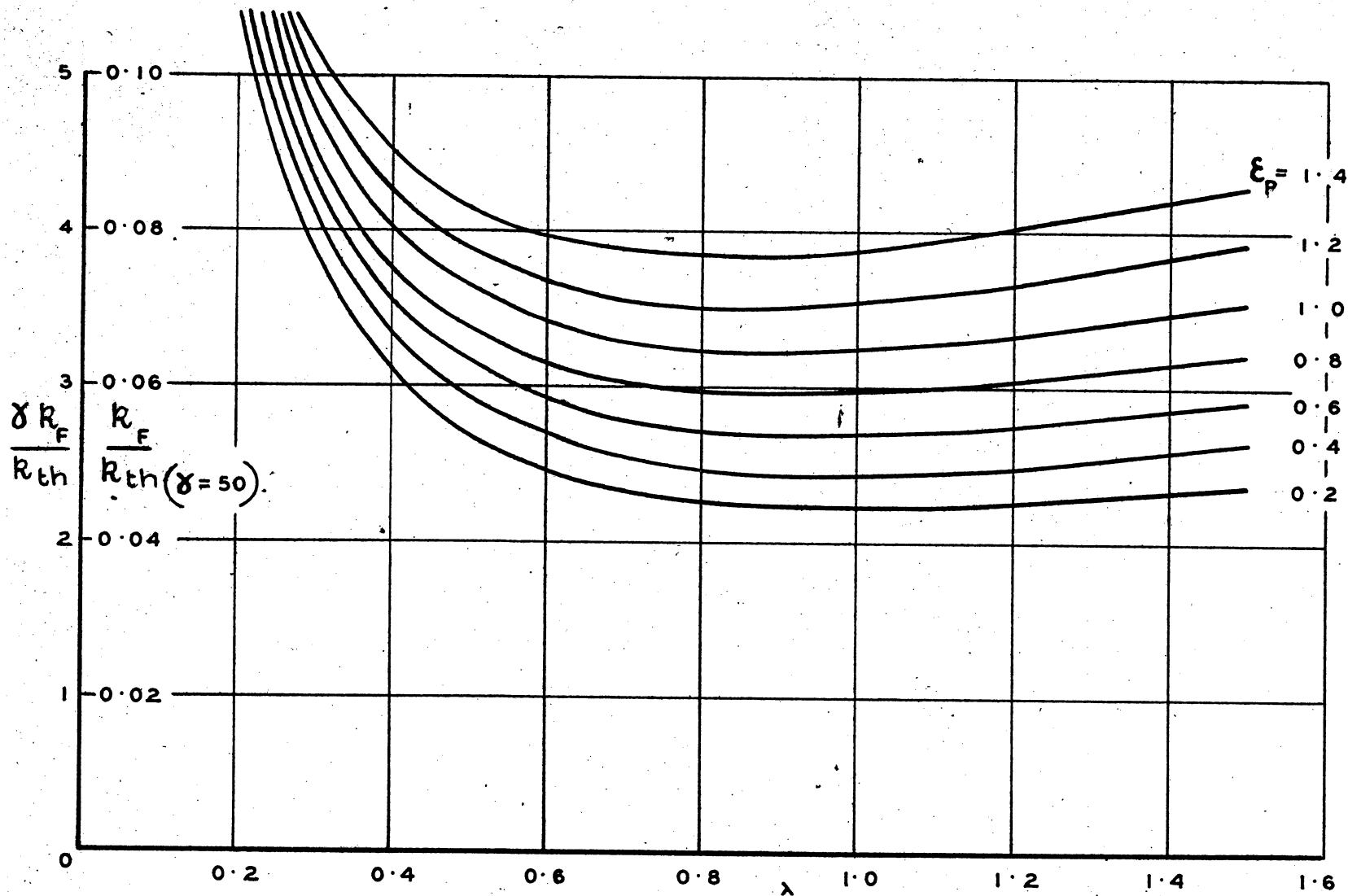
LIFT COEFFICIENTS AND GAP/CHORD RATIOS  
AS FUNCTIONS OF  $\epsilon$  - GENERAL APPLICATION



CAMBER ANGLES AND RECOMMENDED  $\frac{S}{C}$  FOR  
CASCADE TYPE PREROTATORS

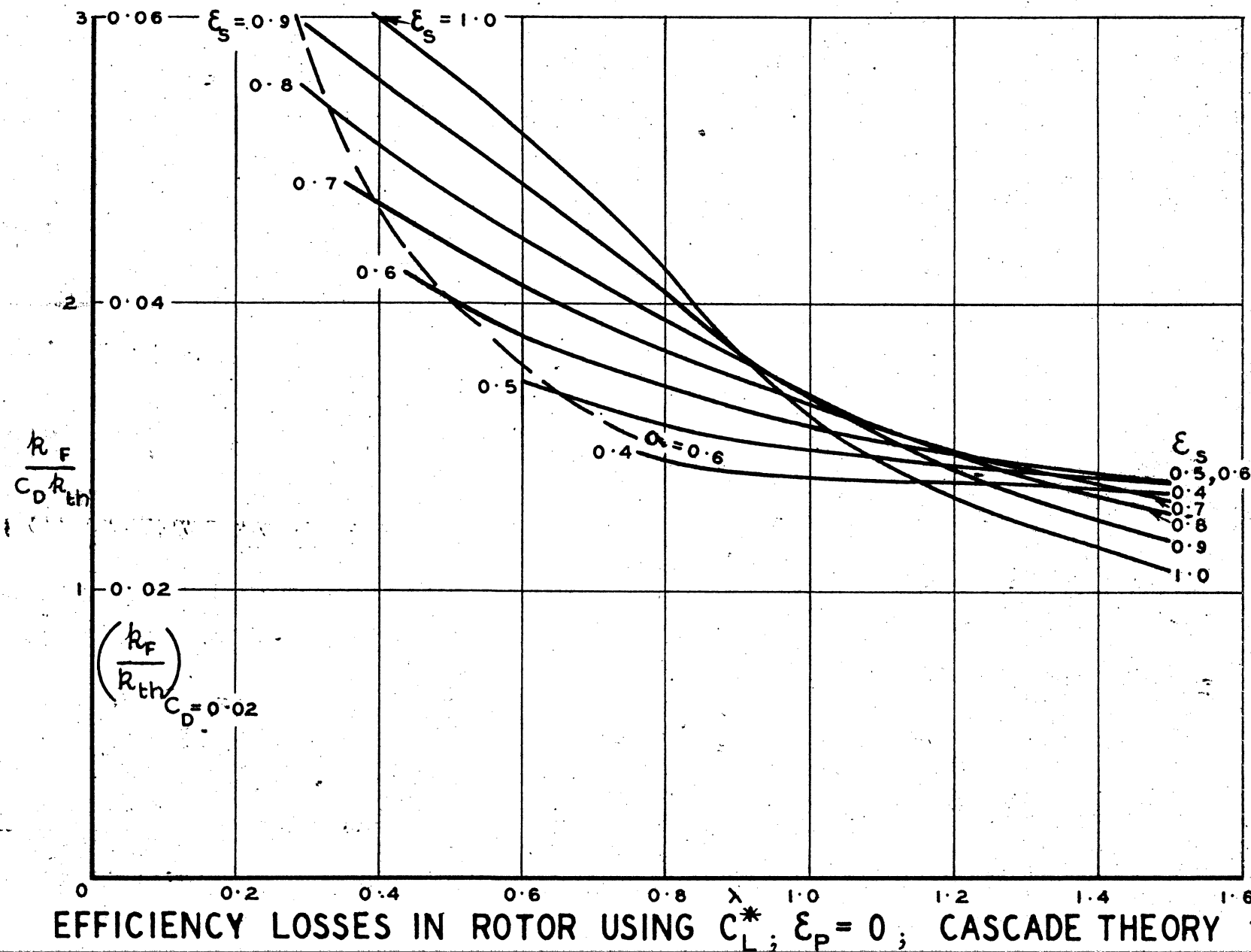


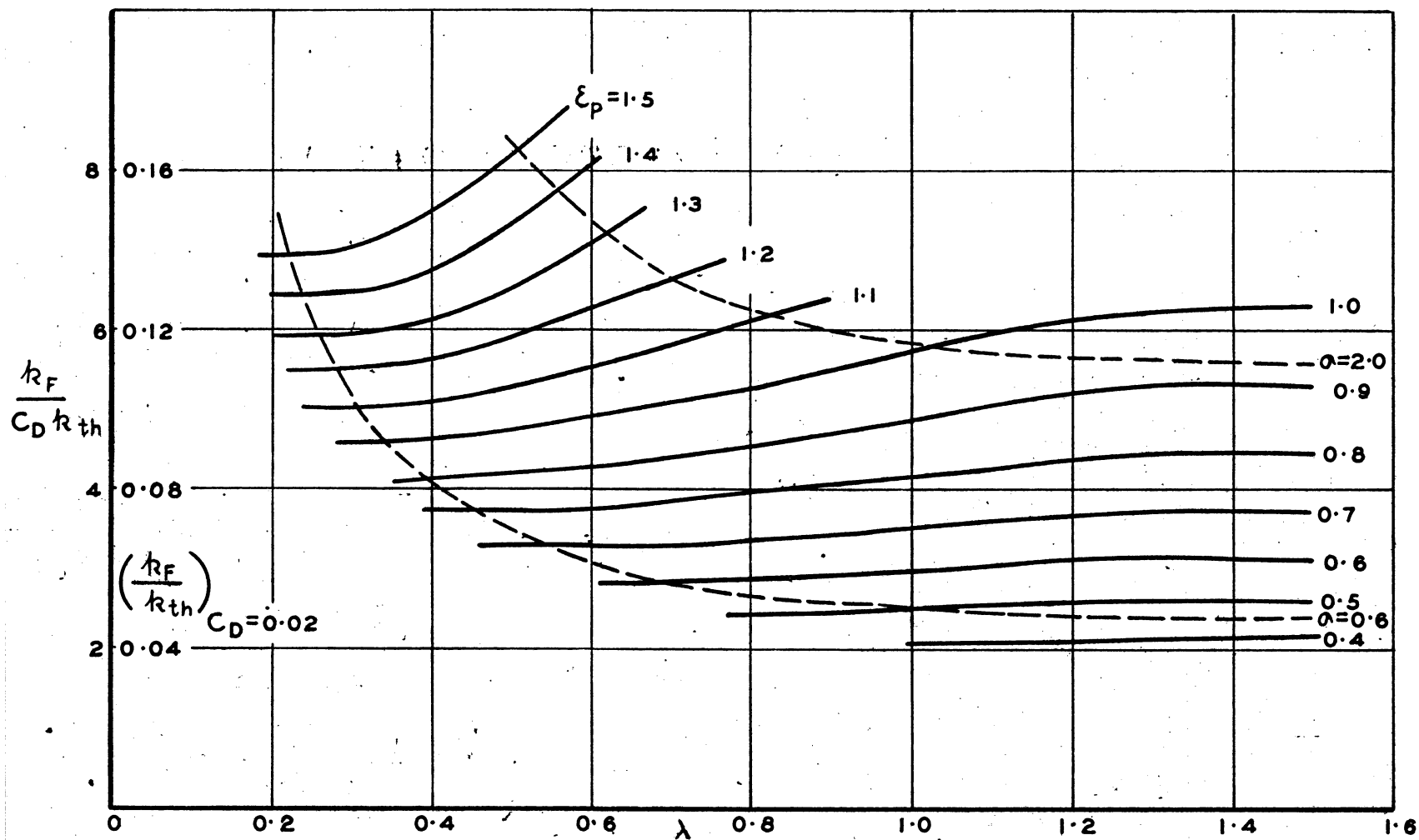
EFFICIENCY LOSSES IN ROTOR FOR  $\epsilon_p = 0$  — GENERAL APPLICATION



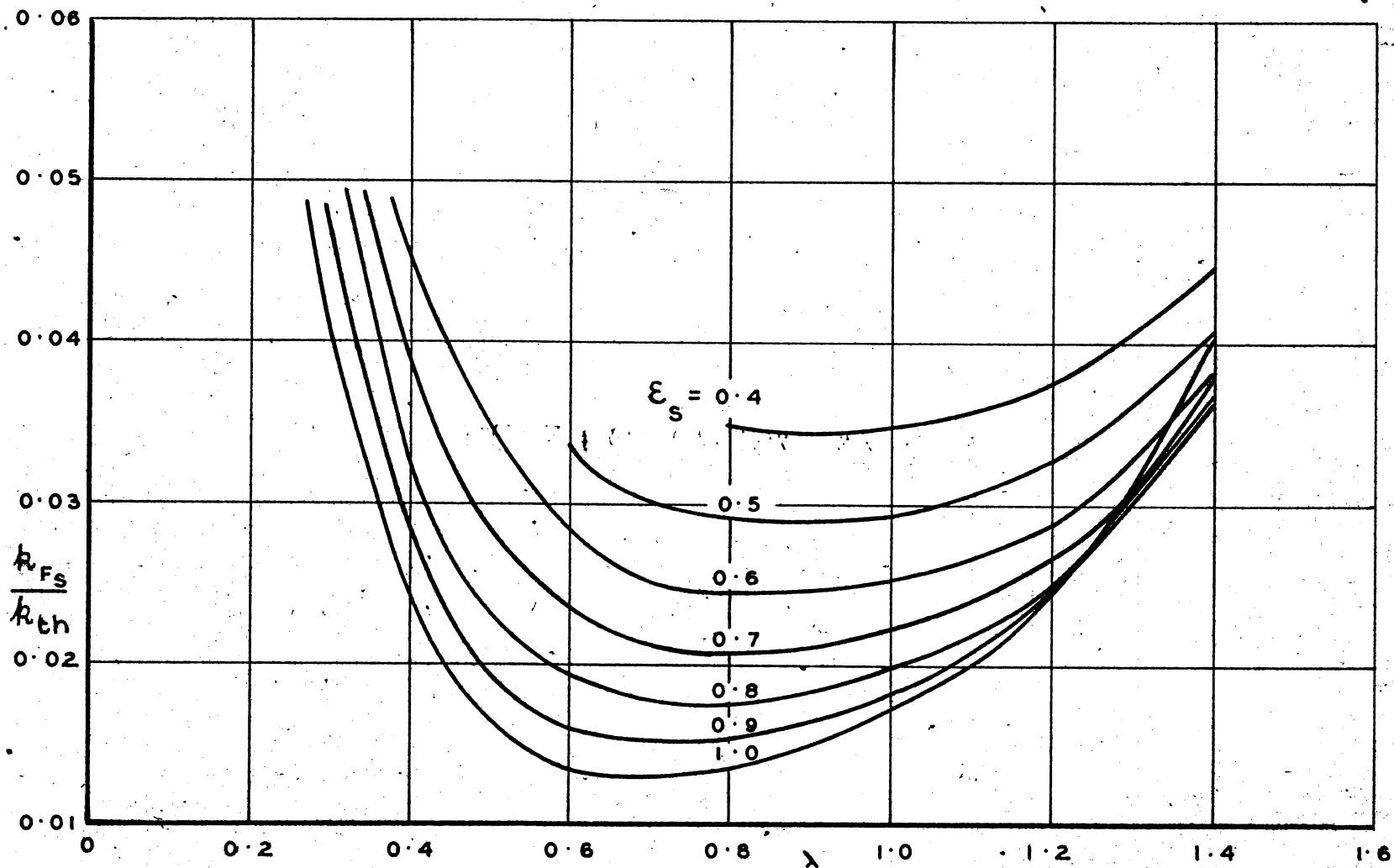
EFFICIENCY LOSSES IN ROTOR FOR  $\epsilon_s = 0$  — GENERAL APPLICATION



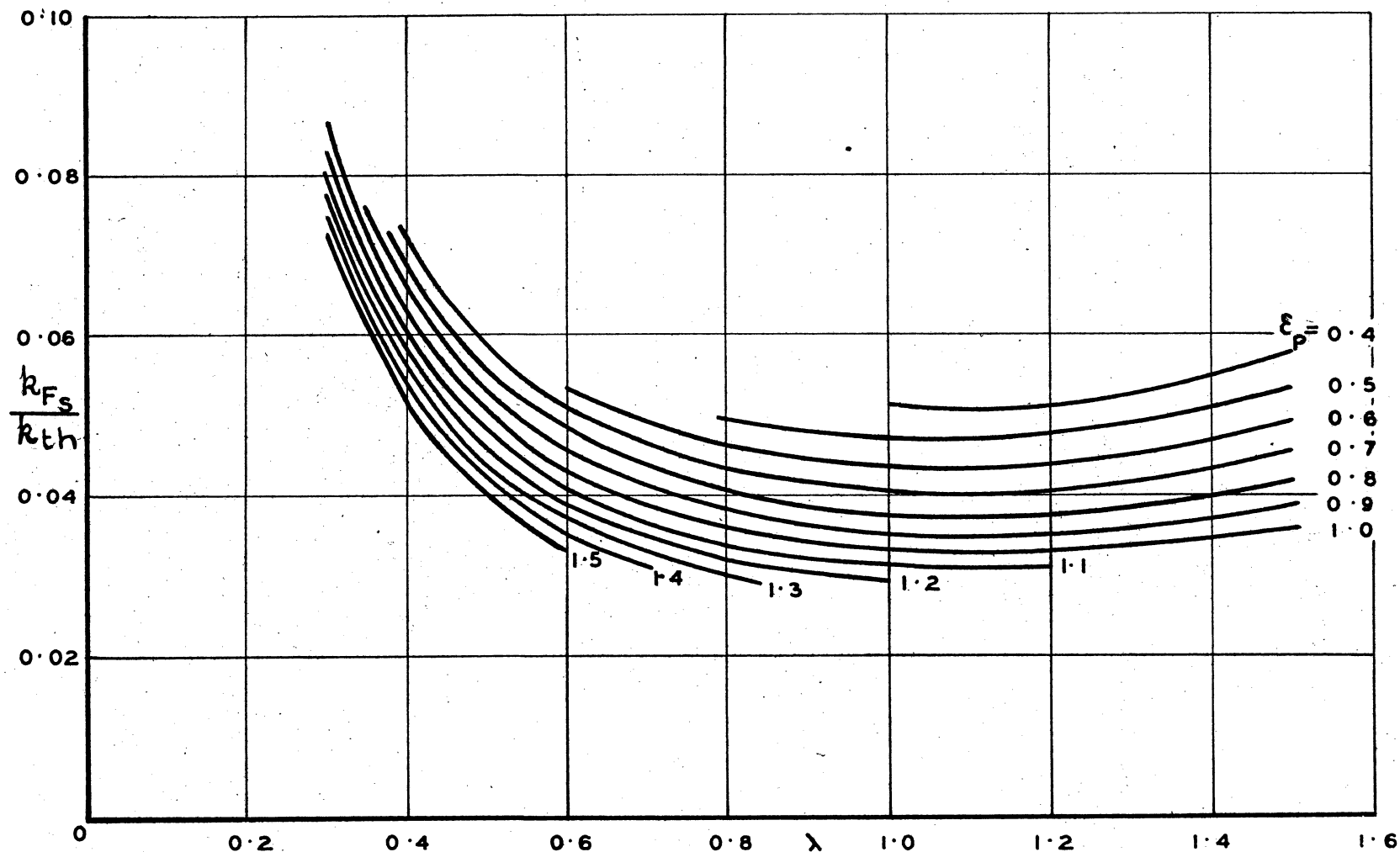




EFFICIENCY LOSSES IN ROTOR USING  $C_L^*$ ;  $\epsilon_s=0$ ; CASCADE THEORY

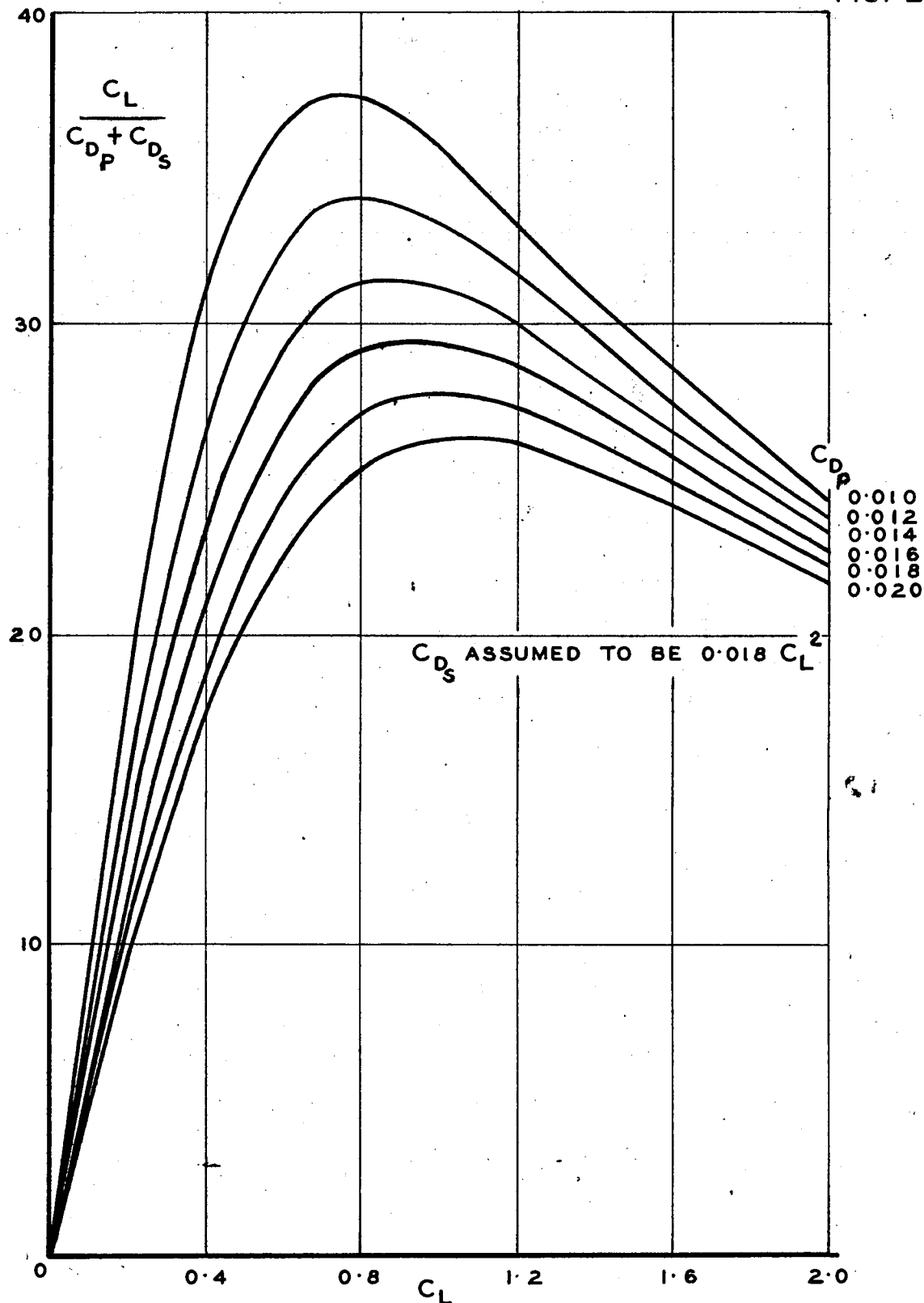


LOSSES DUE TO SECONDARY DRAG,  $\epsilon_p = 0$  — CASCADE THEORY

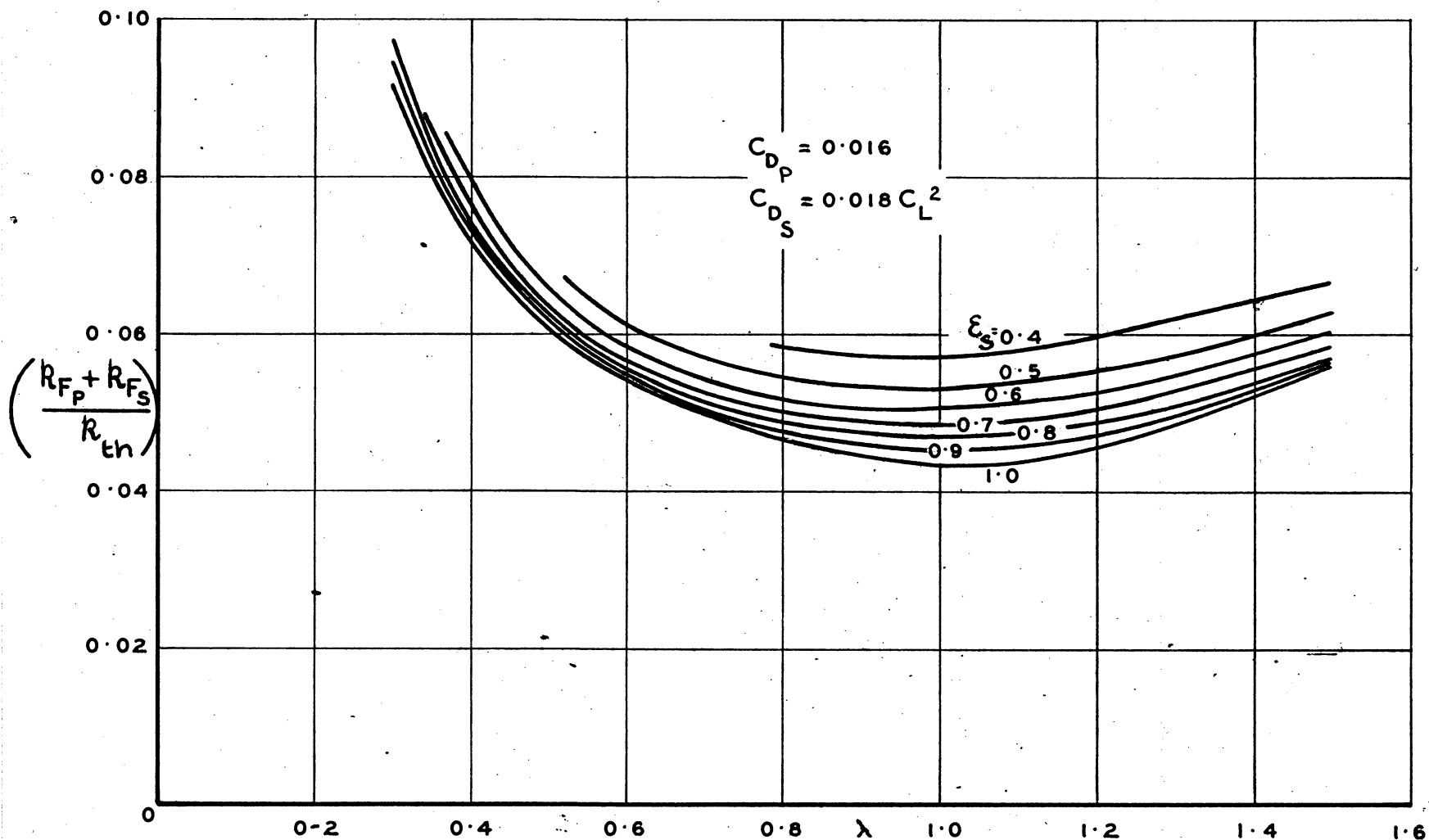


LOSSES DUE TO SECONDARY DRAG,  $\epsilon_s = 0$  — CASCADE THEORY

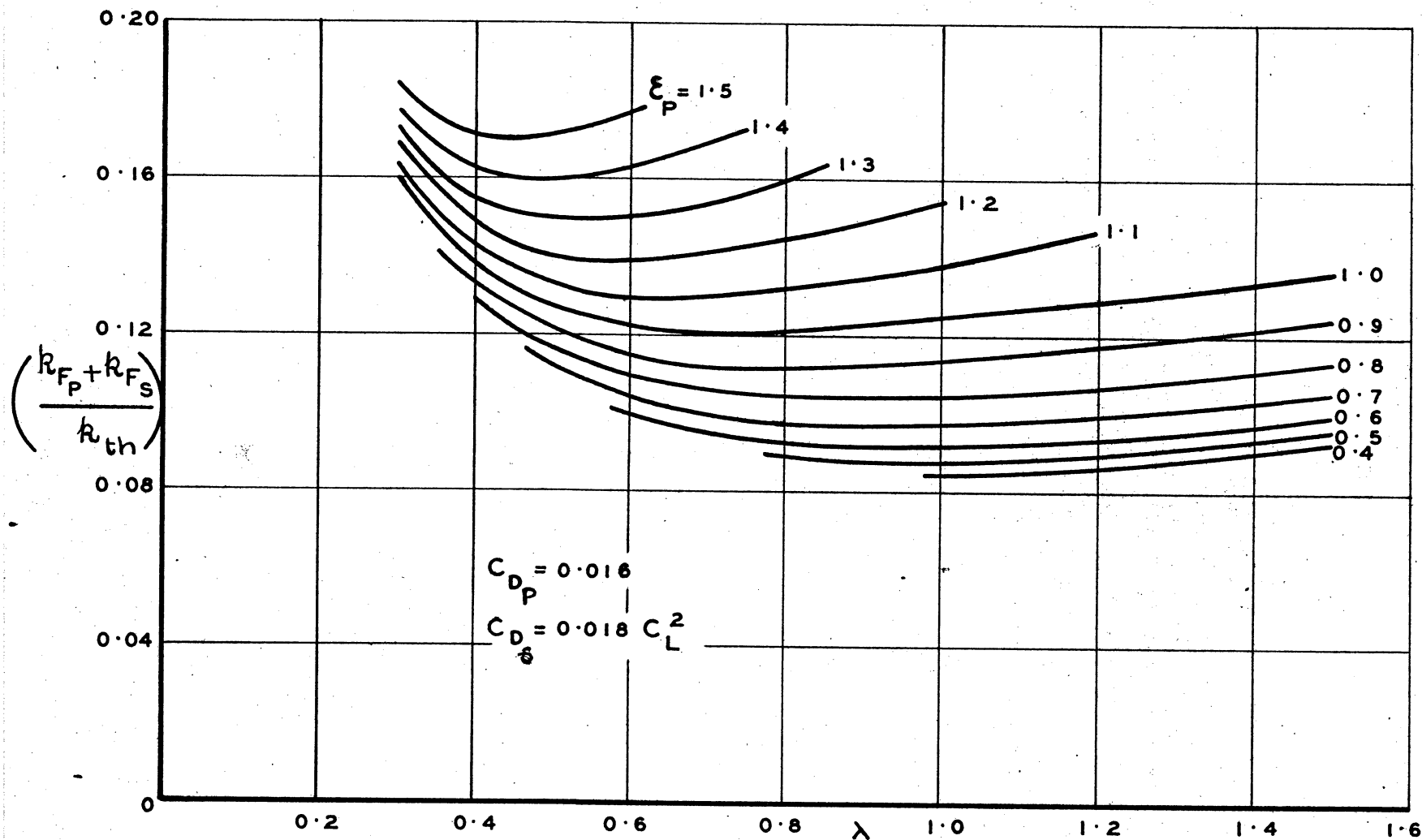
FIG. 27



EFFECT OF  $C_L$  ON LIFT / DRAG RATIO  
GENERAL APPLICATION

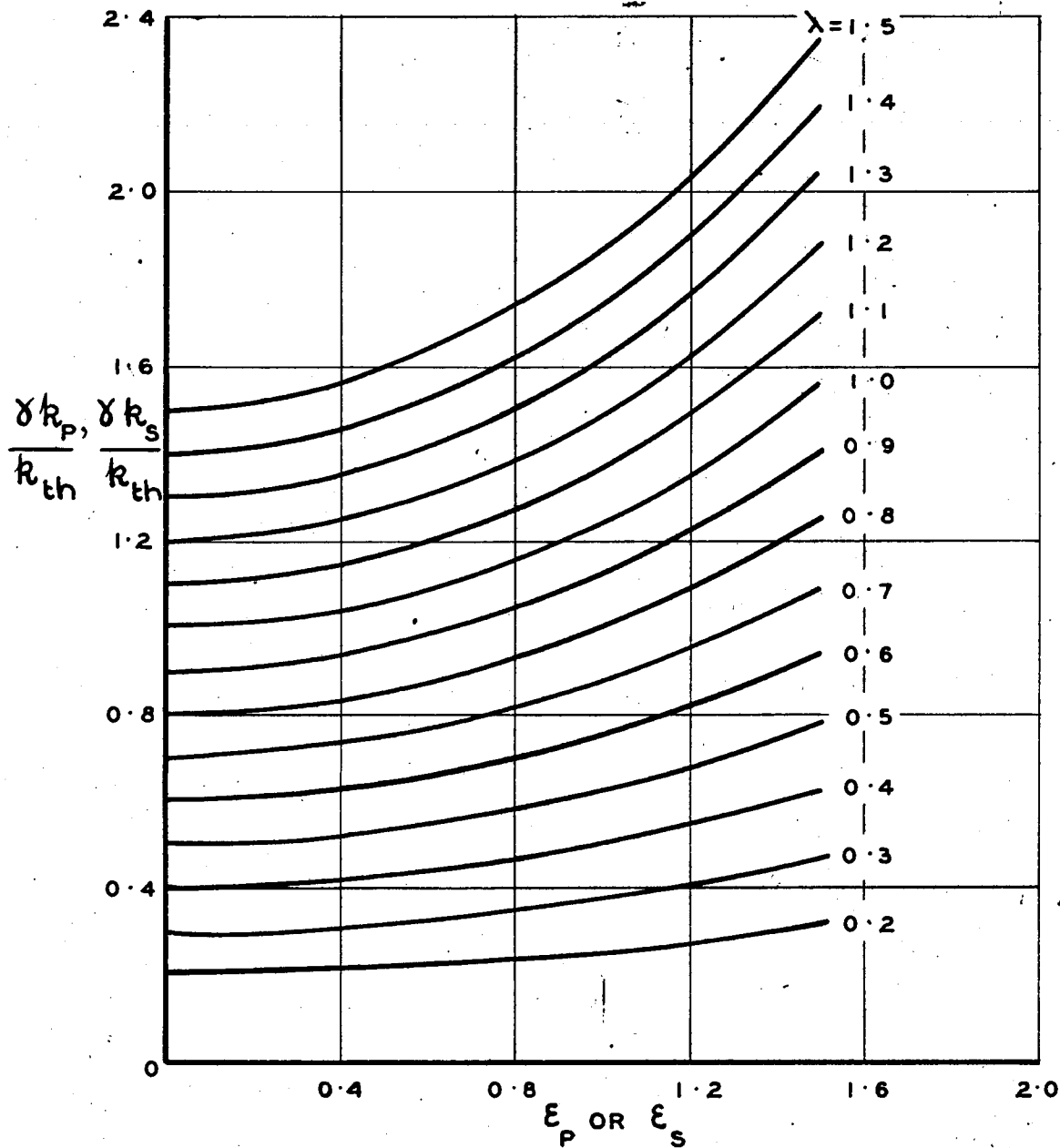


LOSS IN EFFICIENCY DUE TO PROFILE AND  
SECONDARY LOSSES  $\epsilon_p = 0$  — CASCADE THEORY



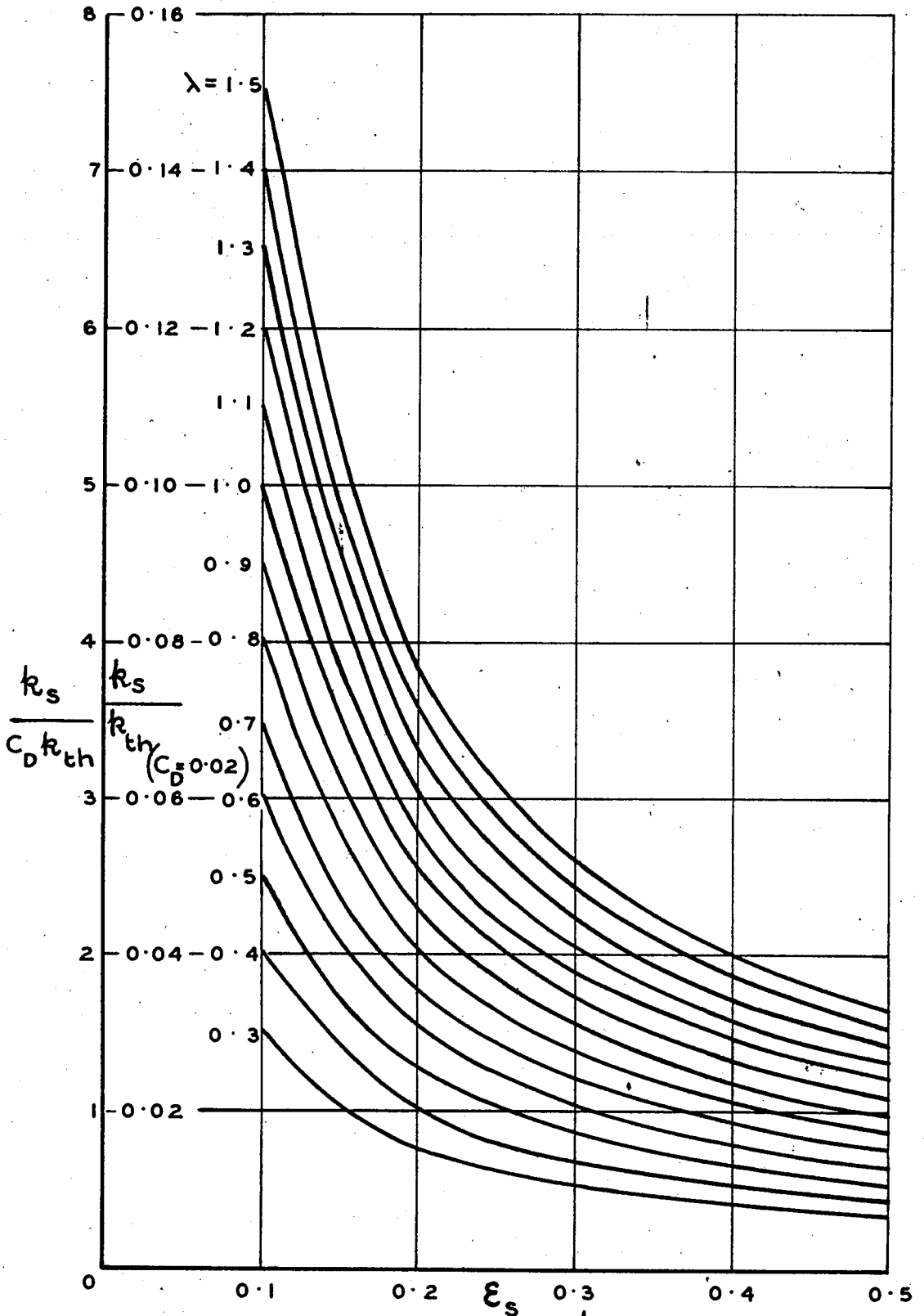
LOSS IN EFFICIENCY DUE TO PROFILE AND  
SECONDARY LOSSES  $\xi_s = 0$  — CASCADE THEORY

FIG. 30



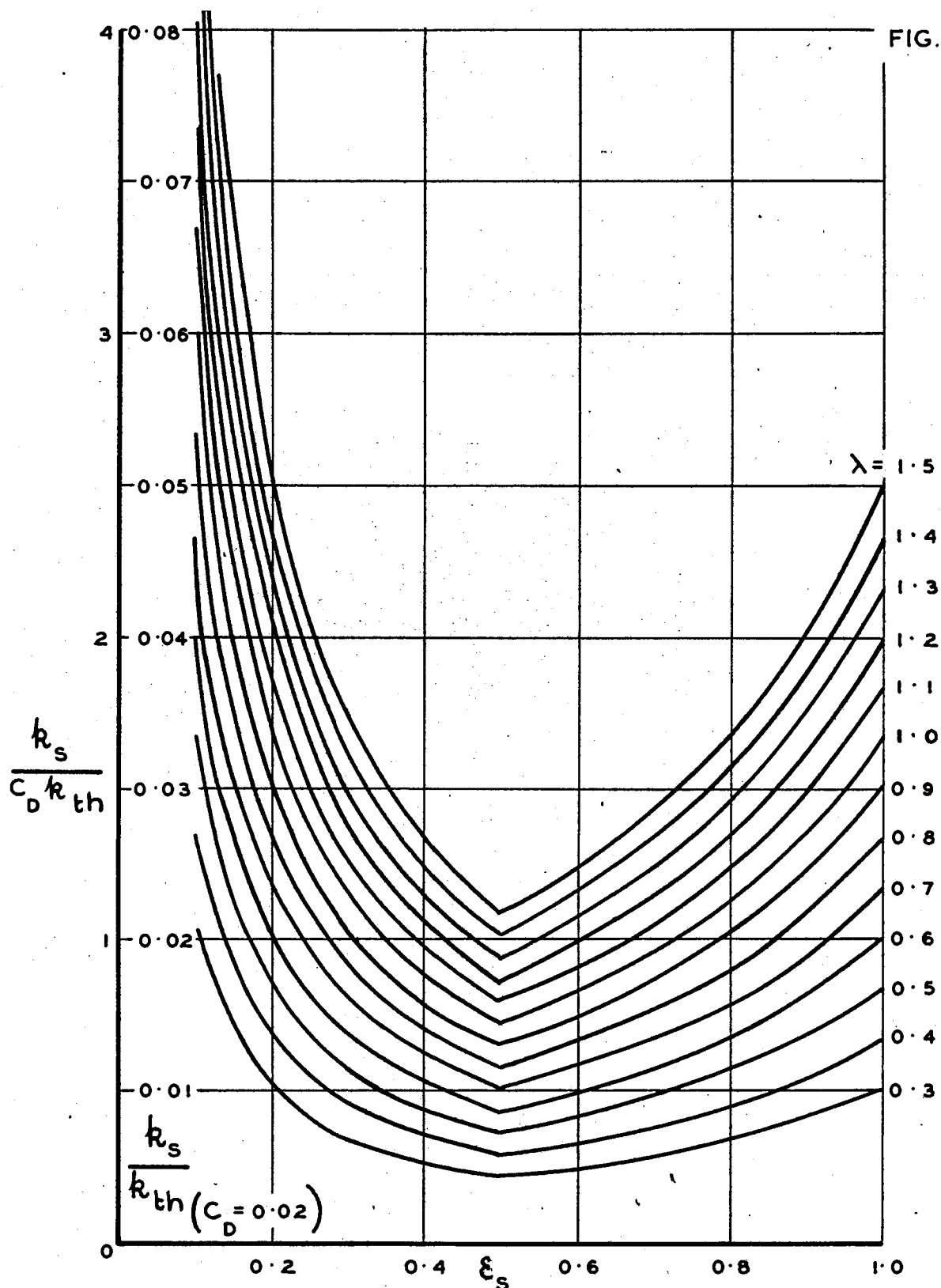
EFFICIENCY LOSSES IN STATORS  
GENERAL APPLICATION





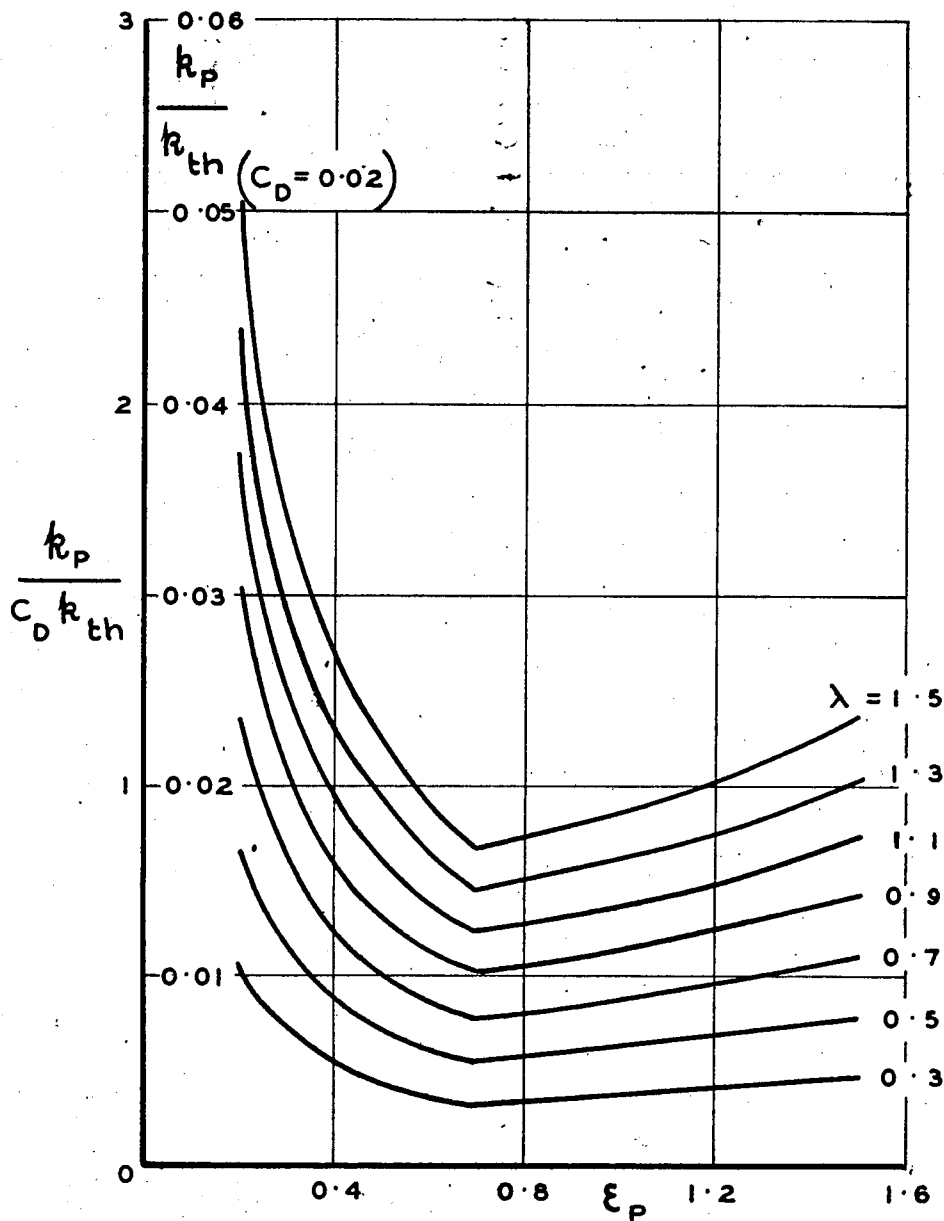
EFFICIENCY LOSSES IN  
N.P.L. TYPE STRAIGHTENERS

FIG. 32



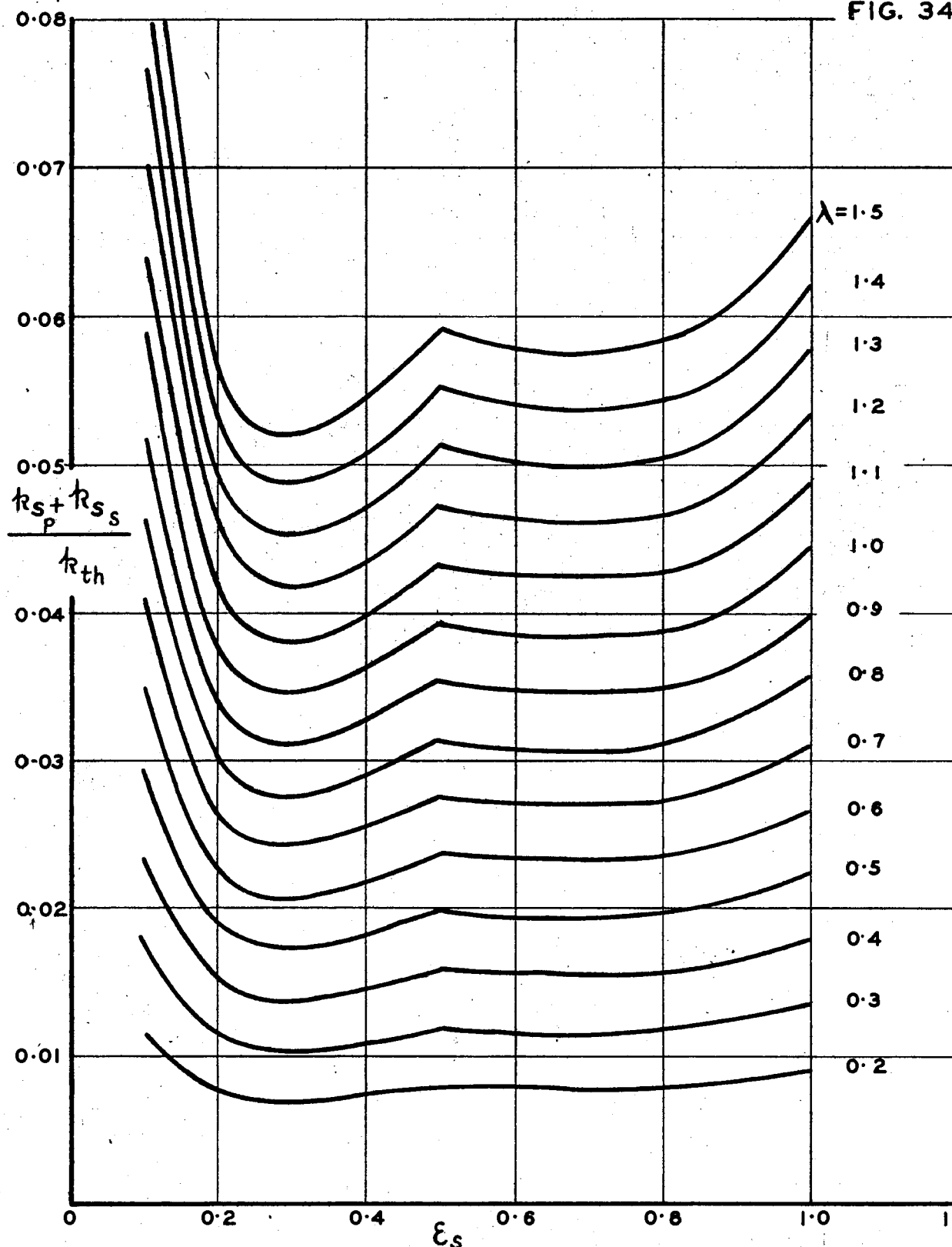
LOSSES IN CASCADE TYPE STRAIGHTENERS FOR  
RECOMMENDATIONS OF SECTION 3.3

FIG. 33



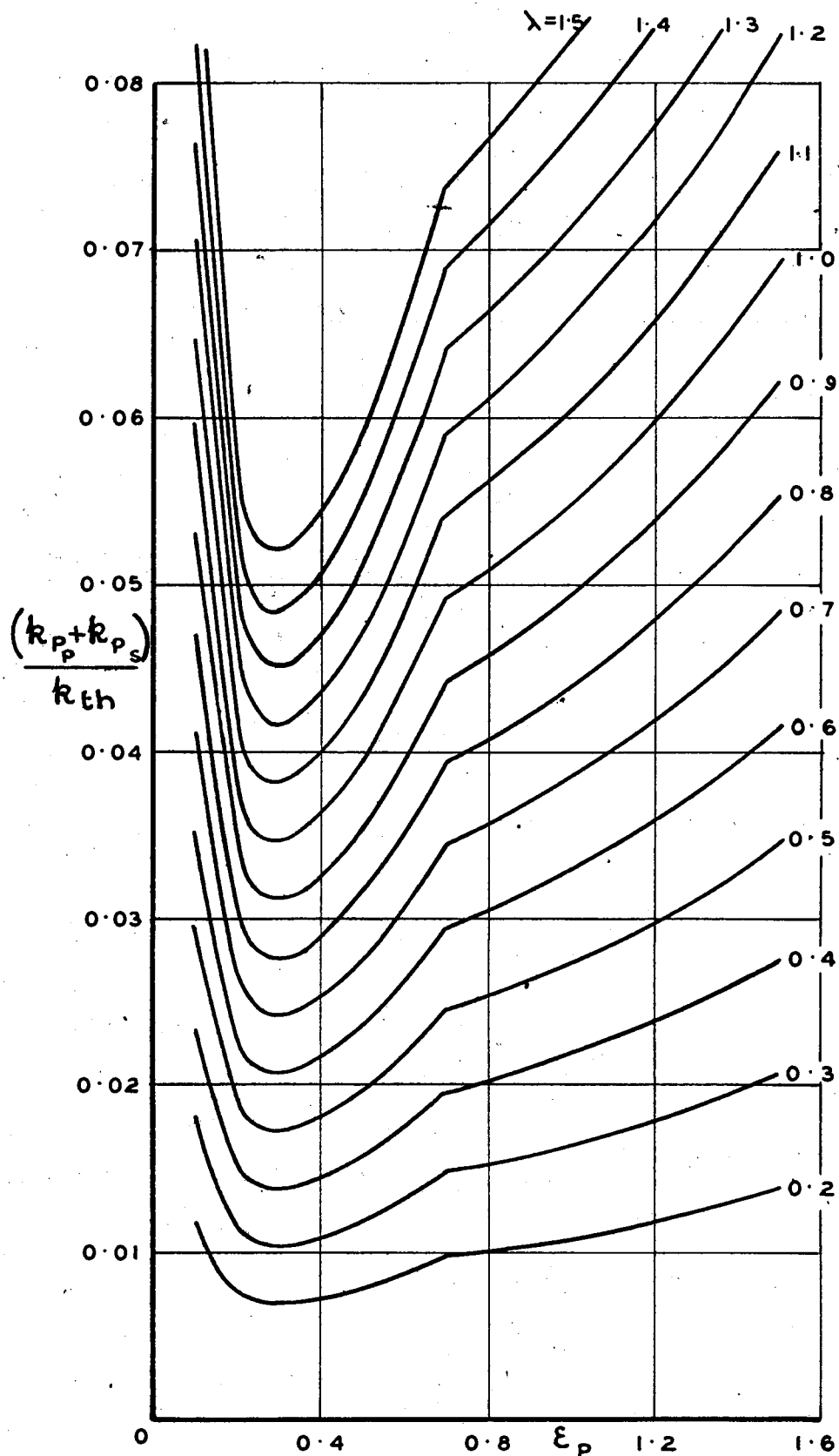
LOSSES IN CASCADE TYPE PREROTATORS FOR  
RECOMMENDATIONS OF SECTION 3.4

FIG. 34



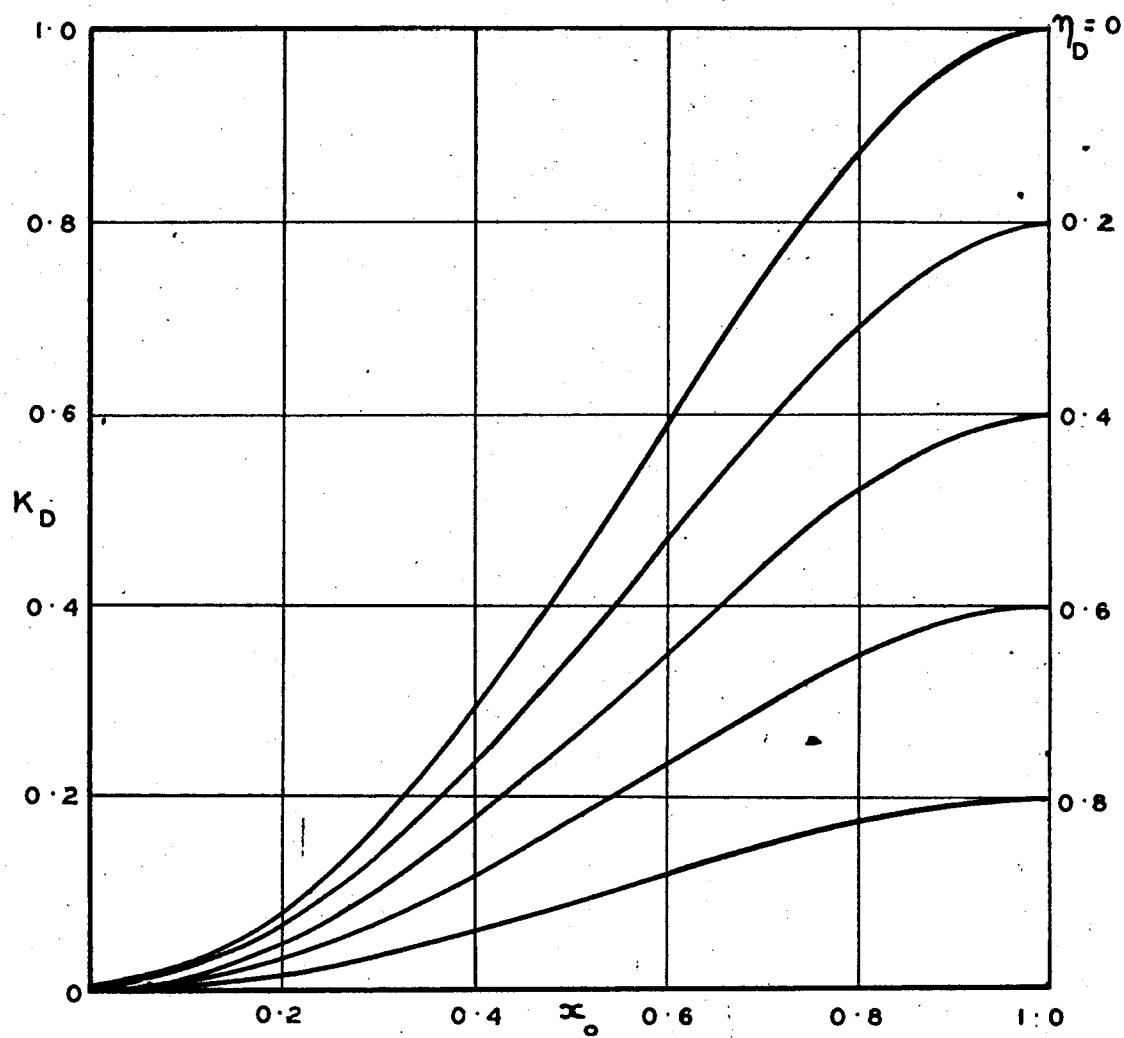
EFFICIENCY LOSSES IN CASCADE TYPE STRAIGHTENERS FOR  
RECOMMENDATIONS OF SECTION 3.3

FIG. 35



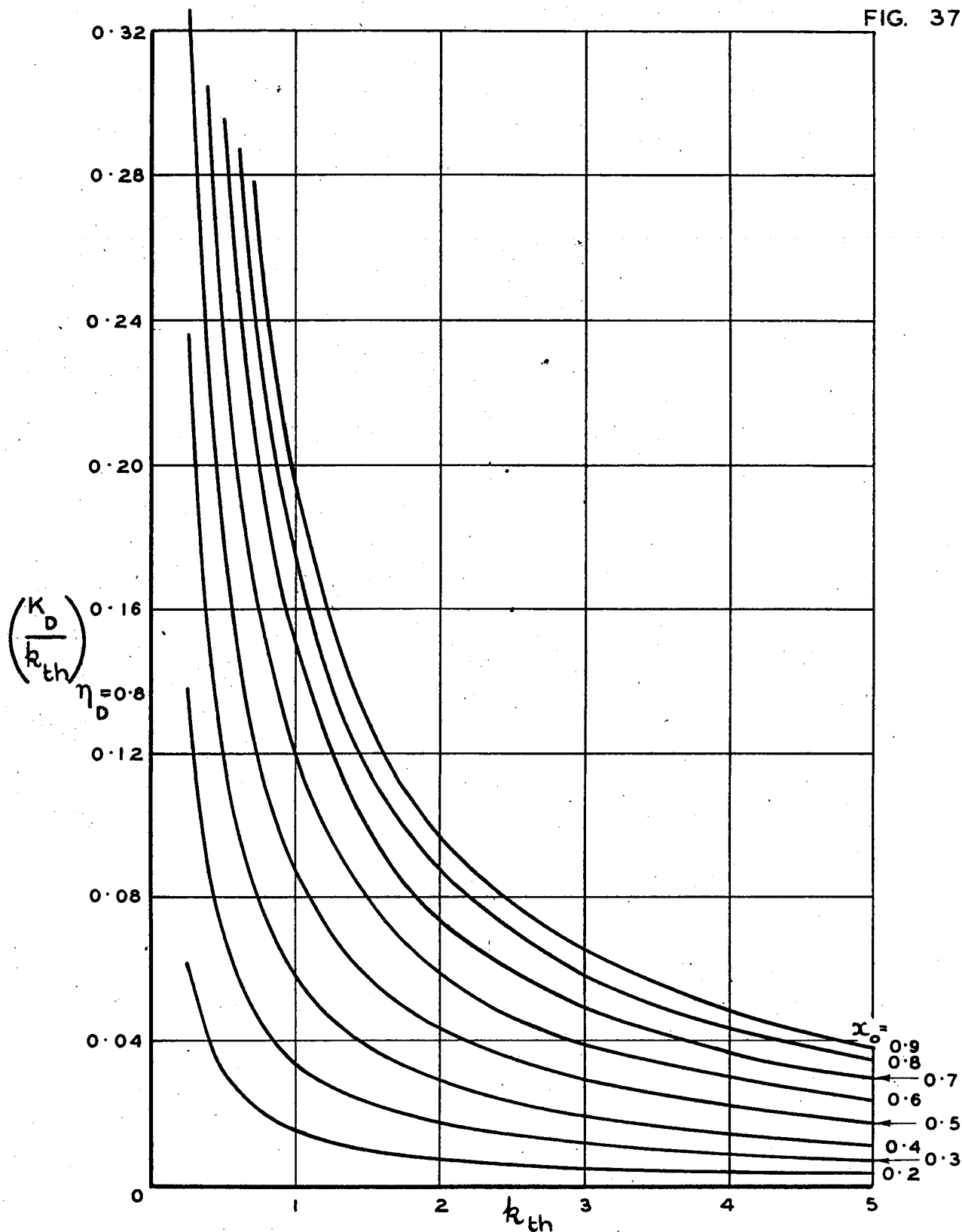
EFFICIENCY LOSSES IN CASCADE TYPE  
PREROTATORS FOR RECOMMENDATIONS OF  
SECTION 3.4

FIG. 36



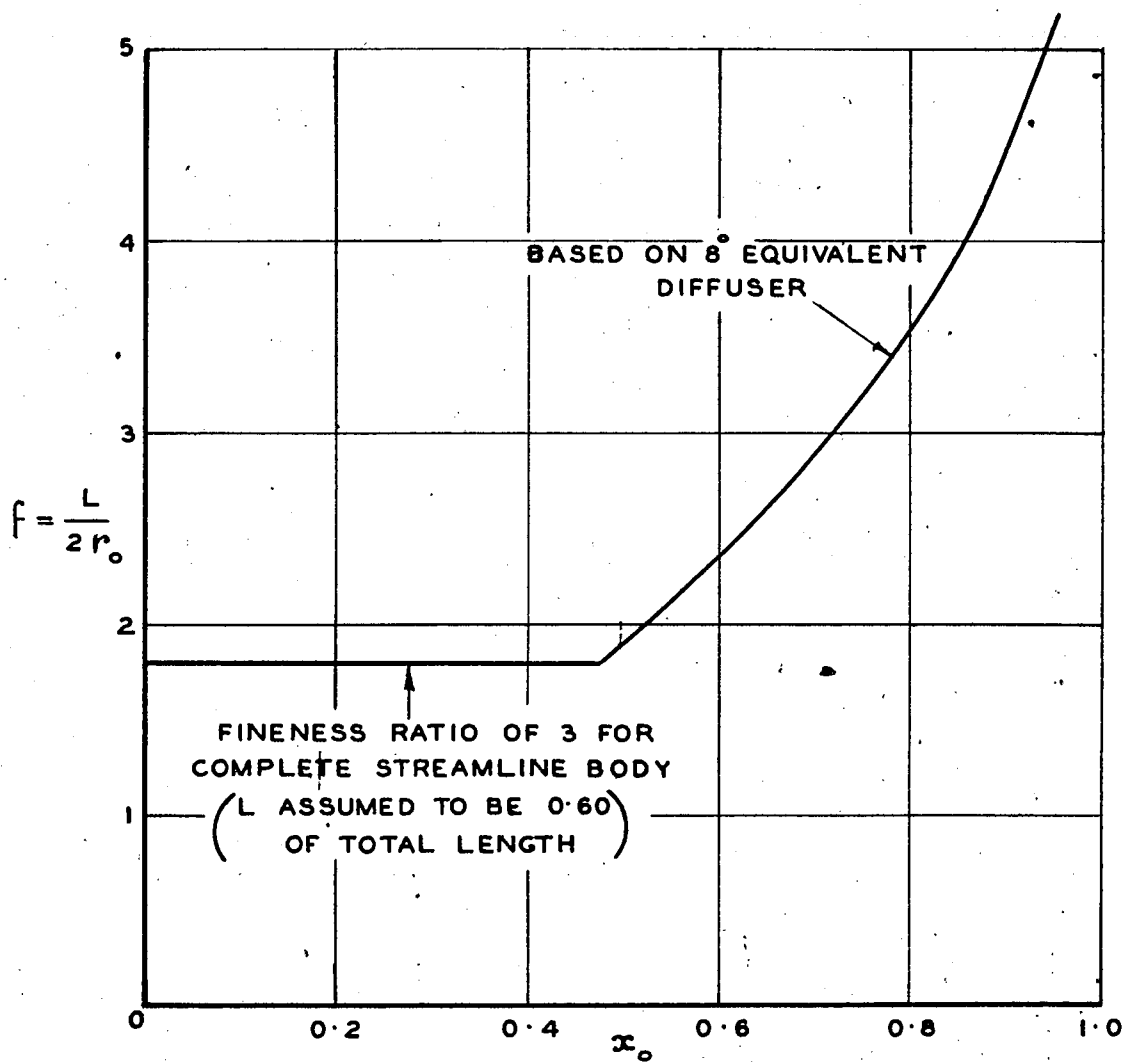
DIFFUSION LOSSES OVER TAIL FAIRING

FIG. 37



LOSS IN EFFICIENCY DUE TO DIFFUSION ( $\eta_D = 0.80$ )

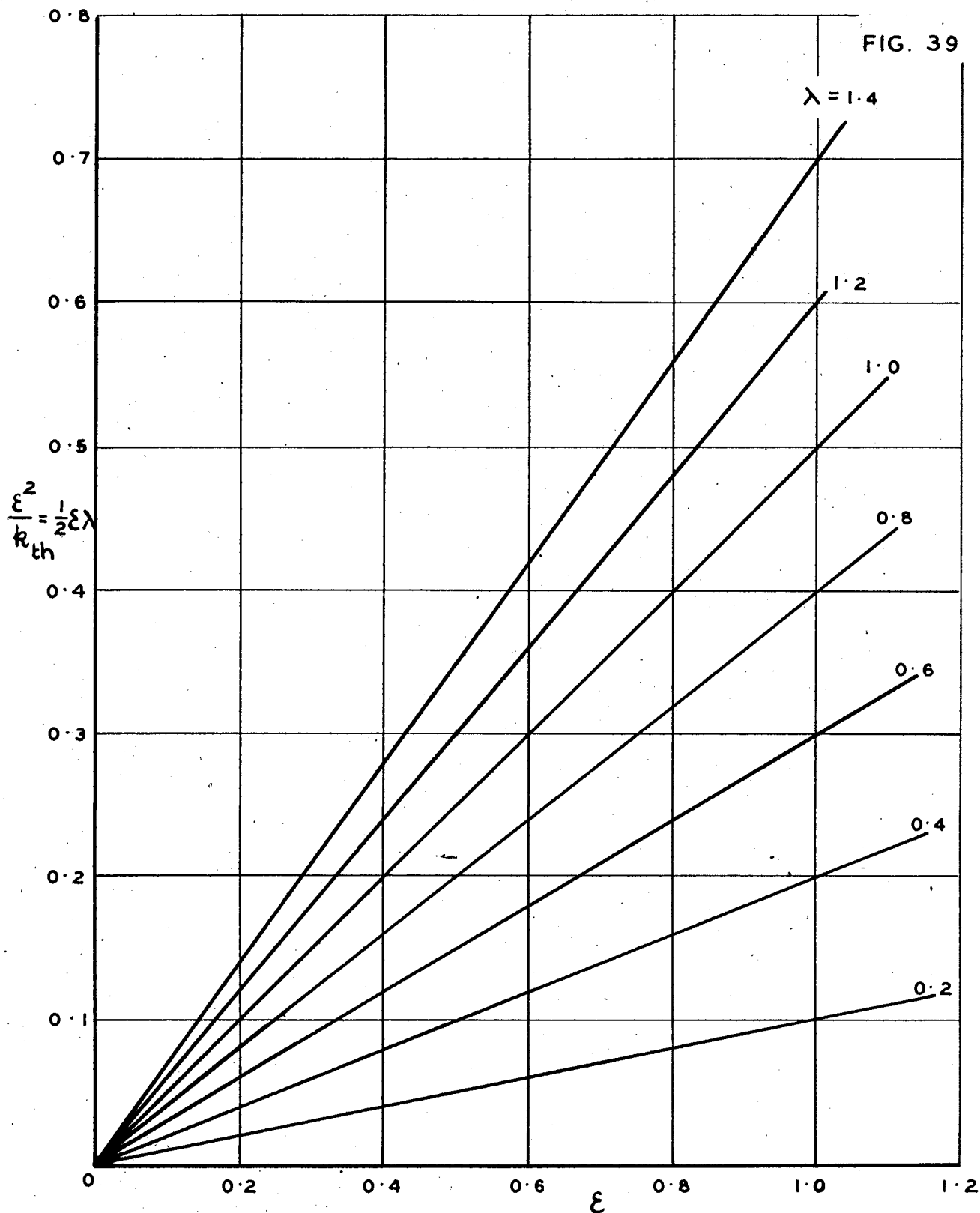
FIG. 38



FINENESS RATIO OF TAIL FAIRING



FIG. 39



EFFICIENCY LOSS DUE TO SWIRL  
NO STATORS PROVIDED

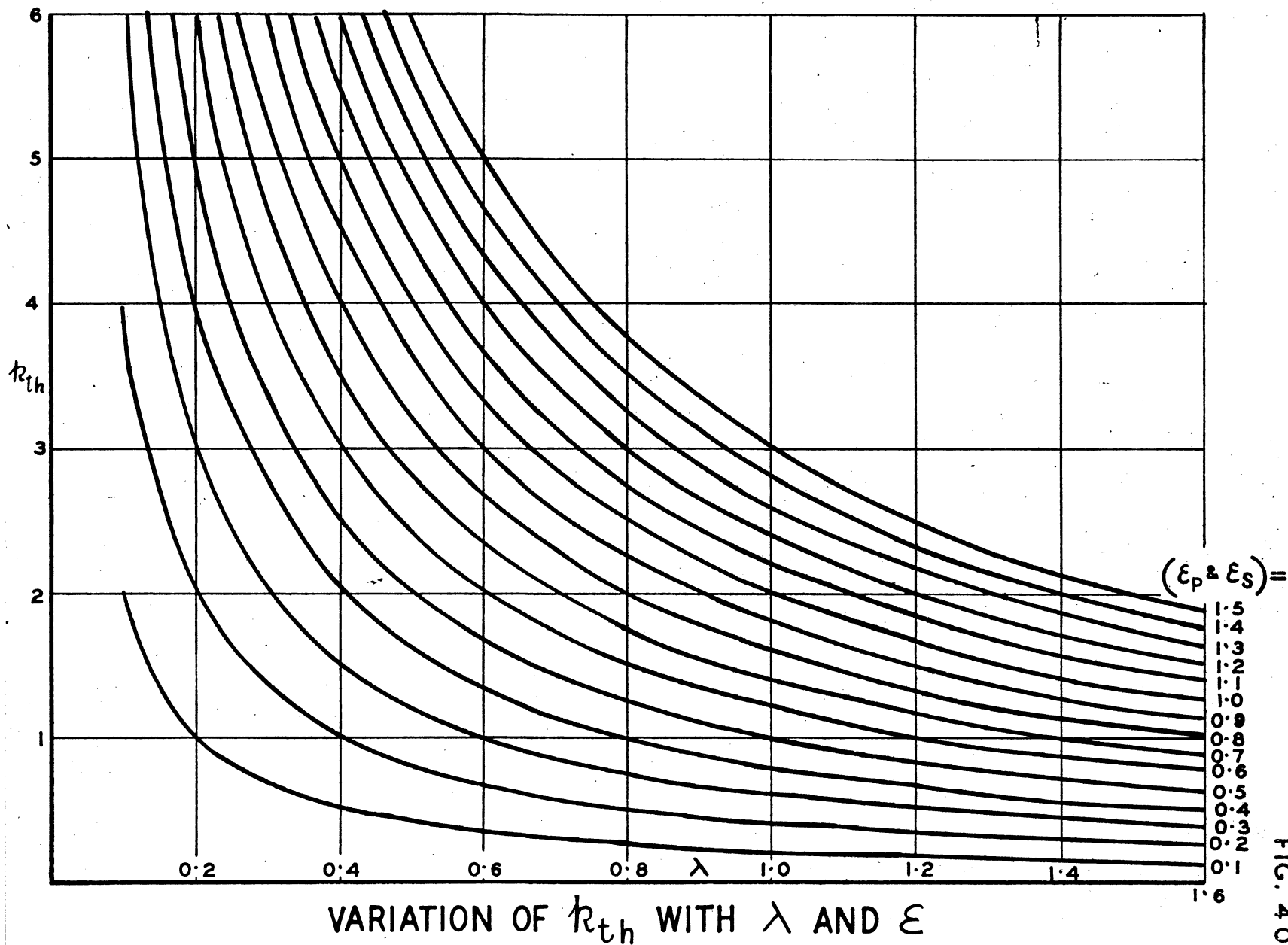
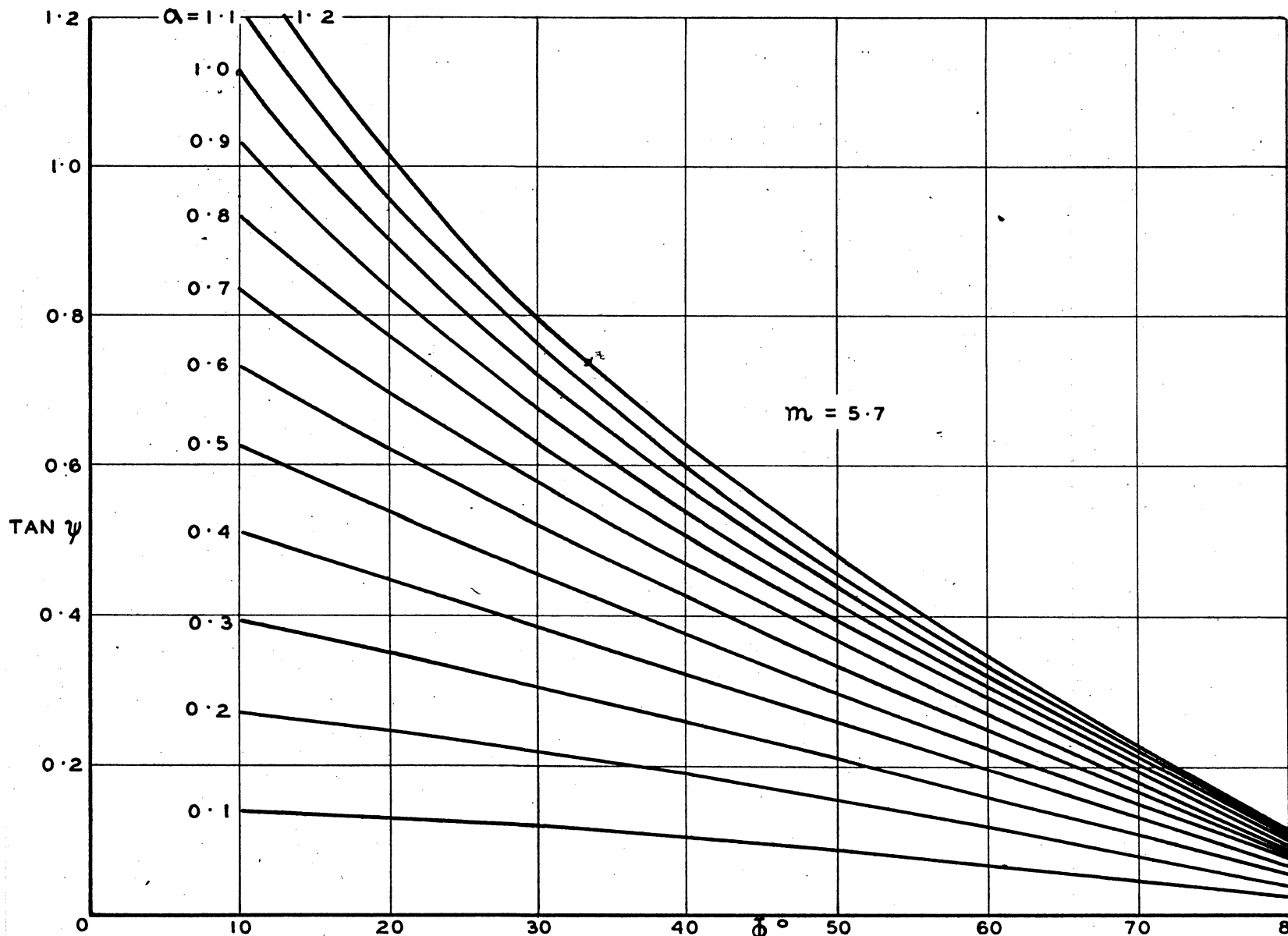
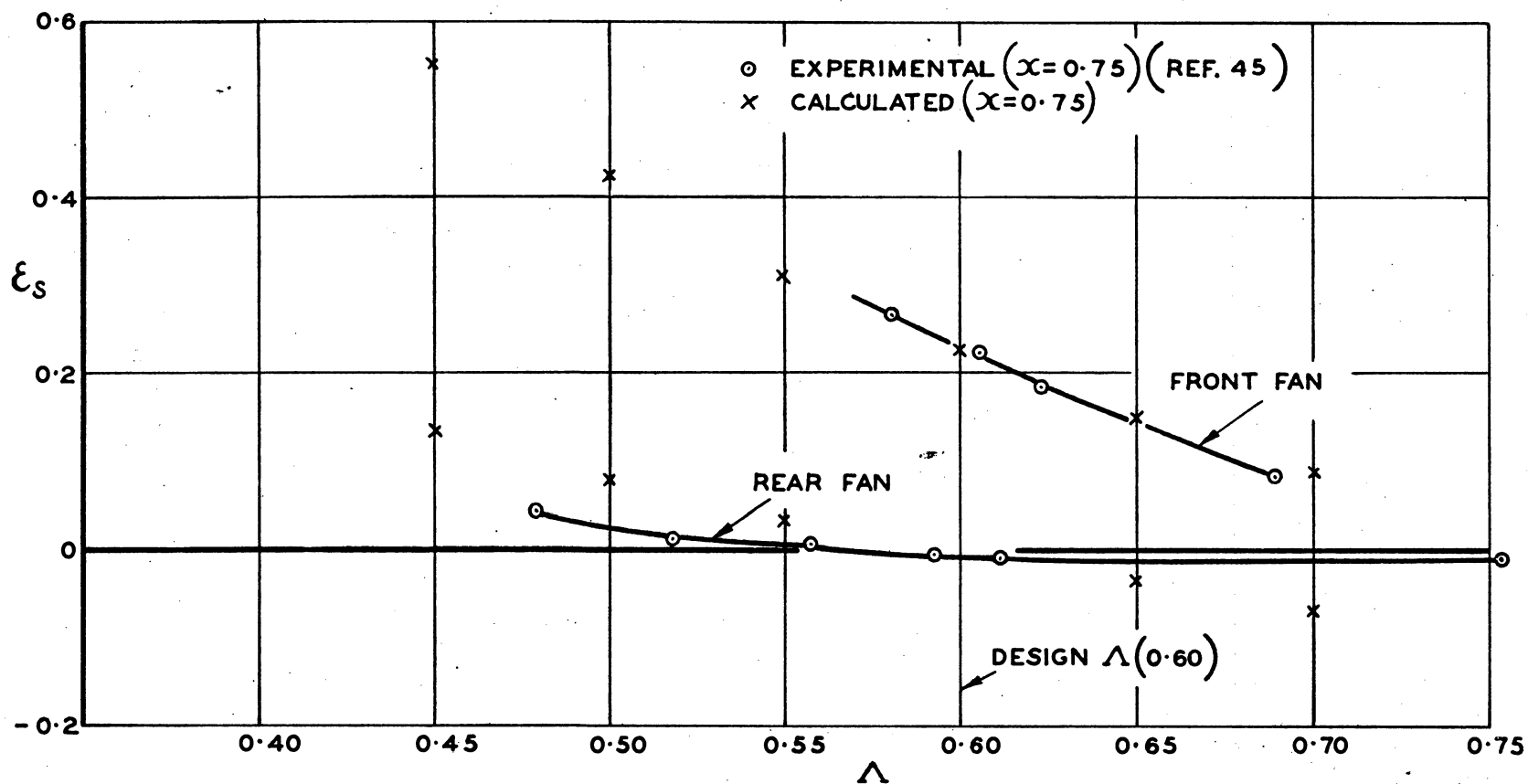


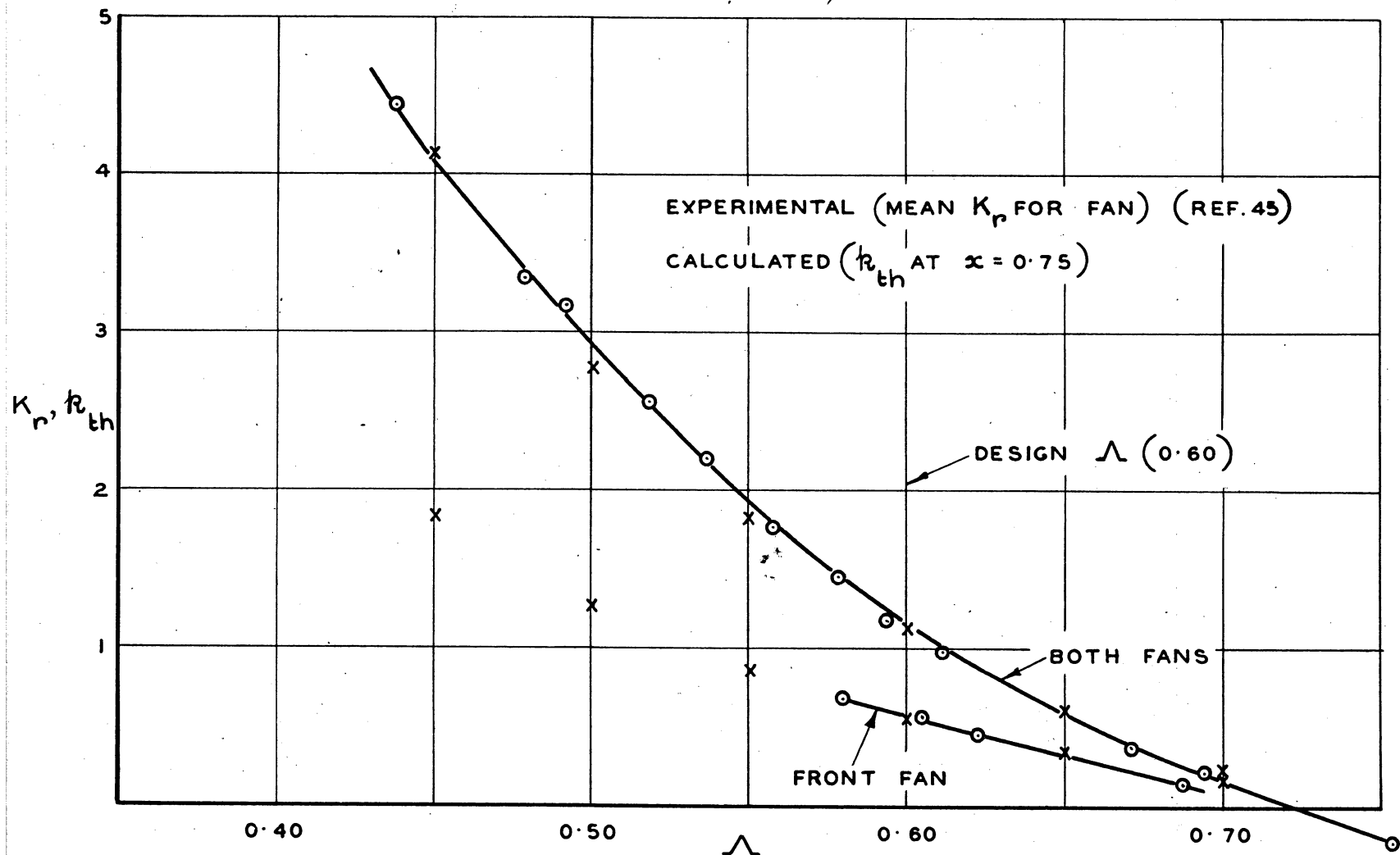
FIG. 40



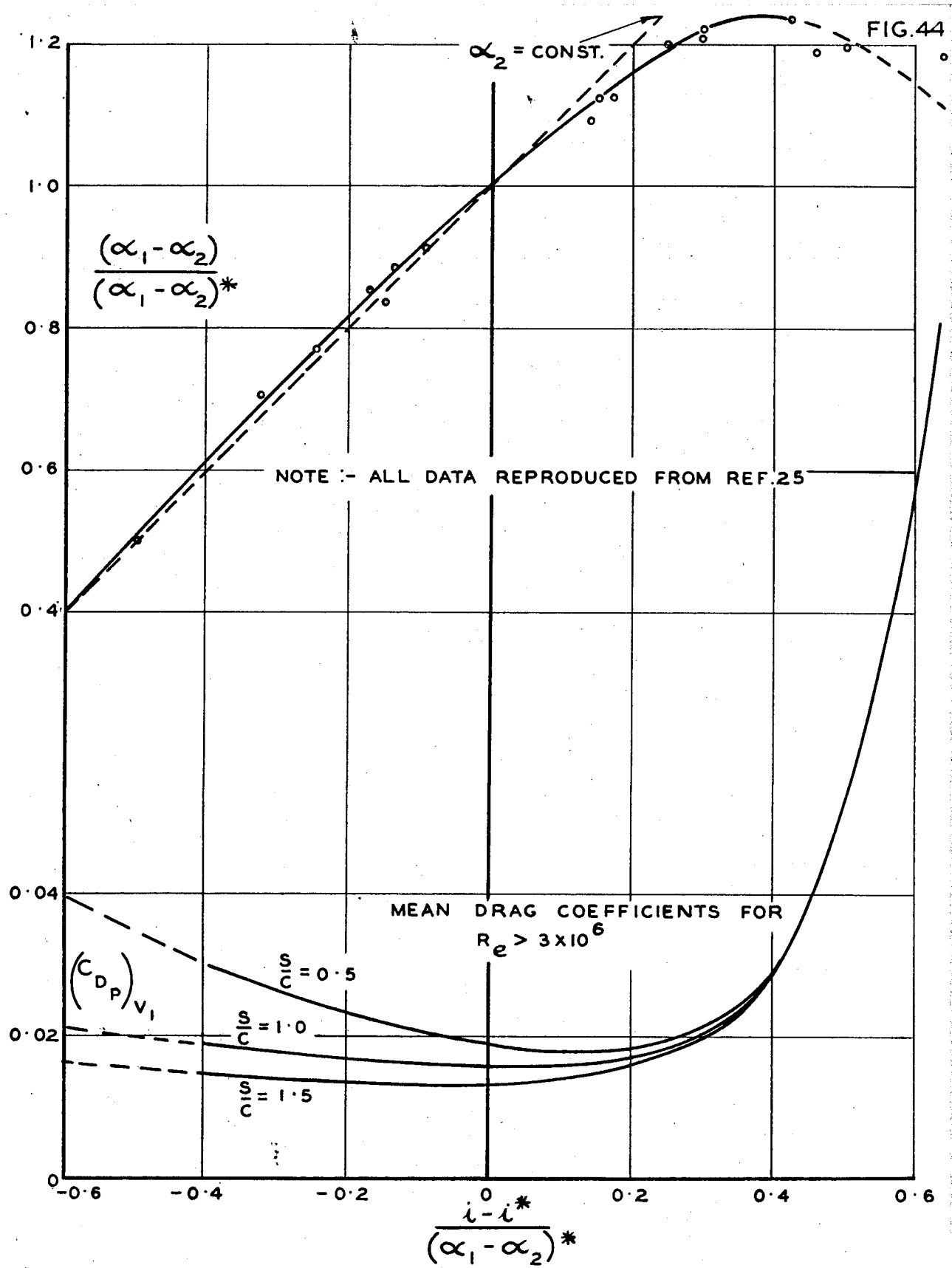
FAN ANALYSIS- $\omega_p r = \text{CONSTANT OR ZERO}$



SWIRL COEFFICIENTS DOWNSTREAM OF CONTRA-ROTATING FANS



TOTAL HEAD RISE ACROSS CONTRA-ROTATING FAN UNIT



CASCADE DATA FOR ANALYSING FANS

PART BTESTS ON SHEET METAL BLADED FANSADDITIONAL NOTATION

- $\Delta h_r$  Total head rise across rotor in elementary annulus at radius  $r$ .
- $k_r$  Coefficient of total head rise across rotor in elementary annulus at radius  $r$   $\left( = \frac{\Delta h_r}{\frac{1}{2} \rho U^2} \right)$
- $K_r$  Coefficient of mean total head rise across rotor
- $U$  Mean axial velocity through rotor.
- The following variables were defined in the notation of Part A but slight modifications are necessary -
- $(\eta_g)$  In the absence of stators in these tests, this efficiency applies to the rotor only, i.e. equals  $\eta_r$
- $(u)$  As before, the axial velocity at radius  $r$  but not a constant.
- The flow and swirl coefficients are  $\Lambda = \frac{U}{\Omega R}$  and  $\epsilon = \frac{\omega r}{u}$  respectively.

11 INTRODUCTION11.1 General.

In industry, axial flow fans fabricated from sheet metal are in universal use, the most common variety employing blades made from simple cambered plates. In general, these have been developed on rough empirical rules which are governed to a certain extent by manufacturing expediency. Usually the aerodynamic shape is poor and the efficiency low. Cambered plate fans have been used, however, in relatively high efficiency aircraft cooling installations (Ref. 59).

At the time this present research was commenced no satisfactory aerodynamic design data were available. Hence as a first step, the two-dimensional characteristics of isolated plates with varying degrees of camber were experimentally determined (Ref. 60). Subsequent to the work of Reference 60, a similar investigation has been carried out in Holland (Ref. 61). Although, to the author's knowledge, no comparable data are available for these aerofoils in cascade, it is usually assumed that they will behave in a similar fashion to orthodox aerofoils with the same camber line provided the inlet flow is approximately tangential to the leading edge of the blade (see Part A). The limitations of this method are discussed in Appendix F.



### 11.2 Description of Fans Tested.

The three fans tested in this present investigation were designed by Patterson's method (Ref.6). Fans No. 1 and 2 were designed for actual installations and since no reliable curved plate data were available at that time, the fans utilized blades which were twisted from root to tip but the blade elements of which were completely flat. The third fan was constructed for the sole purpose of testing a fan designed from the curved plate data of reference 60. As constant chord was a desirable feature in each case, the designs were modified in the manner suggested by Patterson (Ref. 6).

Geometric details are given in Table 17 and the design calculations for No. 3 fan tabulated in Appendix C. Fans No. 2 and No. 3, illustrated in Fig. 45, represent two designs having the same design capacity and total head rise at a given fan speed.

The construction of No. 3 fan was a little unusual. Free vortex design requires a rate of twist which varies along the blade; this condition was readily met by cutting the blades from a cylinder according to the method of reference 62. For completeness, the essential points of this method are reproduced in Appendix G.

### 11.3 General Methods of Fan Testing.

Before discussing the tests on the foregoing fans, it is advantageous to consider in broad outline the

various methods of testing.

In general, most fans are tested in a rig provided with a bellmouth entry, throttling device and a power unit incorporating some form of dynamometer. The pressure and velocity measuring equipment can vary appreciably from rig to rig.

The simplest test procedure consists of fitting a surface static pressure tube in the duct upstream of the nose fairing and one downstream of the tail fairing. Provided the throttle is at the outlet of the rig, the mass flow can be deduced from the upstream static tube since the total head is equal to atmospheric pressure and where the duct area is the same at both stations the difference between the two tubes gives the static pressure rise. In industry, the duty of a fan is usually specified by the static head which, by definition, is the static pressure rise less the mean axial dynamic head. The static head is therefore the downstream static pressure with respect to the upstream total head, which in this case is atmospheric pressure. The power and efficiency can be calculated from dynamometer readings and the above data. When appreciable residual swirl exists downstream of the fan, the above method will be inaccurate due to radial pressure gradients.

The results obtained from the above test procedure are of limited use in developing design methods. A method of overcoming this limitation consists of obtaining radial distributions of velocity upstream of the fan and distributions of total head and flow direction both upstream and downstream of the fan. Mean values are obtained by integration methods. Examples of this experimental approach are given in References 1, 38, 45, 63 and 64. The measuring instruments are usually of the pressure type which are assumed to record mean values.

However, the flow is intermittent due mainly to wakes shed by each blade and it is possible that errors may arise when the instruments are close to the trailing edges of the blades. Because of its quick response the hot wire instrument is very suitable for measuring the instantaneous velocities and this technique has been employed by Weske (Ref. 65) and Pearson (Ref. 66).

Fan design methods based on the calculation of blade shape to give a specified chordwise pressure distribution necessitate a knowledge of the aerodynamic interference between adjacent blades. To elucidate this and other problems associated with rotating blades, different methods of transmitting pressures from the blades have been evolved (Refs. 65, 67 and 68). By this means the actual pressure distributions on the rotating blades can be ascertained.

Certain stalling phenomena can be studied visually by attaching light-weight tufts to the blades and viewing the flow pattern by stroboscopic means.

## 12 FAN TESTS

The experimental work on the fans of section 11.2 is confined to obtaining radial distributions of velocity, total head and flow direction. These data are usually sufficient to permit an evaluation and development of design methods. Detailed results are given for No. 2 and No. 3 fans; only the general characteristics of No. 1 are presented as the details are somewhat similar to those of No. 2.

### 12.1 Equipment.

The test rig in which two of the fans, Nos. 2 and 3, were tested is presented in Figs. 46 and 47 showing No. 2 fan and its accompanying fairings in position; the rig for the smaller No. 1 fan was aerodynamically similar. Both the fairings and fan bearing were supported by very small cylindrical rods in order to reduce interference to a minimum. To enable measurements to be made at any axial station with the condition of a constant mean axial velocity component, the streamlined nose and tail fairings were separated by a cylindrical section which extended some distance upstream and downstream of the fan. The fan was driven by a constant speed electric motor, a set of pulleys and a V belt giving a step-up in speed of approximately 2:1 (Fig. 47). A transmission

dynamometer capable of recording low torques was fitted in conjunction with a pulley to the end of the fan shaft. The torque on the shaft was measured by the twist in a torsion spring, the deflection on the scale being read by stroboscopic means (Fig. 48). On account of the static friction, the unit was calibrated dynamically with a Prony brake; one inch on the scale represented 0.15 lbs. ft. torque.

Readings of total head and yaw were obtained with a  $\frac{1}{2}$ " diameter cylindrical tube having three holes, each with separate pressure leads.

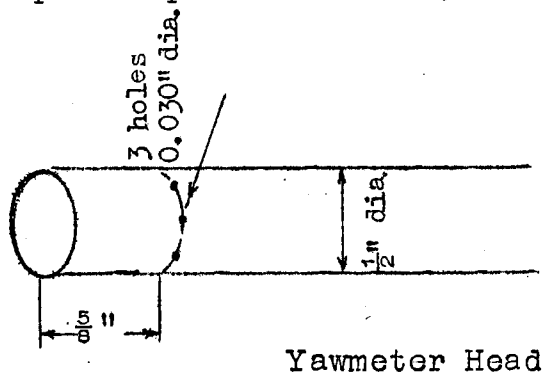


DIAGRAM 14

When the axis of the tube is placed normal to the axis of the tunnel, the direction of the stream can be determined by rotating the tube until the pressures in the side holes are the same, and the centre hole which is precisely midway between the other holes then reads the stagnation pressure, i.e. the total head of the stream. Velocity measurements

upstream of the fan were made with a conventional type pitot-static tube.

## 12.2 Method of Analysis

All three fans were tested over a range of operating conditions, the pressure rise being varied by the addition of wire screens at the entrance of the duct.

The objectives for each condition, were to determine

- (i) the mean velocity of the stream;
- (ii) the distribution of swirl velocity;
- (iii) the distribution of total head added to the stream by the fan;
- (iv) fan speed;
- (v) power absorbed; and
- (vi) fan efficiency.

(i) A velocity traverse upstream of the fan was made for each test condition. The mean velocity was obtained from the integral -

$$U = \int_{r_0}^R \frac{2 ur}{R^2 - r_0^2} dr = \int_{x_0}^1 \frac{2 u x}{(1 - x_0^2)} dx \quad 12.2.1$$

where  $u$  is the local velocity,  $r$  the radius,  $R$  the fan radius,  $r_0$  the boss radius and  $x$  equals  $r/R$ . It is more convenient to express the flow non-dimensionally as  $\Lambda = \frac{\dot{U}}{\Omega R}$  where  $\Omega$  is the angular velocity of the fan.

(ii) The induced or swirl velocity,  $\omega r$ , can be expressed non-dimensionally as  $\epsilon = \frac{\omega r}{u}$  where  $\epsilon$  is the tangent of the effective yaw angle. The effective yaw in these tests was taken to be the difference between any slight yaw upstream of the fan and the angle of yaw downstream.

The torque of the fan can be expressed as the rate of change of the angular momentum of the air; the torque coefficient,  $Q_c$ , is given in section 9 as

$$Q_c = \frac{Q}{\frac{1}{2}\rho U^2 R^3 \pi} \quad \text{where } Q \text{ is the shaft torque. 9.1}$$

$$= 4 \int_{x_0}^1 \left(\frac{u}{U}\right)^2 \epsilon x^2 dx \quad (\text{Ref. 6})$$

$$\text{or } Q_c = 4 \int_{x_0}^1 \epsilon x^2 dx \quad \text{when } u \approx U \text{ as is normally the case. 9.2}$$

Although not the primary reason for measuring  $\epsilon$ , the torque values obtained by this method have been compared with the dynamometer readings.

(iii) The total head distributions were measured directly upstream and downstream of the fan. It was found that the measured total head varied markedly with the station downstream and hence a number of distributions at different positions were obtained.

The difference of total head across the fan for a given elementary annulus can be expressed non-dimensionally as  $k_r = \frac{\Delta h_r}{\frac{1}{2}\rho U^2}$  where  $\Delta h_r$  is the increment of the resultant total head and  $\frac{1}{2}\rho U^2$  is the mean dynamic head of the axial component through the fan. The mean value for the fan can then be expressed (Ref. 45).

$$K_r = \frac{2}{1 - x_o^2} \int_{x_o}^1 k_r x dx \quad 12.2.2$$

(iv) Fan speed was measured with a dial gauge indicator type of tachometer, the calibration of which was checked with a stop watch and a 125 : 1 reduction box, driven from the shaft.

(v) The power was calculated from the expression -

$$\text{H.P.} = \frac{2\pi n Q}{33,000} \quad 12.2.3$$

where  $n$  = R.P.M. and  $Q$  is the fan torque obtained from the dynamometer readings.

(vi) Fan efficiency can be shown (Ref. 45) to be -

$$\eta_a = \frac{K_r \Lambda (1 - x_o^2)}{Q_c} \quad 12.2.4$$

### 12.3 Results

The mean duct velocity upstream of the nose fairing varied around 25 ft./sec. for No. 1 fan and around 38 ft/sec for No. 2 and No. 3 fans.



Stations at which traverses were taken upstream and downstream of the fans are given in Table 18.

#### 12.3.1 Velocity Distribution.

The velocity distributions in all cases are fairly uniform with a slightly increasing velocity towards the boss; this effect is due to the presence of the nose fairing (see Fig. 49). The wall boundary layer at the tips is approximately 0.06 of the fan diameter for each of the three fans. At the boss, the boundary layers are very thin.

#### 12.3.2 Swirl Velocity Distributions.

The rotation of the air can be expressed in terms of the non-dimensional parameter,  $\epsilon$ , as mentioned in the preceding section. This parameter is plotted against  $x$ , the radius ratio, in Figs. 50 and 51 for the various flow conditions under which No. 2 and No. 3 fans were tested. Both the design distributions are superimposed on the results and illustrate the boundary effects at the root and tip. In the intermediate region, the agreement with theory is satisfactory for the No. 3 fan. The tests on No. 2 fan were carried out in a relatively small laboratory and recirculation tended to upset inlet conditions to the test rig. This would tend to reduce the accuracy of the results. The lower values of  $\epsilon$  obtained experimentally for No. 2 fan would suggest that the two dimensional drag near the centre of the span is less than

expected in design. As leading edge separation is almost certainly present on the flat plate blade element at design incidences, difficulty in predicting the drag accurately must be expected.

The distribution for all three fans was found to be a little flatter than assumed in the design. This has also been observed in the contra-rotating fan tests of Reference 45.

The manner in which the swirl changes downstream of No. 3 fan is demonstrated in Fig. 2 for a near design case; for No. 2 fan the distributions at the rear station are superimposed on Fig. 50. The most significant trend is the reduction of  $\epsilon$  at the blade extremities with increasing distance from the fan. A considerable proportion of the momentum associated with the large values of  $\epsilon$  at the extremities is contained in the secondary flows described in Part A. These flows break down into random turbulence and hence such a reduction in  $\epsilon$  must be expected.

Test distributions of  $\epsilon$  are also useful in detecting the stalling characteristics of the fans. For example, the blades of No. 3 fan at a test  $A$  of 0.171 have stalled everywhere with the possible exception of  $x = 0.75$  (see Fig. 51); this is inferred from the manner in which the swirl distribution has been modified.

Distributions such as that at station 3 (Fig. 51) can be taken as representative of a stalled fan.

Although the comparison between theory and experiment is only fair, the behaviour of the fans, on the whole, is satisfactory as will be shown later.

### 12.3.3 Total Head Distribution.

For all three fans, the rise in total head remains reasonably constant along the blade except for regions at the root and tip (see Figs. 53 and 54). The mean values of the total head rise coefficient at various downstream stations are plotted in Fig. 55 for Nos. 1 and 3 fans. It will be seen that the measured value drops rapidly by approximately 10% in the first inch or so downstream. A possible explanation is that, owing to the pulsating nature of the flow, the total head measured immediately downstream of the fan is not the true mean total head. However, it appears likely that mixing and secondary losses account for some of the discrepancy. (A similar phenomenon occurred in Ref. 63 and the 10% loss measured there was attributed to mixing of the flow downstream of the fan.) The change of total head with downstream station is shown in detail in Fig. 56 for the near design case of No. 3 fan. The change is more or less constant along the whole blade suggesting that the wall boundary layers are not the primary reason. Station 2 for

fan No. 2 and station 3 for fan No. 3 have been chosen arbitrarily as giving conditions which are fairly representative of the fans. The corresponding distributions are given in Figs. 53 and 54.

A dimensional plot of the total head rise distributions given by the No. 3 fan is presented in Fig. 57. For the case  $\Lambda = 0.171$ , the blade is stalled over the whole span except at  $x = 0.75$ . This agrees with the conclusion drawn in the previous subsection from Fig. 51. A phenomenon which appears to be associated with tip stalling is the large total head increases achieved locally, (see Figs. 53, 54 and 57); this was most noticeable on the flat plate fans, (Nos. 1 and 2) which are more prone to stall at the tips. The major portion of this increase, however, is associated with large swirl velocity heads of which very little can be recovered as pressure head.

#### 12.3.4 Characteristic Curves.

The mean total head rise coefficient,  $K_p$ , has been plotted against the flow coefficient,  $\Lambda$ , in Figs. 58 to 60, for the three fans tested. Despite deviations of the actual spanwise distributions from the theoretical, as described in the preceding subsections, reasonable agreement with design has been obtained.

Although fans 2 and 3 were designed to fulfil the same design condition, this is not apparent from the above figures. Using these curves, the characteristics have been plotted dimensionally for a fan speed of 2,800 R.P.M. (Fig. 61). Although the fans agree at the design point, the characteristic at higher pressure rises is different.

#### 12.3.5 Power and Efficiency.

The torque coefficient, power and efficiency curves for Nos. 2 and 3 fans are respectively given in Figs. 62 and 63. Efficiency is based on the mean total head rise at stations 2 and 3 for fans 2 and 3 respectively. In both cases, the peak efficiency is approximately at the design point with the cambered blade fan 11 per cent more efficient. The torque of fan No. 1 could not be obtained very accurately and hence power and efficiency curves for this fan are not given.

The torque coefficients, as derived from yawmeter readings, show considerable inconsistency. The results at station 3 of No. 3 fan are given in Fig. 63; those for No. 2 fan were 10% below dynamometer readings when based on station 1. Very close agreement, however, was obtained in References 45, 63 and 64 between yawmeter and dynamometer readings for orthodox aerofoil blades. This suggests that yawmeter torque measurements may not be accurate for the cambered or flat plate type of fan.

LOSSES OVER TAIL FAIRING

Some experimental work was carried out on the No. 3 fan installation to determine the order of the tail fairing losses. Two fairings of different fineness ratios, namely  $f = 1.35$  and  $2.35$ , were tested with and without flow straighteners in the unit. The efficiency as expressed by Patterson (Ref. 54) and elaborated upon in Part A was in the vicinity of 80% for all cases with the exception of the smaller fairing with flow straighteners. Here the efficiency was lower owing to a flow separation on the rear portion of the fairing. The longest tail fairing is based on an equivalent  $8^\circ$  included angle diffuser.

Although no detailed measurements were made of the losses over the tail fairing of the No. 2 fan unit, it was deduced from the measured total loss in the test rig that the efficiency was also approximately 80%.

These efficiencies are lower than the 90% values quoted for a wide range of diffusers in reference 54. In the case of a fan unit however, the tail fairing is an additional wetted surface which, no doubt, is responsible for greater losses.

The nature of the flow in the vicinity of the tail fairing is of interest; velocity and yaw distributions are given in Figs. 64 and 65. The yawmeter was used for measuring velocity having first been calibrated in the duct

upstream of the fan with and without a wire screen at the tunnel inlet. When the direction of the stream is found from the two pressure holes, which are  $90^\circ$  apart, the instrument is turned through  $45^\circ$  so that one gives the total pressure,  $h_o$ , and the other a pressure  $p_1$ , which is a function of the velocity head. For the test Reynolds number range the value

$$\frac{h_o - p_1}{\frac{1}{2} \rho V^2}$$

was approximately constant at 2.08 and independent of the turbulence added by the wire screen.

The addition of straighteners thickens the three dimensional wall boundary layers (Fig. 64) as would be expected. Plotting the axial velocity component distributions (Fig. 64), however, shows that the mass flow has been increased.

As the flow progresses down the tail fairing the law of conservation of angular momentum results in an increase of angular velocity with decreasing radius; this can be demonstrated from Fig. 65.

In comparing the boundary layer profiles for the two fairings (Fig. 64), it should be noted that the traverse for the fairing,  $f = 1.35$ , is slightly more than 12 inches downstream of the end of the fairing. In this distance, a favourable redistribution of boundary layer

momentum would have taken place. Keeping this in mind, it can be inferred from Fig. 64 that the fairing,  $f = 2.35$ , is in no danger of stalling with or without flow straighteners. Hence the recommendation of an  $8^\circ$  included equivalent diffuser angle (Part A) appears satisfactory.

#### 14 CONCLUSION

The tests conducted on fans with sheet metal blades have shown that the free vortex design method is satisfactory. Not only are the design distributions of total head and flow direction approximated in practice, but the efficiency is good and if suitable allowances are made for losses, then the fan can be expected to fulfil design requirements. The order of the tail fairing losses has been determined, demonstrating the need for keeping the boss ratio as low as practicable.

This data, with the design theory of Part A and the cambered plate data of reference 60, enables ducted axial flow fans with sheet metal blades to be designed with confidence. Fans with uncambered metal blades are, for efficiency reasons, not recommended.

#### 15 ACKNOWLEDGEMENTS

The author wishes to acknowledge the assistance of Mr. S.A. Ambrose who carried out the experimental work on No. 3 fan. Grateful acknowledgment is also given to the Chief Scientist, Dept. of Supply for permission to submit the foregoing work.



APPENDIX CDESIGN DETAILS OF NO. 3 FAN.

As mentioned previously, the design of this fan followed the procedure set out in Reference 6 by Patterson. The important design calculations are tabulated below. A 4% cambered plate was used for the blade sections, the aerodynamic characteristics being obtained from the data of reference 60 for a Reynolds number of  $3.14 \times 10^5$ .

The initial design assumptions were

$$k_{th} - k_{FP} = 1.55$$

$$\Lambda = 0.294$$

$$x_o = 0.6$$

$$\eta = 0.92 \text{ (based on profile drag only)}$$

x	0.6	0.7	0.8	0.9	1.0
$\lambda$	0.49	0.42	0.367	0.327	0.294
$\epsilon$	0.413	0.354	0.309	0.276	0.248
$\tan \phi$	0.545	0.453	0.389	0.343	0.305
$\phi$	28.6°	24.4°	21.3°	18.9°	17.0°
$\gamma$	24.9	28.5	32.3	36.0	39.9
$\alpha$	0.7°	1.1°	1.7°	2.3°	3.0°
$C_L$	0.49	0.53	0.58	0.65	0.71
$C_{Dp}$	0.0190	0.0180	0.0176	0.0184	0.0186
$C_y$	0.421	0.475	0.534	0.609	0.674
$\epsilon^2$	0.1710	0.1255	0.0952	0.0760	0.0615
$\sin^2 \phi$	0.2290	0.1700	0.1315	0.1050	0.0851
$y$	0.905	0.712	0.571	0.455	0.376
$yC_L$	0.443	0.377	0.331	0.296	0.267
$C_L(y=0.5)$	0.886	0.754	0.662	0.592	0.534
$\alpha$	4.9°	3.5°	2.6°	1.8°	1.2°
$\phi + \alpha$	33.5°	27.9°	23.9°	20.7°	18.2°

The design equations used were -

$$\epsilon = \frac{(k_{th} - k_{FP})}{2 \cdot \eta} \lambda$$

$$\tan \phi = \frac{\lambda}{1 - \frac{1}{2} \epsilon \lambda}$$

$$\gamma = \frac{(1 - \frac{1}{2} \epsilon \lambda) (\eta - \frac{1}{2} \epsilon \lambda) + \lambda^2}{\lambda (1 - \eta)}$$

$$C_y = C_L \cos \phi - C_D \sin \phi$$

$$y = \frac{2x(k_{th} - k_{FP} - \epsilon^2) \sin^2 \phi}{C_y}$$

The product,  $yC_L$ , was obtained and the blade planform adjusted in the manner suggested in Reference 6. The chord was assumed to be constant and the  $C_L$  range chosen so that the ratio:  $\frac{C_L}{C_{Dp}}$ , was large at all stations. A modified  $\alpha$  was then obtained thus giving the blade setting relative to the plane of rotation as

$$\phi + \alpha$$

Assuming 8 blades and from the expression

$$y = \frac{Nc}{\pi R} \quad (=2x\sigma) \text{ where } N \text{ is the number of blades.}$$

$$c = 1.67 \text{ ins. when } y = 0.5$$

From the above data, the shape of the blade was developed out of a rolled sheet by the method of Appendix G (Ref. 62).

APPENDIX D  
ANALYSIS OF FAN LOSSES  
TEST RESULTS

The losses in a fan rotor are composed of the following main components (see Part A).

- (a) Profile drag.
- (b) Secondary drag.
- (c) Annulus drag.

In Part A, each of these losses is treated in some detail and hence will not be elaborated on here. Due to the relative crudity of sheet metal blades, the above losses will be greater than for a fan using orthodox aerofoil sections. The profile drag losses can be calculated from aerofoil data, but the second and third types of loss are not known with any degree of accuracy. However, the following tentative suggestions are put forward -

The secondary drag coefficient recommended in Part A is -

$$C_{D_S} = 0.018 C_L^2$$

but for sheet metal blades the following relationship based on test results, is suggested

$$C_{D_S} = 0.025 C_L^2$$

Using these figures and the expression developed in Part A namely

$$\gamma \frac{k_F}{k_{th}} = \frac{\lambda}{\sin^2 \phi}$$

we obtain the loss in efficiency due to secondary drag from

$$\frac{K_{FS}}{k_{th}} = \frac{\lambda_m}{(\sin^2 \phi)_m} (0.0250_L)_m$$

where the suffix m denotes the values at the mid-span station.

In Part A, the loss in efficiency due to annulus drag was assumed constant at 2% but for the present type of fan, an increase to 3% is recommended.

#### Efficiency losses for Fans No. 2 and No. 3

Fan	Design value	From above recommendations		Total Efficiency	
	Profile drag loss	Secondary drag loss	Annulus drag loss	Test Value	Calculated from above
No. 2	0.22	0.04	0.03	0.72	0.71
No. 3	0.08	0.05	0.03	0.83	0.84

The numerical subdivision of the losses is somewhat arbitrary due mainly to the limited test data available. Whilst it should be relatively easy to obtain consistent results for cambered plate fans this may not be possible for flat plate fans (e.g. fans Nos. 1 and 2; see section 12.3.2). For cambered plate fans the above recommendations should be of the right order and their adoption is suggested for design purposes.

APPENDIX EANALYTICAL DETERMINATION OF CHARACTERISTICCAMBERED PLATE FAN

$$\tan \psi = \frac{\cos \Phi}{\frac{4}{m\sigma} + \sin \Phi} \quad 10.1.10$$

$$\varepsilon = \frac{2 \tan \psi}{\lambda} [\tan \Phi - \lambda] \quad 10.1.8$$

$$k_{th} = \frac{2\varepsilon}{\lambda} \quad 2.2.8$$

Data:- For  $x = 0.80$ , (assumed to give mean values for fan)

$\phi + \alpha = 23.9^\circ$ ,  $\frac{N_c}{\pi R} = 0.50$  and camber = 4% (Appendix C).

From Fig. 66 a suitable linear lift curve is, no-lift

angle =  $-4.9^\circ$  and  $m = 5.4$ . Hence  $\Phi = 28.8^\circ$  and

$$\tan \psi = 0.308$$

	$\Lambda = 0.17$	$\Lambda = 0.20$	$\Lambda = 0.25$	$\Lambda = 0.30$	$\Lambda = 0.33$
$\lambda$	0.213	0.250	0.313	0.375	0.413
$\tan \Phi - \lambda$	.337	.300	.237	.175	.157
$2 \tan \psi / \lambda$	3.04	2.47	1.97	1.65	1.49
$\varepsilon$	1.025	0.740	0.467	0.288	0.204
$k_{th}$	9.63	5.93	2.99	1.54	0.99
$K_r$ (station 3)	7.0	4.9	2.60	1.37	0.78

The efficiency,  $K_r/k_{th}$ , is in general

greater than the measured efficiency. Hence a curve based on computed values of  $k_{th}$  and the actual efficiency would be pessimistic, as in Appendix A.

APPENDIX F  
DESIGN EXAMPLE

GENERAL

When the design specification permits the use of isolated aerofoil data (Ref. 60) the method is straightforward. The procedure of Part A is more suitable than that due to Patterson (Ref. 6) as it permits the choice of camber to be left to the concluding stages of the design. This ensures the most efficient camber for the  $C_L$  range contemplated (Ref. 60).

With high pressure rise fans necessitating the use of cascade theory it is usual to make the assumptions outlined in section 11.1. However, an experimental investigation of the turning angle through plate prerotators (Ref. 49) suggests that the turning angle is less than that of an orthodox aerofoil with the same camber line; certain objections can be raised to these results\*.

---

\* The results of Ref. 49 were obtained in a convergent annulus and were corrected in an arbitrary fashion for axial flow. Two criticisms can be made of the recommended curve of turning angle versus camber angle for zero local inlet incidence, i.e.  $i = 0$ . Firstly the curve does not tend to the origin which is the case of a flat plate parallel to the stream. Secondly the percentage deviations from the recommendations of the cascade theory (Part A) increase considerably as the camber angle is decreased i.e. as the loading is reduced. These findings fail to satisfy physical reasoning and hence must be treated as suspect.

Conditions which may lead to "underturning" will now be discussed. Difficulties arise from leading edge separation which occurs when the local incidence,  $i$ , of cambered plates exceeds approximately  $2^\circ$ . With increasing incidence, the region of separation spreads towards the trailing edge giving a rapid drag increase and from a potential flow point of view, an effective thickening of the plate towards the trailing edge. This latter effect is equivalent to reducing the camber, which implies "underturning". In the rotor, which has to give a certain non-dimensional pressure rise such a phenomenon would, compared with the design, result in a small flow reduction and an increase in blade incidence. Underturning in either prerotators or straighteners also leads to small flow reductions, e.g. a small residual rotation downstream of the straighteners represents an additional loss which the rotor must overcome.

Since the camber line and not the symmetrical aerofoil with which it is clothed is the main variable which determines the turning angle, an extension to cambered plates appears reasonable. Although the possibility of "underturning" cannot be ignored, insufficient data exist to warrant, at the moment, any modification to the theory of Part A other than a limitation on the local incidence at the leading edge. It is recommended, as before, that the incidence,  $i$ , should be zero at the design point (see also Ref. 64).



Outside the limits of say  $i = \pm 3^\circ$ , the behaviour of a cambered plate will probably start to differ from that of the orthodox aerofoil.

In conclusion it can be said that errors arising from any possible "underturning" will be of a very minor nature provided the above recommendations are followed. If experience showed the above to be incorrect the appropriate place to make the correction would be in Constant's rule (eq. 2.5.3); this would produce a modification to the camber and stagger angles.

#### ACTUAL EXAMPLE.

In the following fan-straightener example, certain conditions have been fixed but no difficulty should be experienced in re-arranging the preliminary design procedure to suit individual requirements.

#### SPECIFICATION

*A ducted axial flow fan fitted with flow straighteners is required to deliver 12,000 C.F.M. through a duct system in which the total head loss is 2.0 inches of water. It is desirable to limit the fan diameter to 30 inches. The fan, which is to operate at sea level, is to be directly coupled to an electric motor (1430 R.P.M.) enclosed in the tail fairing.*

The preliminary design of a possible configuration will be studied in detail; the results are finally tabulated and compared with those obtained from a number of other designs.

Assuming fan diameter = 30 inches

boss diameter = 18 inches

then boss ratio  $x_o = 0.6$

Mean axial velocity through fan

$$u = \frac{\text{C.F.M.}}{60} \frac{1}{\pi(R^2 - r_o^2)}$$

$$= 63.6 \text{ ft./sec.}$$

The dynamic head

$$\frac{1}{2}\rho u^2 = 4.81 \text{ lbs/ft.}^2$$

where  $\rho = 0.002378 \text{ slugs/ft.}^3$  at S.T.P.

Reducing the total head loss in the duct system to the same units as above

$$\Delta H = 2 \times 5.2 = 10.4 \text{ lbs/ft.}^2$$

Assuming an overall efficiency of 0.77, the theoretical total head rise coefficient,  $k_{th}$ , is given by

$$k_{th} = \Delta H / \frac{1}{2}\rho u^2 \frac{1}{\eta_T}$$

$$= 2.81$$

Tip speed of fan

$$\Omega R = \frac{\text{R.P.M.}}{60} 2\pi R$$

$$= 187 \text{ ft/sec.}$$

## Flow coefficient

$$\Lambda = \frac{u}{\Omega R}$$

$$= 0.340$$

with  $\lambda_o = 0.567$  at the root

$$\lambda_m = 0.425 \text{ at the mid span station}$$

For reasons outlined in Part A, the loadings on the rotor and stator blades are more critical at the root section.

From figure 40 for  $k_{th} = 2.81$

$\varepsilon_o = 0.80$  which specifies the maximum stator loading to be encountered. As this is less than unity, the limit suggested in Part A, the stator design is completely practical.

Using the above values of  $\lambda_o$  and  $\varepsilon_o$ , the rotor loading is obtained from Fig. 6.

$$(C_L \sigma)_o = 0.94$$

As this is a relatively high value, a check should be made on the optimum lift coefficient,  $C_L^*$ . From Figure 4, which is based on the cascade theory of design,  $C_L^*$  is obtained as a function of  $\varepsilon_o$  and  $\lambda_o$ .

$$C_{L_o}^* = 0.70$$

The solidity,  $\sigma$ , is therefore found to be

$\sigma_0 = 1.34$  which is in excess of unity, the value recommended as an upper limit for the free aerofoil theory of design. It will be shown later how the free aerofoil theory can be modified at the root to overcome this difficulty.

The losses can be determined approximately as functions of  $\epsilon_m$  and  $\lambda_m$  where the suffix  $m$  denotes the mid-span values. Now

$\lambda_m = 0.425$  and from Fig. 40 we have

$\epsilon_m = 0.60$  from which the loss in efficiency can be obtained in the following manner:-

Firstly the general equation 4.2.4 gives

$$\gamma \frac{K_F}{k_{th}} = 2.21 \quad (\text{see Fig. 21})$$

The loss components will be taken separately

(a) Profile drag.

The lift and drag data of Ref. 60 has been reproduced in Figs. 66 to 69 for two Reynolds numbers, namely  $3.14 \times 10^5$  at  $6.28 \times 10^5$ .

In the present design, the order of the appropriate Reynolds number can be determined for the mid span station by considering only the rotational velocity component. Assuming the chord,  $c$ , is half the blade height

$$R_e = \frac{2 \pi r_m c}{60v} \times \text{R.P.M.} = 240,000$$

and therefore Figs. 66 and 68 will be the appropriate ones.

From the preliminary investigation at the root station a tentative  $C_L$  range along the blade can be assumed, say 0.70 to 0.90; the 6% cambered plate appears the most efficient for this  $C_L$  range (see Figs. 70 and 71) and gives a mean lift/profile drag ratio = 42.

Hence

$$\frac{K_{FP}}{k_{th}} = \frac{2.21}{42} = 0.053$$

(b) Secondary drag loss.

Assuming the mean  $C_L$  is 0.8 the efficiency loss is (see Appendix D)

$$\begin{aligned} \frac{K_{FS}}{k_{th}} &= 2.21 \times 0.025 \times 0.8 \\ &= 0.044 \end{aligned}$$

(c) Annulus drag loss

$$\frac{K_{FA}}{k_{th}} = 0.03 \text{ (see appendix D)}$$

It may be assumed tentatively that the efficiency of the rotor is

$$\eta_F = 0.873$$

The losses in the stators can now be determined. From the general equation 5.2.5 (Fig. 30)

$$\gamma \frac{K_S}{k_{th}} = 0.465 \quad \text{for } \lambda_m = 0.425 \text{ and } \epsilon_m = 0.60$$

Since  $\epsilon$  will be in excess of 0.4, the stators will be designed by the cascade method. For optimum conditions  $C_L$  and hence  $C_{D_S}$  (see appendix D) are known. From reference 60 it can be shown that the profile drag coefficient for optimum lift/profile drag ratio is approximately 0.022 for all cambers. The above data permits  $\gamma$  to be expressed as a function of  $\epsilon$  for optimum conditions (see Fig. 72).

For the present design

$$\gamma = 20$$

and the loss in efficiency

$$\frac{K_S}{k_{th}} = \frac{0.465}{20} = 0.023$$

Tail fairing losses are the last major contribution to the fan unit losses. When 80% diffuser efficiency is assumed we obtain for  $x_o = 0.6$  and  $k_{th} = 2.81$

$$\frac{K_D}{k_{th}} = 0.042 \quad (\text{see Fig. 37})$$

The total efficiency of the fan unit is then

$$\eta_T = 0.808$$

say 80%

This is 3% more efficient than was originally assumed. Hence a correction can now be made for  $k_{th}$ .

$$k_{th} = 2.81 \times \frac{0.77}{0.80}$$

$$= 2.71$$

The small corrections to  $\epsilon_o$  and  $\epsilon_m$  due to the change in  $k_{th}$  would not affect the foregoing calculation to any worthwhile extent; the estimates are only of a preliminary nature.

Whilst this design is satisfactory, it might not represent the optimum from an efficiency point of view. As a rule it is not only desirable, but usually necessary, to complete a number of these preliminary designs. These can be set out in the following tabulated form where design B is the one just described in detail.

C.F.M. = 12,000 and  $\Delta H = 2.0$  ins. of water (1430 R.P.M.)

Design	A	B	C	D	E
Fan diameter = $2R$ (ins.)	30	30	30	27	27
Boss diameter = $2r_o$ (ins.)	20	18	16	20	18
$x_o = \frac{r_o}{R}$	0.667	0.6	0.533	0.741	0.667
$u = \frac{\text{C.F.M.}}{60 \pi (R^2 - r_o^2)} \text{ (ft/sec.)}$	73.4	63.6	57.0	111.1	90.6
Dynamic head = $\frac{1}{2} \rho u^2$ (lb/ft <sup>2</sup> )	6.41	4.81	3.86	14.7	9.76
$k_{th} = \frac{\Delta H / \frac{1}{2} \rho u^2}{\eta_T} \text{ } (\eta_T = 0.77)$	2.10	2.81	3.51	0.91	1.38
Tip speed = $\frac{\text{R.P.M.}}{60} 2\pi R$ (ft/sec)	187	187	187	168	168
$\Lambda = \frac{u}{\text{tip speed}}$	0.392	0.340	0.305	0.663	0.540
$\lambda_o = \frac{\Lambda}{x_o}$	0.588	0.567	0.572	0.894	0.811
$\lambda_m = \frac{\Lambda}{x_m}$	0.471	0.425	0.398	0.761	0.649
$\epsilon_o$ (from Fig. 40)	0.61	0.80	1.00	0.40	0.56
$(C_L \sigma)_o$ (from Fig. 6)	0.72	0.94	1.24	0.61	0.81
$C_{L_o}^*$ (from Fig. 4)	0.90	0.70	0.54	1.14	0.94
$\sigma_o$	0.79	1.34	> 2	0.54	0.87



Design	A	B	C	D	E
$\epsilon_m$ (from Fig. 40)	0.50	0.60	DESIGN IMPRACTICAL AS SOLIDITY LIMIT HAS BEEN EXCEEDED	0.36	0.44
$\gamma^{k_F/k_{th}}$ (from Fig. 21)	2.12	2.21		1.75	1.78
$\frac{C_L}{C_{DP}}$ (assumed see Fig. 70)	42	42		48	42
$K_{FP}/k_{th}$	0.051	0.053		0.036	0.042
$K_{FS}/k_{th}$	0.048 ( $C_L=0.9$ )	0.044 ( $C_L=0.8$ )		0.044 ( $C_L=1$ )	0.040 ( $C_L=0.9$ )
$K_{FA}/k_{th}$	0.03	0.03		0.03	0.03
$\eta_F$	0.871	0.873		0.89	0.888
$\gamma^{k_S/k_{th}}$ (from Fig. 30)	0.50	0.465		0.78	0.68
$\gamma$ (from Fig. 72)	19.5	20.0		21.2	20.3
$K_S/k_{th}$	0.026	0.023		0.037	0.034
$K_D/k_{th}$ (from Figs. 37)	0.066	0.042		0.176	0.100
$\eta_T$	0.779	0.808		0.677	0.754

A survey of the five designs establishes the second as the most suitable. The most significant factor influencing the overall efficiency of the fan unit is the tail fairing loss. Although rotor efficiency increases with  $A$ , it is more than countered by the above diffusion loss. The third figure in the total efficiency is not a significant one and has only been included for comparison purposes.

The power required to drive the chosen fan is

$$\frac{\text{C.F.M.} \times \text{total head rise}}{33,000 \times \eta_T}$$

$$= \frac{12,000 \times 5.2 \times 2.0}{33,000 \times 0.80}$$

$$= 4.73 \text{ H.P.}$$

As the frame size of a suitable 5 H.P. motor will be less than the 18 inches diameter of the fan boss, the original requirement concerning the housing of the motor in the rear fairing will be readily met.

It will be assumed that the total head rise coefficient  $k_{th}$  and the axial velocity component,  $u$ , are both constant along the blade span (see Part A for design assumptions)

The first basic design equation is

$$\frac{k_{th} \lambda}{2 \epsilon} = 1 \quad (2.2.8) \text{ where } k_{th}, \lambda \text{ and } \epsilon \text{ are respectively}$$

non-dimensional measures of the head rise, flow and torque respectively for any blade element. From this equation, the unknown,  $\epsilon$ , can be determined.

Secondly,

$$\tan \phi = \frac{\lambda}{1 - \frac{1}{2} \epsilon \lambda} \quad (2.2.5) \text{ where } \phi \text{ is the angle}$$

which the resultant velocity has to make with the plane of rotation in order to maintain the correct relationship between the axial, swirl and blade components of velocity.

Knowing the velocity vectors it is possible to calculate the loading on the blades. This gives the third design equation as

$$C_{L\sigma} = 2 \epsilon \sin \phi \quad (2.3.1)$$

This completes the first part of the detail design; the results of the calculations for the design example are tabulated below:

$x = \frac{r}{R}$	0.6	0.7	0.8	0.9	1.0
$\lambda = \frac{\Lambda}{x}$	0.567	0.486	0.425	0.378	0.340
$\varepsilon = \frac{k_{th}\lambda}{2}$	0.768	0.658	0.576	0.512	0.461
$1 - \frac{1}{2}\varepsilon\lambda$	0.782	0.849	0.878	0.903	0.921
$\tan \varphi = \frac{\lambda}{1 - \frac{1}{2}\varepsilon\lambda}$	0.725	0.578	0.484	0.418	0.369
$\varphi$	35.9°	30.0°	25.8°	22.7°	20.3°
$\sin \varphi$	0.586	0.500	0.435	0.386	0.347
$C_L \sigma$	0.900	0.658	0.501	0.395	0.320

When the tabulated design data of tables 2 and 3 (Part A) are plotted to a convenient scale,  $\varphi$  and  $C_L \sigma$  can be read directly as functions of  $\varepsilon$  and  $\lambda$ .

The blade element details will now be considered. Three simple methods of fixing the blade plan form are to

- (a) assume a constant chord
- (b) assume a constant  $C_L$ , and
- (c) assume a linear variation of chord along the blade.

Before choosing the planform of this design, the root condition will be re-examined for the modified value of  $k_{th}$ , namely 2.71. From Fig. 4

$$C_{L_o}^* = 0.74 \text{ for } \lambda_o = 0.567 \text{ and } \varepsilon_o = 0.768$$

and hence

$$\sigma_o = 1.215$$

When constant chord is assumed, the  $C_L$  at the tip is 0.44 which for a 6% cambered plate, (tentatively chosen,) is unacceptable for efficiency reasons (See Fig. 70). In this design the second method, namely constant  $C_L$  has been chosen with a slight modification. For efficiency reasons a lift coefficient of 0.8 is more desirable than 0.74 for stations other than at the root (see Fig. 70).

The final stage of the design can now be completed -

x	0.6	0.7	0.8	0.9	1.0
$C_L$	0.74	0.8	0.8	0.8	0.8
$\sigma$	1.215	0.822	0.626	0.494	0.400
Nc (ins.)	68.7	54.2	47.2	41.9	37.7
c(N=16) ins.	4.29	3.39	2.95	2.62	2.36
$\alpha$ (see Fig. 66)	1.9°	2.6°	2.6°	2.6°	2.6°
$\alpha + \phi$	37.8° (38.7°)	32.6°	28.4°	25.3°	22.9°

It will be remembered that the solidity at the root is in excess of that normally used in the free aerofoil theory. Hence a check of this station along the lines of the cascade theory appears warranted.

From Fig. 13 the optimum camber angle (Part A) is  $\theta = 20.5^\circ$  at the root station and from Fig. 15 the stagger angle (Part A).

$$\xi = 50.3^\circ$$

Now the stagger angle is equal to

$$90^\circ - (\alpha + \phi) \quad \text{and hence from the cascade}$$

theory we obtain

$$(\alpha + \phi) = 39.7^\circ$$

The camber/chord ratio is given by equation 2.5.11

$$\left(1 - \cos \frac{\theta}{2}\right) / 2 \sin \frac{\theta}{2} \quad \text{which for}$$

$$\theta = 20.5^\circ \text{ is } 0.045.$$

When we assume a stagger angle of  $50.3^\circ$ , the angle of incidence is  $3.8^\circ$  ( $\phi = 35.9^\circ$ ) and interpolating for a 4.5% cambered plate in Fig. 66 we get a lift coefficient of 0.82. The incidence at which a 6% cambered plate free aerofoil attains a lift of 0.82 is  $2.8^\circ$ , and hence the amended angle of setting at the root station is

$$\alpha + \phi = 38.7^\circ$$

From the above the lift of the aerofoil in cascade divided by the lift of a free aerofoil is 0.85 which is of the right order (see Reference 9).

The blade details are now known from the foregoing table, the amended figure being included in brackets.

Finally the torque is given by

$$Q = Q_c \frac{1}{2} \rho u^2 \pi R^3 \quad 9.1$$

or

$$Q_c = k_{th} \Lambda (1 - x_o^2) \quad 9.3$$

$$= 0.59$$

$$\therefore Q = 17.4 \text{ ft. lbs.}$$

and the thrust by

$$T = T_c \frac{1}{2} \rho u^2 \pi R^2 \quad 9.4$$

$$\begin{aligned} \text{when } T_c &= k_{th} \eta_F (1 - x_o^2) + \frac{1}{2} k_{th}^2 \Lambda^2 (\log_e x_o) \quad 9.8 \\ &= 1.292 \end{aligned}$$

$$T = 30.5 \text{ lbs.}$$

Two further portions of the fan unit remain to be designed. These are the straightener vanes and the nose and tail fairings.

As mentioned previously, the cascade stator design method will be used. When it is assumed that the flow enters the vane along the tangent at the leading edge, this being the most favourable condition for cambered plates, the optimum design is a function of only one variable, namely,  $\epsilon$ . This enables all the vane details to be presented as in Figs. 17 and 18.

Taking the values of  $\epsilon$  from the fan design for the various radial stations, the following design results

x	0.6	0.7	0.8	0.9	1.0
$\varepsilon$	0.768	0.658	0.576	0.512	0.461
$s/c$	0.74	0.98	1.22	1.46	1.50
$\theta$	48.3°	44.9°	41.9°	39.5°	36.7°
% Camber	10.7	9.9	9.3	8.7	8.1
$\xi$	13.4°	10.8°	8.9°	7.5°	6.7°
S (ins.)	3.77	4.40	5.03	5.66	6.29
c(N=15) ins	5.09	4.49	4.12	3.88	4.19

The number of stator vanes, namely 15, differs by one from that used in the rotor design; this is to reduce the noise resulting from the beat of a number of rotor blades passing a similar number of vanes simultaneously.

When the above design is set out graphically it will be seen that the vane differs only slightly from a conical shape. Hence for practical purposes the vane design may be adjusted to make use of the simple geometric shape if so desired. Such adjustments include small chord increases (a decrease is not recommended), and maintenance of the local angle of incidence,  $i$ , within the limits  $\pm 3^\circ$ . Small deviations from the vane outlet angle necessary to give pure axial flow are not serious since small residual swirls are usually of little consequence.



The nose and tail fairings should preferably be good streamlined shapes. One such shape is given in Reference 56; the co-ordinates are reproduced below.

<u>Distance from nose</u>	0	0.0125	0.025	0.05	0.10	0.20	0.30	0.40	0.50	0.60	0.70	0.80	0.90	0.95	1.00
Total length															
<u>Diameter at point</u>	0	0.2478	0.3480	0.4841	0.6615	0.8660	0.9682	1.00	0.9765	0.9049	0.7818	0.6001	0.3469	0.1869	0
Max. diameter															

It is usually convenient to consider the nose and tail fairings separately, that is, the portions forward and aft of the 40% position respectively. Nose fairings should be kept relatively short whilst tail fairings may have to be long if flow separation is to be avoided. When the recommendations of Part A are used, the fineness ratio,  $f$ , can be expressed as a function of  $x_0$ , provided there is no divergence of the duct walls (Fig. 38). For this design example the appropriate value is 2.35 which proved satisfactory in No. 3 fan installation where the boss ratio was also 0.6. A suitable fineness ratio for the nose fairings is 1.2 as this provides a good entry to the fan. An alternative nose fairing is a hemisphere; the total losses are much the same in both cases.

The final design is illustrated in Fig. 73.

APPENDIX GCONSTRUCTION METHOD FOR CAMBERED BLADES (Ref. 62)

Irrespective of the method used in designing a fan, the final requirements are a certain camber, chord and blade setting at each station along the blade. As the chief advantage of using cambered blades of sheet material is to facilitate manufacture it is essential to have a simple but accurate procedure for producing the blades.

The method outlined here is best illustrated in diagram 15 where the blade is set at an angle to the axis of a cylinder in order to obtain the correct degree of twist. The simplest application of this method is when the fan design is arranged with constant chord and camber along the blade.

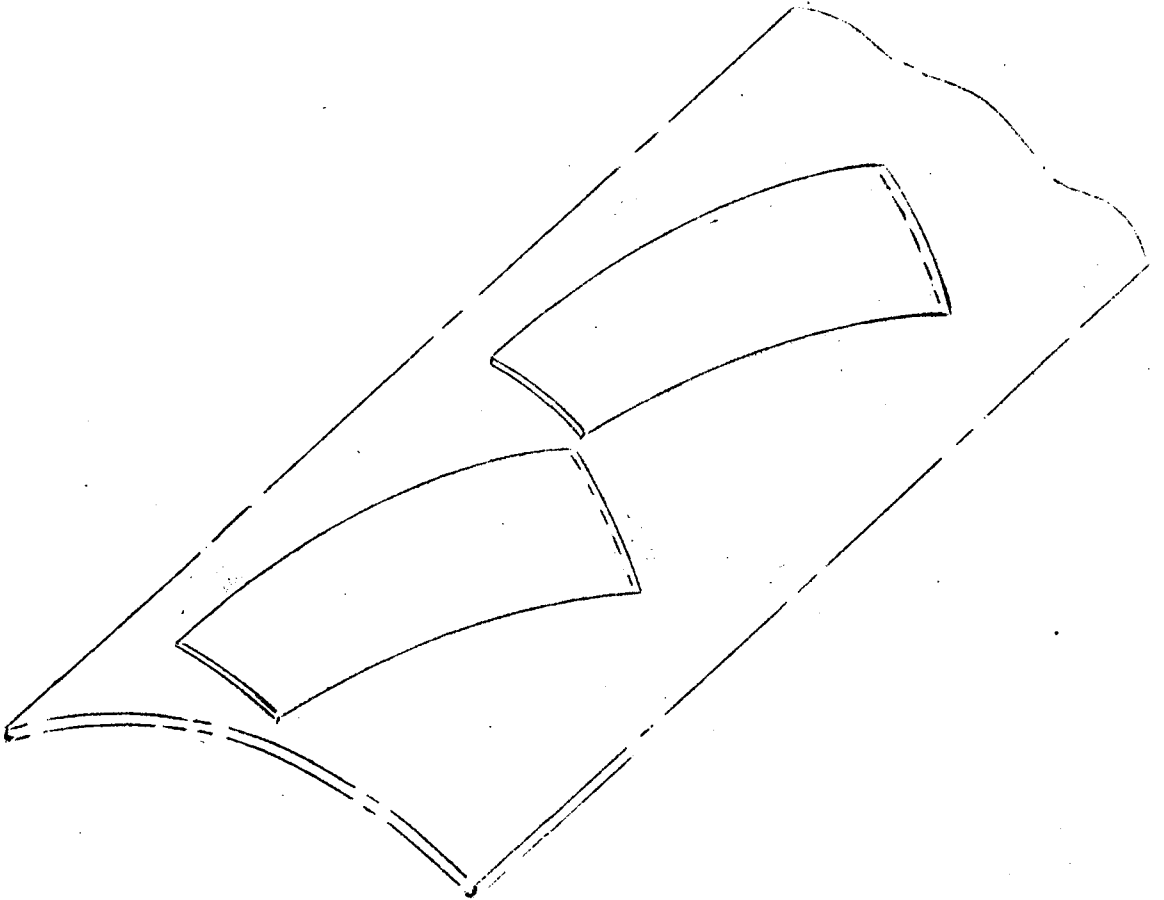


DIAGRAM 15

The blades are marked out on a sheet of flat metal by means of a template. After rolling the plate into a part cylinder with its axis in the appropriate direction, the blades can be profiled out on a bandsaw.

In setting out the blade, it is assumed that the line joining the mid-chord points at the root and tip is perpendicular to the chord line (see diagram 16).

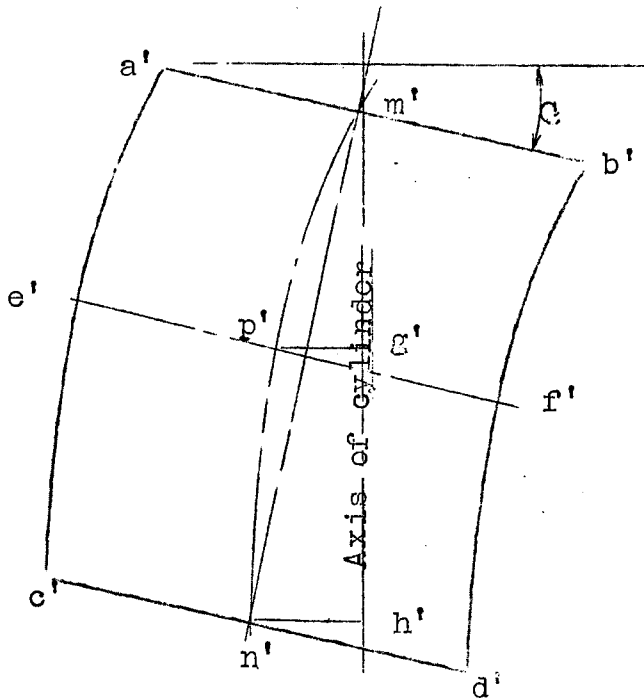
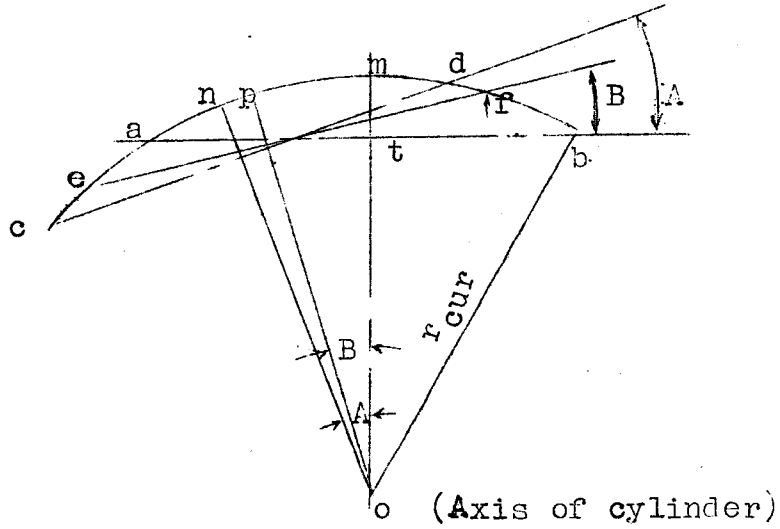


DIAGRAM 16

From diagram 16 it can be seen that  $m'h'$  and  $ob$  are the axis and radius of curvature respectively. The cross section of the blades is no longer circular but elliptical. However, when the camber is small, which is usually the case, the section is, for all practical purposes, circular, with a radius of curvature given by

$$R_{\text{cur}} = \left\{ \frac{\text{camber}}{2} + \frac{\text{chord}^2}{8 \times \text{camber}} \right\} = \left\{ \frac{a}{2} + \frac{c^2}{8a} \right\}$$

where  $a = mt$

$c = a'b'$

The radius to which the sheet has to be rolled is then given by

$$r_{\text{cur}} = \left\{ \frac{a}{2} + \frac{(c \cos C)^2}{8a} \right\}$$

If  $D$  were the desired angle of twist between blade sections  $c'd'$  and  $a'b'$ , the angle  $A$  will then be

$$A = \tan^{-1} \left( \frac{\tan D}{\cos C} \right)$$

Once the angle  $C$  is determined, it is then possible to set out the blade. Let the length of the blade equal  $l$ . Then

$$\sin C = \frac{n' h'}{l}, \quad \text{also}$$

$n'h' = r_{\text{cur}} \sin A$ , hence

$$\sin C = \frac{r_{\text{cur}} \sin A}{l}$$

$$= \frac{\left( \frac{a}{2} + \frac{c^2 \cos^2 C}{8a} \right) \left( \sin \tan^{-1} \frac{\tan D}{\cos C} \right)}{l}$$

This equation can be solved very readily by substituting an assumed value for  $\cos C$  in the  $\sin A$  term. This method of approximations gives a rapid convergence to the true value of  $C$  as small changes in  $\cos C$  have only a second order effect on the equation. The  $\sin A$  term can now be replaced by  $\sin A'$  where  $\sin A'$  is calculated using the assumed value of  $\cos C$ . By writing  $1 - \sin^2 C$  for  $\cos^2 C$  the following quadratic is obtained

$$L \sin^2 C + l \sin C - M = 0$$

$$\text{where } L = \frac{c^2 \sin A'}{8a} \text{ and } M = L + \frac{a \sin A'}{2}$$

$$\text{hence } \sin C = \frac{-l \pm \sqrt{l^2 + 4LM}}{2L}$$

After a little experience, one or two approximations usually suffice in the determination of  $C$ .

If  $E$  were the angle of twist between sections  $e'f'$  and  $a'b'$  then the angle  $B$  would be

$$\tan^{-1} \frac{\tan E}{\cos C}$$

The arc length  $pm$  is then the product of  $r_{cur}$  and  $B$  where  $B$  is in radians. Other stations along the blade can be treated in a similar manner.

Hence once  $C$  has been determined it is then possible to find the radius  $r_{cur}$  and set out the curved centre line of the blade. After modifications have been made to the root, to allow for fixation to the boss, and to the tip for duct clearance, it is possible to construct a template from which the blades are marked out. Only two operations are then required to produce the blade, namely the rolling of the material to the desired curvature and shaping with a power saw. A desirable refinement, especially when the material is thick relative to the chord, is the rounding of the leading and trailing edges of the blades.

The above geometrical treatment can be applied to blades of tapering plan form but in this case the aerodynamic design problem has to assume a trial and error procedure owing to the varying amount of camber along the blade.

When the correct aerodynamic twist is maintained along the blade, the leading and trailing edges form spiral curves, which, if the boss diameter were less than half the fan diameter, would assume an extreme shape for fan blades. However, as it is difficult to design an efficient fan for a boss ratio less than half, the above limitation will not be serious.

TABLE 17DETAILS OF FANS

FAN		1	2	3
Diameter of fan (ins.)		10.75	17	17.5
Diameter of boss (ins.)		5.375	8.5	10.2
Blade Chord (ins.)		2	2.5	1.65
Number of blades		6	8	8
Blade setting relative to plane of rotation, ( $\phi + \alpha$ )	x			
	0.5	56.5°	38.6°	—
	0.6	47°	31.5°	33.5°
	0.7	41°	26.5°	27.9°
	0.8	36°	23.1°	23.9°
	0.9	31°	20.4°	20.7°
	1.0	29°	18.2°	18.2°

TABLE 18DETAILS OF MEASURING STATIONS DOWNSTREAM OF FANS

Fan	Distances from Longitudinal $\phi$ of fans (ins.)			
	Station 1	Station 2	Station 3	Station 4
1	1.25	2.00	3.25	5.36
2	0.95	2.95	—	—
3	0.65	1.33	2.35	4.35

N.B. Upstream stations were immediately in front of fan.





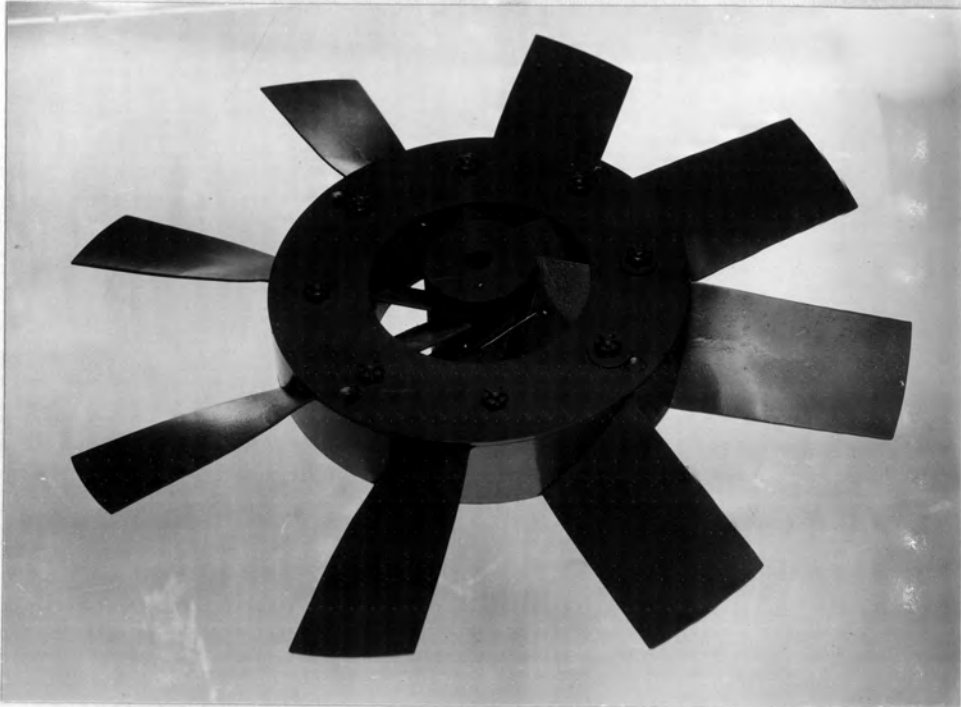


Fig. 45(a)

No. 2 Fan

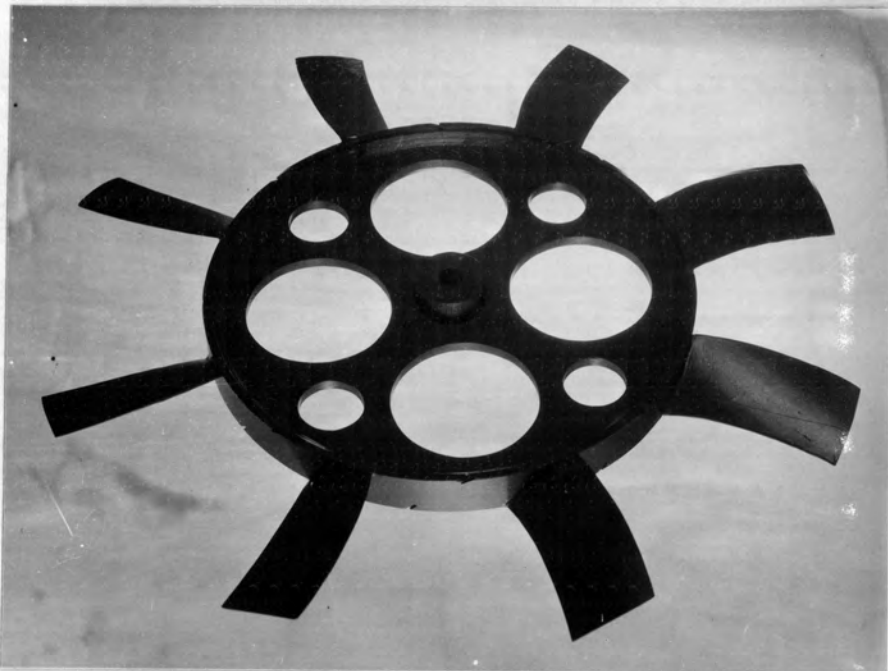
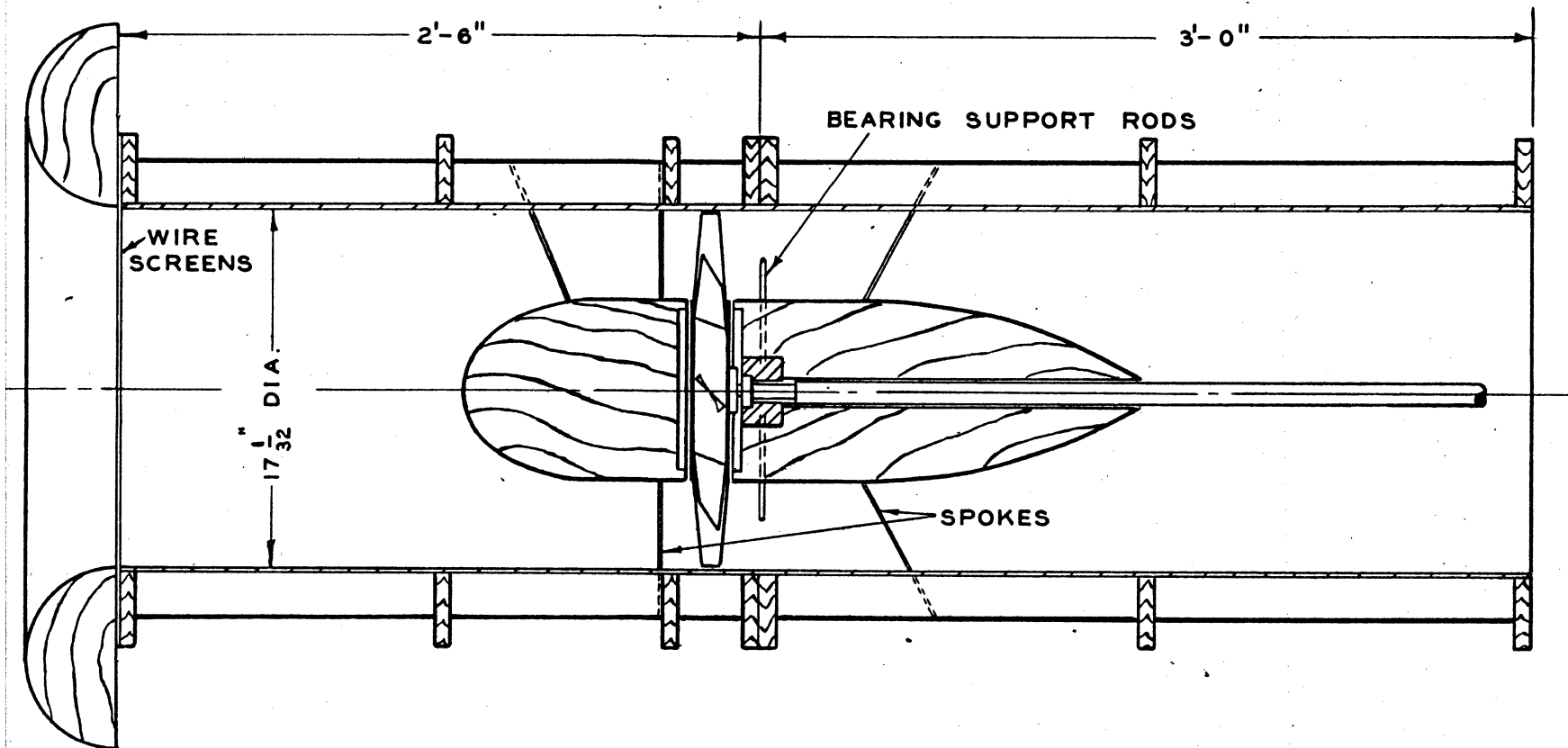


Fig. 45(b)

No. 3 Fan

GENERAL VIEW OF FANS



FAN TESTING TUNNEL

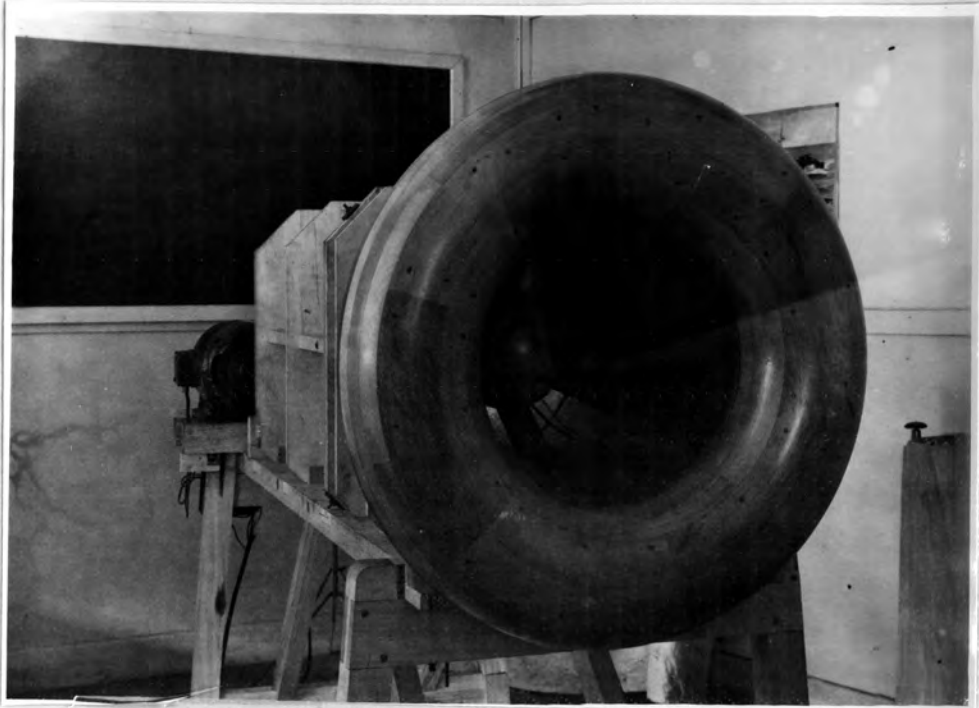


Fig. 47(a) Bellmouth entry to test rig

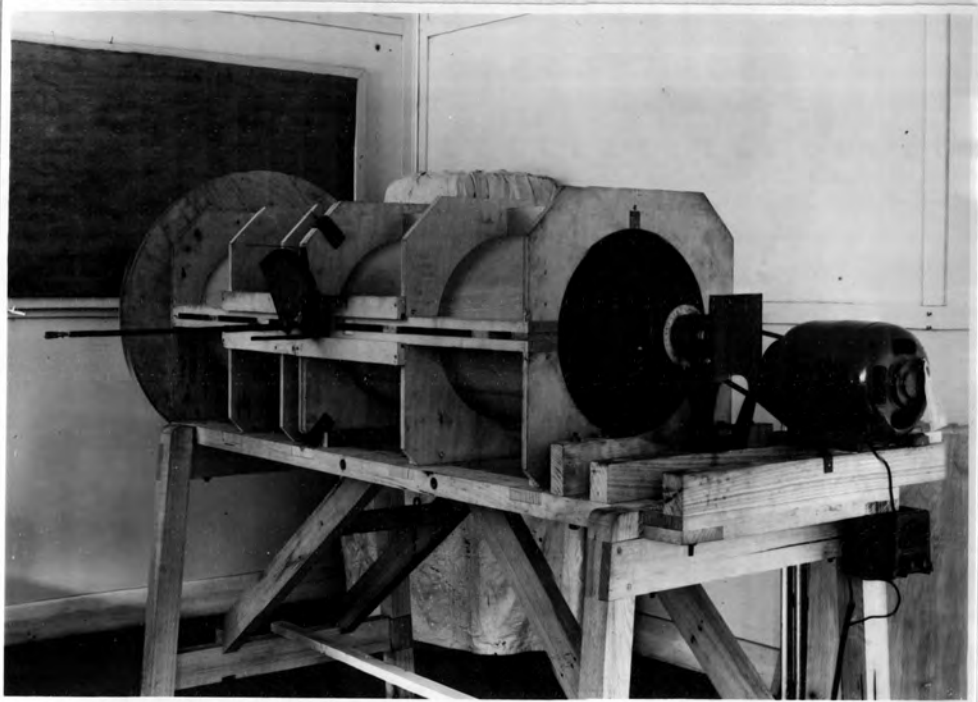
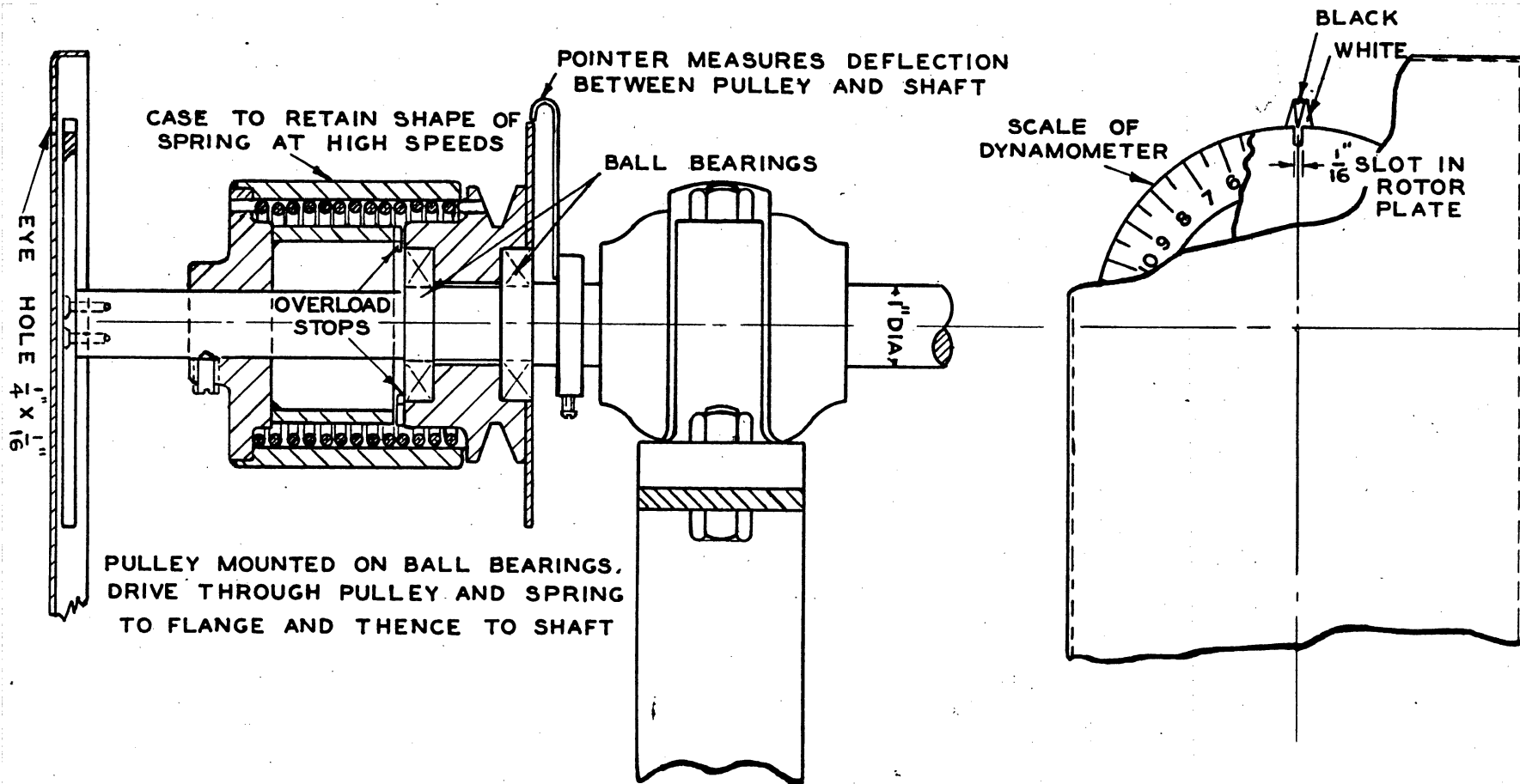


Fig. 47(b) General side view of test rig

GENERAL VIEW OF TEST RIG



DYNAMOMETER

FIG. 49

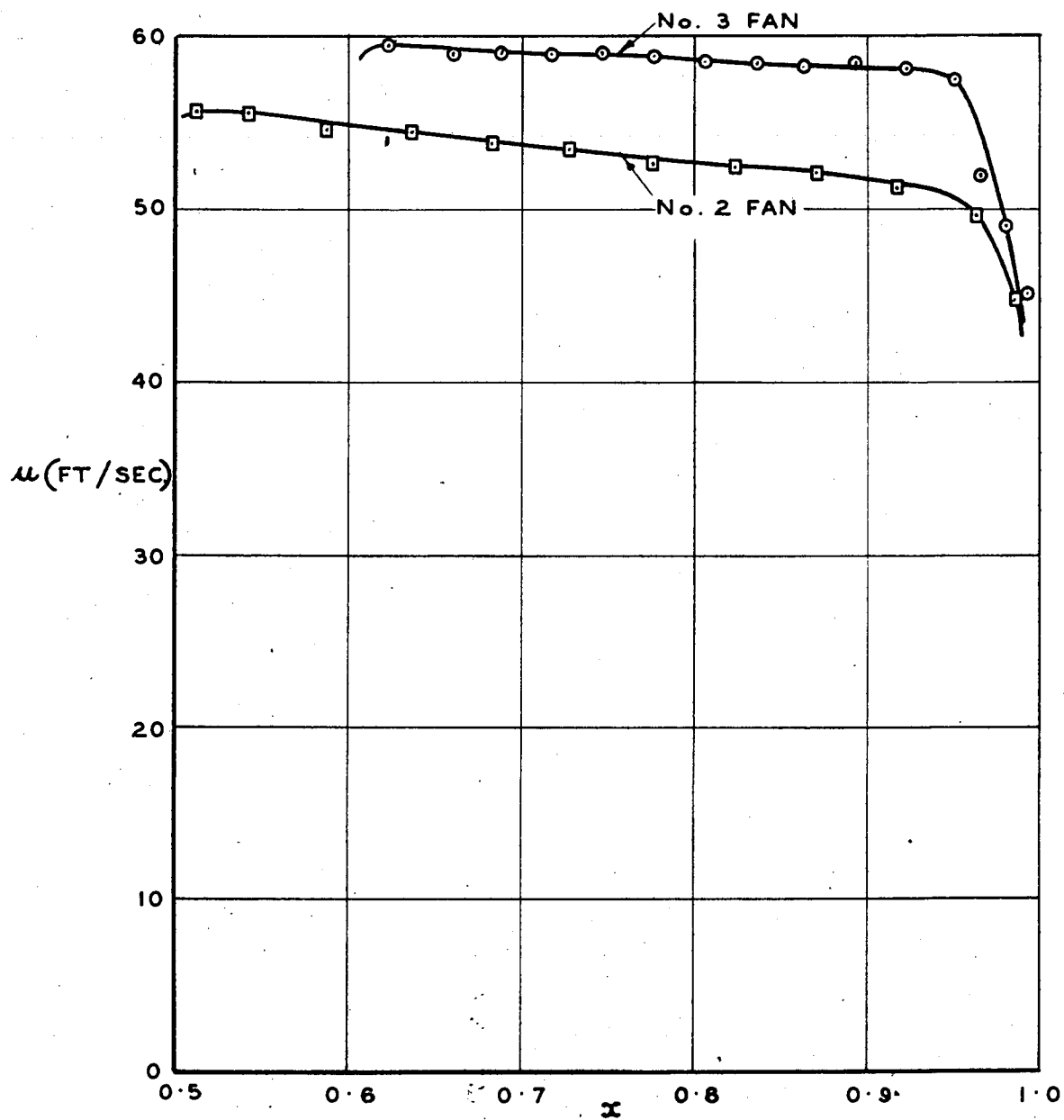
TYPICAL VELOCITY DISTRIBUTIONS  
UPSTREAM OF FANS

FIG. 50

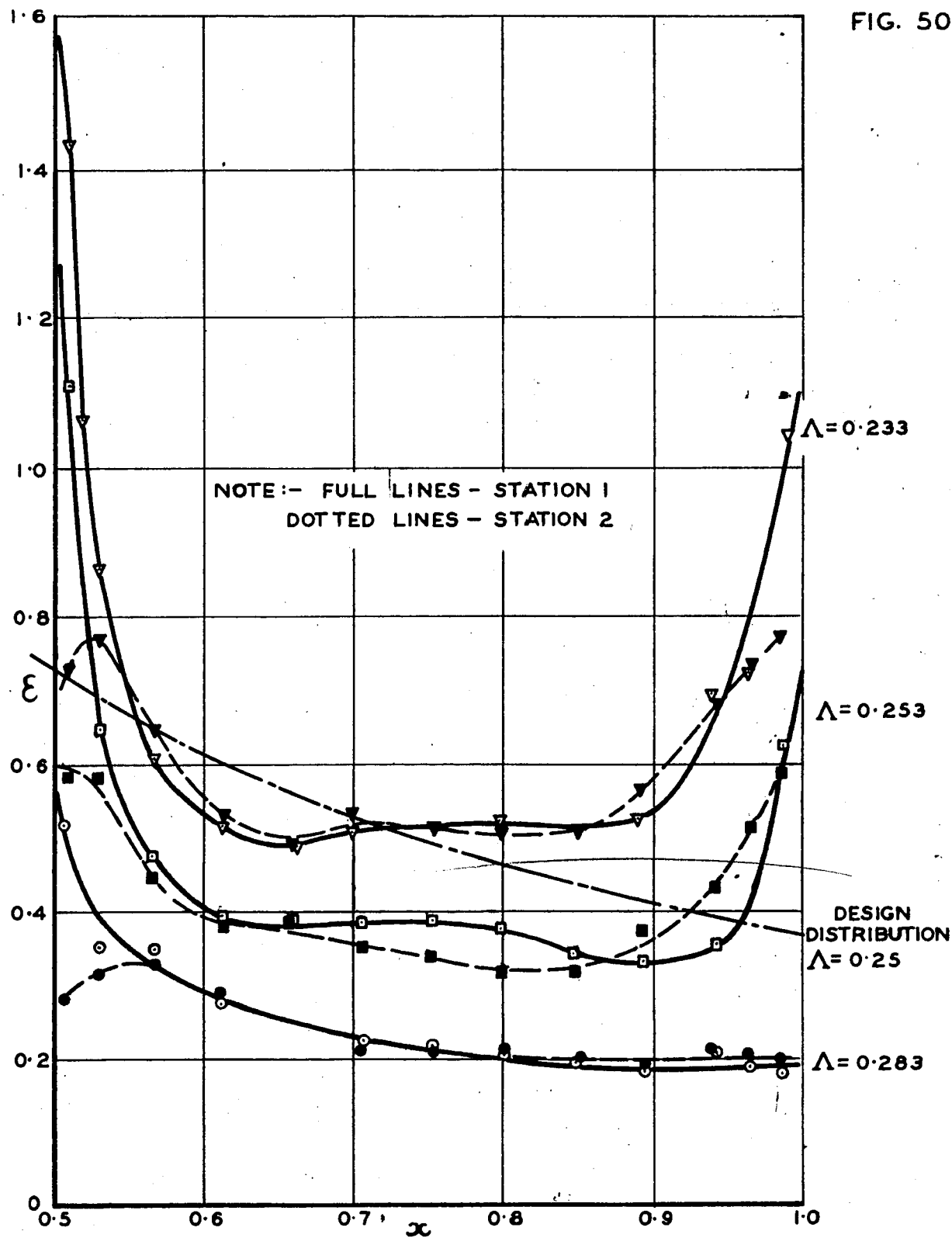
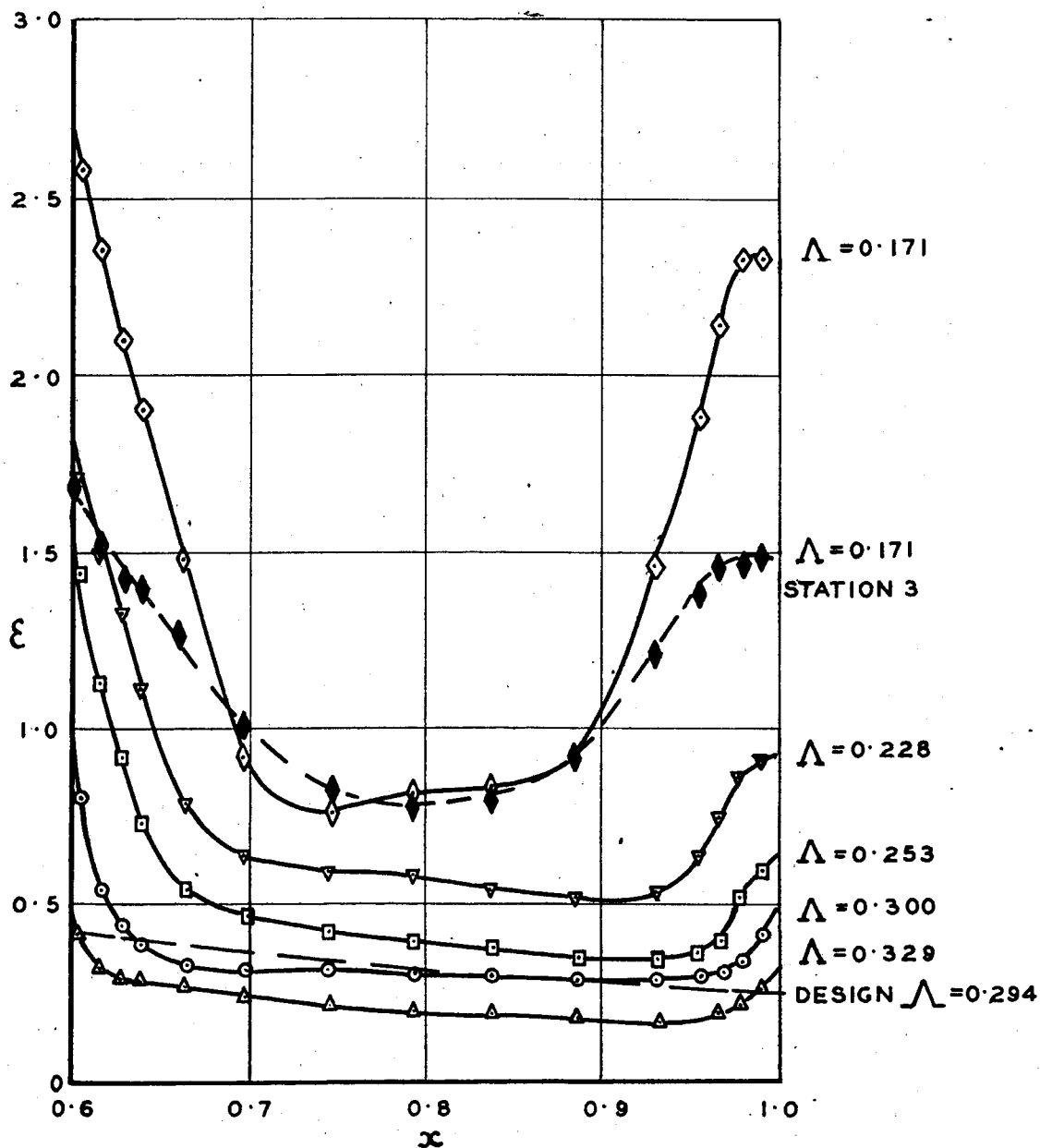
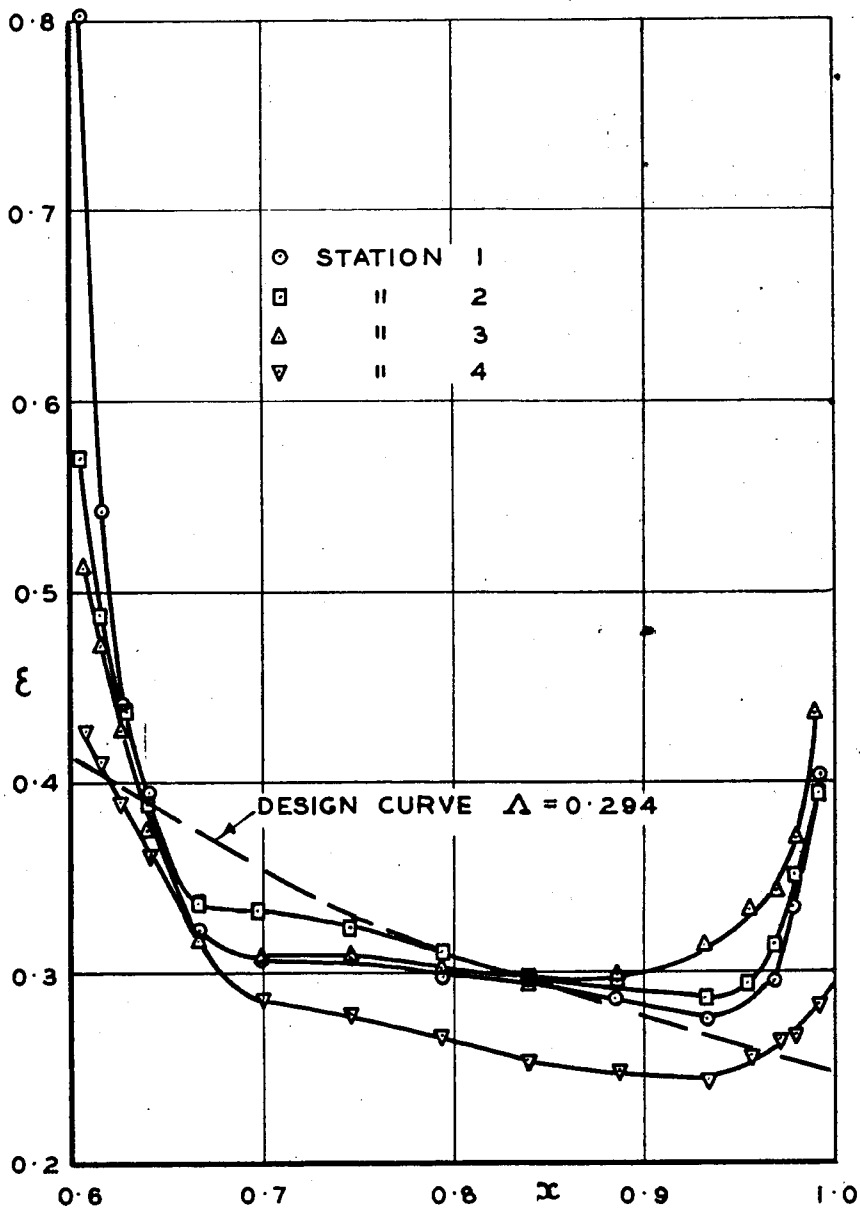


FIG. 51



VARIATION OF  $\varepsilon$  ALONG BLADE  
(STATION 1) No. 3 FAN

FIG. 52



VARIATION OF  $\epsilon$  ALONG BLADE ( $\Delta = 0.300$ )  
No. 3 FAN



FIG. 53

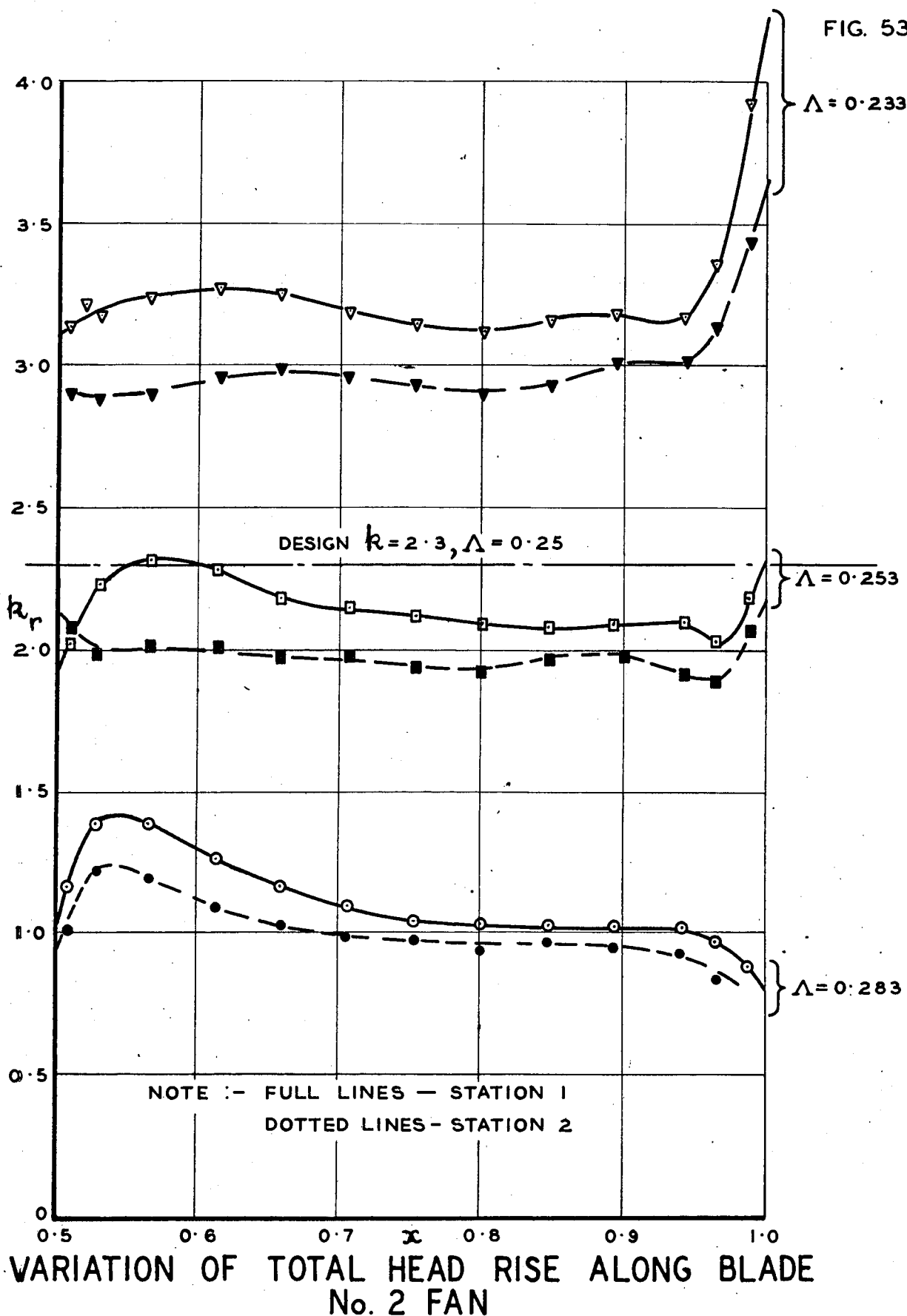
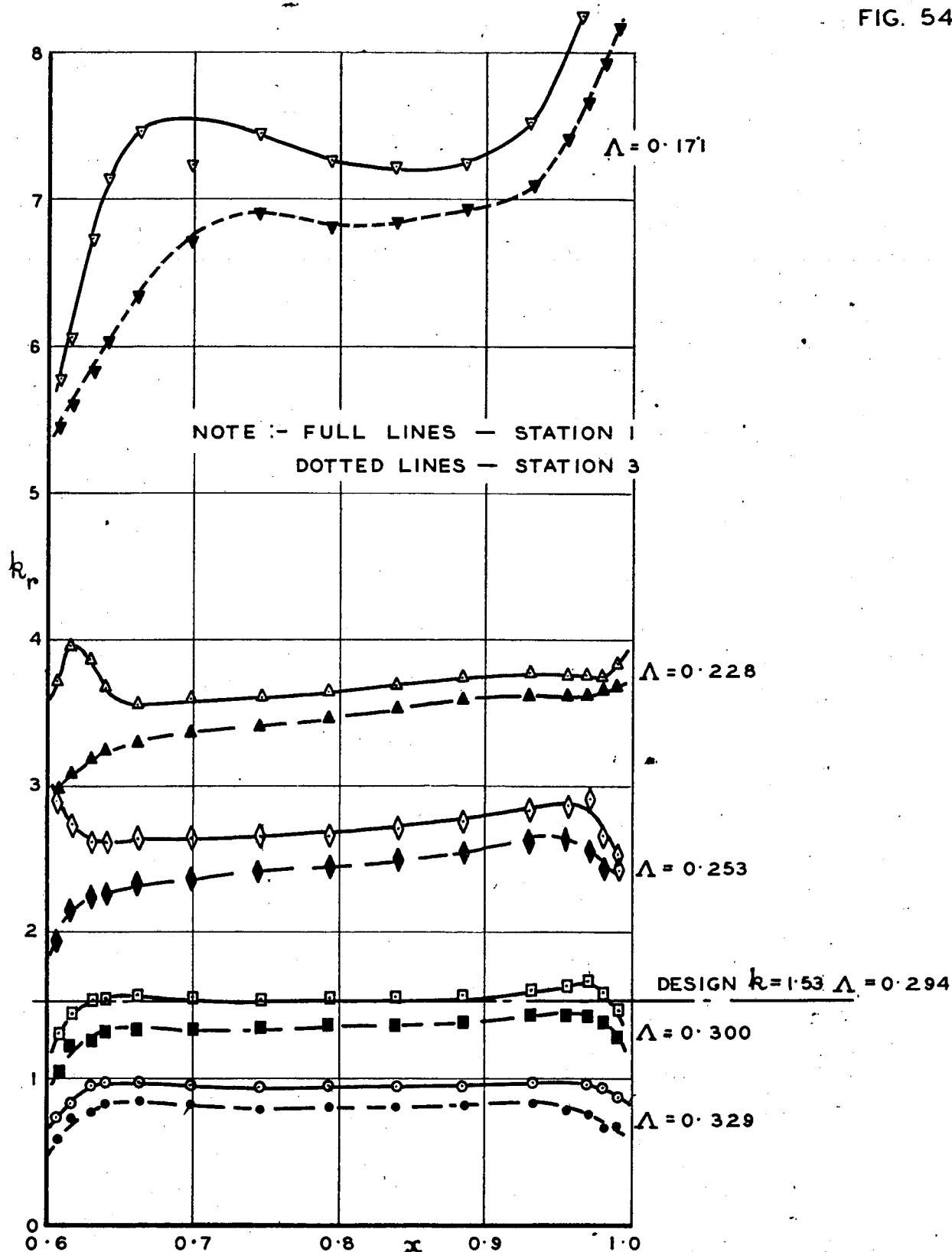
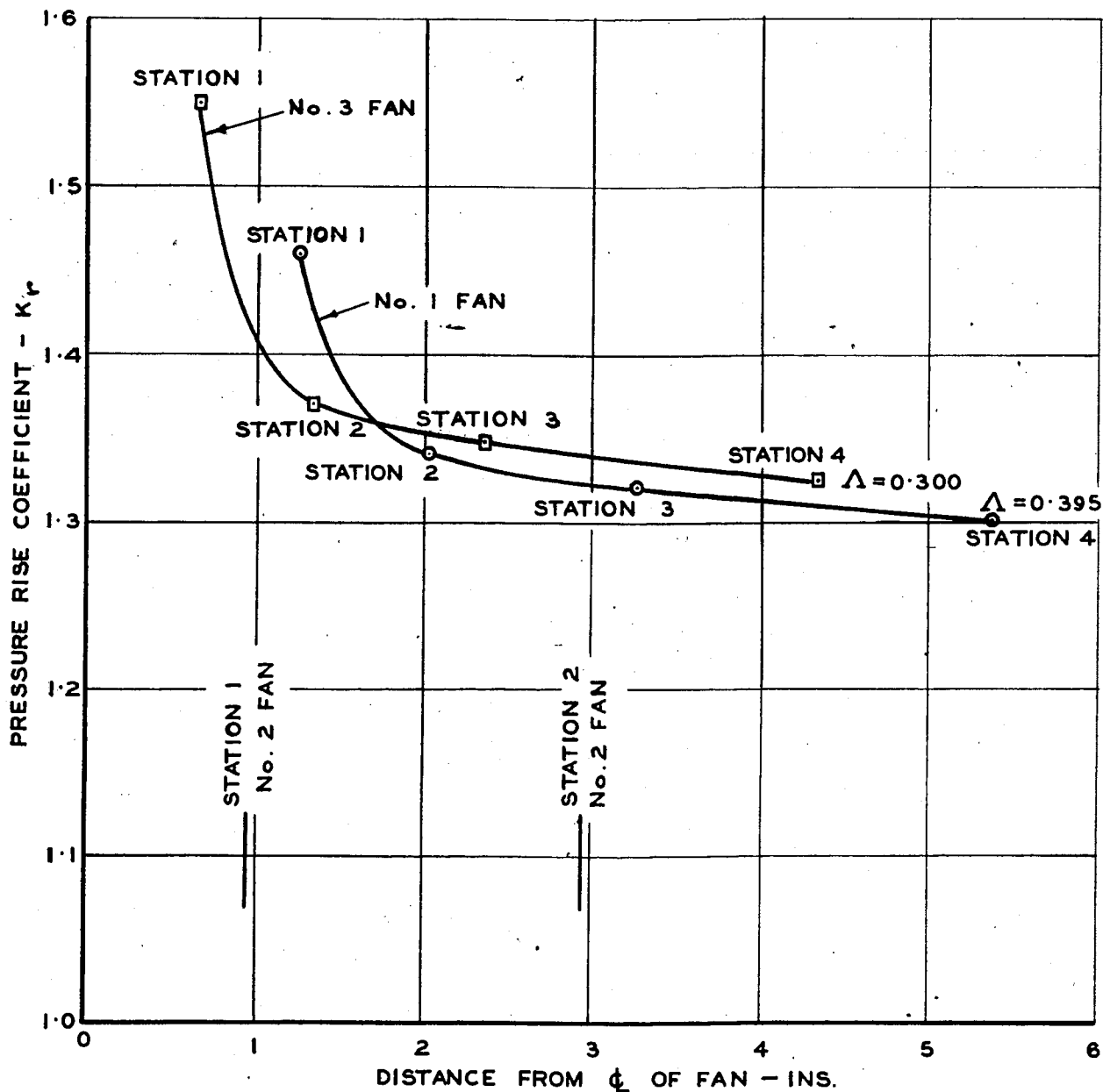
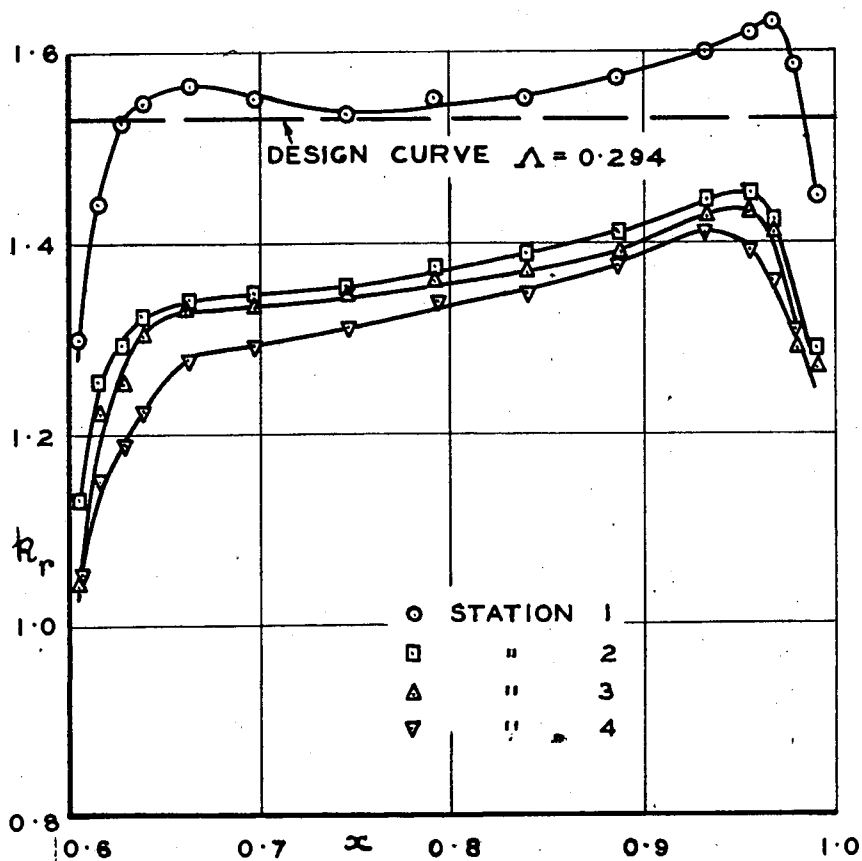


FIG. 54



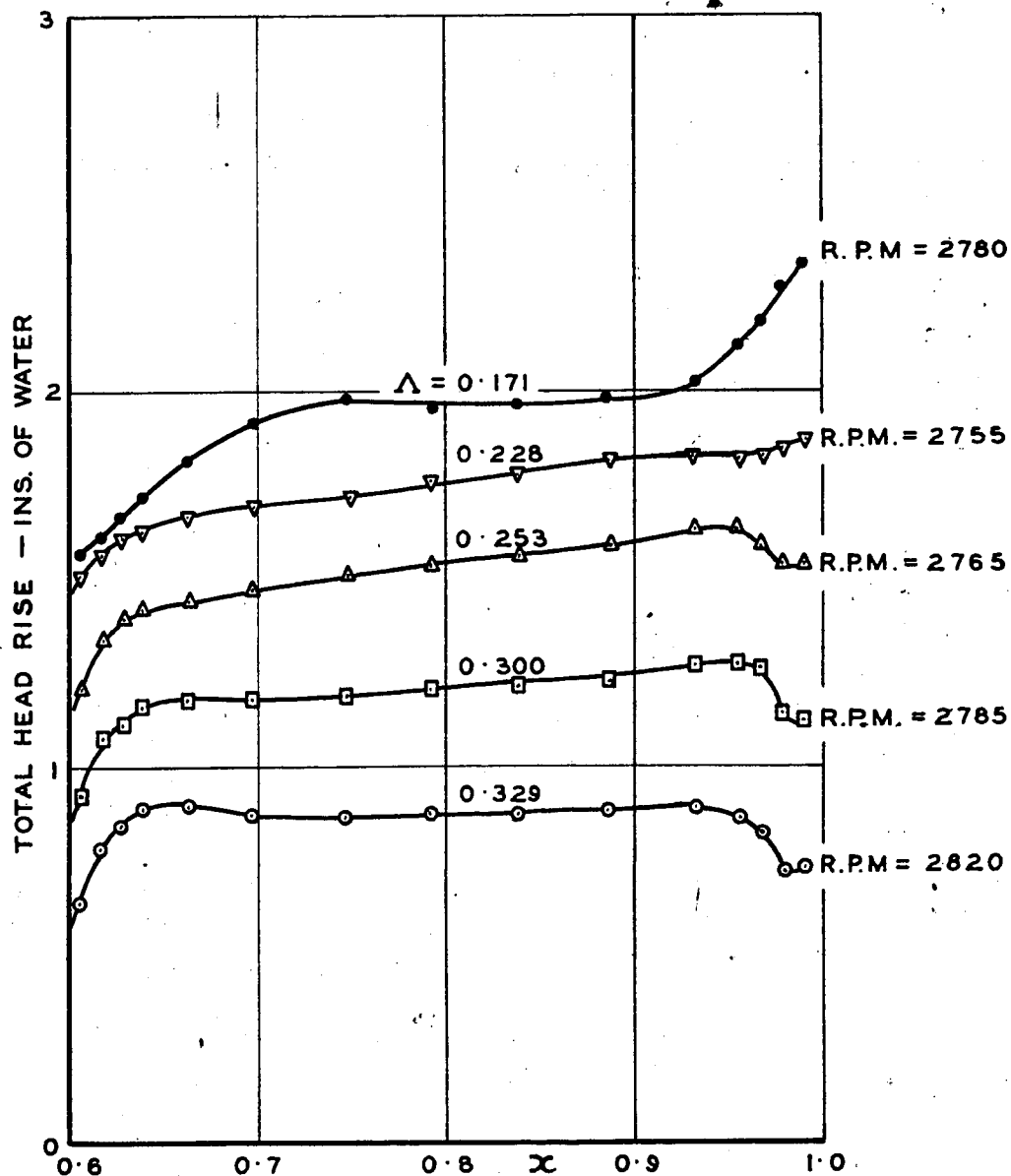


VARIATION OF  $K_p$  WITH DISTANCE DOWNSTREAM OF FAN  
No. 1 AND No. 3 FANS

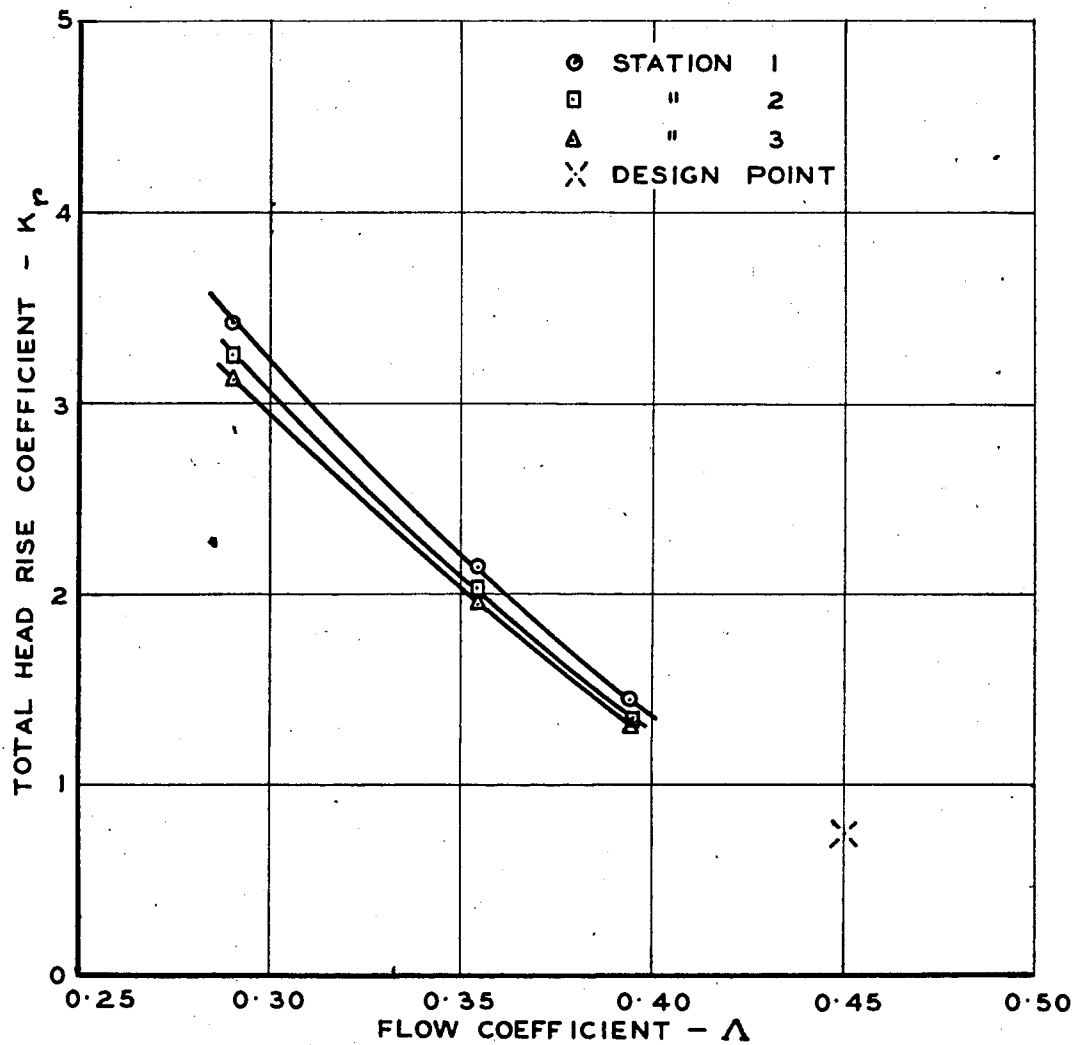


VARIATION OF TOTAL HEAD RISE ALONG BLADE ( $\Delta = 0.300$ )  
No. 3 FAN

FIG. 57

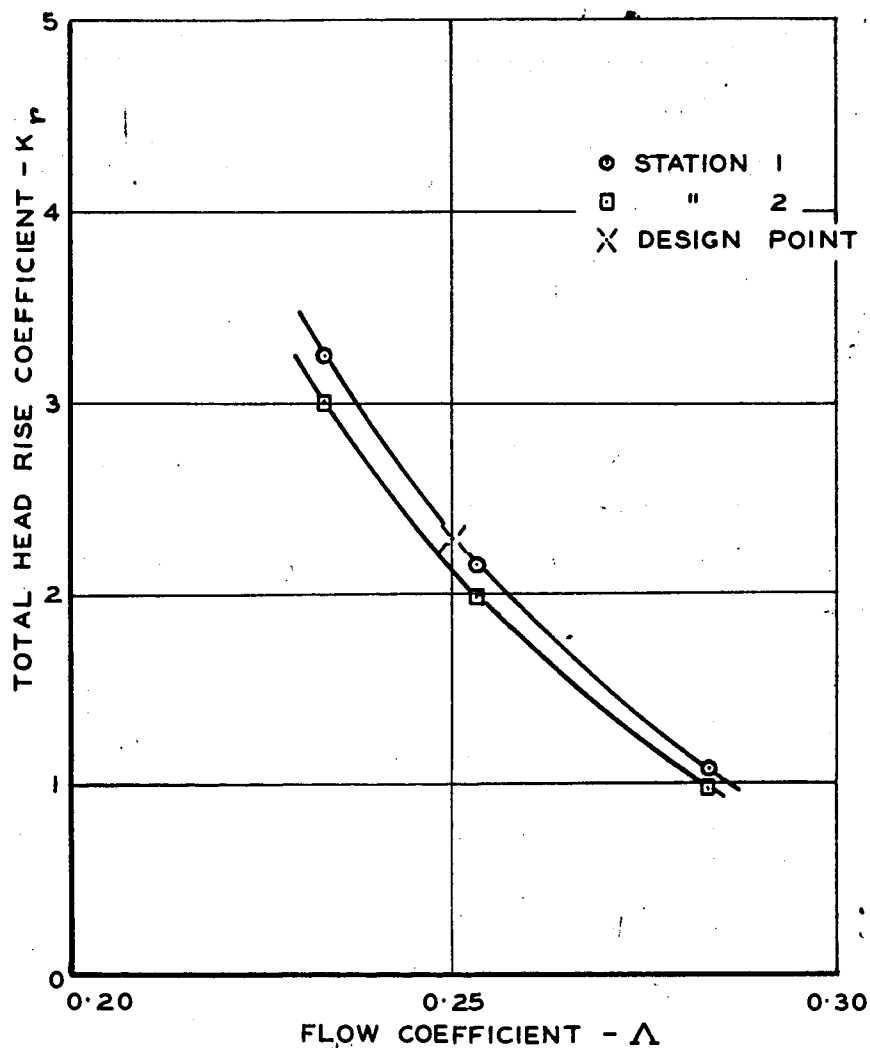


VARIATION OF TOTAL HEAD RISE ALONG BLADE  
(STATION 3) No. 3 FAN



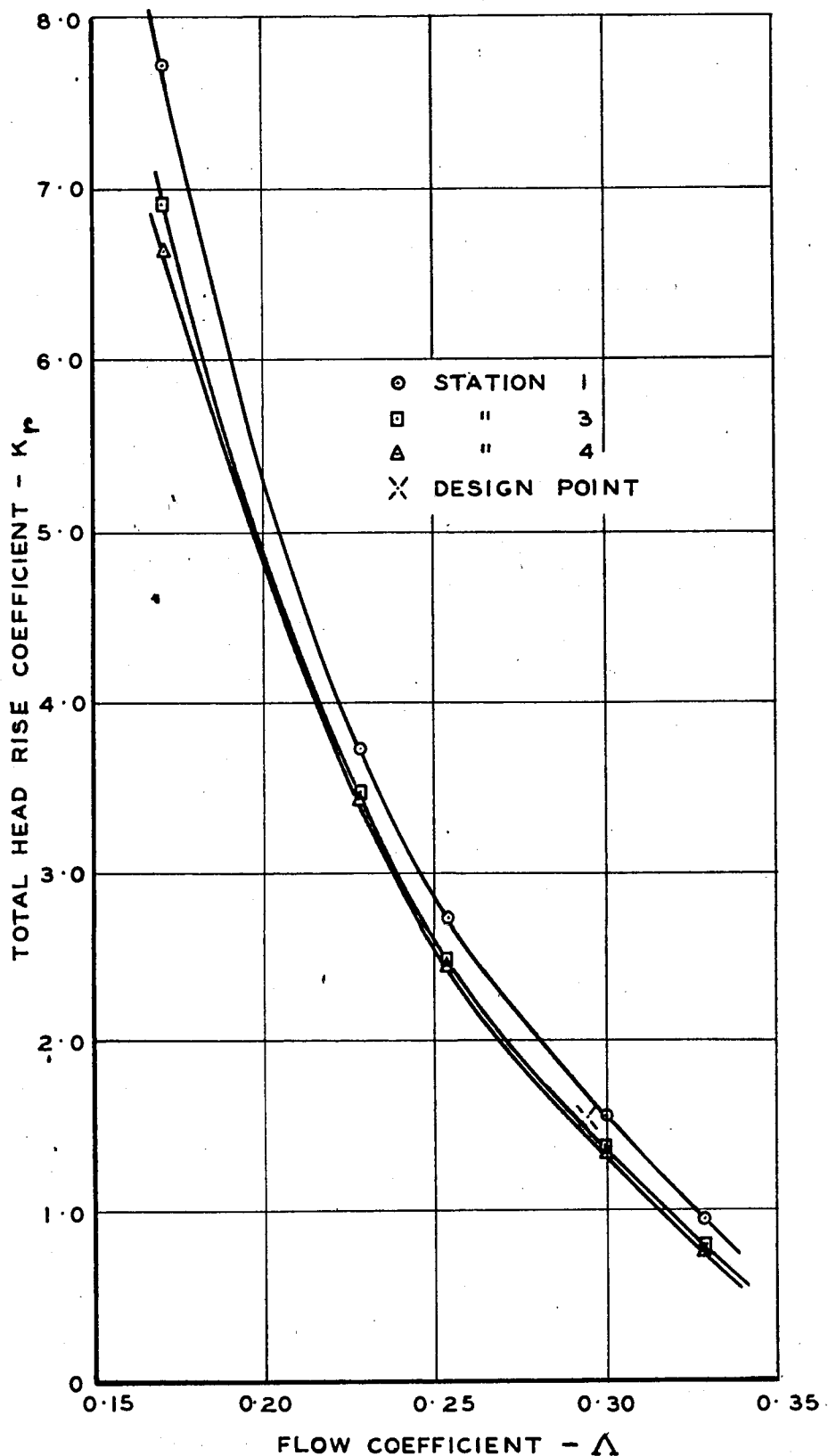
CHARACTERISTIC CURVE FOR No.1 FAN

FIG. 59



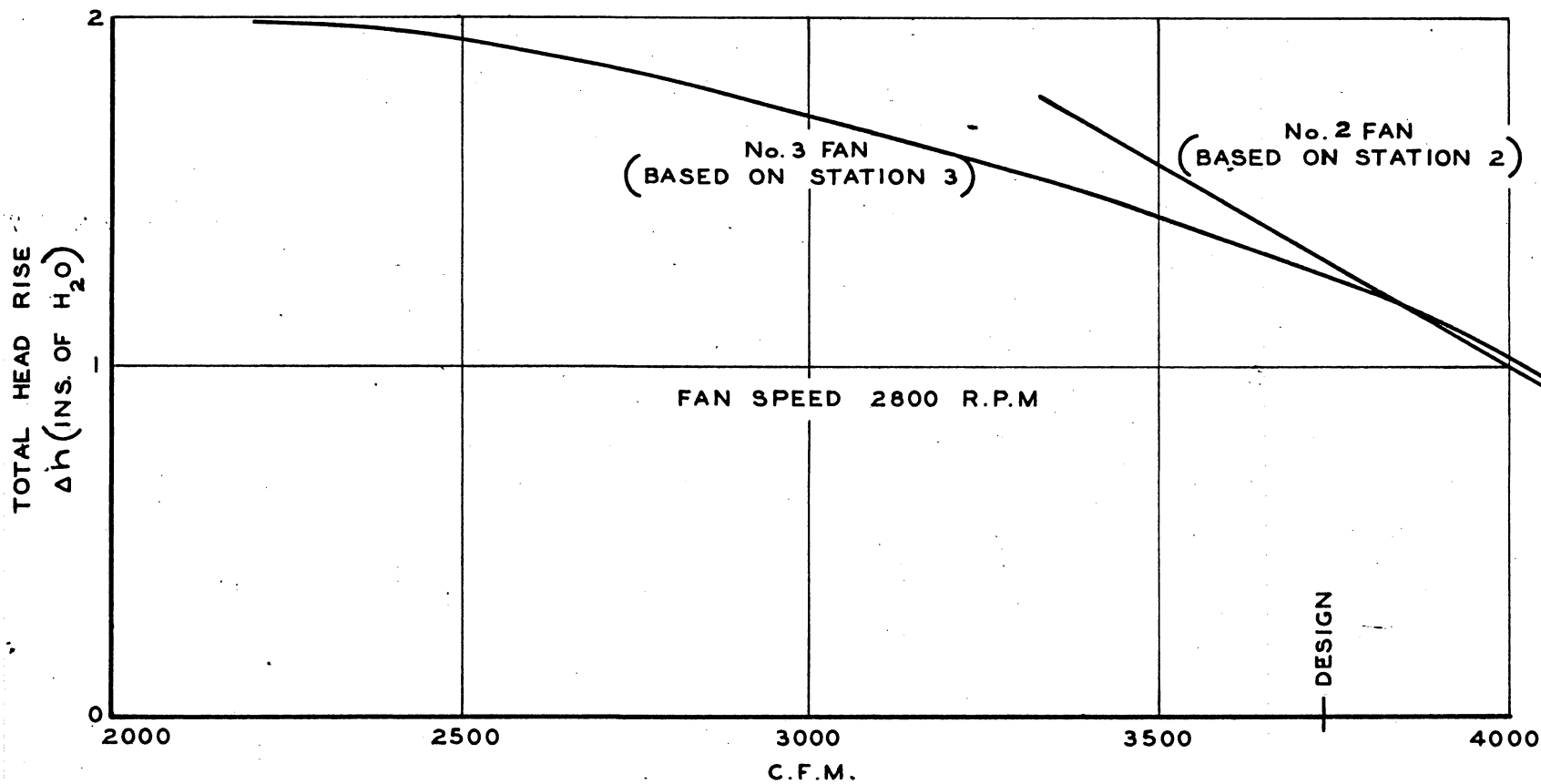
CHARACTERISTIC CURVE FOR No. 2 FAN

FIG. 60



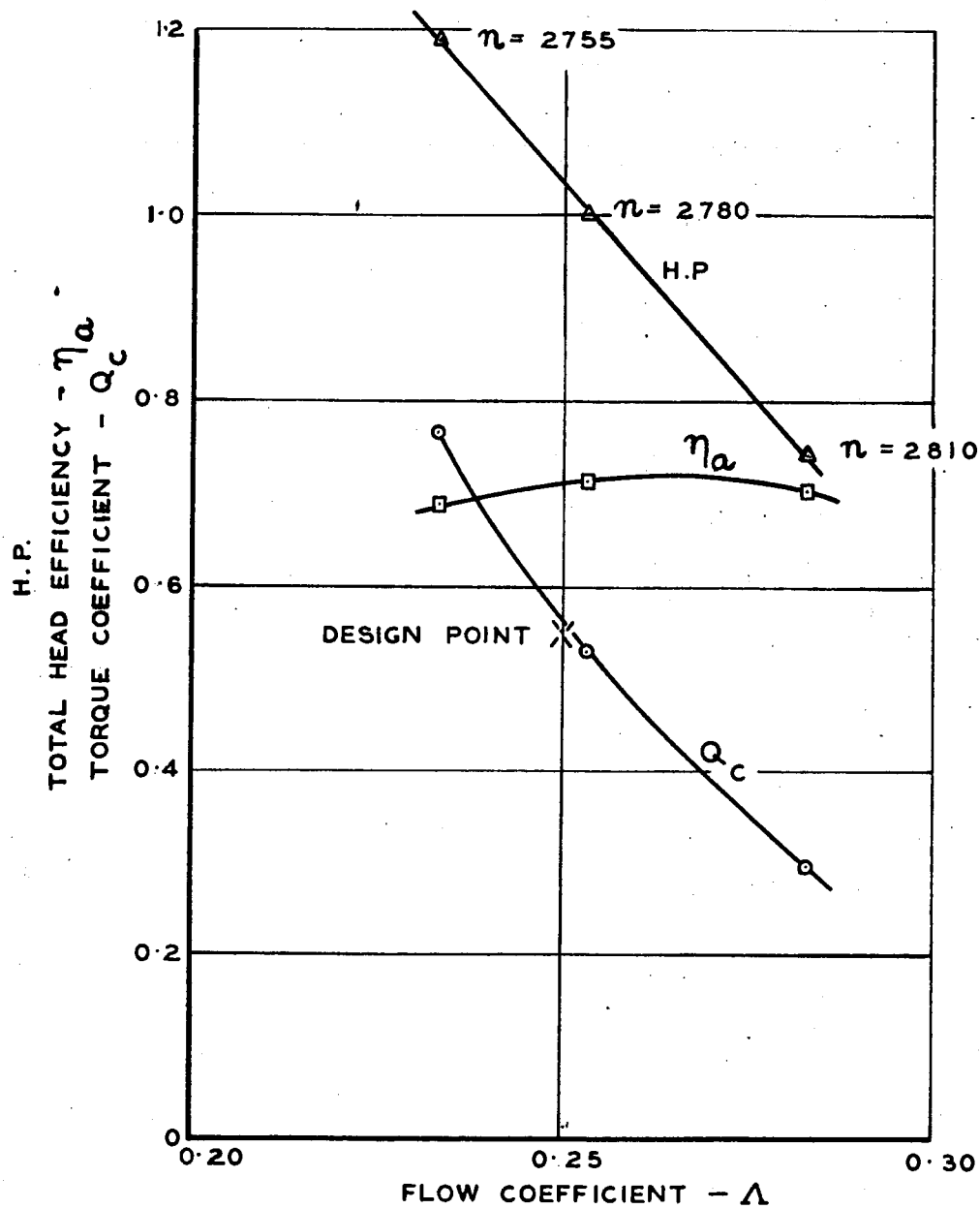
CHARACTERISTIC CURVE FOR No. 3 FAN



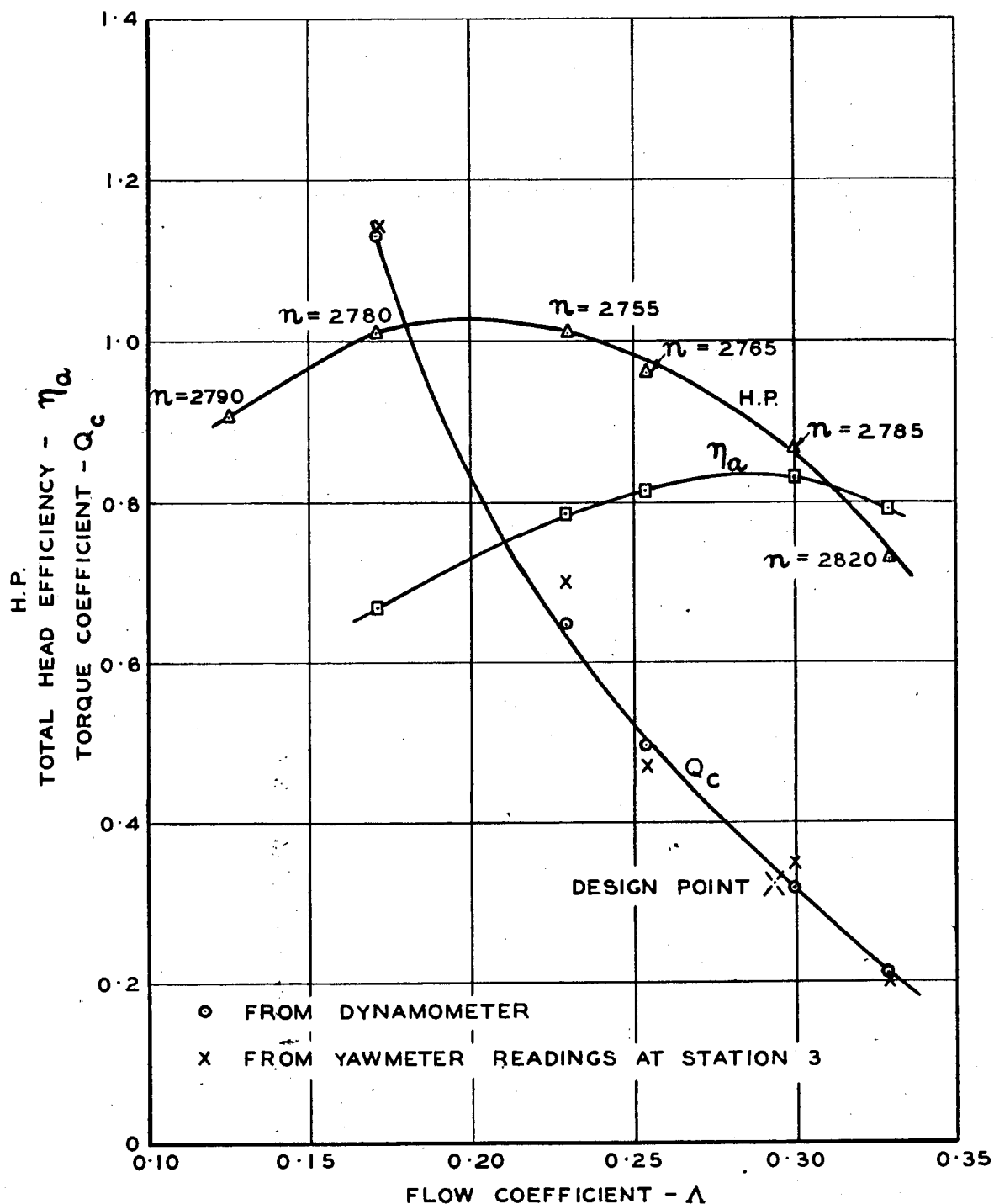


COMPARISON OF No.2 AND No.3 FANS

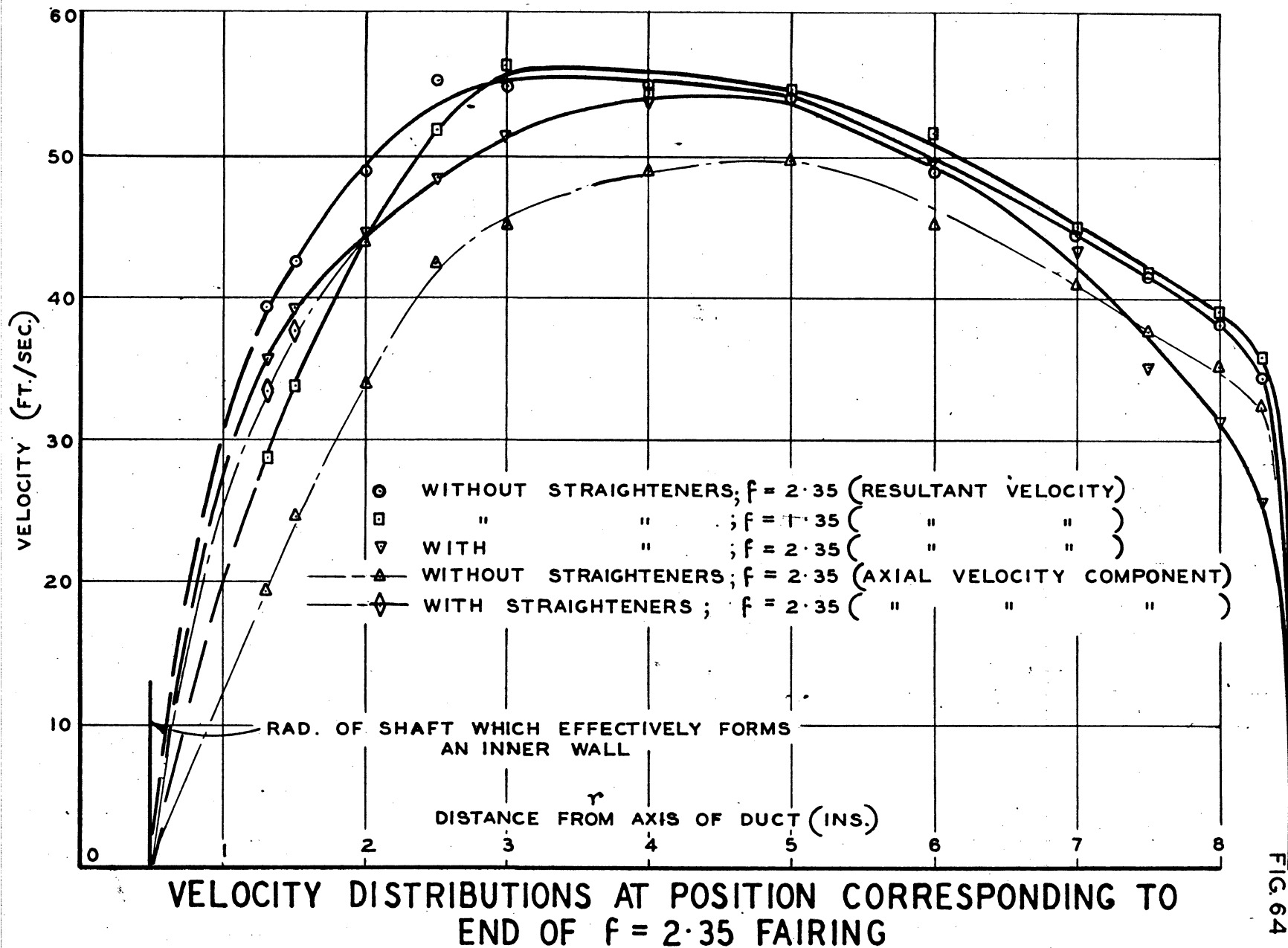
FIG. 62

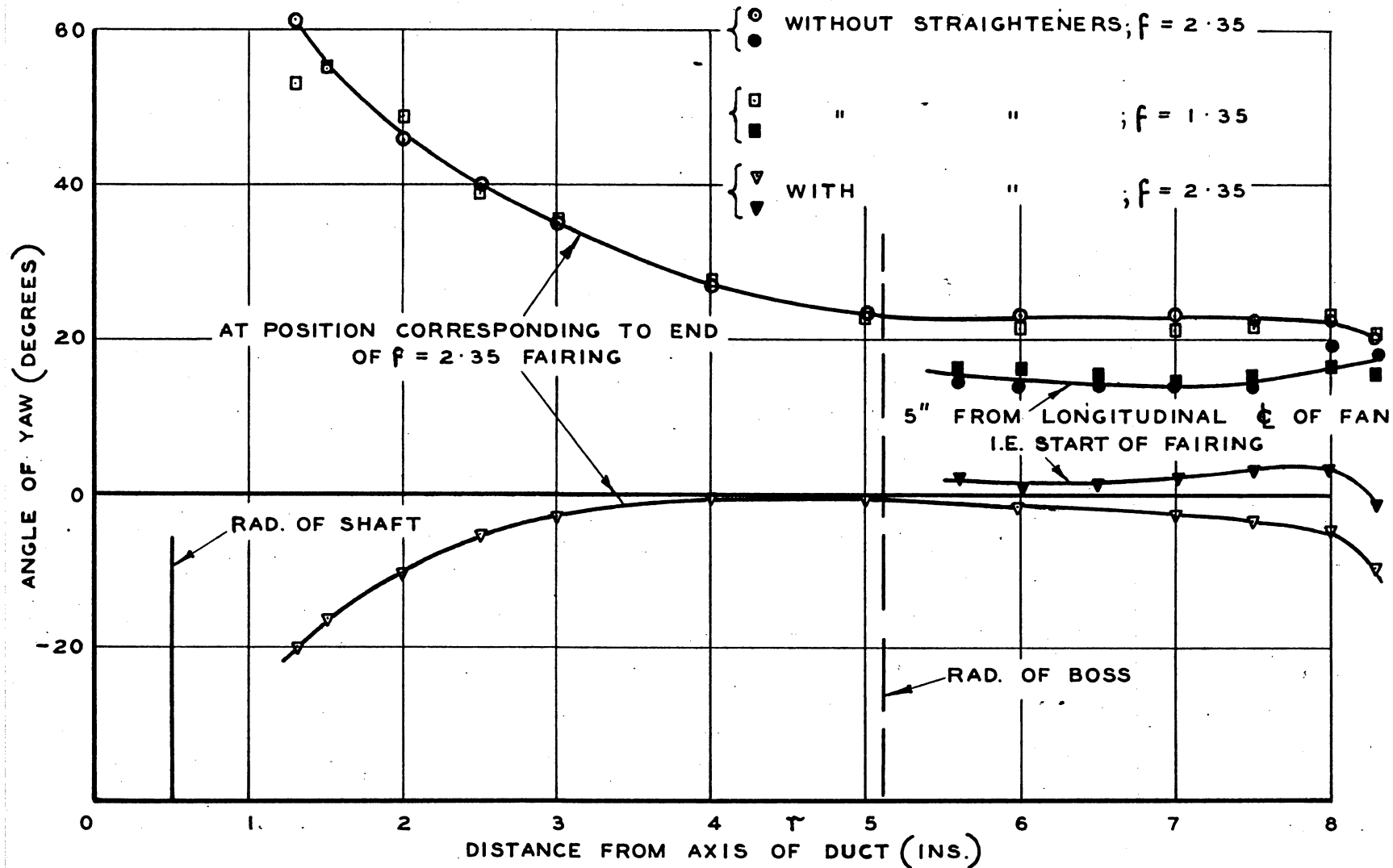


EFFICIENCY AND POWER OF No.2 FAN

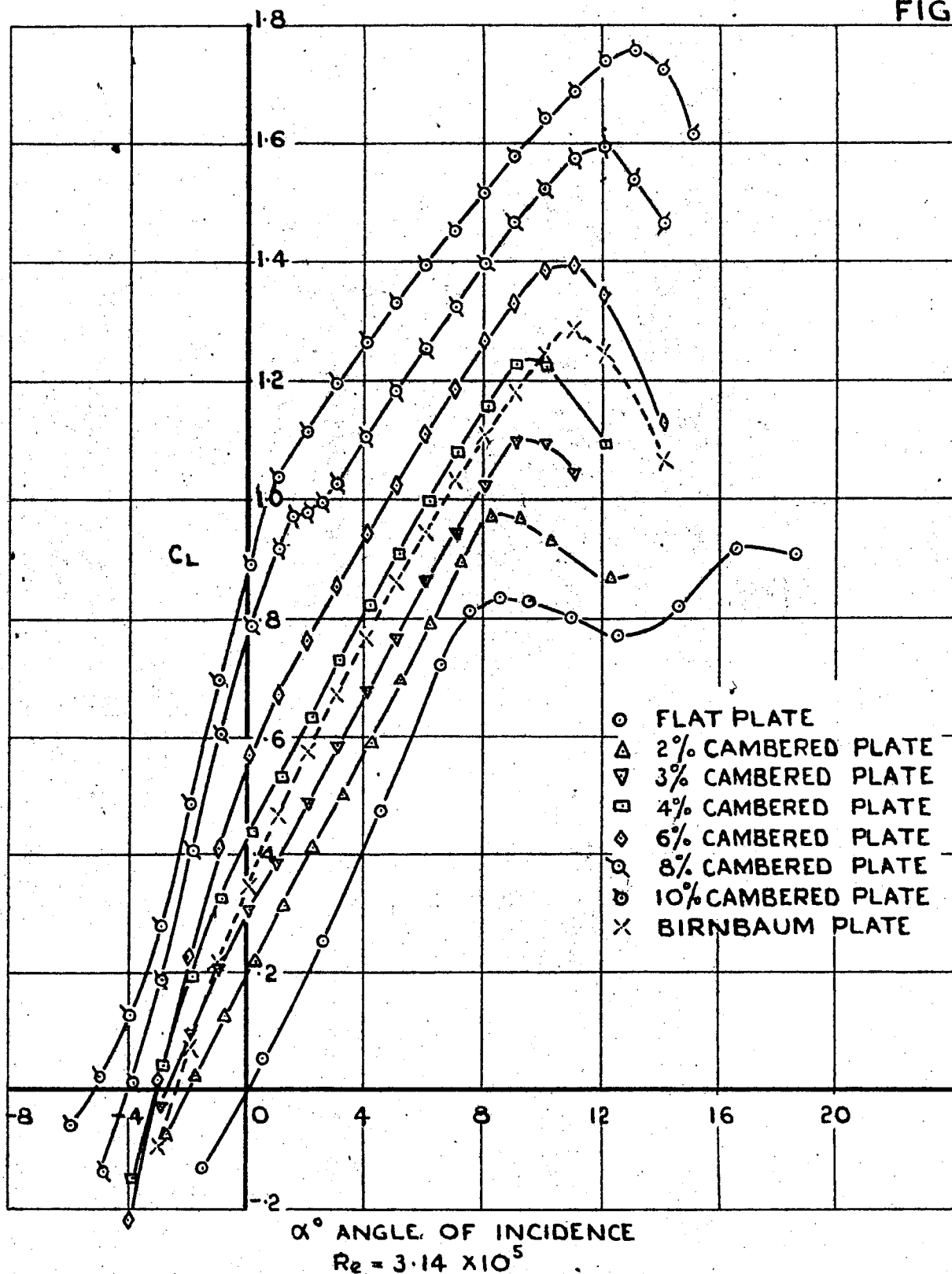


EFFICIENCY AND POWER OF No. 3 FAN



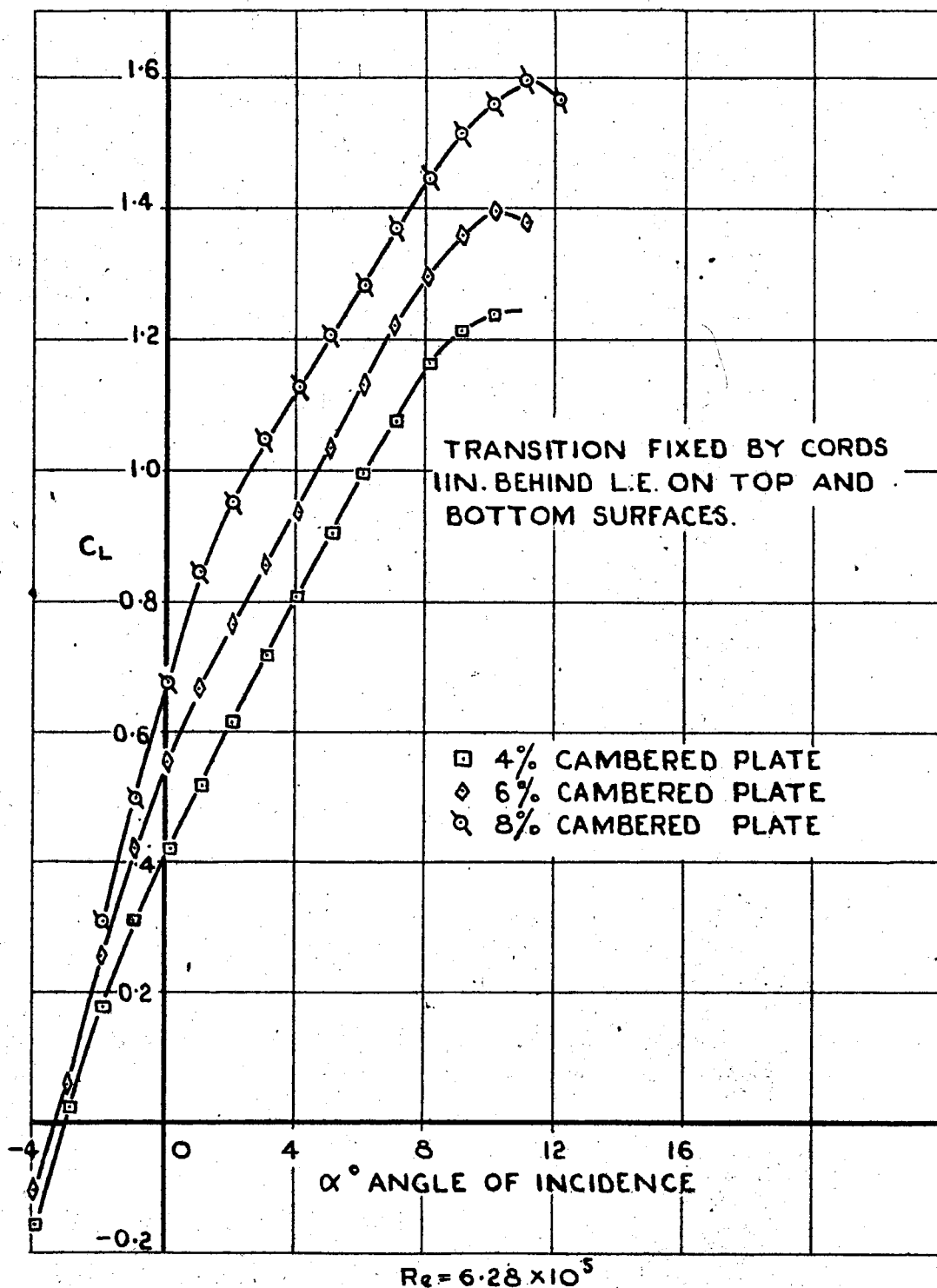


DISTRIBUTION OF YAW NEAR TAIL FAIRING



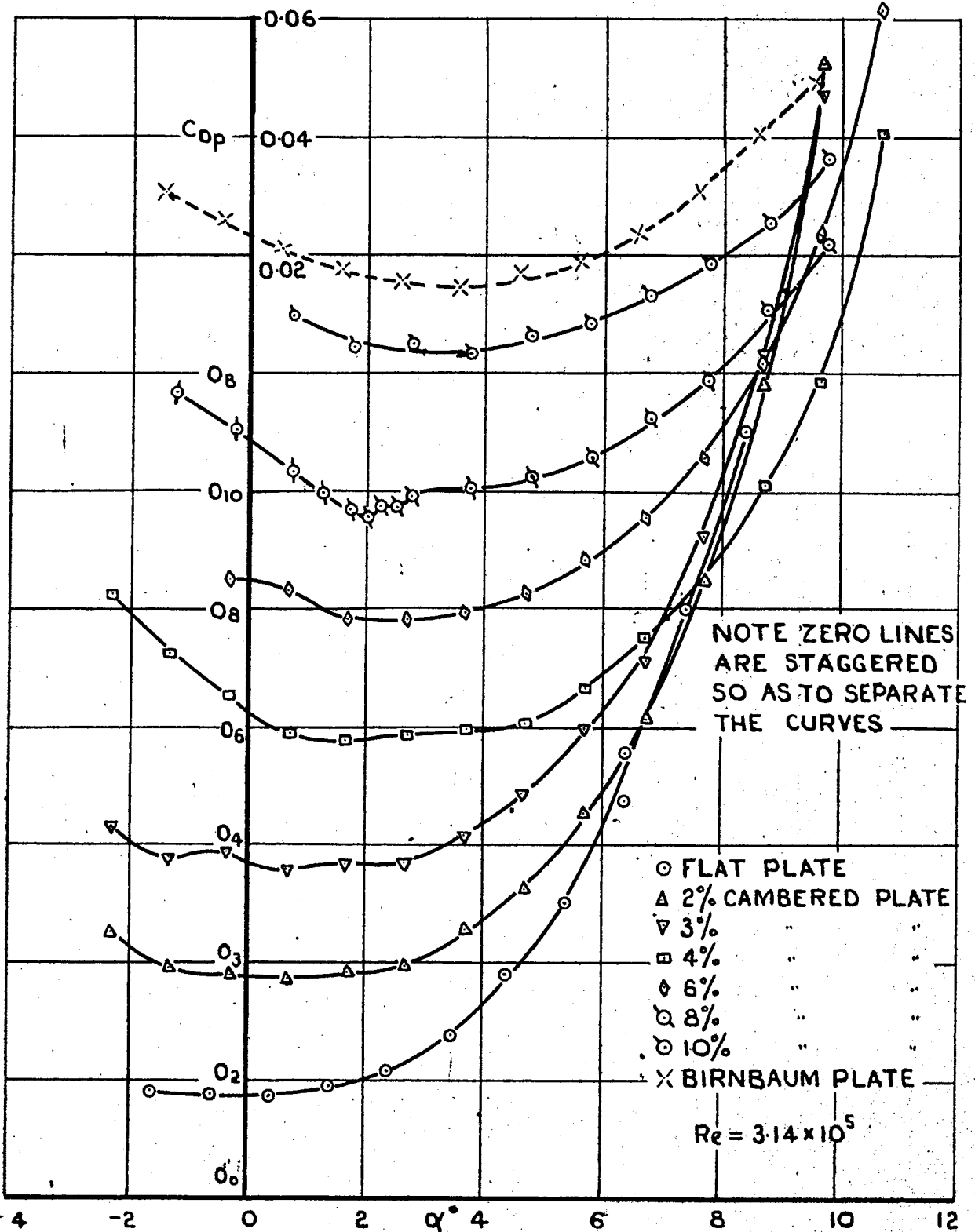
TWO-DIMENSIONAL LIFT CHARACTERISTICS

FIG.67



## TWO-DIMENSIONAL LIFT CHARACTERISTICS

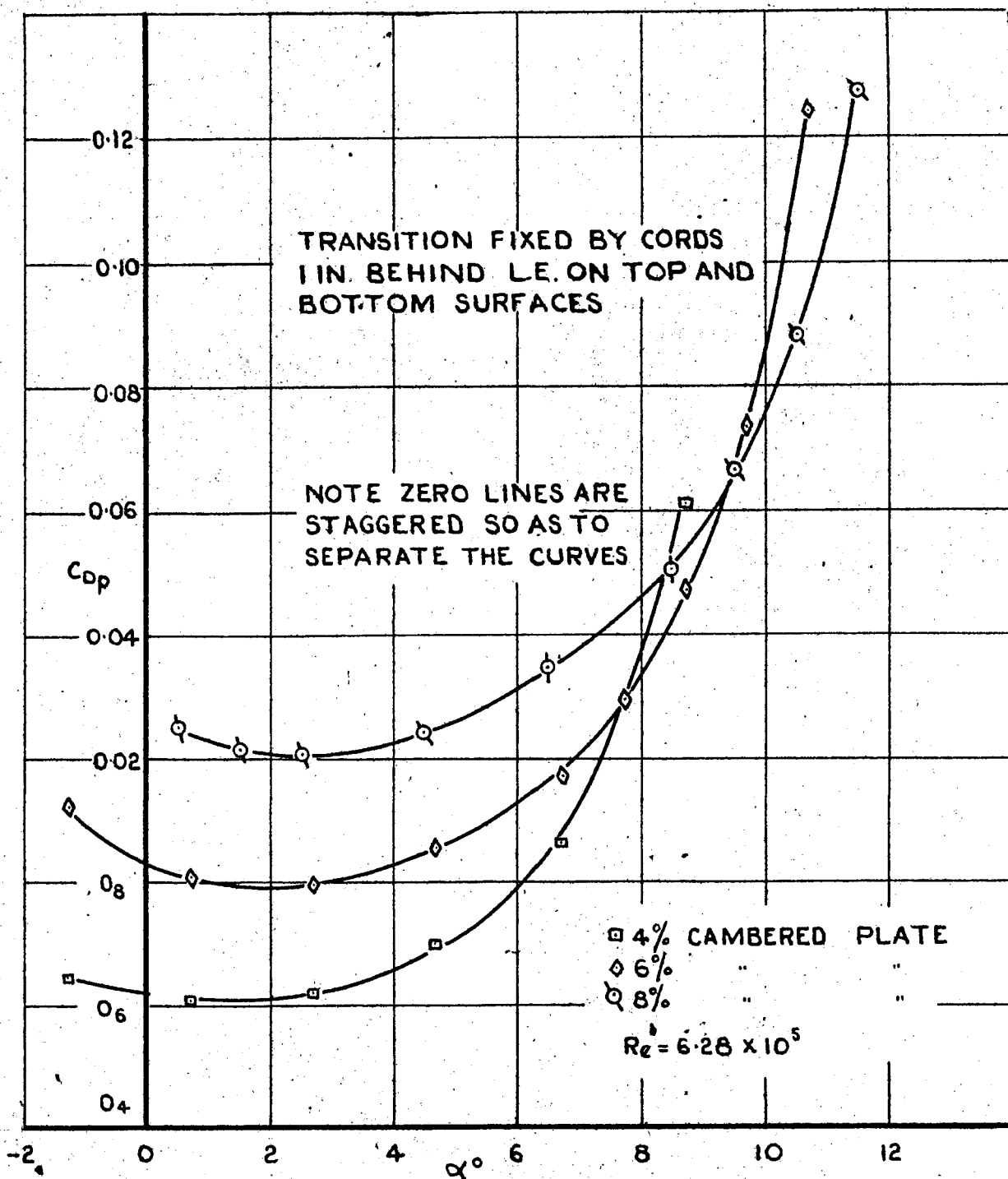
FIG. 68



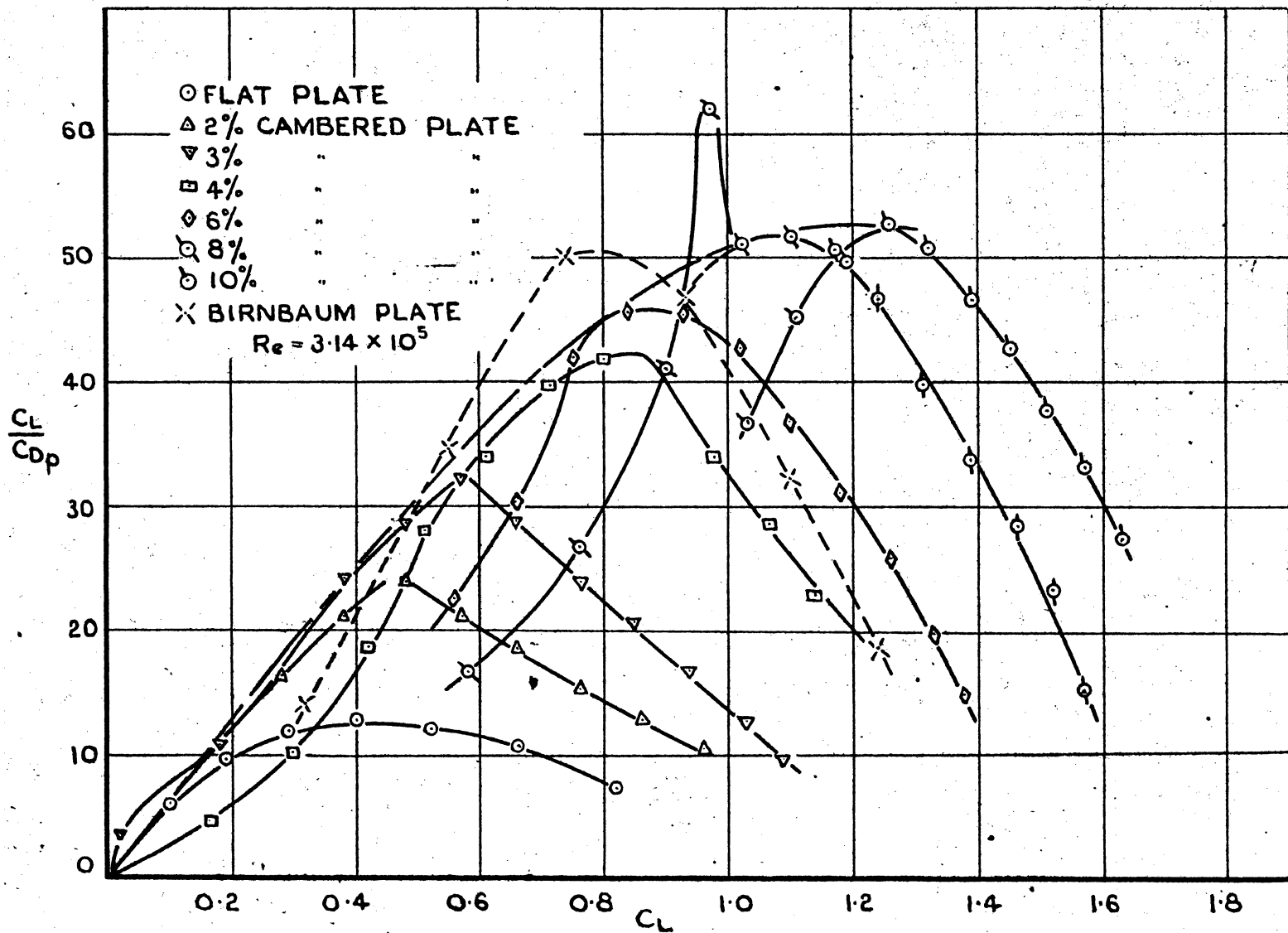
PROFILE DRAG CHARACTERISTICS



FIG. 69



PROFILE DRAG CHARACTERISTICS



LIFT  
PROFILE DRAG

CHARACTERISTICS

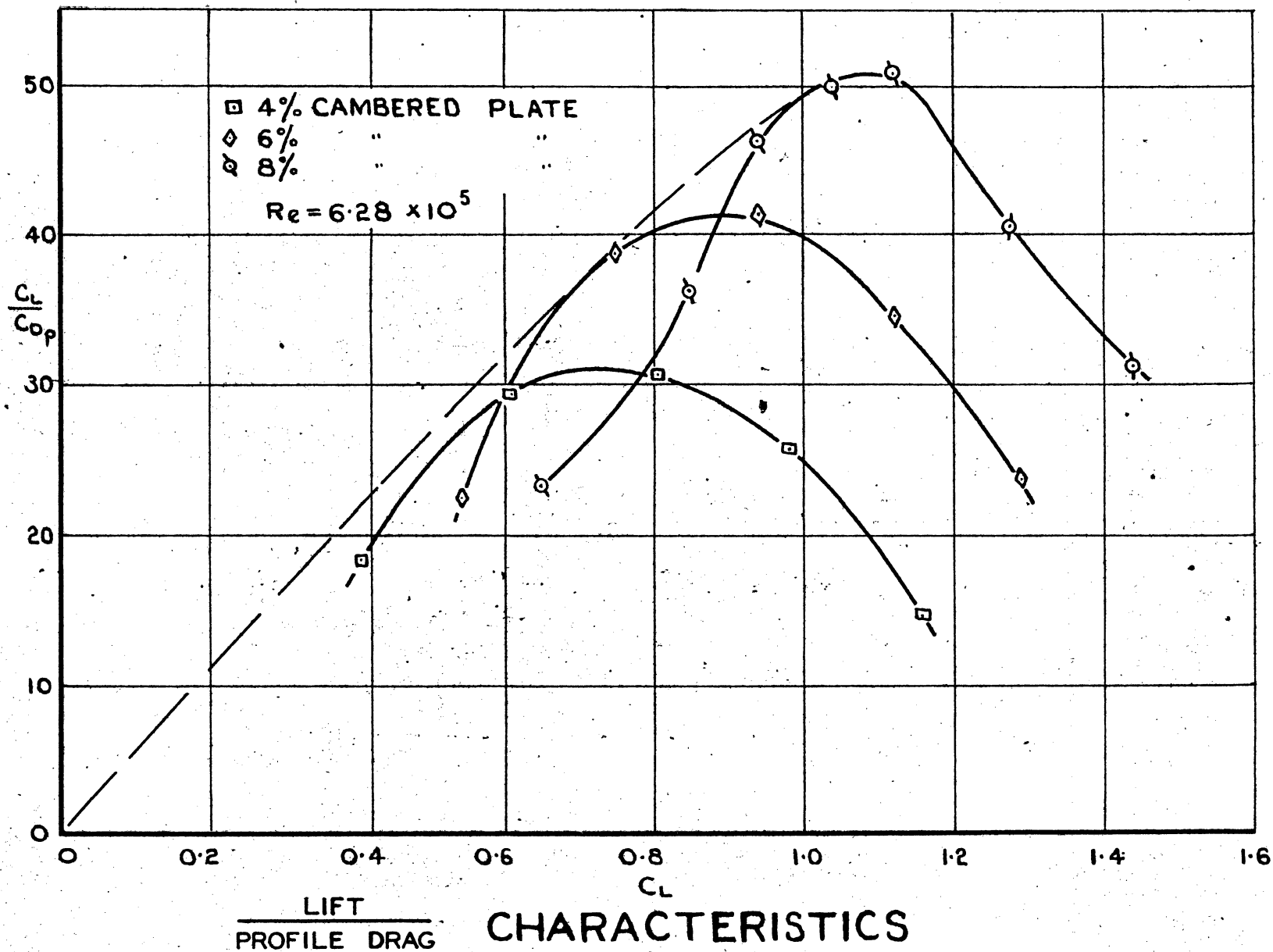
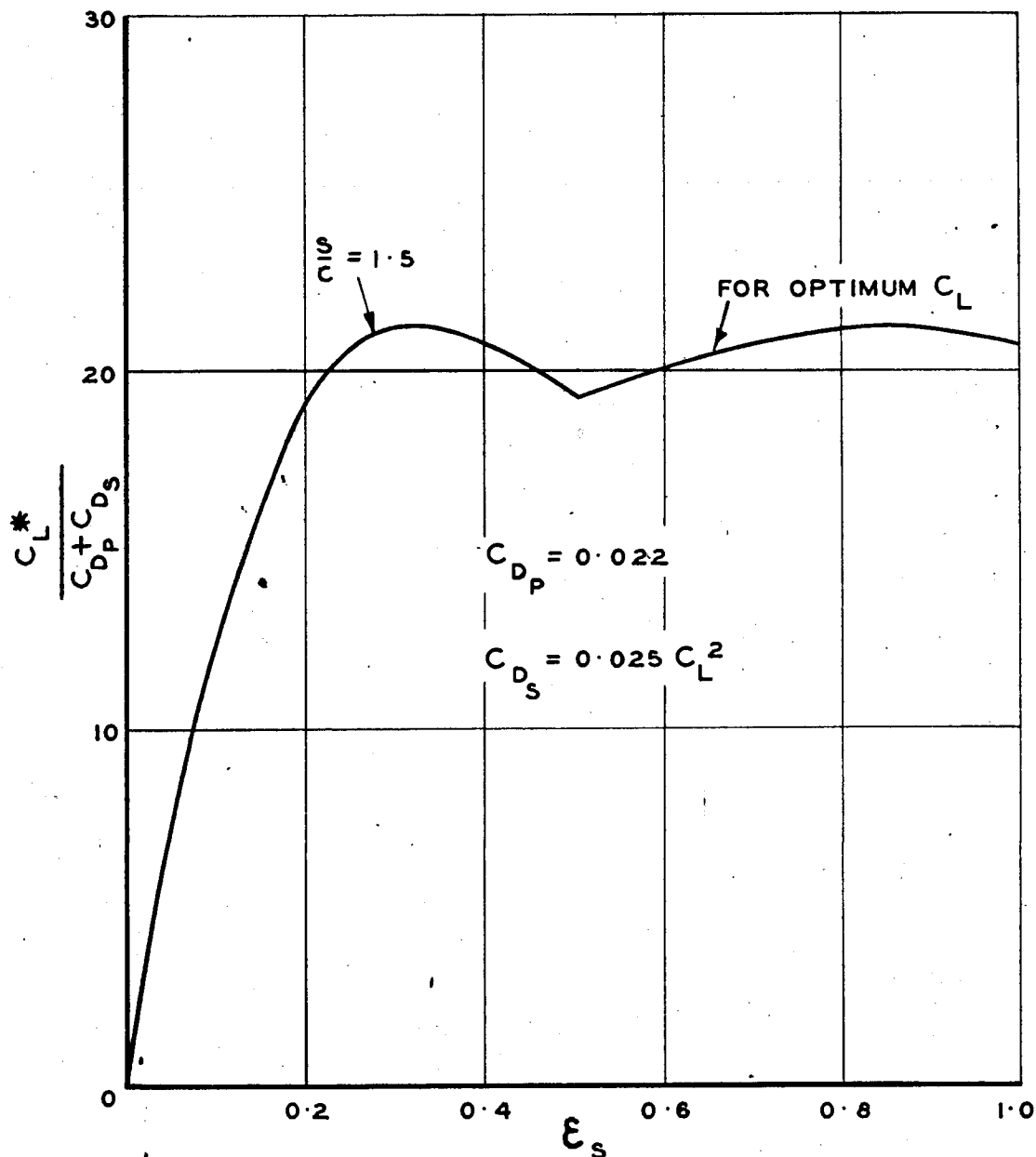
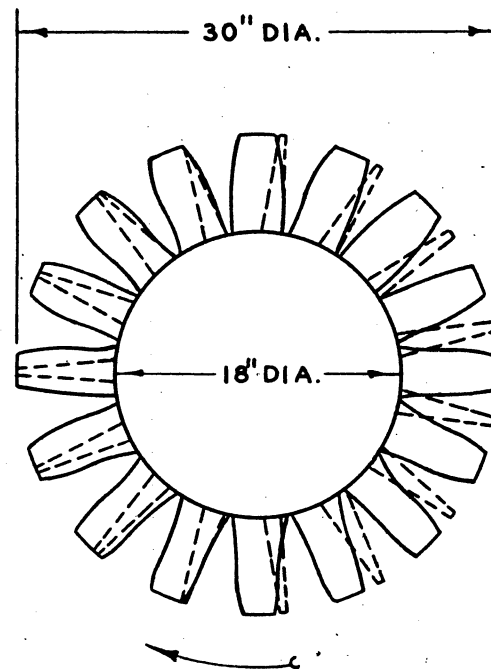
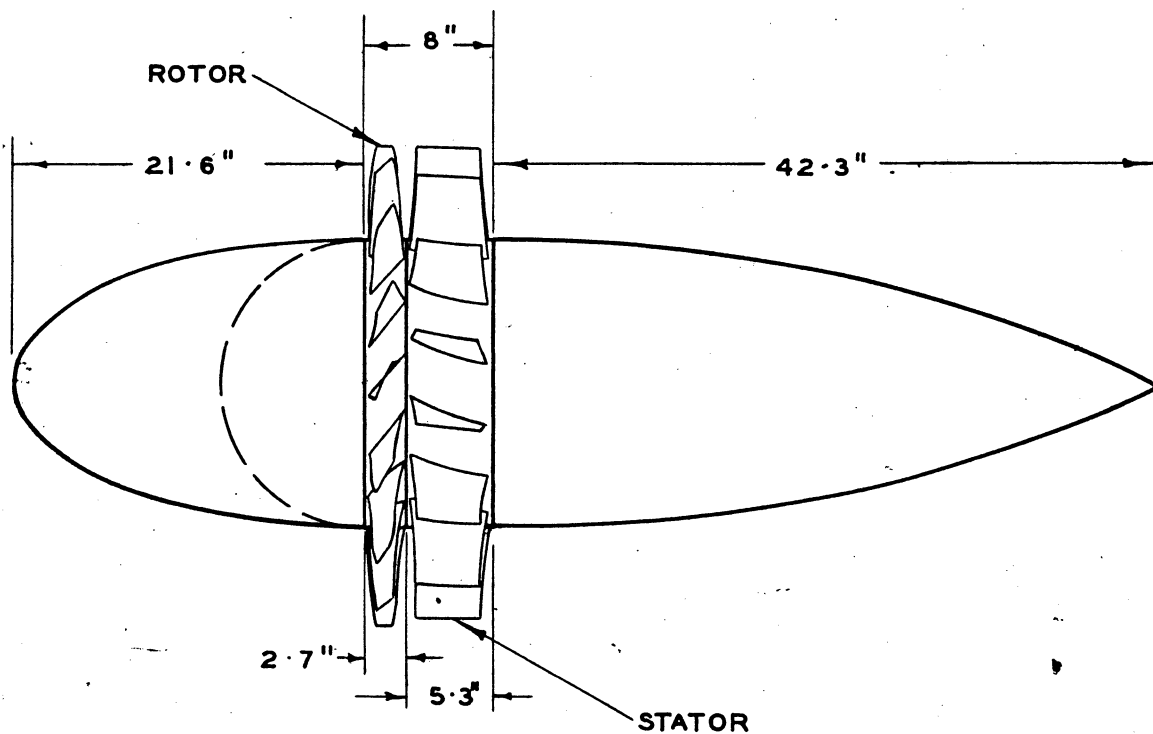


FIG. 71

FIG. 72



LIFT/DRAG RATIO FOR SHEET METAL CASCADE  
TYPE STRAIGHTENERS — OPTIMUM CONDITIONS



SCALE :- 1" = 1 FOOT

DESIGN EXAMPLE — APPENDIX F

## REFERENCES

1. A. Kahane                      Investigation of axial flow fan and compressor rotors designed for three-dimensional flow. NACA Technical Note 1652 (July, 1948).
2. H.B. Finger                    Method of experimentally determining radial distributions of velocity through axial flow compressor. NACA Technical Note 2059 (April, 1950).
3. A.R. Howell                    The present basis of axial flow compressor design. Part II. Compressor theory and performance. RAE. Report E.3961. (December, 1942).
4. A.R. Collar                    The design of wind tunnel fans R. & M. 1889, (August, 1940).
5. W.A. Mair                      The design of fans and guide vanes for high speed wind tunnels. R. & M. 2435, (June, 1944).
6. G.N. Patterson                Ducted fans: design for high efficiency. Australian Council for Aeronautics. Report ACA-7, (July, 1944)
7. C. Keller                      The theory and performance of axial flow fans (Edited by L.S. Marks and J.R. Weske) First Edition 1937, McGraw-Hill Book Company.
8. Y. Shimoyama                Experiments on rows of aerofoils for retarded flow. Memoirs of the Faculty of Engineering, Kyushu Imperial University, Fukuoka, Japan. Vol.VIII, No.4, 1938.
9. A.R. Collar                    Cascade theory and the design of fan straighteners. R. & M.1885, (January, 1940).

10. E. Struve  
Theoretical determination of axial flow performance .  
Report 295 of the Central Aero-Hydro dynamical Institute, Moscow, 1937. Translated in NACA Technical Memo 1042 (April, 1943).
11. P. Ruden  
Investigation of single stage fans Luftfahrtforschung, Vol.14 No.7, July, 1937, Translated in NACA Technical Memo 1062, (April, 1944).
12. G. Krober  
Vane grids for the deflection of fluid flows with small energy losses.  
Ingenieur - Archiv, Vol.3, No.6, 1932, Translated in NACA Technical Memo 722.
13. A. Betz  
Diagrams for calculation of aerofoil lattices. Ingenieur - Archiv Vol.2, No.3, September, 1931, Translated in NACA Technical Memo 1022 (July, 1942).
14. W. Merchant  
Flow of an ideal fluid past a cascade of blades. R. & M.1890. (July, 1940)
15. R.E. Meyer  
A contribution to the theory of axial blade grids.  
Aeronautical Research Council Report 8869, (July, 1945).
16. A.R. Howell  
Note on the theory of arbitrary aerofoils in cascade, RAE. Note E.3696 (March, 1941).
17. S. Katzoff,  
R.S. Finn and  
J.C. Lawrence  
Interference method for obtaining the potential flow past an arbitrary cascade of aerofoils.  
NACA. Technical Note 1252, (May, 1947).

18. L. Diesendruck  
Iterative interference methods  
in the design of thin cascade  
blades. NACA. Technical Note  
1254 (May, 1947).
19. M.J. Lighthill  
A mathematical method of  
cascade design.  
R. & M. 2104 (June, 1945).
20. A.G. Hansen  
and  
P.L. Yohner  
A numerical procedure for  
designing cascade blades with  
prescribed velocity distribution  
in incompressible potential flow  
NACA. Technical Note 2101,  
(June, 1950).
21. G.R. Costello  
Method of designing cascade  
blades with prescribed velocity  
distributions in compressible  
potential flows.  
NACA. Report 978. (1950)
22. A.W. Goldstein  
and  
M. Jerison  
Isolated and cascade aerofoils  
with prescribed velocity  
distribution.  
NACA. Report 869  
(1947).
23. G.R. Costello  
R.L. Cummings  
and  
J.T. Sinnette  
Detailed computational procedure  
for design of cascade blades with  
prescribed velocity distributions  
in compressible potential flows.  
NACA. Technical Note 2281,  
(February, 1951).
24. S.M. Bogdonoff  
Blade design data for axial flow  
fans and compressors.  
NACA. ACR. L5F07a (July, 1945).
25. A.R. Howell  
The present basis of axial flow  
compressor design Part I. Cascade  
theory and performance.  
RAE. Report E.3946, (June, 1942).
26. A.D.S. Carter  
The low speed performance of  
related aerofoils in cascades.  
Aeronautical Research Council  
Current paper 29. (September, 1949).



27. J. Reeman  
Performance of cascades of  
aerofoils at positive stagger.  
Power Jet Memorandum M.1203  
(March, 1947).
28. A.R. Howell  
and  
A.D.S. Carter  
Fluid flow through cascades of  
aerofoils. Sixth International  
Congress of Applied Mechanics.  
(September, 1946)  
(National Gas Turbine Establish-  
ment Report R.6).
29. J.R. Erwin  
and  
J.C. Emery  
Effect of tunnel configuration  
and testing technique on cascade  
performance. NACA Report 1016,  
(1951).
30. S. Katzoff  
and  
M.E. Hannah  
Further comparisons of theoretical  
and experimental lift and pressure  
distributions on aerofoils in  
cascade at low subsonic speed.  
NACA. Technical Note 2391,  
(August, 1951).
31. J.L. Koffman  
Fans for traction applications  
Diesel Railway Traction  
Part I (March 1951), Part II  
(April, 1951).
32. A.R. Howell  
Fluid dynamics of axial com-  
pressors, Institution of Mechanical  
Engineers, Proceedings Vol.153  
War Emergency Issue 12 (1945)
33. A. Mager,  
J.J. Mahoney  
and  
R.E. Budinger  
Discussion of boundary layer  
characteristics near the wall  
of an axial flow compressor.  
NACA. Report 1085 (1952)
34. A.D.S. Carter  
Three dimensional flow theories  
for axial compressors and tur-  
bines. Institution of Mechanical  
Engineers, Proceedings Vol.159  
War Emergency Issue No.41 (1948)
35. H.B. Squire  
and  
K.G. Winter  
The secondary flow in a cascade  
of aerofoils in a non-uniform  
stream, Journal of Aeronautical  
Sciences, Vol.18, No.4, (April 1951)

36. W.R. Hawthorne      Secondary circulation in fluid flow. Proceedings of Royal Society, Vol.206, No.A.1086, (May, 1951).
37. A.G. Hansen,  
H.Z. Herzig  
and  
G.R. Costello      A visualization study of secondary flows in cascades. NACA. Technical Note 2947 (May, 1953).
38. S.M. Bogdonoff  
and  
L.J. Herrig      Performance of axial flow fan and compressor blades designed for high loadings. NACA. Technical Note 1201 (February, 1947).
39. G.N. Patterson      Ducted fans: Approximate method of design for small slipstream rotation, Australian Council for Aeronautics, Report ACA.8 (August, 1944).
40. G.N. Patterson      Ducted fans: Effect of the straightener on overall efficiency, Australian Council for Aeronautics. Report ACA.9. (September, 1944).
41. G.N. Patterson      Ducted fans: High efficiency with contra-rotation. Australian Council for Aeronautics, Report ACA.10 (October, 1944).
42. B. Thwaites      A note on the design of ducted fans. Aeronautical Quarterly, Vol.3, Part III, (November, 1951).
43. F.G. Blight      An introduction to the aerodynamic theory of compressors and turbines. Aeronautical Research Laboratories (Melb.) Engines Report E.56 (May, 1947).
44. S. Gray      Fluid dynamic notation in current use at N.G.T.E. National Gas Turbine Establishment Memorandum M.93 (July, 1950).

45. J.F.M. Scholes  
and  
G.N. Patterson  
Wind tunnel tests on ducted  
contra-rotating fans.  
Australian Council for  
Aeronautics. Report ACA.14  
(February, 1945).
46. J.F.M. Scholes  
Ducted fans: a nomogram  
method of analysis.  
Australian Council for  
Aeronautics. Report ACA.32,  
(February, 1947).
47. B. Thwaites  
A note on the performance of  
ducted fans.  
Aeronautical Quarterly, Vol.5,  
Part I, (February, 1953).
48. D.B. Welbourn  
Axial flow ducted fan theory.  
The Engineer, Vol.186, page 86,  
(July 22, 1949).
49. S. Lieblein  
Turning angle design rules  
for constant thickness circular  
arc inlet guide vanes in axial  
annular flow.  
NACA. Technical Note 2179  
(September, 1950).
50. A.D.S. Carter  
and  
E.M. Cohen  
Preliminary investigation  
into the three dimensional  
flow through a cascade of  
aerofoils. Power Jets  
Report R.1180. (February, 1946).
51. P.S. Granville  
A method for the calculation of  
the turbulent boundary layer  
in a pressure gradient.  
David W. Taylor, Model Basin,  
Report 752, (May, 1951).
52. E. Boxer  
Influence of wall boundary  
layer upon the performance of  
an axial flow fan rotor.  
NACA. Technical Note 2291,  
(February, 1951).

53. D.G. Ainsley      Performance of axial flow turbines. Institution of Mechanical Engineers, Proceedings Vol. 159 War Emergency Issue 41, (1948).
54. G.N. Patterson      Modern diffuser design. Aircraft Engineering, Vol. 10, 115. (September, 1938).
55. P. Rebuffet      Aérodynamique Expérimentale (pg.281) Librairie Polytechnique Ch. Beranger, 2nd Edition (1950).
56. E.P. Warner      Airplane Design - Performance (pg. 349) McGraw-Hill Book Company. 2nd Edition (1936).
57. E.B. Bell  
    and  
    L.J. De Koster      The effect of solidity, blade section and contravane angle on the characteristics of an axial flow fan. NACA. ARR. December, 1942.
58. I.H. Abbott  
    and  
    A.E. von Doenhoff      Theory of Wing Sections, pg. 321 1st Edition, McGraw-Hill Book Company (1949).
59. K. Campbell      Engine cooling fan theory and practice. S.A.E. Journal (transactions) Vol. 52 No. 9 (September, 1944).
60. R.A. Wallis      Wind tunnel tests on a series of circular arc plate aerofoils. Aeronautical Research Laboratories Aerodynamics Note 74 (August, 1946).
61. Zwaaneveld      The aerodynamic properties of circular arc plate sections (Dutch) J. Polyt. Tijd. No. 6 (March 1951).
62. R.A. Wallis      Sheet metal blades for axial flow fans. Engineering Vol. 171 No. 4454 (8th June, 1951).
63. R. Fail      Tests on a high solidity engine cooling fan in the R.A.E. full scale fan testing tunnel. R.A.E. Aero. Report 2068 (July, 1945).

64. R. Fail Tests on an impulse type engine cooling fan in the R.A.E. full scale fan testing tunnel.  
R.A.E. Aero Report 2101 (December, 1945).
65. J.R. Weske An investigation of the aerodynamic characteristics of a rotating axial-flow blade grid.  
N.A.C.A. Technical Note 1128 (Feb. 1947).
66. C.E. Pearson Measurement of instantaneous vector air velocity by hot wire methods.  
Journal of Aeronautical Sciences  
Vol. 19 No. 2 (February, 1951).
67. J.F. Runckel and R.S. Davey Pressure distribution measurements on the rotating blades of a single stage axial flow compressor.  
N.A.C.A. Technical Note 1189 (Feb. 1947).
68. K.H. Khalil Rotational effects on a cascade of aerofoil blades.  
The Engineer Vol. 193 No. 5030  
(20th June, 1952).